STATE OF CALIFORNIA • DEPARTMENT OF TRANSPORTATION

TECHNICAL REPORT DOCUMENTATION PAGE

TR0003 (REV 10/98)

ADA Notice

For individuals with sensory disabilities, this document is available in alternate formats. For information call (916) 654-6410 or TDD (916) 654-3880 or write Records and Forms Management, 1120 N Street, MS-89, Sacramento, CA 95814.

1. REPORT NUMBER CA14-1723	2. GOVERNMENT ASSOCIATION NUMBER	3. RECIPIENT'S CATALOG NUMBER
4. TITLE AND SUBTITLE Investigation of Methacrylate Rehabilitation Strategy to Extend the Service Life of Concrete Bridge Decks		5. REPORT DATE September 2013 6. PERFORMING ORGANIZATION CODE
7. AUTHOR Eli Cuelho and Jerry Stephens		8. PERFORMING ORGANIZATION REPORT NO. MSU G&C #4W2179
9. PERFORMING ORGANIZATION NAME AND ADDRESS Western Transportation Institute PO Box 174250 Montana State University – Bozeman Bozeman, Montana 59717-4250		10. WORK UNIT NUMBER 11. CONTRACT OR GRANT NUMBER 65A0294
12. SPONSORING AGENCY AND ADDRESS California Department of Transportation Division of Research Innovation, and Systems Information, MS-83 P.O. Box 942873 Sacramento, CA 94273-0001		13. TYPE OF REPORT AND PERIOD COVERED Final Report July 2008– September 2013 14. SPONSORING AGENCY CODE

15. SUPPLEMENTARY NOTES

16. ABSTRACT

Deterioration of bridge decks is an ongoing problem faced by transportation agencies across the country. California has a bridge inventory of over 12,300 structures, many of them are a box girder design. Maintenance of these structures can be challenging due to the fact that the bridge deck is integrally cast as part of the load bearing structure. Several rehabilitation treatments are available to help extend the life of distresses concrete bridge decks, but the long-term performance and optimum treatment time of these treatments have not been fully established. The focus of this study was to investigate the effectiveness of high molecular weight methacrylate (HMWM) treatments applied at various stages of bridge deck deterioration in order to determine their effectiveness in extending the life of concrete bridge decks. To accomplish this objective, eight full-scale deck panels (four sets of two panels each) were cast to Caltrans specifications and fixed to a support structure to simulate a box girder design configuration. A fully-automated, 20-kip, rolling wheel load simulator was used to traffic the test panels. Six of the eight test panels subsequently were treated with HMWM at various traffic levels, (up to 2,000,000 cycles at various cycle increments), with two panels being treated at each level, resulting in four treatment/traffic combinations including untreated (control) samples. Evaluation of performance was based on cracking behavior and flexural stiffness of the test panels over time. This result was most evident in the two sets of deck panels that were treated at 1,000,000 load cycles and then trafficked for an additional million load cycles. Test panels treated at earlier times also showed a benefit, but to a much lesser extent. Based solely on traffic-induced stresses and not environmental induced deterioration, performance comparisons generally indicated that later applications of HMWM will likely result in greater structural benefit.

17. KEY WORDS methacrylate, concrete bridge deck, box girder, accelerated testing	18. DISTRIBUTION STATEMENT No Restrictions. This document is available through the National Technical Information Service, Springfield, VA 22161	
19. SECURITY CLASSIFICATION *(of this report)* Unclassified	20. NUMBER OF PAGES 162	21. COST OF REPORT CHARGED

Reproduction of completed page authorized.

DISCLAIMER STATEMENT

This document is disseminated in the interest of information exchange. The contents of this report reflect the views of the authors who are responsible for the facts and accuracy of the data presented herein. The contents do not necessarily reflect the official views or policies of the State of California or the Federal Highway Administration. This publication does not constitute a standard, specification or regulation. This report does not constitute an endorsement by the California Department of Transportation (Caltrans) of any product described herein.

For individuals with sensory disabilities, this document is available in braille, large print, audiocassette, or compact disk. To obtain a copy of this document in one of these alternate formats, please contact: the California Department of Transportation, Division of Research Innovation, and Systems Information, MS-83, P.O. Box 942873, Sacramento, CA 94273-0001.

INVESTIGATION OF METHACRYLATE REHABILITATION STRATEGY TO EXTEND THE SERVICE LIFE OF CONCRETE BRIDGE DECKS

Final Project Report

by

Eli Cuelho and Jerry Stephens

of the

Western Transportation Institute, College of Engineering
Montana State University – Bozeman

prepared for the

California Department of Transportation
Department of Research and Innovation

September 2013

DISCLAIMER STATEMENT

The contents of this report reflect the views of the authors, who are responsible for the facts and the accuracy of the data presented herein. The contents do not necessarily reflect the official views or policies of the State of California or the Federal Highway Administration. This report does not constitute a standard, specification or regulation. The United States Government does not endorse products or manufacturers. Trade and manufacturers' names appear in this report only because they are considered essential to the object of the document.

ACKNOWLEDGMENTS

The authors gratefully acknowledge the financial support provided by Caltrans and the Research and Innovative Technology Administration of the U.S. Department of Transportation to fund this research project. The authors greatly appreciate the contribution of Steve Sahs of Caltrans for his support throughout the project. Methacrylate overlay materials were graciously donated by Kwik Bond Polymers (Benicia, CA). The assistance and contribution from the following individuals (listed in alphabetical order) during all phases of this project is also greatly appreciated:

- Michelle Akin – helped with data acquisition system and instrumentation
- Andy Gilbert – graduate student on the project responsible for static load test
- Jason Harwood – research associate responsible for design, construction and setup of laboratory test experiment
- Jeremy Miller – graduate student on the project responsible for carrying out trafficking study
- Steve Quenneville – designed and constructed the accelerated testing device through Applied Research Associates, Inc. (headquartered in Albuquerque, NM)
- Adam Stordahl – graduate student on the project responsible for designing support frame, concrete sampling during concrete pours, and finite element analyses
- Zac Zupan – graduate student and research associate responsible for carrying out trafficking study, maintaining the trafficking device and analyzing long-term data

EXECUTIVE SUMMARY

Deterioration of bridge decks is an ongoing problem faced by transportation agencies across the country. With a bridge inventory of over 12,300 structures, Caltrans is one such agency, particularly since many bridges in California utilize a box girder design. While this design offers several advantages (greater torsional resistance, longer span lengths, prefabrication, modular construction, etc.), maintenance of these structures can be problematic. This type of bridge construction uses a driving surface (deck) that is an integral part of the basic load carrying elements of the structure. Replacing the deck of a box girder bridge is therefore difficult, making the use of surface treatments to address deck deterioration a particularly attractive option (as opposed to replacement). Caltrans currently uses several different rehabilitation techniques to extend bridge deck life (high molecular weight methacrylate (HMWM), polyester overlay with partial deck removal, polyester overlay without deck removal, Portland cement overlay, and asphalt concrete overlay), with HMWM often being used. The choice of treatment strategy depends, in part, on the extent and severity of the damage. The long-term effectiveness of using these techniques, however, has not been fully validated, nor has the optimum time to apply these various treatments been fully established. Furthermore, current analytical performance models alone are not sufficiently developed to answer these questions.

The objective of this project was to develop information on the timing and performance of various deck treatments under fatigue loading that could be used by Caltrans in selecting more effective deck rehabilitation strategies in any given situation. The decision was made to obtain this information by testing various treatments under realistic load conditions. While the original intent was to evaluate several different treatment approaches, the experimental program was modified to be able to use larger test specimens that would more realistically represent in-service structural conditions, which in turn resulted in a corresponding reduction in the rehabilitation strategies considered to simply HMWM. Thus, the objective of this research was to determine the optimal timing of the application of HMWM deck sealants to maximize their effectiveness in extending the life of Caltrans concrete bridge decks.

In pursuit of the project's objective, eight full size concrete deck panels were trafficked under a moving wheel load. The panels were 8 ft 5½ inches long by 7 ft wide by 6½ inches thick, and were representative of Caltrans box girder deck sections with respect to thickness, transverse span and reinforcement layout. The panels were reinforced following typical Caltrans practices and cast using a concrete mixture based on that used in a typical Caltrans bridge structure. The panels were clamped in a test frame to generate a stress environment generally consistent with the local transverse stresses expected in an actual bridge structure in which the decks are cast integral with the webs of the box beams. An automated bridge deck tester was used to fatigue the test panels under a 20-kip moving wheel load that ran down the center of the deck panels, parallel to their clamped edges. Data recorded during trafficking consisted of applied load and

center and quarter point deflection midway along each panel in the direction of wheel travel. These measurements were used to determine changes in slab stiffness as cycling proceeded, where stiffness was simply calculated as applied load divided by deformation. Panel condition (cracking and spalling) was visually assessed and documented periodically as the load cycles were applied. Performance of the test panels was determined using both the cracking behavior and flexural stiffness.

The panels were tested in two groups of four panels each, with panels variously experiencing approximately 600,000 to 2,100,000 wheel passes. Six of the eight panels were treated with HMWM Kwik Bond Polymers (Benicia, CA) KBP 204 HMWM primer/sealer at different points during trafficking. The panels were steel shot blasted and cleaned using compressed air in accordance with California's Standard Specifications prior to HMWM application. HMWM treatments were applied at approximately 25,000, 250,000 and 1,000,000 traffic cycles, and one set of panels were left untreated (i.e., controls). In all, four different treatment–traffic combinations were evaluated, each with two panels.

All of the test panels experienced cracking as trafficking proceeded, although no spalling or delamination of the concrete was observed. Top cracking in the test panels was inhibited by HMWM treatment. Existing cracks were sealed and only a few (or no) new cracks formed in the treated test panels under continued loading. Cracking on the bottom surface of the panels generally was not affected by HMWM treatment of the top surface. Overall, while significant differences were observed in the absolute amount of cracking in similarly configured and loaded test panels, patterns in the progression of this cracking and the effect of HMWM treatment were similar across all panels, and any differences in specific panel performance can be attributed to vagaries in material properties and support conditions (i.e., edge fixity) between panels.

Flexural stiffness of the deck panels was also used to characterize their performance over time during trafficking. Independent of specific level of initial stiffness, all panels demonstrated similar behavior as cycling proceeded, consisting of a sharp decline in stiffness in the first 25,000–100,000 load passes, a subsequently more gentle decrease in stiffness through approximately 250,000 load passes, and finally, a very gradual further decay in stiffness until testing was terminated.

Panel stiffness generally increased after HMWM treatment. As may be obvious, HMWM application did not fully restore panel stiffness to precracked conditions, as only the top surface of the panels were treated (i.e., internal and bottom surface distress was not remediated). The greatest increase in stiffness was observed for the M1000 panels, in which stiffness increased by an average of 10 percent as a result of the HMWM treatment. As would be expected, the percentage increase in stiffness of the treated panels was proportional to the degree of top cracking the panels had experienced at the time of treatment.

Across all cyclic load intervals, greater relative degradation in stiffness occurred in the untreated versus treated test panels. The most pronounced difference in stiffness performance with HMWM treatment was seen following application of HMWM to the M1000 panels at 1,071,820 cycles of applied load, following which the average stiffness in the treated panels decreased by only 4 percent over the next 1,000,000 load cycles, compared to a decrease of 34 percent in the untreated panels.

Overall, this project successfully began the characterization of the behavior of full-scale bridge deck panels fatigued using a large, automated trafficking device and then treated with high molecular weight methacrylate coatings on their top surfaces. Based solely on traffic-induced stresses, and evaluated based on cracking behavior and flexural stiffness calculations, performance comparisons between panels treated at various levels of traffic generally indicated that later applications of HMWM will likely result in greater structural benefit. This result was most evident in the two sets of panels that were trafficked for over two million load cycles. Test panels treated at earlier times (approximately 25,000 and 250,000 traffic cycles) also showed a benefit from the treatment, but to a much lesser extent (retaining only 1 to 4 percent more stiffness upon subsequent cycling relative to comparable untreated panels). Due to time and resource constraints, however, these panels could not be trafficked over the long term, which would have made it possible to characterize the effect of these early HMWM treatments on longer term performance. Furthermore, while the results of this project appear to suggest that later application of HMWM may be more beneficial, environmental effects and ingress of water and/or chlorides which are known to accelerate damage in untreated bridge decks was not considered. Early sealing could play an important role in mitigating damage from these mechanisms.

Recommendations for future work include:

- making redundant any instrumentation used to make critical measurements,
- revising the panel edge support design to better ensure consistent and full restraint conditions along the edge of the test panels,
- continued trafficking of the panels treated at approximately 25,000 and 250,000 cycles of load to observe the effect of these treatments over the long term (say, to the 2,000,000 load cycle level used on other panels),
- increasing the magnitude of the applied wheel load (possibly to 25 kips) to accelerate fatigue damage, and
- further testing of other rehabilitation techniques such as polyester concrete overlays, Portland cement overlays, asphalt concrete overlays.

TABLE OF CONTENTS

Introduction 12
Background 15
Concrete Bridge Deck Deterioration 15
Bridge Deck Overlay Rehabilitation Strategies 17
HMWM Sealants 18
Polyester, Portland Cement and Asphalt Concrete Overlays 20
Polyester Concrete Overlay 20
PCC Overlay 21
Asphalt Concrete Overlay 22
Summary 23
Caltrans Bridge Deck Rehabilitation Practices and Procedures 23
Rolling Wheel Load Fatigue Testing of Full-Scale Bridge Deck Elements 24
Laboratory Test Set Up 24
Fatigue Life 26
Summary 29
Experimental Design 30
Design of the Bridge Deck Test Panels 31
Construction of the Concrete Bridge Deck Test Panels 36
Design and Construction of Reaction Frame 38
Fatigue Life Predictions 45
Automated Bridge Deck Tester 47
Response Monitoring 49
Instrumentation and Data Acquisition 49
Visual Distress Assessment 51
Concrete Compression Tests 51
Concrete Core Tests 52
Testing 54
Response Monitoring/Data Collection 54
Deck Rehabilitation 56
Analysis and Results 61
Cracking Analysis 61
General Cracking Behavior 61
Quantitative Analysis of Cracking Distress 70
Conclusions from Cracking Distress 74

Flexural Stiffness Analysis 75
Conclusions and Recommendations 83
References 86
Appendix A – Deck Slab Reinforcement Details 92
Appendix B – Caltrans Concrete Mix Design 93
Appendix C – Support Frame Design Schematic 94
Appendix D – CRT TEst Results 96
Appendix E – Product Data Sheet for Kwik Bond Methacrylate 106
Appendix F – Crack Maps 111

LIST OF TABLES

Table 1: Mix Designs and Wet Mix Properties of Test Panel Concrete Pours 37
Table 2: Testing Matrix for Concrete Cores 52
Table 3: Test Panel Traffic Levels at Treatment and Completion Times 54
Table 4: Summary of Top Cracking Distresses of Treated Panels Prior to Treatment 56

LIST OF FIGURES

Figure 1: Concrete box girder bridge in Nevada County, CA (photo by Mark Yashinsky) 13
Figure 2: Cracking Mechanisms in Concrete Structures (Transportation Research Circular, 2006) 16
Figure 3: Isometric View and Cross Section of Testing Frame (El-Gamal et al., 2005). 25
Figure 4: Tension/compression moment resisting connection (from Yoshitake et al., 2010). 26
Figure 5: Fatigue life curves for full-scale concrete bridge decks (El-Ragaby et al., 2007). 29
Figure 6: Dimensions and reinforcement details of test specimens. 32
Figure 7: Transverse steel layout in the bridge deck (Section 3 from Figure 6). 32
Figure 8: Idealized moment behavior of the deck in the transverse direction. 33
Figure 9: Three-dimensional geometry and VA FEA mesh of the full-scale deck model. 34
Figure 10: Comparison of transverse stresses in the test specimen and full bridge models. 34
Figure 11: Transverse stresses in the top of the deck under the rolling wheel load as it moves along the specimen. 35
Figure 12: Close-up of reinforcement layout. 36
Figure 13: Finished slabs with concrete curing compound on surface. 38
Figure 14: Automated bridge deck tester. 39
Figure 15: Three-dimensional rendering of support frame. 40
Figure 16: Test slabs mounted on reaction frame. 41
Figure 17: Clamping detail for test specimen. 41
Figure 18: Frame setup showing LDPE pads for single panel. 42
Figure 19: Comparison of transverse stresses in the top of the deck for the fully-restrained slab model and rest frame model. 43
Figure 20: End view of static load test setup. 44
Figure 21: Side view of static load test setup. 44
Figure 22: Predicted fatigue life of test panels as a function of applied load. 46
Figure 23: Drive cable and carriage assembly. 49
Figure 24: Locations of displacement measurements under each test panel. 50
Figure 25: Photo of LVDT sensors attached to underside of a test panel. 51

Figure 26: Results from rapid chloride permeability tests on concrete cores. 53
Figure 27: Results from rate of absorption tests on concrete cores. 53
Figure 28: Timeline of events for Control and M1000 test panels (Panel Set 1). 55
Figure 29: Timeline of events for M250 and M25 test panels (Panel Set 2). 56
Figure 30: Shot blasting the deck panels in preparation for the HMWM application. 57
Figure 31: Concrete surface before and after shot blasting. 58
Figure 32: Crack in deck surface after shot blasting. 58
Figure 33: Application of HMWM surface treatment. 59
Figure 34: Close-up of methacrylate-filled crack. 60
Figure 35: Top cracking in $Control_a$ test panel at various traffic levels. 62
Figure 36: Bottom cracking in $Control_a$ test panel at various traffic levels. 63
Figure 37: Longitudinal crack in top surface. 64
Figure 38: Top cracking in all test panels at about 250,000 traffic passes. 66
Figure 39: Top cracking in M1000 and Control test panels at 1,071,820 traffic passes. 67
Figure 40: Bottom cracking in M250, M1000 and Control test panels at 250,000 load cycles. 69
Figure 41: Bottom cracking in M1000 and Control test panels at 1,071,820 traffic passes. 70
Figure 42: Percent top cracking for both panel sets. 71
Figure 43: Top crack length for both panel sets. 71
Figure 44: Percent bottom cracking in Panel Set 1. 73
Figure 45: Percent bottom cracking in Panel Set 2. 74
Figure 46: Flexural stiffness of Panel Set 1 based on center-point displacements. 76
Figure 47: Flexural stiffness of Panel Set 1 based on quarter-point displacements. 77
Figure 48: Average flexural stiffness of Panel Set 1. 77
Figure 49: Flexural stiffness of Panel Set 2 based on center-point displacements. 78
Figure 50: Flexural stiffness of Panel Set 2 based on quarter-point displacements. 78
Figure 51: Average flexural stiffness of Panel Set 2. 79
Figure 52: Percent cracking versus percent increase in stiffness. 81
Figure 53: Percent change in stiffness as a function of traffic. 81
Figure 54: Average flexural stiffness as a function of top cracking for the Control test panels. 82

INTRODUCTION

California's highway system includes over 12,300 bridges. These structures have a median age of approximately 40 years. The bridges are exposed to a variety of potentially damaging conditions, including marine environments along the coast and the use of deicers in the northeast part of the state (Environmental Area III). According to a survey by Aktan and Fu (2003), the service life of concrete bridge decks operated by Caltrans is believed to be 40 years or less under current average traffic levels. This life span is significantly shorter than the standard design life of bridges (usually about 75 years). Various distresses in the forms of transverse cracking, spalling, and reinforcement corrosion reportedly have been observed in these bridge decks (Aktan and Fu, 2003; Russell, 2004; Rahim et al., 2006). Based on this information, considerable resources are needed to rehabilitate or replace concrete bridge decks in California. Upkeep related to corrosion alone is projected to cost the state hundreds of millions of dollars per year.

In California, the problem of maintaining aging bridge infrastructure is complicated by the widespread use of concrete box girder bridges (Figure 1). This type of bridge construction utilizes a driving surface (deck) that is cast integrally with the main load carrying elements. In contrast, the deck in an open girder bridge design is a distinct element from the rest of the structure. The significance of this difference is most pronounced when it becomes necessary to replace or rehabilitate an in-service bridge deck. Replacing the deck of a box girder bridge is difficult since it requires removing part of the structure needed to carry basic loads on the system. In light of this situation, deck preservation/rehabilitation using surface treatments is a particularly attractive option for box girder bridges.

One important preservation strategy employed by Caltrans is the use of deck protection systems, including deck crack filling/sealing and overlays. Currently, high molecular weight methacrylate (HMWM) is the primary type of deck crack sealant used in California. Deck overlays are used to address a variety of deck deterioration conditions. Partial-depth overlays involve removal of the top several inches of deck concrete followed by recasting the partial deck section with Portland cement concrete (PCC) or polyester concrete. Direct overlay methods can also be used and entail constructing a new deck over the deteriorated deck without removal of existing concrete.

Figure 1: Concrete box girder bridge in Nevada County, CA (photo by Mark Yashinsky[1])

While significant resources are expended each year to rehabilitate concrete bridge decks, a survey of existing research shows a lack of knowledge in how to best implement the rehabilitation methods given above. While there have been many laboratory studies performed to evaluate the effectiveness of these strategies (Kushner et al., 1987; Sprinkel et al., 1995), these relatively simple investigations have not been able to model all of the complexities in the behavior of real bridge decks. Thus, there is a recognized disconnect between positive laboratory results for rehabilitation/repair strategies and their subsequent performance in the field, particularly with HMWM sealants (Marks, 1988; Meggers, 1998). Consequently, little research is available to help inform Caltrans on how and when bridge decks can best be rehabilitated. As a result, the decision of when to implement a certain rehabilitation measure is commonly made based on professional judgment of experienced personnel. In light of the significant value and critical role of these elements of the highway infrastructure, as well as the substantial cost of the rehabilitation measures themselves, it would be beneficial to research and more formally establish engineering relationships between deck condition and appropriate rehabilitation strategy (i.e., type and timing) to optimally extend deck life.

The objective of this research was to determine the optimal timing of the application of HMWM deck sealants to maximize their effectiveness in extending the life of Caltrans concrete bridge decks. While the original intent of this project was to also study Portland cement, polyester and asphalt concrete deck overlays, the experimental program was modified to use larger and more realistic test specimens, which resulted in a corresponding reduction in the rehabilitation strategies that could be accommodated.

[1] http://creativecommons.org/licenses/by-nc-sa/3.0/

In pursuit of the project's objective, eight full size concrete deck panels were trafficked under a moving wheel load of 20 kips. The panels were 8 ft 5½ inches long by 7 ft wide by 6½ inches thick, and were representative of Caltrans box girder deck sections with respect to thickness, transverse span and reinforcement layout. The panels were clamped in a test frame to generate longitudinal fixed edge conditions generally consistent with those expected in an actual bridge structure in which the decks are cast integral with the webs of the box beams. The moving wheel load ran down the center of the deck panels, parallel to their clamped edges. Data recorded during trafficking consisted of applied load and center and quarter point deflection midway along each panel in the direction of wheel travel. Panel condition (cracking and spalling) was visually assessed and documented periodically as load cycles were applied. Panel condition was quantified by calculating crack densities from these visual inspections.

The panels were tested in two groups of four panels each, with panels variously experiencing approximately 600,000 to 2,100,000 wheel passes. Six of the eight panels were treated with HMWM sealant at different points during trafficking, with attendant changes in their stiffness and degradation as a result of treatment application being monitored as traffic loading proceeded.

This report begins with a literature review presented in Chapter 2 covering bridge deck deterioration, rehabilitation practices and fatigue testing methods, prior to reporting on the conduct and outcome of the test program. This information is followed in Chapter 3 by a description of design and construction of the test specimens and load frame, validation of the load frame performance and establishment of the basic instrumentation and testing protocols. Test results and analyses are then presented in Chapter 4, focused on the basic deformation response of the test panels and their deteriorated condition as a function of wheel passes and treatment conditions. Finally, Chapter 5 summarizes the work performed, significant findings and recommended future work.

BACKGROUND

This project consisted of an experimental investigation of concrete bridge deck and bridge deck treatment performance. In preparation for its execution a general review was done on bridge deck deterioration, deck rehabilitation treatments, Caltrans bridge deck rehabilitation practices and laboratory approaches to bridge deck testing. Following the original scope of the project this review considered HMWM sealants and Portland cement, polyester, and asphalt concrete overlays. The primary focus, however, was placed on HMWM sealants, as only this rehabilitation methodology was subsequently physically tested. Relative to test methods, the decision was made prior to the beginning of the project that testing would be conducted on deck panel elements under rolling wheel loads, and the literature review was focused in this direction.

Concrete Bridge Deck Deterioration

National attention has been focused on premature deterioration of bridge decks since the mid-1950s, when this problem was ranked as the fourth principal problem faced by bridge maintenance engineers (McGovern, 1955). The late 1950s saw increased use of chloride-based deicing salts (deicers) on highways, which were later found to significantly aggravate concrete scaling and concrete cracking and spalling. Since then, deterioration of concrete bridge decks, especially corrosion-related deterioration, has received ever increasing attention and been frequently indicated as the top structural concern of state departments of transportation (DOTs) including Caltrans (NCHRP, 1970; NCHRP, 1979; Babaie and Hawkins, 1987; Krauss and Rogalla, 1996; Hadidi and Saadeghraziri, 2003; Russell, 2004; Rahim et al., 2006).

Bridge decks do not usually fail due to insufficient concrete strength to bear traffic loading; instead, inadequate or improper maintenance techniques have been constantly cited as the primary cause of failure. Bridge deck deterioration generally consists of concrete deterioration and reinforcement corrosion. Concrete deterioration usually appears in the form of scaling, mortar flaking, alkali-aggregate reactivity, mechanical (traffic) fatigue, abrasion damage, or cracking and spalling (Krauss and Rogalla, 1996; Russell, 2004). Although each distress has a different cause, most premature distresses are closely related to cracking (Mehta, 1991; Hobbs, 1999). In bridge decks, cracks are the precursors to more significant problems since they allow for the ingress of harmful chemicals and substances. Deck cracking can aggravate reinforcement corrosion, lead to deterioration and leaching of concrete, and damage structural components beneath the deck.

Cracking seems to be a universal problem that occurs across many different types of bridge decks and in most geographical locations and climates. Cracks in concrete structures can be divided into two categories based on whether they initiate before or after hardening (see Figure 2), and bridge decks are susceptible to both types of cracking.

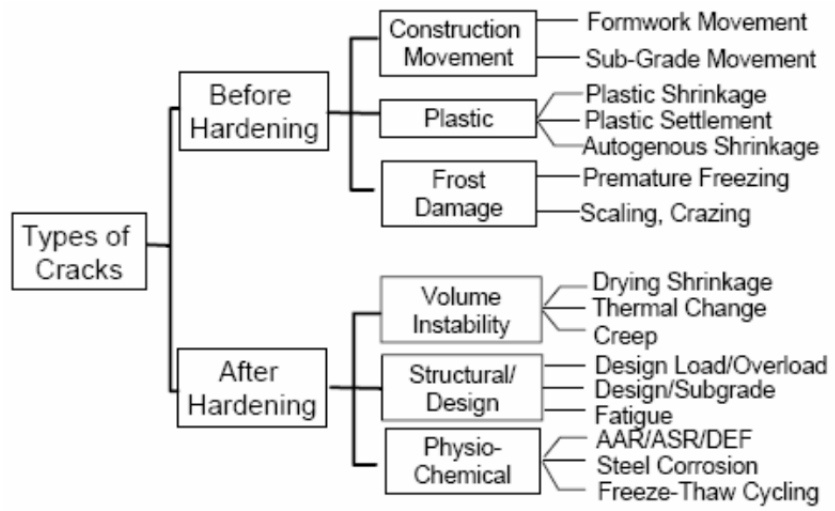

Figure 2: Cracking Mechanisms in Concrete Structures (Transportation Research Circular, 2006)

Cracking occurs in concrete when internal stresses exceed the concrete's tensile capacity. Concrete's relatively low tensile strength (about 15 percent of its compressive strength) makes it particularly prone to cracking. In bridge decks, the concrete often is restrained as part of the structural design, and tensile stresses due to shrinkage (plastic, autogenous, and drying) or temperature induced volume changes may lead to cracking (Carden and Ramey, 1999). Other stresses that lead to cracking can have a variety of origins, including chemical reactions and structural loading (ACI 224.1R-93, 1993). Once initiated, the cracks can be aggravated by several factors, including physical design of the bridges and decks, concrete mixture design, material properties, environmental conditions, and construction practices (Krauss and Rogalla, 1996; Burrows, 1998; Weiss et al., 1999; Juenger and Jennings, 2002). According to the Portland Cement Association (PCA), transverse cracking is the predominant mode of deck cracking, with a lesser degree of longitudinal, diagonal, or map cracks observed in most concrete bridge decks (Carden and Ramey, 1999; ACI 345R-91, 1991).

Reinforcement corrosion involves electrochemical reaction of the steel with oxygen and water in the concrete (Hausmann, 1998; Hartt and Nam, 2004). Corrosion of reinforcement in concrete can be initiated, or significantly accelerated, by the ingress of chloride ions above a concentration of 0.6 to 0.9 kg/m^3 (1.0 to 1.5 lb/yd^3) on the rebar surface. Corrosion of reinforcement in concrete can debond the steel-concrete interface and reduce the structural capacity of bridge decks. Reinforcement corrosion can also generate significant hoop stress around the reinforcing bars, leading to cracking and spalling of concrete cover. Cracking and spalling due to reinforcement corrosion in turn provide chlorides, water, oxygen, and carbon dioxide ready access to the reinforcement and exacerbate reinforcement corrosion (Samples and Ramirez, 1999; Sagues and Kranc, 1997). Excessive concrete cracking or spalling, if not well attended, can also significantly shorten the service life of bridge decks. Rebar corrosion due to

chloride ingress from highway deicer application and/or marine exposure has been recognized as the primary cause for structural failure of bridge decks (Page et al., 1986; Hartt and Nam, 2004).

As concerns grew regarding deicer-related deck deterioration in the 1960s, highway engineers started to develop strategies to protect bridge decks. Early protection strategies targeted mitigating salt scaling by using high-quality air-entrained concrete and periodic applications of linseed oil. More protective strategies were developed after 1972 when FHWA required that deck protective systems be used on federal-aided structures to deal with concrete cracking and spalling due to deicing chlorides. Today, numerous strategies are available to protect bridge decks, including modification of concrete mix design, adjustment of structural design and construction practices, and employment of deck protection systems involving sealants, overlays, membranes, impregnants, or electrochemical approaches such as cathodic protection and electrochemical removal of chlorides and/or injection of corrosion inhibitors (Aktan and Fu, 2003; Russell, 2004; Rahim et al., 2006).

A high-quality concrete bridge deck that can lead to a long service life and minimum maintenance incorporates low chloride permeability, a top surface that does not deteriorate from freeze-thaw or abrasion damage, cracking limited to fine flexural cracks associated with the structural behavior, and smooth rideability with adequate skid resistance. Service life of decks can be significantly extended by using measures to prevent ingress of detrimental substances from the external environment. Since detrimental substances usually intrude into decks from deteriorated concrete surfaces (mainly cracks), an effective way to slow down the deterioration process is to seal the cracks or to provide a protective overlay (ACI 345R-91, 1991). The state-of-the-practice involves various systems to prevent the ingress of detrimental substances, with an emphasis on preventing ingress of chloride and water in case of reinforcement corrosion. According to the 2004 NCHRP Synthesis, crack filling/sealing, overlay, and surface coating using water-proof membranes are the most commonly used protection systems (Russell, 2004).

Bridge Deck Overlay Rehabilitation Strategies

As stated earlier, the prevalence of box girder bridges in California has lead the California Department of Transportation (Caltrans) to prefer deck surface treatments to deck replacement. While there are many rehabilitation techniques currently used by Caltrans (HMWM, polyester overlay with partial deck removal, polyester overlay without deck removal, Portland cement overlay, and asphalt concrete overlay), this project has focused its attention on HMWM overlays/sealants.

Overlays are placed on bridge decks as a barrier against water and chemical ingress, wheel load damage and loss of skid-resistance. Bridge deck overlays generally can be divided into three categories: thin overlays (thickness generally less than a half inch), cement-based overlays, and asphalt-based overlays, of which the latter two types are usually thicker than 1 inch. Desired properties for all the three types of overlays include sufficient adhesion or bond to existing

bridge deck concrete, adequate cohesion or resistance to shear stress induced by turning and braking of the heaviest vehicles, and satisfactory skid resistance and durability. Overlays should also be able to expand and contract harmoniously with bridge decks as temperature and moisture conditions change to avoid a loss of bond between them. In addition, overlays used as waterproofing barriers should be designed to be impermeable against moisture and deleterious materials such as chlorides.

HMWM Sealants

HMWM sealants are a common concrete bridge deck rehabilitation material used across the country. In a survey of 16 states conducted by the Minnesota Department of Transportation (Johnson et al., 2009), HMWM was found to be the second most common crack sealant used on bridge decks. Rahim et al. (2006) reported in their survey on state deck sealing practices that 43 percent of the forty states that responded used HMWM deck sealants.

HMWM sealants are adhesive resins consisting of two or more liquid methacrylate monomers that can be mixed and poured directly onto the cracked surface. The resins fill the cracks and bond to the concrete. By filling cracks, HMWMs are able to help prevent chloride and water intrusion. By forming a strong bond with the concrete, the HMWM sealants are able to restore some of the concrete's stiffness as well. Laboratory tests have shown HMWMs to be able to restore 100 percent of a cracked concrete member's flexural stiffness (Rahim et al., 2006). Despite these promising laboratory findings, HMWMs have had mixed results in field applications. The treatment success seems to depend heavily on variables such as the width of the cracks being treated, the surface preparation prior to treatment, the temperature, and the exact formulation of the HMWM (Rahim et al., 2006). The performance of HMWM, however, is usually evaluated based on its ability to penetration into cracks, strength of the bond to concrete, its cured mechanical properties, and other durability factors.

The performance of HMWMs for crack sealing has been frequently studied under laboratory conditions. Kushner et al. (1987), for example, applied three HMWMs with different monomers to concrete samples containing cracks. All the materials were shown to be very effective in sealing cracks with widths above 0.5 mm, and up to 100 percent flexural strength was restored for most samples. In another laboratory study, Sprinkel and DeMars (1995) reported adequate crack sealing, satisfactory freeze-thaw durability, and up to 100 percent flexural strength restoration for three HMWM sealants in a temperature range from 4° to 38°C (40° to 100°F). Finally, Tsiatas and Robinson (2002) found HMWM performed best in an evaluation of HMWM, cementitious based and epoxy sealants.

The performance of HMWM sealants, however, has not always been good, especially in field conditions. Reports on a number of unsuccessful applications of HMWM sealants can be found in the literature. In a 1986 field application, for example, the Iowa DOT used a HMWM resin to seal a cracked bridge deck. Significant water leakage was found from numerous cracks of the

repaired deck on rainy days, even after double application (Marks, 1988). A HMWM used by the Minnesota Department of Transportation appeared to be effective in holding a D-cracked pavement together for less than 18 months (Engstrom, 1994). In a three-year field study conducted in Kansas, none of the three HMWMs considered were found to prevent chloride penetration (Meggers, 1998). Both traffic-induced strain and temperature-induced strain across cracks have been found to significantly reduce the longevity of HMWM sealed cracks. HMWM in treated cracks was itself cracked after one year in service, even though up to 0.5 inches HMWM penetration had been achieved (Sprinkel et al., 1993). Moisture in cracks was once observed to reduce HMWM penetration, although adequate penetration could be still achieved (Mangum et al., 1986).

The current knowledge of HMWM field performance overwhelmingly builds on individual case studies by different highway agencies. Literature reviewed indicated that in most cases failure was attributed to one or two major factors closely related to the specific features of the bridges and decks, sealant application practices, or local environmental conditions. Nevertheless, there are some common factors that have been frequently cited as the major causes of failure, such as crack width and sealant application practices.

Crack width was frequently linked to the penetration depth of the sealant and seems to be the most important factor that affects the performance of HMWMs. Usually a minimum crack width is specified for effective sealant penetration. HMWMs are found to successfully seal cracks wider than 0.04 in., although a national survey indicates that most departments of transportation tend to limit their use to cracks narrower than 0.0625 in. (Rahim et al., 2006; Attanayaka et al., 2003; Soriano, 2002). For cracks narrower than 0.04 in., HMWM can attain satisfactory effect by following with an application of penetrant sealants such as silanes, siloxanes or siliconates, which is commonly referred to as a “dual system” (Xi et al., 2003). The dilemma of crack-width-based evaluation of HMWM performance is that HMWMs have been successfully used on cracks across a large range of sizes, from 0.002 in. to 0.5 in. (Tsiatas and Robinson, 2002; Xi et al., 2003), which indicates that crack width may not be the deterministic factor that defines their performance. Caltrans, for example, observed a reasonable degree of sealant penetration across a variety of crack widths and depths in an extensive field sampling of HMWM treated bridges (Lee and Reis, 2010).

Proper conditions and procedures for sealant application are critical to the success of HMWM treatment. For new decks, it was found that HMWM applied three to six months after construction could effectively control chloride concentration below the corrosion threshold value. For old decks, to achieve good bonding, the application surface must be dry and free of dust, oils, and debris. Other quality assurance practices include specifying surface temperatures for the concrete (10° to 30°C, or 50°F and 85°F) at the time of HMWM application, applying HMWMs during the lowest temperature of the day to ensure that the cracks are the most open, and applying HMWMs directly to the cracks and allowing a few minutes for the sealant to seep

down into the cracks (ACI 345R-91, 1991). Other factors including traffic and environmental loading were also found to affect the field performance of HMWMs. Premature sealant cracking was related to the crack moving and changing due to repeated traffic loading and daily temperature variation (Sprinkel et al., 1993). The Louisiana Department of Transportation and Development evaluated the application of HMWM in sealing a badly cracked deck in 2004. Extracted cores showed that the top one inch was sealed, which was not effective to repair the seriously deteriorated deck (Rahim et al., 2006).

In any event, the long-term effectiveness of using HMWM-based crack sealant in California to rehabilitate bridge decks has not been fully validated, nor has the optimum time to apply these various treatments been fully established. Current analytical performance models alone are not sufficiently developed to generate performance information. Thus, the objective of this research was to determine the optimal timing and durability of HMWM on full-scale concrete deck panels.

Polyester, Portland Cement and Asphalt Concrete Overlays

Polyester Concrete Overlay

Polyester resins, as dense, impermeable polymers when cured, have been used by many DOTs as the binder material for bridge deck overlays. Polyesters are the products of chemical reactions between difunctional alcohols and anhydrides of dibasic organic acids (ACI 503R-93, 1993). Initiators and promoters are often used at the time of application. Polyester resin overlay material can cure rapidly over a large range of temperatures (from 40°F to 100°F), so that traffic can be allowed over the surface within an hour after application. Polyester resin can be formulated to match the elasticity and thermal expansion of existing concrete. Polyester concrete, when used as thin overlay or thicker partial-depth overlay, requires no modifications to curbs, manholes or catch basins and can be applied on bridges without significantly increasing the dead load. Multiple coats can be applied, giving a final thickness of at least 6mm (1/4 inch). Well-constructed polymer concrete overlays can provide good skid resistance and effective protection against chloride intrusion for up to 25 years (Sprinkel et al., 1993). Caltrans currently uses polyester concrete and Portland cement concrete (PCC) on bridge decks. Polyester concrete, as a major overlay material in both partial and complete overlays, has been used in California for the last 10 to 15 years.

Numerous studies have been conducted on the performance of polyester overlays on bridge decks, focusing on polyester overlays' resistance to abrasive wear, cracking, spalling, debonding from the underlying concrete and fatigue under traffic, and on their anti-intrusion capability against moisture and chloride in bridge deck conditions. Similar to the situation with HMWM as a crack sealant, applications of polyester overlays on bridge decks have had mixed success. A comprehensive study conducted by the Virginia DOT compared the performance of polymer overlays, high-early-strength hydraulic cement concrete overlays, sealers, and patches from the

stand-point of performance characteristics (mainly mitigating chloride penetration) and service life (Sprinkel et al., 1993). The study showed that premixed polyester styrene overlays with a methacrylate primer showed a useful service life up to 25 years when applied as a protection or rehabilitation treatment, and outperformed sealers and patches in retarding the infiltration of chlorides. A seven-year durability comparison between polyester overlays and epoxy concrete overlays conducted by New York Department of Transportation in 1991 found that both overlays performed similarly and satisfactorily (Doody and Morgan, 1993). In another side-by-side study of the capability of polyester concrete overlays and epoxy-based concrete overlay systems after a five-year service life, the polyester resin concrete overlays appeared to be susceptible to oxidation and ultraviolet degradation and showed a moderate amount of cracking, spalling and de-bonding from the underlying concrete. The rapid deterioration of polyester overlays was attributed to construction problems that might lead to rich resin in the overlay (Ramirez, 1995).

Fifteen different resinous binders with different formulations were evaluated as overlays in a California-based study on the impacts of wheel characteristics and temperature on their durability and skid resistance. Seven were applied near Sacramento where freezing rarely occurs and eleven were applied at Kingvale, which sees low temperatures and where severe snowplow and chain wear is encountered. All except one of the Sacramento binders were found in good condition after three and one-half years of service. One Kingvale polyester seal coat applied in three layers over an epoxy primer showed good durability but low skid resistance after nearly three years of service. Kingvale polyester overlays without an epoxy primer did not even survive the first winter (Rooney and Shelly, 1969). In an Alabama study, polyester overlays were found to offer the poorest performance of several overlay systems evaluated including epoxy-based, asphalt-based, urethane-based, and polyester-based overlays. The unsatisfactory performance might be due to the relatively high temperature and moisture levels that caused the premature degradation of the polyester material (Ramey and Derickson, 2003).

PCC Overlay

PCC overlays exhibit all of the beneficial behaviors that lead to using a concrete deck in the first place, such as a strong, durable driving surface. However, Portland cement concrete needs to be applied in relatively thick layers (one to four inches), thus adding considerable dead load to the structure. This increase in thickness also causes alignment issues with the roadway if the top surface of the existing deck is not removed.

PCC overlays can be constructed using conventional PCC, latex-modified PCC, polyester-modified PCC, low-slump dense PCC, fast-setting PCC, with some variations involving steel fiber or silica fume, or high-range water-reducing mixtures. The primary function of PCC overlays is to replace deteriorated concrete or asphalt wearing surfaces with a durable and low-permeability material. Performance of PCC overlays has been found to vary considerably from one region to another, depending on design/construction factors and local climates. According to

the ACI Committee 345 (ACI 345.1R-92, 1992), shrinkage and surface cracking of concrete overlays could be significant factors in dry and windy climates or in cold climates where deicing salts are used as compared to locations where there is little use of deicing salts; high-slump mixes (slump over 4 in.) should be avoided on decks with longitudinal grades exceeding 2 percent; and the use of steel fibers, or admixtures such as silica fume or super-plasticizers, can also be expected to improve impermeability and crack resistance.

Asphalt Concrete Overlay

Asphalt concrete overlays on bridge decks, or more broadly the asphalt-based overlays, include two general sub-categories: combined systems consisting of a waterproofing membrane overlaid with one or two courses of asphalt concrete (1½ to 2 inches thick each), and asphalt concrete overlays without a waterproofing membrane. Both systems can add significant dead load to bridge structures. The total thickness of a combined system is usually between 2 and 4 inches. The economics of asphalt mixtures makes asphalt-based overlays a desirable option, which also provides good ride quality. There are many types of membranes including hot applied rubberized membranes, sheet membranes and liquid-applied polymer membranes (NCHRP, 1995). The membranes should be capable of bonding to concrete, bridging cracks, waterproofing, and bonding to AC overlays without being affected by temperatures as high as 150°C from hot repaving. A study involving 119 bridges conducted by the Maine Department of Transportation showed that for as-built wearing surfaces, bituminous concrete overlays with a membrane were more durable and effective in preventing chloride content increases in the deck concrete than reinforced concrete overlays or integral concrete (Kolb et al., 1992). For replacement wearing surfaces, bituminous concrete overlays with membrane waterproofing were also more durable and effective than unreinforced conventional PCC overlays. Research studies conducted by a number of other highway agencies also reported positive experiences with combined systems with respect to their capability in mitigating penetration of chloride and moisture (Hughes, 1994; Al-Qadi et al., 1992). Membrane debonding from concrete, however, could occur when exposed to heat and sunlight, which could lead to vapor pressure and weakening of the bond. Combined systems were reported as not performing satisfactorily on badly delaminated decks with corroded reinforcing bars close to the surface (NCHRP, 1995).

Asphalt concrete overlays without a waterproofing membrane have been used on bridge decks to provide a smooth riding surface and help reduce traffic-caused fatigue of decks (ACI Committee 345.1R-92, 1992). AC overlays are also commonly used as a protective-wearing surface for existing AC-membrane combined systems or polymer sealed decks. The deck surface ought to be dry and primed with an effective sealer and a bonding agent before an AC overlay is placed to ensure good adhesion. Poorly compacted asphalt mixtures could more easily lead to deck deterioration (ACI Committee 345.1R-92, 1992). The use of AC overlays without a waterproofing membrane or sealed cracks, however, should be avoided since the asphalt concretes are relatively porous and entrap salt-laden moisture which can promote deck

deterioration due to alkali-silica reactivity and/or rebar corrosion. Moreover, such deteriorating effects can usually be aggravated by increased permeability of AC with age. The obscured deck deterioration below the asphalt has been found to be difficult to detect or measure (Caltrans, 2006). AC overlays and the concrete underneath the overlay require periodic inspection.

Summary

Similar to other agencies, Caltrans does not have a proven test method to predict the effectiveness and durability of HMWM as a deck sealant. Similarly, the performance of other deck rehabilitation treatments in California has not been verified. Current application of treatment systems, like in most other states, is based mainly on practical experience. Thus, a clear understanding of their deterioration mechanisms will help Caltrans use them more effectively with respect to appropriate design, construction practices, and optimum timing of their deployment. Research is needed to identify the critical factors that influence their performance and to investigate the deterioration rate in order to predict appropriate application time and frequency and better define Caltrans' bridge deck rehabilitation strategies.

Caltrans Bridge Deck Rehabilitation Practices and Procedures

Caltrans routinely assesses the condition of their bridge decks as part of their maintenance and asset management program. Common bridge deck defects and deficiencies include cracking, spalling, delamination, scaling, efflorescence, wear and chloride contamination. A maintenance/asset management training presentation provided by Caltrans was used to develop the summary found in this section (Caltrans, 2007).

HMWM is the preferred treatment for addressing cracking on bridge deck surfaces, but can also be used to address severe efflorescence or efflorescence in California Environmental Area II (moderate climate: occasional freeze-thaw, salts used, low ADTT chain wear) and Environmental Area III (severe climate: significant freeze-thaw, frequent salting, high ADTT chain wear). HMWM treatment is used to bond cracks back together and inhibit moisture intrusion by filling the cracks. This method is primarily used in California to treat cracks under the following conditions:

- Deck cracking is moderate size <u>and</u> density, or severe size <u>and</u> density. This corresponds to the CoRe Smart Flag 358 (cracking) at Condition State 3 or 4 (AASHTO, 2011). Narrow-moderate cracks are about 0.0625–0.125 inches wide and medium-severe cracks are greater than 0.125 inches wide (AASHTO, 2011).
- Deck cracking is moderate size <u>or</u> density (CoRe Smart Flag 358 at Condition State 2), and the soffit has between 2 and 25 percent distress/rust stain (CoRe Smart Flag 359 (efflorescence) at Condition State of 3 or more).
- Deck cracking is moderate size <u>or</u> density (CoRe Smart Flag 358 at Condition State 2) in California Environmental Areas II and III.

- Bridges with heavy truck traffic and deck cracking is moderate size or density (CoRe Smart Flag 358 at Condition State 2).

Fatigue-related cracking is a direct result of load-driven mechanical damage to the structural section that can reduce the load carrying capacity of the bridge deck over time. There are several stages of fatigue damage, as briefly summarized below.

- Stage I – Cracks develop on the bottom face of the deck slab in the transverse direction, mainly from shrinkage at first, but can be exaggerated over time by traffic.
- Stage II – Longitudinal cracks develop on the bottom face of the deck slab creating a network of cracks in orthogonal directions, and transverse cracks on the top face of the deck slab. At this level of deterioration, spacing is about two times the spacing of the top mat of reinforcement.
- Stage III – Further wear of cracks due to cyclic traffic loading. Moisture intrusion can lubricate the cracked surfaces and accelerate damage. Efflorescence may be evident in these cases.
- Stage IV – Cracks through the deck are fully worn, meaning that all shear interlock at the crack face is lost. There is significant loss of load distribution in the longitudinal direction resulting in the deck behaving like a series of transverse "beams" or "planks" rather than a single plate.
- Stage V – Complete loss of structural support due to shear failure of deck reinforcement. Spalling, depressions on the top surface, punching failures and holes are evidence of this level of deterioration.

Recommended maintenance actions for Stage I is to apply HMWM to the deck surface to arrest early crack formation by bonding the crack back together. For similar reasons, HMWM may also be used to address Stage II and III fatigue distresses, but should be based on a case-by-case basis depending on the cost and benefit of such action. Alternatively, polyester concrete overlays are another method of addressing these levels of deterioration. Stage IV may be addressed by and V require deck augmentation or replacement.

Rolling Wheel Load Fatigue Testing of Full-Scale Bridge Deck Elements

Laboratory Test Set Up

Relative to bridge deck test methods, this literature review focused on approaches to reproduce in the laboratory structural behaviors common in full size, in-service bridge decks that are continuous across supporting members. A methodology successfully used in stationary concentrated load testing of such full-size bridge deck models is introduced, as well past methods and results from rolling wheel load tests. While considerable laboratory testing has been done on full-scale bridge deck models in which the panel edges were clamped to mimic the

boundary conditions of a deck slab continuous across interior supports (e.g., Newhook, 1997; Khanna et al., 2000; Hassan et al., 2002), El-Gamal et al. (2005) was the first to conduct such tests using what would be considered an economical approach. Edge restraint in earlier tests was accomplished by monolithically/compositely casting the deck panels on the attendant supporting steel beams of the testing frame with welded steel studs anchoring the deck to the beams. In the research conducted by El-Gamal and his colleagues (2005), slab edge restraint was more simply provided by clamping the edges of the deck panel to the steel support beams using a double row of bolts, as shown in Figure 3. This approach allows the test slabs to be precast independent of the test frame, both simplifying test preparations and maximizing available time to traffic specimens in the test frame.

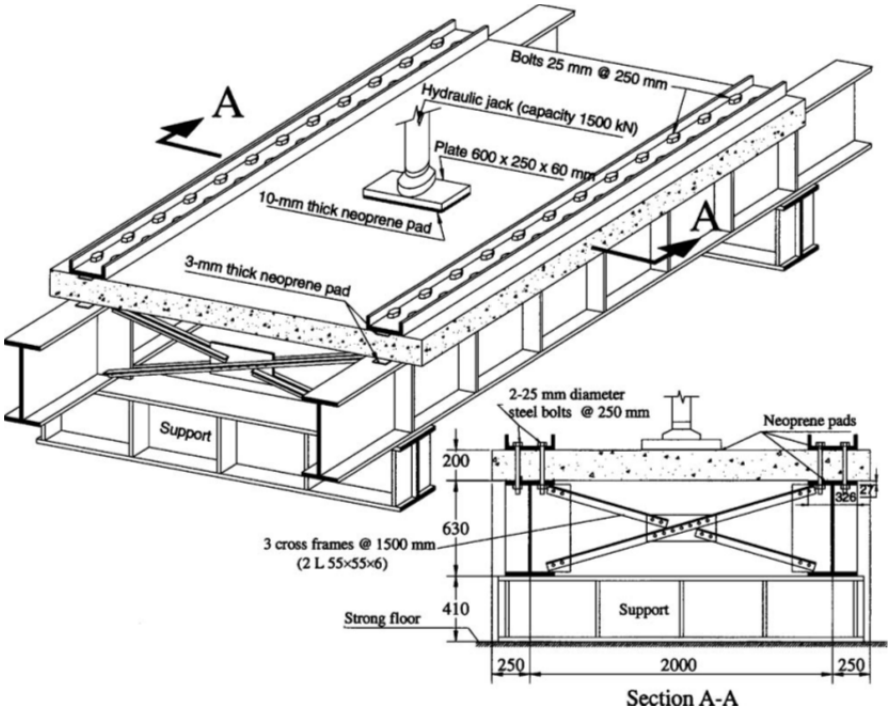

Figure 3: Isometric View and Cross Section of Testing Frame (El-Gamal et al., 2005).

This test setup was developed and used by El-Gamal et al. (2005) to study the behavior of concrete bridge decks reinforced with fiber reinforced polymer (FRP) bars under static loads. Each deck slab was tested to failure using a monotonically applied, concentrated load. El-Ragaby et al. (2007) used the same test setup to investigate the fatigue life of full-scale deck models reinforced with FRP bars. The deck slabs were pre-cracked and then tested under concentrated cyclic loading until failure. In the tests done by both El-Gamal et al. (2005) and El-Ragaby et al. (2007), the test slabs were approximately 10 feet long, 8 feet wide, and 8 inches thick. The width and thickness dimensions were chosen to represent common bridge decks in Canada, while the length dimension was selected to include the area that would be affected by a punching shear failure.

El-Gamal et al. (2007) verified that the deck panel support system used in these various tests provided a restrained edge condition using the results from static tests conducted on four full size test specimens. The observed crack patterns and the measured displacements within the deck slabs indicated that that the expected distribution of flexural stresses from a restrained boundary condition existed within the slabs. These flexural stresses included transverse tensile stresses in the top of the deck near the face of the supports (negative moment condition), and compressive stresses in the top surface at the mid-span (positive moment condition).

Yoshitake et al. (2010) have more recently used a slightly different approach to that of El-Gamal et al. (2007) to generate translational and rotation fixity along the edge of full size laboratory deck slab models. Rather than using a double row of clamping bolts along each edge of the panel, they elected to use a single row of bolts at the extreme outer edge of the panel, complemented by an adjacent roller, to create a tension/compression moment resisting couple along the panel edge, as shown in Figure 4.

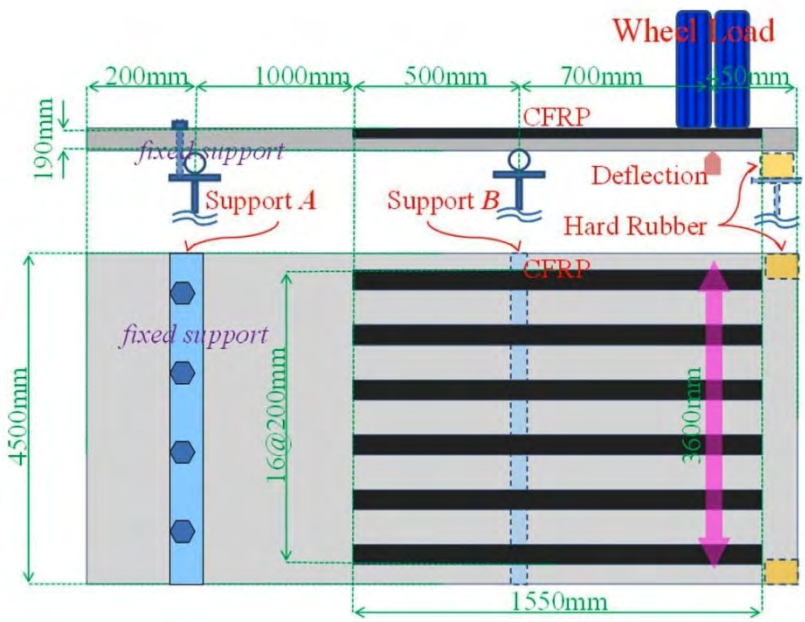

Figure 4: Tension/compression moment resisting connection (from Yoshitake et al., 2010).

Fatigue Life

A considerable amount of research has been done on fatigue testing full-scale bridge deck slabs. Most of this work, however, has been done using stationary pulsating as opposed to rolling loads (e.g., Graddy et al., 2002; Roesler and Barenberg, 1999; Kuang and Morley, 1992). Much of the moving load work that has been done in the laboratory was performed by Perdikaris and Beim (1988), and by a group of investigators in Japan (Yoshitake et al., 2010; Gebreyouhannes et al., 2008; Maekawa et al., 2006; Matsui et al. 2001; Sonoda and Horikawa, 1982). Perdikaris and Beim (1988) performed both pulsating load and rolling wheel load tests on scale models of

reinforced concrete slabs. Their tests revealed that the moving wheel load produced far more damage in the concrete slabs than the fixed pulsating load. This significant reduction in fatigue life using a moving wheel load rather than a pulsating fixed position load was also reported in work done by Gebreyouhannes et al. (2008).

One issue with rolling wheel load testing, which is moot for stationary pulsating load testing, is if uni-directional or bi-directional trafficking can/should be used. Bi-directional trafficking can considerably shorten testing time, recognizing that tests often are conducted for millions of cycles of load, and testing times can be reduced by one-half if bi-directional loading is used. In asphalt pavement research, uni-directional loading is thought to yield different results and to be more indicative of real-world traffic loading than bi-directional trafficking (Byron et al., 2004). When a pavement is loaded in the unidirectional mode, ruts develop substantially faster and rut profiles differ from those loaded in the bidirectional mode (Harvey et al., 2007). This sensitivity to the direction of travel can be attributed to the fact that asphalt concrete exhibits viscoelastic properties. In a viscoelastic material, non-transverse or longitudinal shear stress path patterns are different under unidirectional loading compared to bidirectional loading. This difference in stress path results in different levels of deformation in the material. Specific to tests done on asphalt concrete (AC) overlays, researchers have found that there is a difference in the rate of accumulated permanent deformation between loading in the unidirectional and bidirectional mode.

The situation relative to the effects of unidirectional versus bi-directional loading in Portland cement concrete structures is less clear. In the various moving load fatigue tests of concrete bridge decks identified in this effort (e.g., Yoshitake et al., 2010; Gebreyouhannes et al., 2008; Maekawa et al., 2006; Sonoda and Horikawa, 1982; Perdikaris and Beim, 1988), it was generally unclear from the available test descriptions whether unidirectional or bidirectional loading was used. Direct communication with three investigators who have conducted such tests found that their tests were carried out using bi-directional loading (Bousias, 2009; Perdikaris, 2009; Petrou, 2009). Accelerated pavement tests have been performed on Portland cement concrete (PCC) overlays in both directions of travel (Embacher et al., 2001; Harvey et al., 2007), but no companion unidirectional results are available for comparison. As a non-viscous material, and in light of the apparent lack of concern among researchers in reporting on this item, it was concluded that direction of loading is not of concern in rolling wheel load tests on concrete deck panels.

One outcome of laboratory fatigue tests on concrete deck slabs is fatigue life curves. Again, while considerable information of this type is available for the stationary pulsating load case (e.g., Graddy et al., 2002; Roesler and Barenberg, 1999; Kuang and Morley, 1992), information from moving wheel load tests is more sparse. The limited information that is available on moving/rolling loads consistently indicates that the fatigue life of concrete slabs is significantly reduced (by factors from approximately 1/100 to 1/1000) in the moving versus stationary load

case (e.g., Gebreyouhannes et al., 2008; Perdikaris and Beim, 1988). The fatigue life curves that are available for the rolling load case typically are expressed in terms of cycles to failure at a given level of normalized demand. Normalized demand is variously expressed as the ratio of the applied shear force to the shear capacity, the applied load to the statically applied failure load, or some other measure of cyclic demand to corresponding monotonic capacity. In all cases (and as is typical of many fatigue phenomena), level of demand and associated fatigue life are logarithmically related. One such relationship was developed by Matsui et al. (2001) (as referenced by El-Ragaby et al., 2007) from experiments conducted on full-size bridge deck slabs under a moving wheel load. The tests were conducted on 7-inch thick, simply supported, reinforced concrete slabs and led to the development of the following fatigue life relationship:

$$\log \frac{P}{P_s} = -0.07835 \log(N) + \log(1.52)$$ **Equation 1**

where, P is applied load, P_s is the punching shear capacity of the deck slab, and N is number of cycles to failure. The equation was reported to be valid only for values of N greater than 10,000 cycles. Since the relationship was reported to be valid for different types of concrete bridge deck slabs, El-Ragaby et al. (2007) made an effort to verify this fatigue life model. Using regression analysis and interpretation of their fatigue test results on full-scale slabs reinforced with FRP's and tested with clamped edges, El-Ragaby et al. (2007) developed the following fatigue life equation to compare to the one developed by Matsui et al. (2001):

$$\frac{P}{P_s} = 0.0034(\log N)^2 - 0.11873(\log N) + 1.0752$$ **Equation 2**

As seen in Figure 5, the fatigue life relationships are in good agreement for values of N greater than 10,000 cycles.

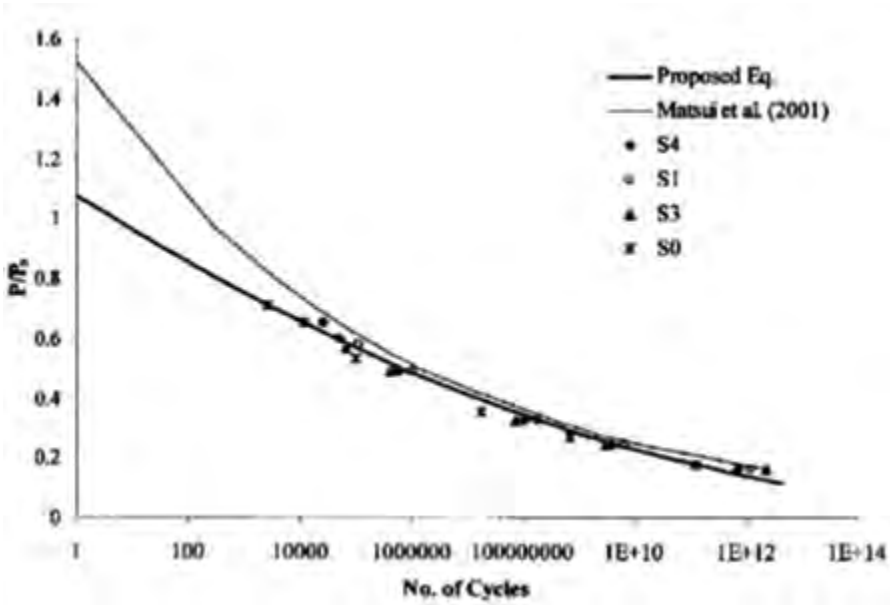

Figure 5: Fatigue life curves for full-scale concrete bridge decks (El-Ragaby et al., 2007).

In both of the fatigue life curves shown in Figure 5, the ultimate static strength of the deck slabs was assumed to be the punching shear capacities of the slabs. This assumption was verified by Graddy et al. (2002) who investigated the punching shear behavior of bridge decks under fatigue loading. Graddy et al. (2002) established that the predominant failure mode for concrete bridge decks tested using static, pulsating, or moving wheel loads is punching shear and not flexure.

On general fatigue behavior, Petrou et al. (1994) observed that if the applied load on the slab was slightly below that of the cracking load, the fatigue life of the slab would be up to 40 times greater than if it were loaded at the cracking load.

Summary

The basic test setup developed by El-Gamal, et al. (2005) for testing full size deck panels in the laboratory was considered a potentially attractive approach to be used in this test program. The approach has been used to test similar deck panels under monotonic and cyclic loads, providing a fixed edge longitudinal restraint condition generally consistent with in situ conditions for deck slabs continuous across internal supports. Further, fatigue life models developed by others from tests on full size deck panels were found to be available that could be applied in some manner to estimate the performance of the deck panels to be tested in this program.

EXPERIMENTAL DESIGN

In light of the complexity of the phenomena being studied, and in consultation with Caltrans, the decision was made to move forward and test full size deck panels in the laboratory under a rolling wheel load. The intent in this decision was to provide the level of control offered in laboratory rather than field testing, coupled with the level of confidence provided by testing full size deck models under realistic structural loads.

The experimental design consisted of the design and construction of the test slabs, their support frame, and an automated loading facility, as well as planning the data collection effort to monitor their response during testing. The final test setup consisted of the following attributes.

- Test slabs – The test slabs were 7 feet wide by 8 feet 5½ inches long by 6½ inches thick, generally representative of the deck section of a box girder bridge face-to-face between girder webs. The slabs were reinforced following typical Caltrans practices and cast using a concrete mixture based on that used in typical Caltrans bridge construction.
- Test frame – The test slabs were mounted in a test frame that was designed and constructed to provide fixed/clamped boundary conditions along the longitudinal edges of the slabs (i.e., parallel to the direction of trafficking) and simply supported boundary conditions across their transverse edges (i.e., perpendicular to the direction of trafficking). The frame accommodated four slabs/panels trafficked sequentially by the automated loading device.
- Automated bridge deck tester – WTI's automated bridge deck tester (ABDT), designed and fabricated by Applied Research Associates, Inc. (Randolf, VT), is capable of applying up to a 30-kip load on a dual tire assembly along a testbed 35 feet in length. This device is capable of uni- and bi-directional trafficking. This device can apply about 13,800 load cycles per day travelling at 8.8 ft/second and operating in the bi-directional mode. In this test program the ABDT was set to apply a 20-kip wheel load in the bi-directional mode at the fastest speed of 8.8 ft/sec.
- Performance monitoring – In consultation with Caltrans, the decision was made to monitor a) applied wheel load and b) test slab deflections at the midspan and quarter point along the transverse bisector of each slab. These measurements were used to determine changes in slab stiffness with cyclic load application. Additionally, slab condition (i.e., cracking, spalling, etc.) was visually documented at various intervals throughout testing. Finally, chloride and moisture permeability tests were conducted at the end of testing to potentially obtain a more direct indication of compromised deck condition based on cracking.

Each of these activities is described in more detail below. Note that after various test parameters were established (i.e., test slab configuration, magnitude of applied load, etc.), the expected fatigue life of the slabs was estimated using the fatigue life curves introduced in the previous section of this report. These predictions were performed in an effort to ensure that the test slabs would experience an acceptable degree of degradation in a reasonable amount of time (say, several months of cyclic testing versus several years), as is also further discussed below.

Design of the Bridge Deck Test Panels

The deck test panels were designed to represent a section of a deck in a typical box girder bridge used by Caltrans. After considering a variety of specimen configurations, including a single flat panel, flat panels with edge beams (to introduce the effects of the box beam webs), and two flat panels with edge and center beams (again, to introduce the effects of the box beam webs), the decision was made to move forward with flat panel specimens, as shown in Figure 6. These specimens are 8 feet 5½ inches long, 7 feet wide, and 6½ inches thick and are reinforced with two mats of reinforcing steel. Test panels built to this configuration were expected to generally reproduce in the laboratory pertinent stress conditions experienced in the transverse direction by a section of a full size, in-service bridge under vehicle loads. These stresses are a function of the slab materials, cross section, and plan geometry; as well as their support and loading conditions.

Any material and cross-section geometry effects were simply accounted for by using materials and a cross-section employed by Caltrans in actual box girder construction. The slabs were 6.5 inches thick, which is the thinnest deck used by Caltrans in box girder construction. The reinforcing steel in the test panels was sized and arranged in accordance with standard design details provided by Caltrans for their box girder bridges (deck slab reinforcement details provided in Appendix A). The reinforcing consisted of two mats of Grade 60 steel using #4 and #5 bars in straight, bent, and truss bar configurations (see Figure 6). With respect to capturing responses related to the specific layout of the reinforcing steel in the transverse direction, this specimen configuration specifically offered three replications in the pattern of the positive and negative moment steel, centered across the longitudinal length of the specimen. This feature of the test specimen configuration is illustrated in Figure 7. Effectively, three of these replications are within the central region of the models in which the stress conditions are predicted to be similar to those in a full size bridge (as discussed further below). Accurately representing the layout of the reinforcing steel in the deck panels is relatively important, because under moving loads, cracking tends to follow the reinforcing grid (Perdikaris et al., 1989). The concrete used in panel construction was based on a mixture design provided by Caltrans for a 4,000 psi concrete used on an actual bridge project (Hanson Mix, July 2007, Appendix B).

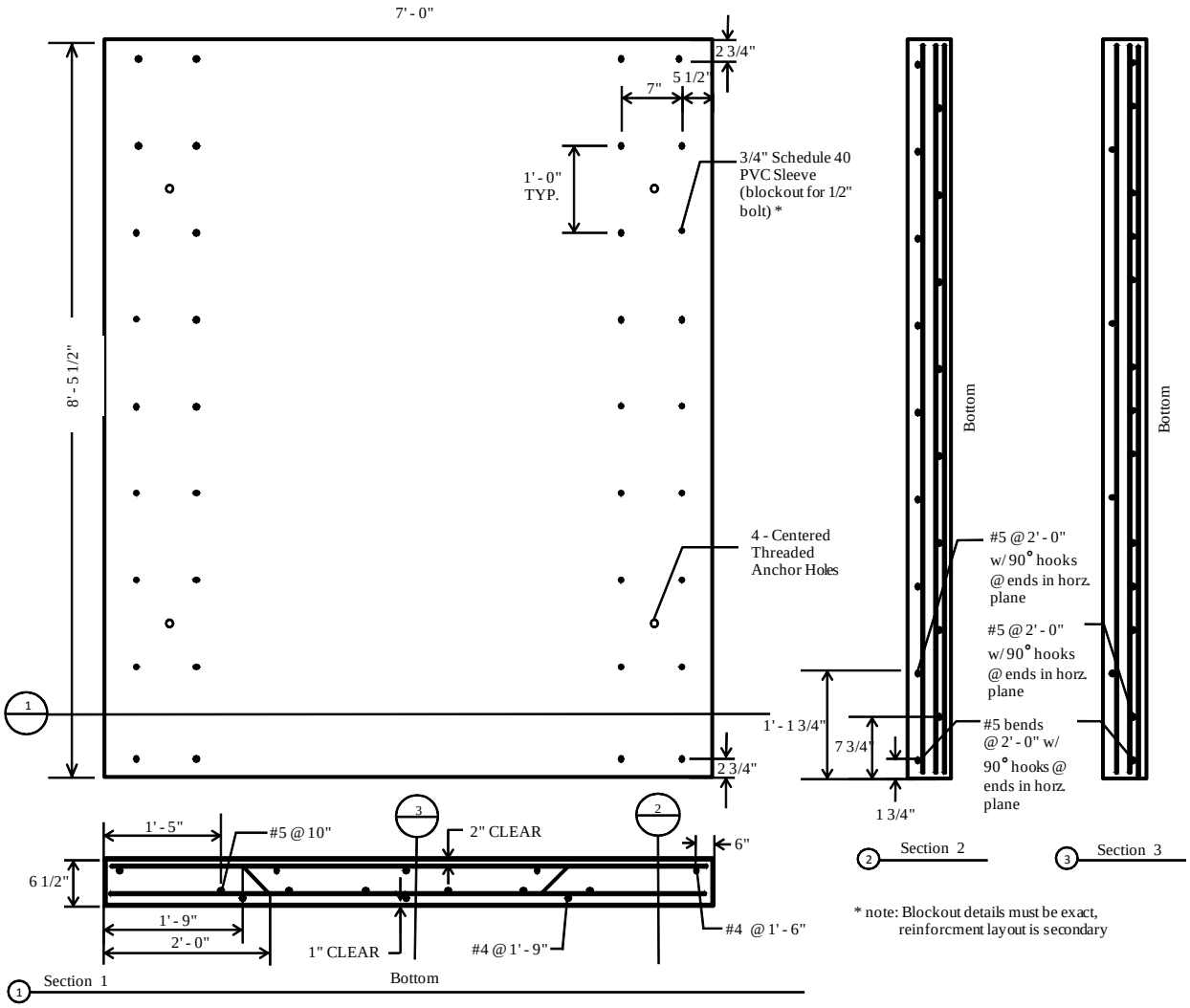

Figure 6: Dimensions and reinforcement details of test specimens.

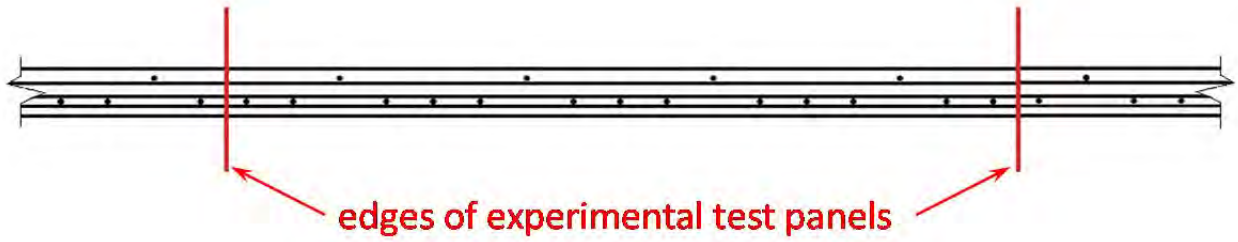

Figure 7: Transverse steel layout in the bridge deck (Section 3 from Figure 6).

The plan geometry and support conditions for the test panels were specifically determined based on matching the local transverse flexural stresses in the panel with those experienced in an actual bridge deck. Note that these local stress excursions in the transverse direction under each passing wheel load were judged to be more critical in the fatigue performance of the deck than the global longitudinal stress excursions generated by transmitting vehicle loads longitudinally to the bridge supports. Simply stated, these local transverse stresses consist of tensile stresses in the top of the deck over the webs of the box girders (negative moment) and compressive stresses in the top surface of the deck between webs (positive moment), as shown in Figure 8.

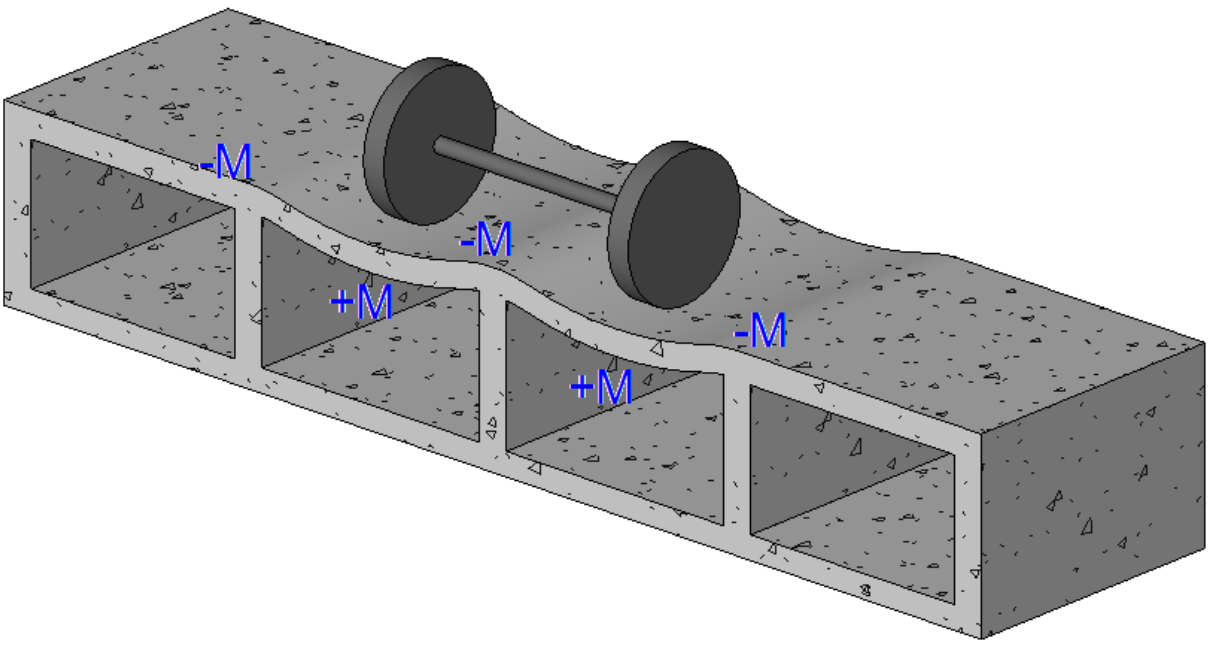

Figure 8: Idealized moment behavior of the deck in the transverse direction.

Having established the deck thickness and reinforcing configuration, and assuming that the load could be applied along the longitudinal centerline of the panel, the distribution of the transverse flexural stresses in the test slabs was affected by the plan dimensions of the panels and their edge support conditions. Relative to developing a general target distribution for these stresses, an analytical model of a full bridge (four cells wide, with each cell nominally four feet deep and six feet wide) with a span of 80 feet was created in the finite element package, Visual Analysis (see Figure 9). Using a linear elastic analysis, this model was used to determine the distribution of flexural stresses transversely across the deck in the interior of the longitudinal span under a 15 kip patch load centered on one of the cells. This stress distribution was compared with that produced in an analytical model of a flat panel of the same thickness with clamped edge conditions, with the 15 kip load applied at the longitudinal centerline of the panel. The stress distributions in the two analytical models were similar in shape and magnitude, as shown in Figure 10.

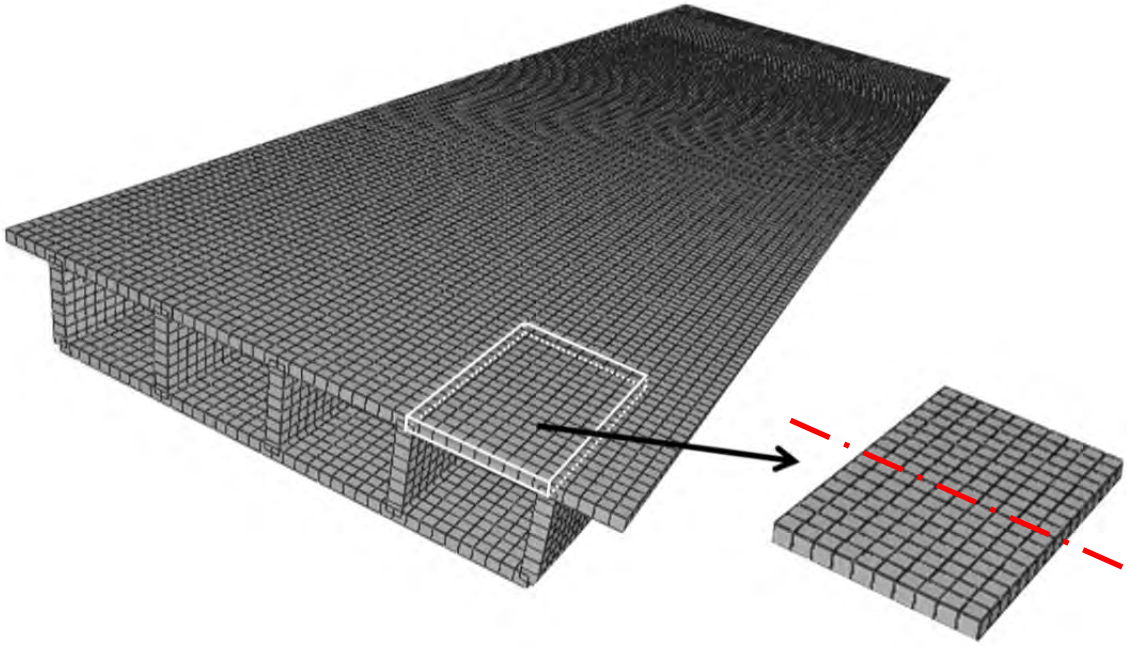

Figure 9: Three-dimensional geometry and VA FEA mesh of the full-scale deck model.

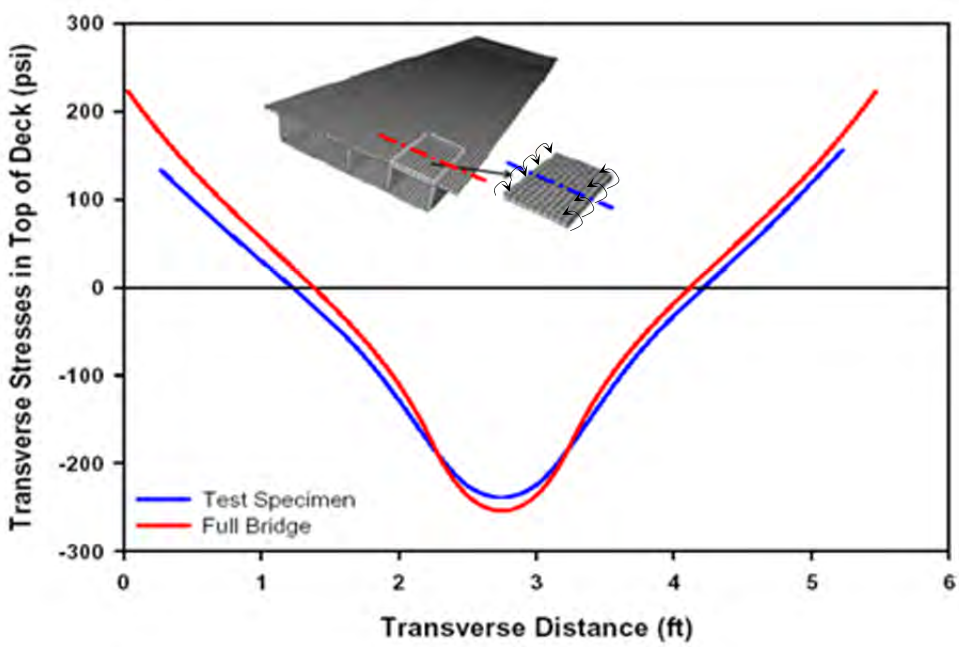

Figure 10: Comparison of transverse stresses in the test specimen and full bridge models.

With respect to magnitude, the peak positive flexural stresses are about 7 percent higher in the model of the test specimen compared to those at an equivalent location in the model of the full bridge. Conversely, the peak negative moment stresses are about 10 to 20 percent lower in the test specimen model compared to the full bridge model.

Finite-element modeling was also used to determine whether the leading and trailing transverse edges of the deck panels should be supported during testing. In the absence of support at these locations, as the wheel starts onto the specimen large deflections and relatively high stresses would be induced at these "free" edges. These relatively large stresses could have initiated cracks that would then propagate to the interior of the specimens, possibly leading to premature failures not representative of actual bridge deck behavior. Supporting these edges eliminated this issue, but did result in significantly lower stresses in these edge zones when compared to an actual bridge. The transverse stress in the deck under the wheel at various longitudinal positions of the load axle for the supported case is shown in Figure 11. Referring to Figure 11, boundary effects from the lead and trailing transverse edges of the models are evident, with approximately 3.5 feet of length in the center of the panel experiencing relatively constant stress response (longitudinal positions 2.5 to 6.0 feet). In the remaining edge affected zones of the panel, the stresses quickly diminish to zero at the panel edge. As a stress deviation in edge affected zones of the panels was inevitable, it seemed more desirable for the stress to be lower in these regions than in the actual case (supported condition) rather than higher than in the actual case (unsupported condition), so that premature damage from this area would not propagate to the interior section. Therefore, the decision was made to simply support the transverse edges of the panels.

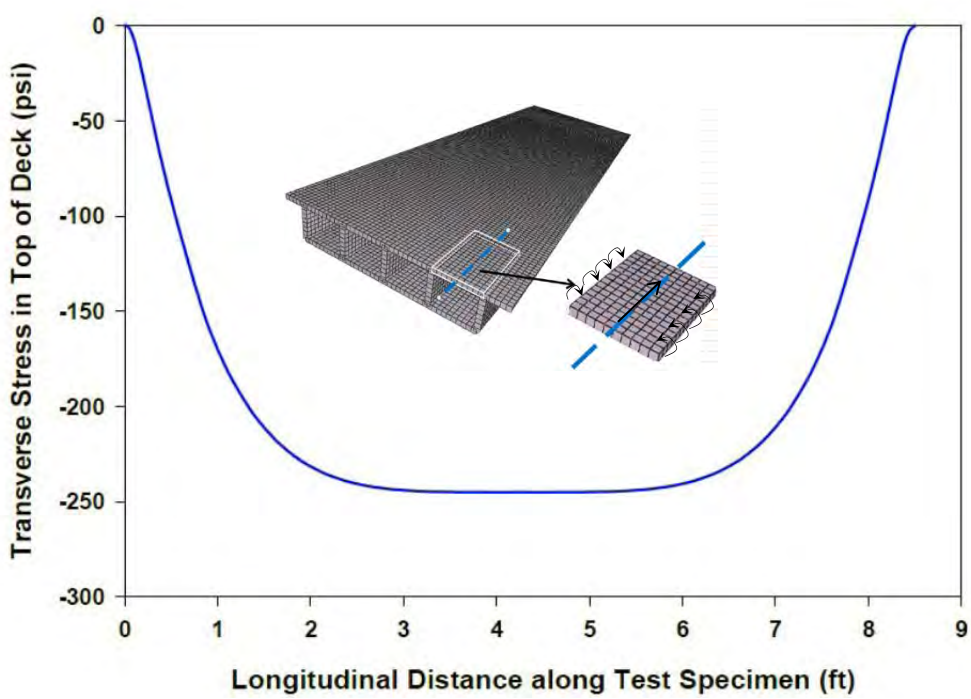

Figure 11: Transverse stresses in the top of the deck under the rolling wheel load as it moves along the specimen.

Construction of the Concrete Bridge Deck Test Panels

Eight test panels were cast for this project in two separate pours of four panels each. The first set of four panels was cast on November 16, 2010 and the second set of four panels was cast on March 29, 2011. Typical formwork and rebar cage is shown in Figure 12. A double row of blockouts were placed along both longitudinal edges of each panel to accommodate the bolts to hold the test slabs to the reaction frame during testing. Tensile tests were conducted on the reinforcement to characterize their strength properties, namely, yield strength and ultimate strength. Three #4 and three #5 bars were tested. Average yield and ultimate strengths for the #4 bars were 65,200 psi and 110,100 psi, respectively, and average yield and ultimate strengths for the #5 bars were 63,200 psi and 104,100 psi, respectively. These values are all within the appropriate ASTM specifications for Grade 60 reinforcing steel.

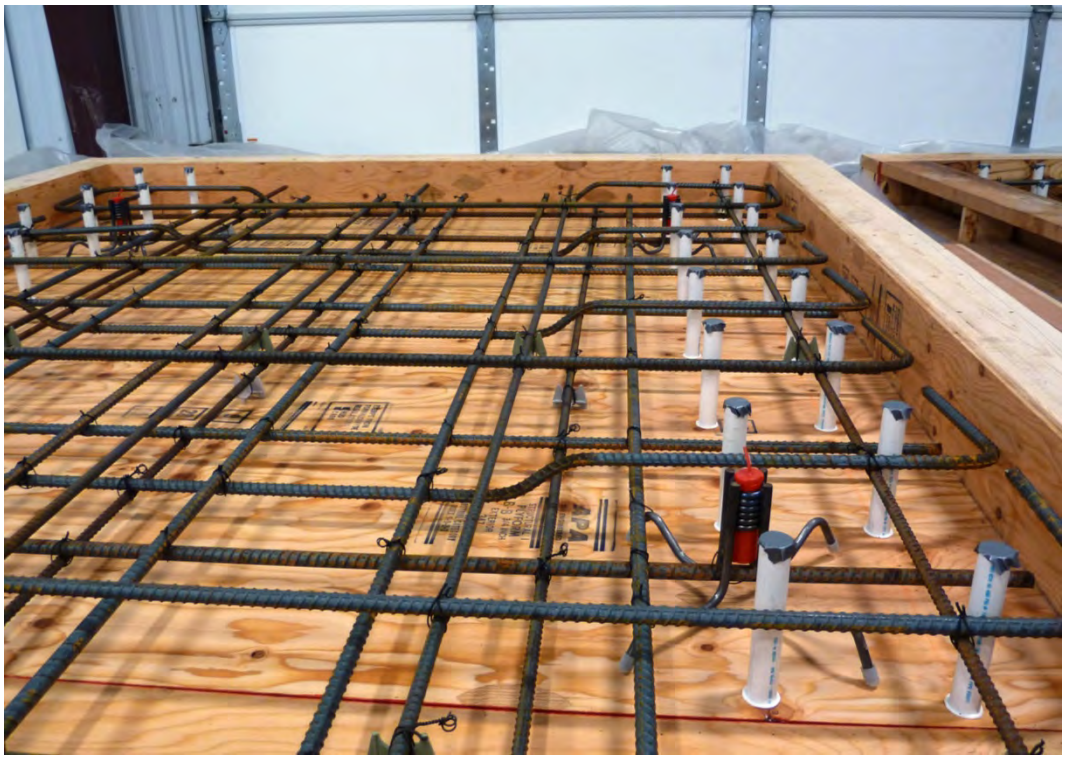

Figure 12: Close-up of reinforcement layout.

The concrete mixes used for the test panels were based on a mix design provided by Caltrans from a typical bridge project ("Hanson" mix, Appendix B). The mix designs are presented in Table 1, along with the results of slump and air entrainment tests conducted at the time of casting. The minimum required compressive strength of the concrete was 4,000 psi. The surface of the concrete was trowel-finished smooth, and a pigmented curing compound was applied (Figure 13). The test slabs were cured in accordance with the Caltrans' specifications for curing bridge deck slabs, which involves applying a pigmented curing compound immediately after

finishing the slab and then wet-curing the slab for seven days with water saturated burlap (Caltrans, 1991).

Fifteen 4 x 8 inch compression test cylinders and 12 rupture beams were cast with each batch of concrete. Three specimens from each group were moist cured for 28 days and then tested to confirm the basic capacity of the concrete. The 28-day compressive strengths of the concrete for the first and second set of bridge deck panels were 5,120 psi and 4,540 psi, respectively (minor adjustments were made to the mix design to reduce the strength between the first and second pour dates). The additional compression test cylinders and rupture beams were cured with each deck specimen and were tested during the fatigue test program (i.e., at the initiation and conclusion of testing.

Table 1: Mix Designs and Wet Mix Properties of Test Panel Concrete Pours

	Design Quantities (per yd^3)	
Ingredient	**Panel Set 1 (Nov. 16, 2010)**	**Panel Set 2 (Mar. 29, 2011)**
Course aggregate (lb.)	1672	1672
Concrete sand (lb.)	1366	1405
Type I/II cement (lb.)	423	424
Class F fly ash (lb.)	141	140
Air admixture (oz.)	2.1	1.5
Water reducer admixture (oz.)	28.2	14
Water (gal.)	30	33
Mix Characteristics		
Water/cement ratio	0.444	0.490
Slump (in.)	3.5	3.5
Entrained air (%)	4.9	2.1
28-day strength (psi)	5120	4540

Figure 13: Finished slabs with concrete curing compound on surface.

Design and Construction of Reaction Frame

For testing, the deck panels were anchored in a reaction frame positioned under the rolling wheel loading device, as shown in Figure 14. To generate the expected stresses in the panels, this reaction frame was designed to provide the support conditions assumed in the analysis described above, i.e., full restraint (no rotation or vertical translation) along the longitudinal edges of the panels, and simple support across the transverse panel edges. Another very important practical design consideration for the frame was that the bottom side of the panels had to be reasonably accessible for the purposes of monitoring crack development and measuring displacements.

The basic configuration of the reaction frame was patterned after the test setup developed by El-Gamal et al. (2005), as previously shown in Figure 3. The frame designed for this effort is shown in Figure 15. The frame was designed to simultaneously test four deck panels and consisted of two continuous support beams along the longitudinal edges of the panels with short cross beams under the transverse edges that are shared between adjacent panels (Figure 16). Fixed support along the longitudinal panel edges was provided using a double row of ½ inch diameter bolts spaced at 12 inches on center by clamping a top channel to the support beams below (Figure 17). All bolts were tightened to the same level of torque (90 ft-lb), to provide uniform edge restraint across all models. Low Density Polyethylene (LDPE) plastic strips (1/8-inch thick) were used at all interfaces between the supporting steel members and the deck panels (Figure 18). The flanges of the W 24 x 104 support beams were further stiffened using ¾ inch

web plate stiffeners spaced at 10 inches on center along their length. The leading and trailing edges of each deck panel rested on a W 24 x 104 cross member.

Figure 14: Automated bridge deck tester.

W-sections were selected for the main longitudinal support members of the test frame because they offered simplicity in implementing the bolted panel restraint system. These support beams were stiffened to increase their resistance to the torsional loads from the panels. The depth of the wide flange beams (24 inches) was mainly driven by the physical height required for access to the underside of the test specimens. Access holes (20 inches by 20 inches) were cut into the webs to provide this access, and to facilitate cabling and instrumentation. A flange width of approximately 12 inches was selected to allow for practical installation of the clamping bolts straddling the beam web. Engineering drawings and specifications of the support frame are provided in Appendix C.

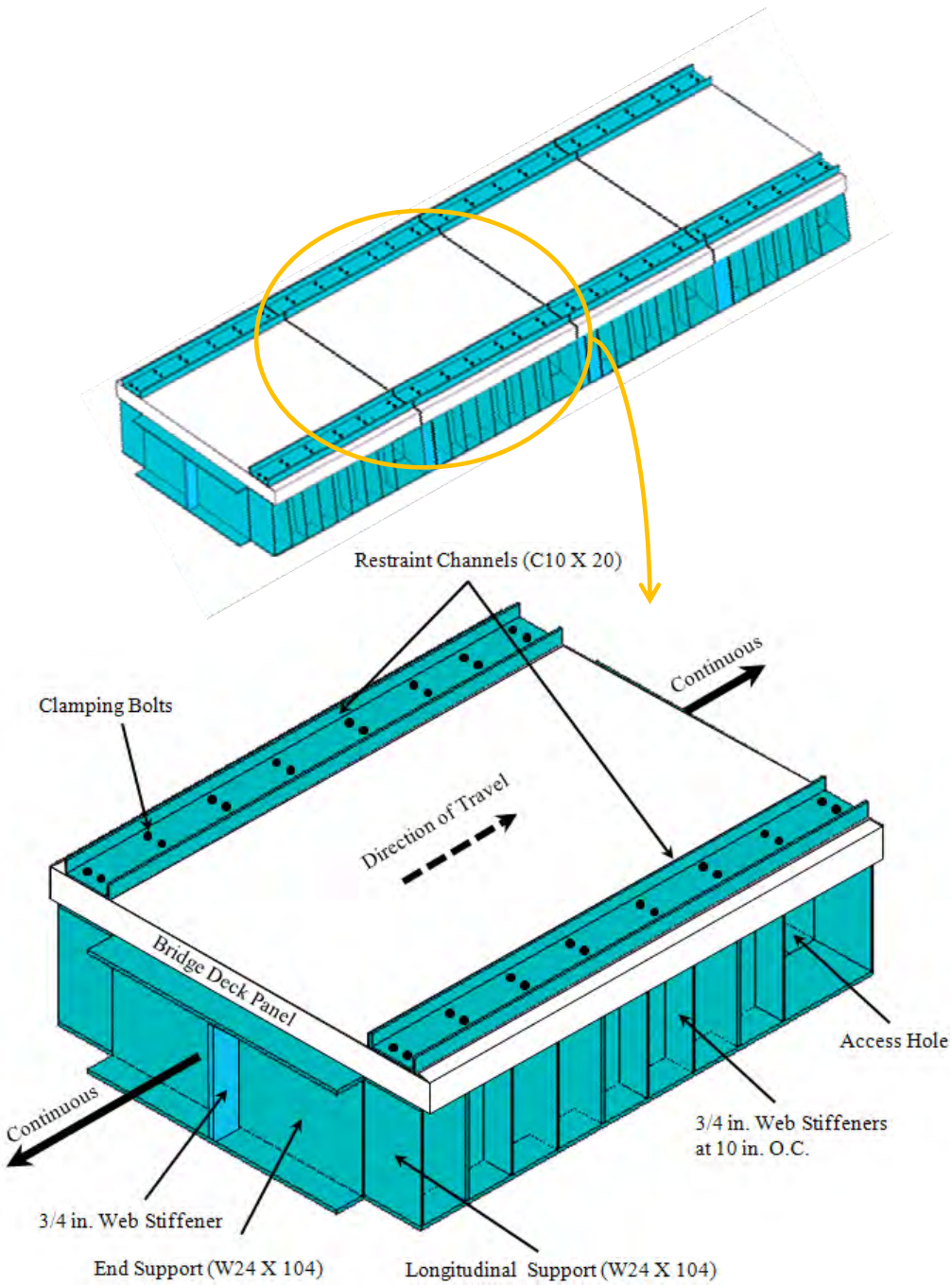

Figure 15: Three-dimensional rendering of support frame.

Figure 16: Test slabs mounted on reaction frame.

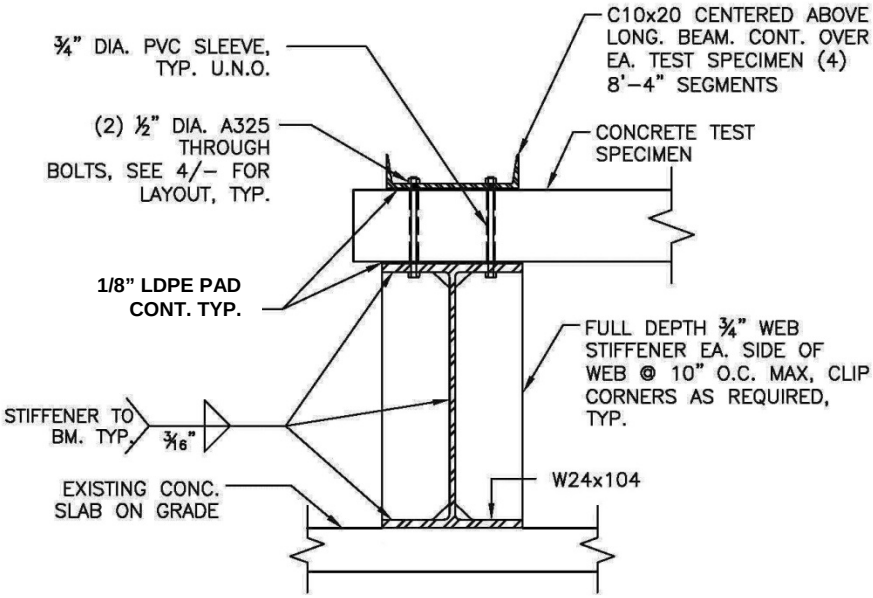

Figure 17: Clamping detail for test specimen.

Figure 18: Frame setup showing LDPE pads for single panel.

The location and size of the access hole along each section of the longitudinal support members was similarly selected in conjunction with finite element analyses such that it did not significantly affect the stiffness of the member while providing the necessary access to the underside of the test specimens.

In designing the reaction frame, multiple finite element analyses were done of the complete test setup (i.e., the reaction frame, clamping system and test panels) to confirm that the stresses generated in the test panels would be consistent with their required fixed edge support condition in the transverse direction (Gilbert, 2011). Linear elastic ANSYS analyses were done using an applied patch load of 15 kips. The initial frame design, for example, did not include web stiffeners for the longitudinal support beams. Subsequent finite element analyses revealed that these beams twisted when load was applied to the test panel, reducing the negative moment at the clamped edges of the panel and increasing the positive moment at the center of the panel. To address this problem, various web stiffener arrangements were analytically investigated iterating on stiffener size and spacing until the observed transverse stresses in the test panel were close in magnitude to those analytically predicted for a panel with perfectly fixed longitudinal edges (see Figure 19).

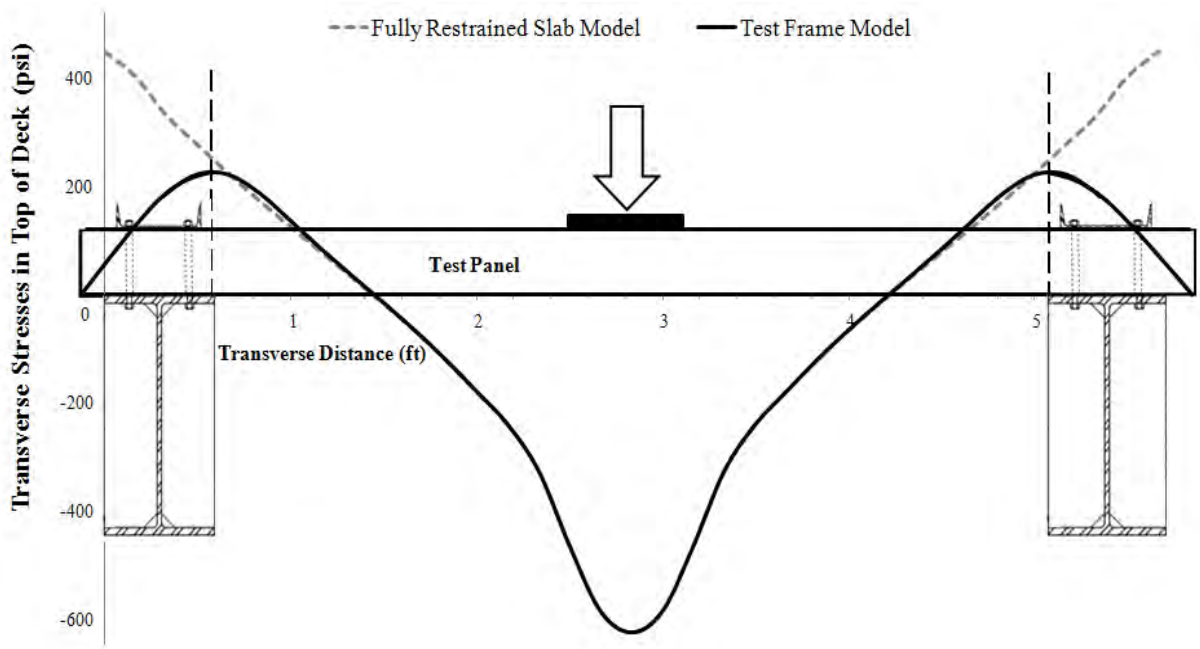

Figure 19: Comparison of transverse stresses in the top of the deck for the fully-restrained slab model and rest frame model.

A further verification of the performance of the reaction frame was conducted by physically loading to failure a single test panel mounted in one of the interior bays of the frame (Figure 20 and Figure 21). The specific specimen used in this test had the same geometry and reinforcing arrangement as the already described fatigue test specimens, with a 28-day concrete strength of 7,618 psi (8,040 psi on the day it was tested). The panel was clamped in the reaction frame using the procedure outlined above. Load was applied using a 2.5-inch thick A-36 steel loading plate with a contact area of 12 x 20 inches (representing a dual truck tire assembly).

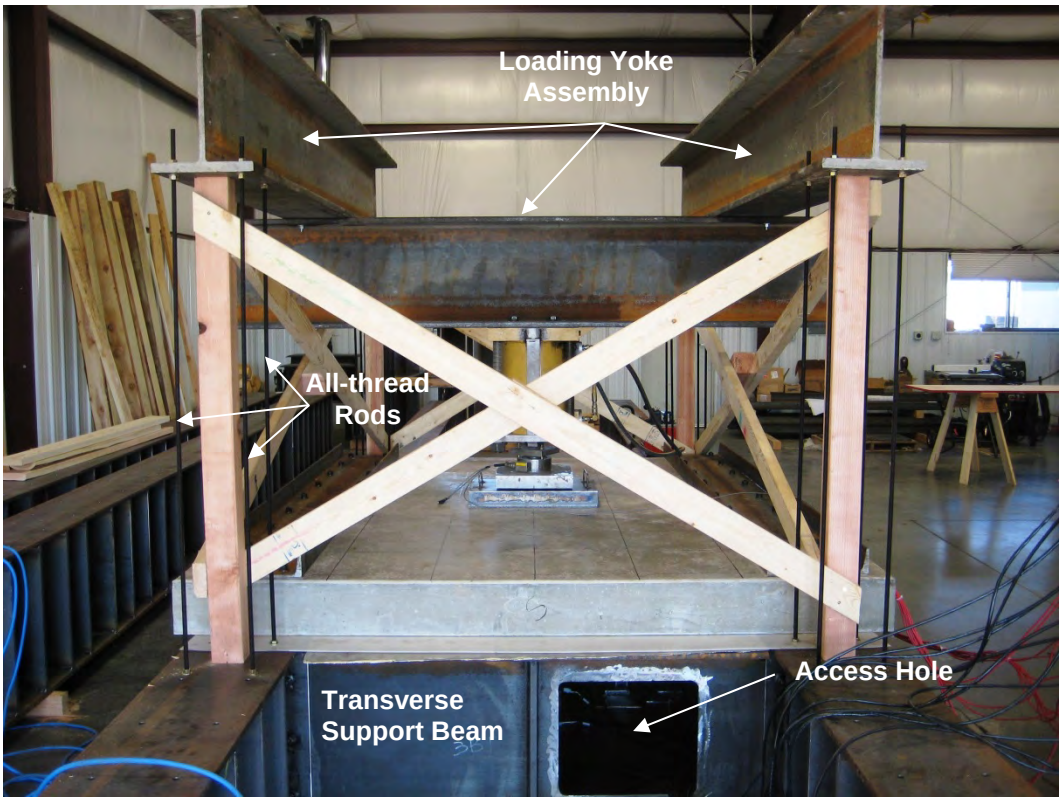

Figure 20: End view of static load test setup.

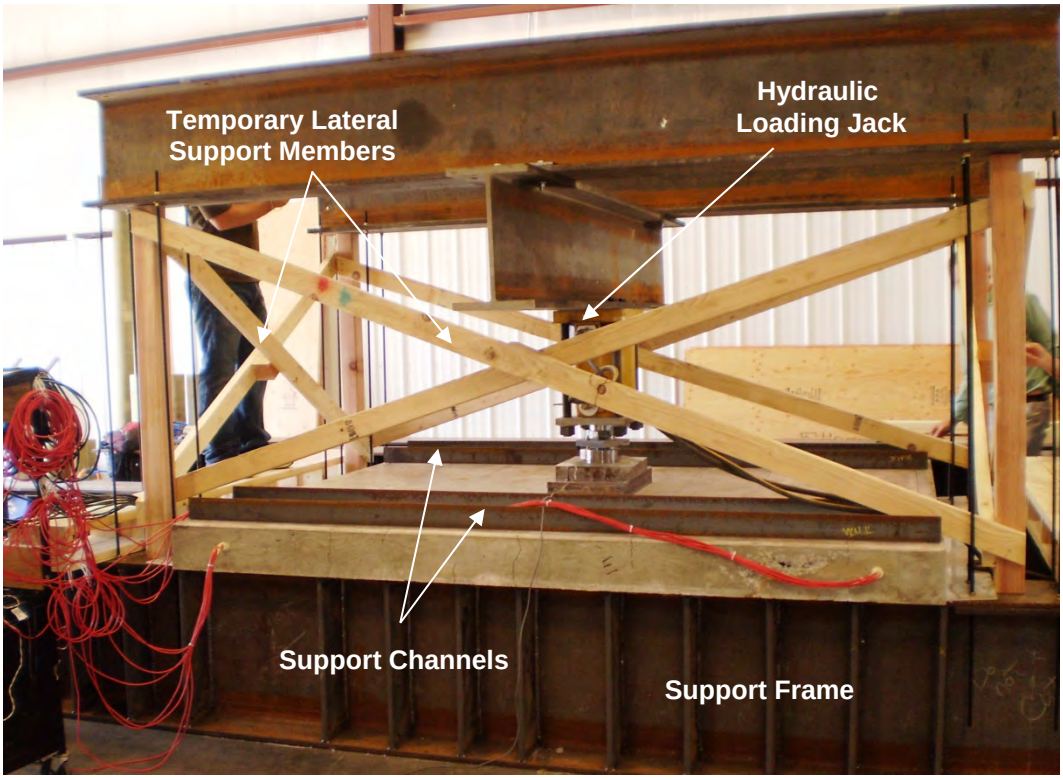

Figure 21: Side view of static load test setup.

Internal strain measurements made in the transverse direction of the panel during this test confirmed that the reaction frame offered a high degree of rotational fixity along the longitudinal edges of the slab (Gilbert, 2011). The strains measured near the clamped edges were tensile in the top of the deck and compressive in the bottom (negative moment) for loads up to 75 kips. Furthermore, the measured strains closely matched those obtained in an FE analysis of the slab in which full rotation and translation restraint was assumed along the longitudinal edges. A tensile strain of 30 microstrain and a compressive strain of 37 microstrain were recorded in the static load test, while the ANSYS model with ideally clamped edges experienced a tensile strain of 35 microstrain, and a compressive strain of 46 micro-strain. These tensile and compressive strains were higher than the experimental results by only 17 and 23 percent, respectively. Finally, the observed crack patterns in the test slab were also consistent with the expected distribution of stresses, that is, all of the top surface cracks initiated in the expected tension zone along the face of the supports, and bottom surface cracks were concentrated in the expected tension zone directly under the applied load.

Fatigue Life Predictions

Another important task prior to initiating the trafficking of the test panels was to estimate the number of traffic cycles that would be needed to produce the degree of deck deterioration needed in this study. This degree of deterioration was defined as the maximum level of distress at which an HMWM treatment would still be used as a rehabilitation treatment. Thus, for the test panel configuration defined above, an effort was made to predict the magnitude and number of load cycles that would be required to reach this deteriorated condition. These predictions were made generally following the form of fatigue life prediction equation previously introduced by Matsui et al. (2001), in which the number of load cycles to failure was expressed as a function of the applied load normalized by the ultimate capacity of the deck slab (Equation 1). This equation was first evaluated with failure being defined as a complete loss of structural load carrying capacity. The failure capacity of a typical slab was established in a previously described test by Gilbert (2011) to be 192 kips (with the failure mechanism being punching shear). This value was adjusted for relative concrete strength (the concrete in the Gilbert slab had an unconfined compression strength of 8,040 psi, compared to a target concrete strength in these test panels of 4,000 psi) and was then used for the normalizing value, P_s, in Equation 1. The resulting fatigue life curve is presented in Figure 22 (upper curve in this figure). Notably, across a range of possibly reasonable magnitudes for the rolling wheel load of 15 to 25 kips, the predicted fatigue life was effectively infinite.

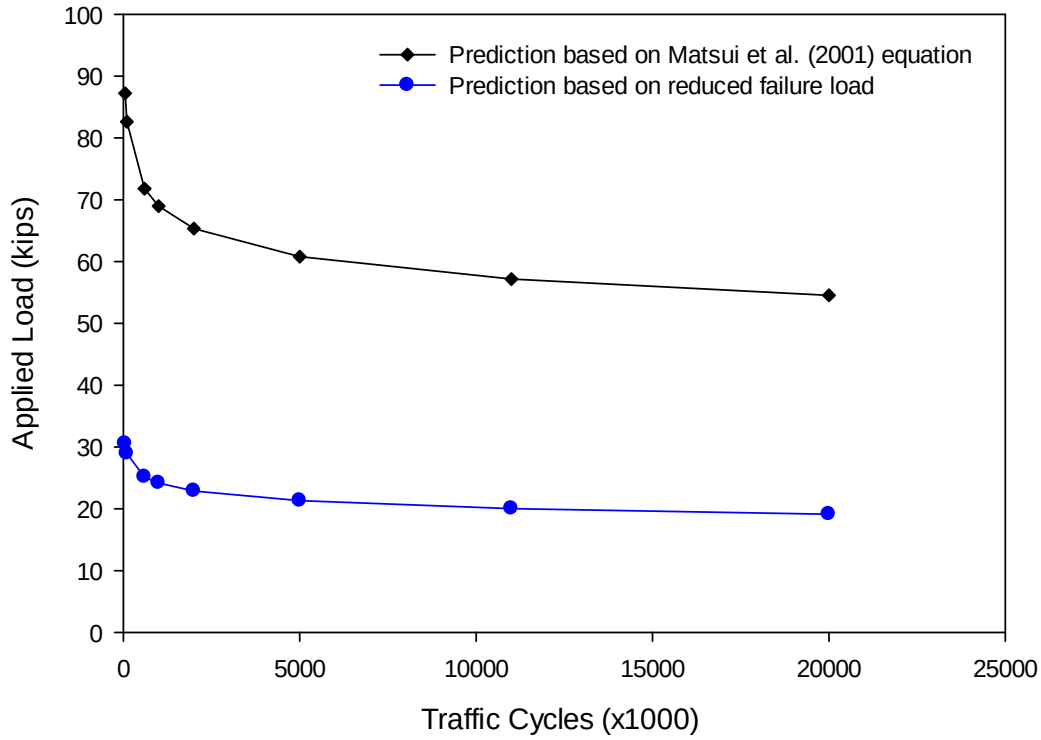

Figure 22: Predicted fatigue life of test panels as a function of applied load.

The Matsui et al. (2001) fatigue prediction equation was subsequently re-evaluated to estimate the number of load cycles required to deteriorate a test panel generally to the level at which HMWM treatment would be considered. This modification was simply introduced by adjusting the "failure load", P_s, used in the ratio, P/P_s to a value consistent with this intermediate distress state rather than that for total structural failure. However, the deteriorated condition at which a deck is optimally rehabilitated using HMWM is not objectively known (hence, the need for this study). Further, how this deteriorated condition correlated with an appropriate value of P_s to be used in this fatigue life prediction equation was also uncertain. The Michigan DOT published a guide on deck rehabilitation (Nowak et al., 2000) which included a matrix relating observed deck condition to candidate rehabilitation strategy. This guide appears to be based on Michigan's experience with deck maintenance over the years, and the guide comments that typically treatments should be applied when the decks are still in relatively good condition to maximize their effectiveness. Relative to rehabilitation versus replacement, the guide suggests that if more than 30 percent of the top and bottom surface of the deck has or had spalling problems and the National Bridge Inventory rating is as low as 2 to 4, replacement should be considered (an asphalt overlay under this situation is only expected to provide one to three years of additional service life). Work done for the Utah Department of Transportation (UDOT) on deck inspection and maintenance (Linford, 2006; Tuttle, 2005) states that many departments of transportation recommend maintenance action when crack widths exceed 0.0625 inches with moderate crack density or when cracking is accompanied by efflorescence. Huang et al. (2004) indicated that

the maximum tolerable condition index at which bridge deck treatments are still effective corresponds to when a deck reaches 35 percent of its design life. Caltrans considers the use of HMWM when deck cracking on the bottom surface has formed a regular network in orthogonal directions, deck cracking on the top surface is predominantly transverse and spacing is about two times the spacing of the top mat of reinforcement, and crack widths are between 0.0625 in. and 0.125 in wide. Polyester concrete overlays are recommended for higher levels of deck deterioration characterized by wider cracks and/or loss of load distribution in the longitudinal direction of the bridge deck from through-cracks that are fully worn and have lost all shear interlock at the crack face (Caltrans, 2007).

Based on these various observations and recommendations, and recognizing that only a very approximate estimate of the expected load cycles required to reach the deck distress of interest in this study might be obtained (say, within an order of magnitude), P_s was set equal to 35 percent of the estimated monotonic failure load for the test panels – 47 kips. The associated relationship between applied load and cycles to "failure" generated using the Matsui et al. (2001) fatigue life equation (Equation 1), based on a lower value of P_s, is presented in Figure 22 (lower curve in this figure). Note that this relationship generally appeared reasonable, in that based on Gilbert's test results (2011), first cracking of the slab was expected at a load of 21 kips. Referring to Figure 22, at applied cycling load levels above this cracking load, the number of cycles required to generate the desired deterioration condition steadily and noticeably decreased, while at cycling load levels below this cracking point, the number of cycles required to generate the desired deterioration condition practically became infinite. Referring again to Figure 22, across the range of wheel loads of 20 to 25 kips, 11,000,000 to 600,000 cycles of applied load would be necessary to bring the test panel to the general distress level of interest. If as described below the ABDT ran continuously at 13,800 cycles per day, 800 and 43 days, respectively would be required to bring the panels to this point under the 20 and 25 kip applied loads. Relative to minimizing test time, the 25-kip load was desirable. Relative to a) maintaining a closer connection to actual expected stress magnitudes in in-service bridge decks, b) staying within allowable load levels of standard tires, and c) reducing wear on the ABDT, the 20-kip load was desirable, and it was selected for this project.

Automated Bridge Deck Tester

The automated bridge deck tester (ABDT), designed and fabricated by Applied Research Associates, Inc. (Randolf, VT), was used to distress the test panels (Figure 14). This device is able to apply a rolling wheel load across a testbed 35 feet in length at loads up to 30 kips. The load is applied through a single dual-wheel assembly equipped with 315/80 R 22.5 HSU2 tires rated for high load carrying capacity (load rating L = 9,090 lb per tire for duals). Application of the load is accomplished through two 12-inch pneumatic cylinders which react against a stiff frame. The wheel carriage assembly was pulled back and forth across the test panels using a

cable and winch assembly (Figure 23). The ABDT has the capability of applying load either unidirectionally or bidirectionally, with the loading in this project being applied bidirectionally. The total length of the ABDT is about 55 feet to accommodate runoff tables on both ends of the test area. The runoff tables provide sufficient acceleration and deceleration distance for the wheel to reverse direction and resume trafficking the test panels at a constant speed. The wheel carriage assembly traveled at 8.8 ft/sec in these tests, the maximum speed of the device. At this speed the ABDT was able to make 575 passes per hour, 13,800 passes per day (total counting both directions). The height of the ABDT (and consequently the elevation of the applied load) is adjustable to accommodate a variety of sample heights. Concrete ballast blocks were cast to provide additional reaction for higher applied loads (greater than about 15 kips). The ballast blocks were positioned on top of the test frame at both ends.

Figure 23: Drive cable and carriage assembly.

Response Monitoring

Applied wheel load and center-point, quarter-point and edge slab deflections were made throughout testing. These measurements were used to determine changes in slab stiffness as cycling proceeded, where stiffness was simply calculated as applied load divided by deformation. Additionally, slab condition (i.e., cracking, spalling, etc.) was visually documented at various intervals throughout testing. Finally, chloride and moisture permeability tests were conducted at the end of trafficking to obtain a more direct indication of compromised deck condition based on cracking.

Instrumentation and Data Acquisition

Displacement and load were the primary measurements made using instrumentation. Vertical displacement measurements were made in three locations on the underside of each test panel. Linearly variable displacement transformers (LVDTs) were placed along the transverse centerline of the test panel at the center point, quarter point and near the edge of the reaction frame (as shown in Figure 24 and Figure 25) to make these measurements. Three additional LVDTs were used to monitor movement of the reaction frame with respect to the concrete floor, and another LVDT was simply placed on the floor, not attached to anything, to monitor potential creep or drift in the gauges. The LVDTs were calibrated to have a total range of 0.25 inches and

an accuracy of ±0.0001 inches. Deformation was calculated as the difference between either center or quarter point deflection and the edge deflection. Load was measured indirectly using a pressure gauge in line with the two pneumatic cylinders that applied the downward force through the load carriage. The number of passes was collected using an optical sensor. All of the information from these sensors was sent to a CR5000 data logger (Campbell Scientific, Inc. (Logan, UT)). The data logger was programmed to scan the LVDTs and pressure cell at 200 Hz and record a single maximum and minimum value for each sensor over a five minute period, resulting in two stored data points for each sensor every five minutes.

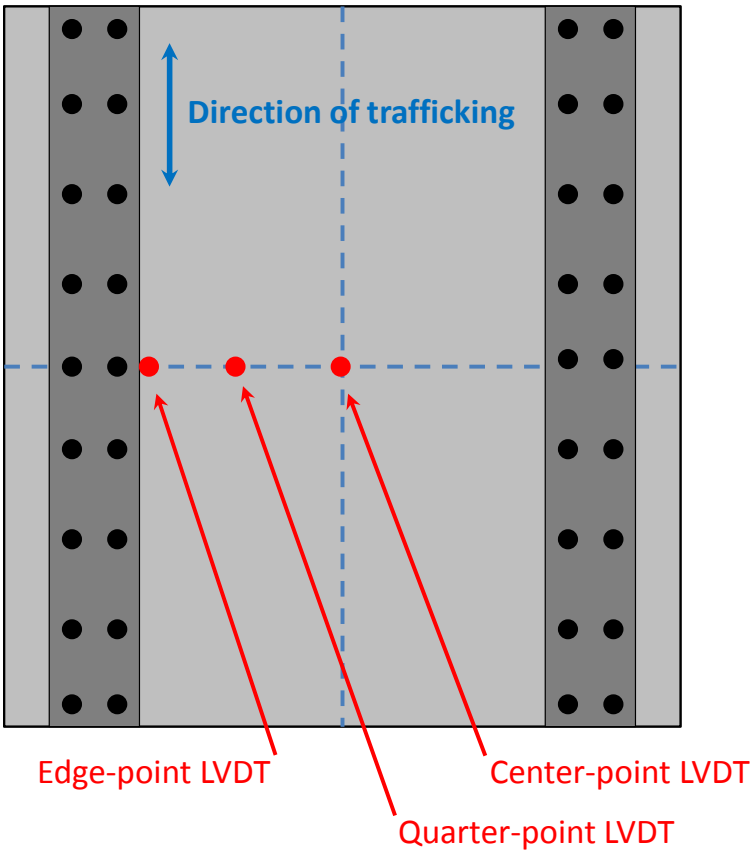

Figure 24: Locations of displacement measurements under each test panel.

Figure 25: Photo of LVDT sensors attached to underside of a test panel.

Visual Distress Assessment

The condition of the test panels was visually assessed periodically as cycling proceeded. Physical condition was characterized in terms of distress location, extent, and severity. A 12 x 12-inch reference grid was used on the top and bottom surface of each test panel to facilitate crack mapping. A chain drag was used to locate delaminated areas – although none were found during this research.

To more easily compare the cracking behavior between panels, the percent cracked area and total crack length was calculated for each test panel for both the top and bottom surfaces. The percent cracked area was calculated using a 3 x 3 inch grid superimposed over the crack maps. Percent cracked area was simply calculated as the number of grid squares containing cracks divided by the total number of squares that comprised the panel. The 3 x 3 inch grid size was selected by successively repeating the percent cracked area calculation at smaller grid sizes until the calculated result was relatively constant. Total crack length was measured on the crack maps.

Concrete Compression Tests

Concrete compressive strength and modulus of rupture were determined in substantial accordance with ASTM C39 *Standard Test Method for Compressive Strength of Cylindrical Concrete Specimens* (ASTM C39, 2010) and ASTM C78 *Standard Test Method for Flexural Strength of Concrete (Using Simple Beam with Third-Point Loading)* (ASTM C78, 2010),

respectively. Test cylinders and rupture beams cast when the deck panels were constructed were used in this evaluation. All test samples were cured with the deck panels. Test cylinders were 4 x 8-inch samples and the rupture beams were 6 x 6 x 20 inches. Strength and modulus of rupture values are an average of three tests.

Concrete Core Tests

Concrete cores were removed from the trafficked deck panels to obtain an indication, through permeability and chloride ion tests, of the internal degradation in the concrete. Cores were removed from the deck panels in areas of high stress/distress, as well as areas where there was less visible evidence of distress, allowing for an assessment of the cyclic load related distress. These cores were removed at the conclusion of testing to avoid affecting slab response. Comparisons were made to cores removed from rupture beams cast at the same time the deck panels were cast, allowing for a clear assessment of the cyclic load related distress. Two specimens from each slab were tested. The matrix of tests conducted on these samples is summarized in Table 2.

Table 2: Testing Matrix for Concrete Cores

Sample	Treatment / Source	Condition
1	Rupture beam	Control (un-trafficked)
2	Untreated slab	Uncracked
3	Untreated slab	Cracked
4	HMWM-treated slab	Uncracked
5	HMWM-treated slab	Cracked

Concrete cores were removed from the deck surface using a 4-inch diameter, diamond tooth, core drill bit. The drill bit did not penetrate the deck entirely, but was allowed to penetrate about 4 inches into the slab. The core concrete was then gently freed from the surrounding material. The core samples were prepared in accordance with sample preparation procedures outlined in ASTM C1202 *Electrical Indication of Concrete's Ability to Resist Chloride Ion Penetration* (ASTM C1202, 2010) and ASTM C1585 *Measurement of Rate of Absorption of Water by Hydraulic-Cement Concretes* (ASTM C1585, 2011). The specimens were sliced to the required 50 mm thickness, sealed, packaged and shipped to Concrete Research and Testing, LLC (Columbus, OH) for testing. Due to higher variability, duplicate samples were prepared for the C1202 tests while only single specimens were tested in the C1585 tests. Test results from CRT are provided in Appendix D. In general, the chloride permeability results indicated moderate potential for chloride ion penetration for untreated concrete cores when compare to samples treated with HMWM (low potential), but it was difficult to distinguish differences between cracked and uncracked samples (Figure 26). The results from the rate of absorption tests on

concrete core samples did not show a clear trend between cracked and uncracked, treated and untreated (Figure 27).

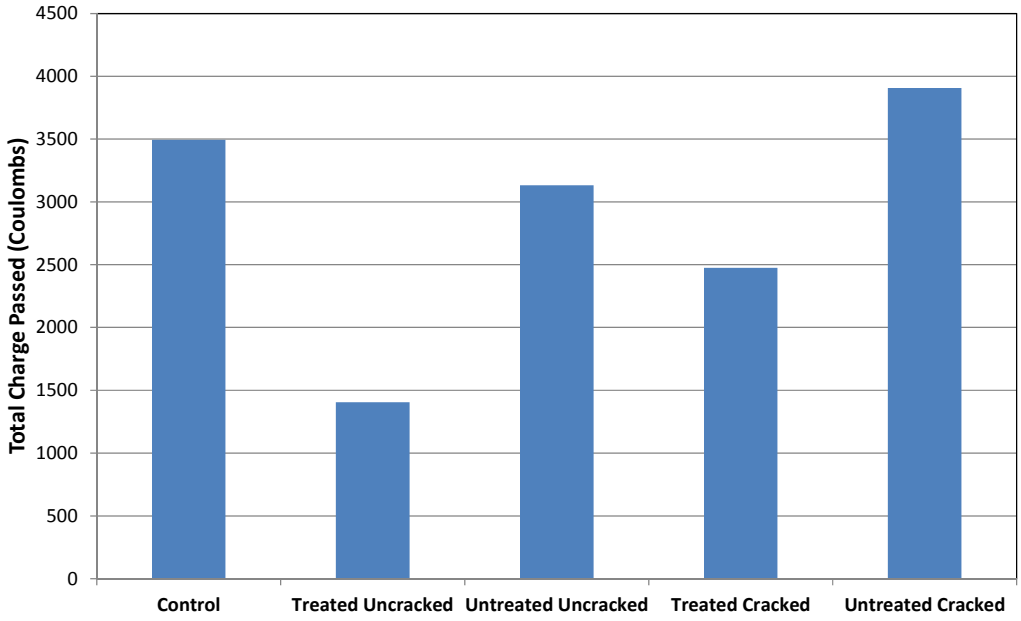

Figure 26: Results from rapid chloride permeability tests on concrete cores.

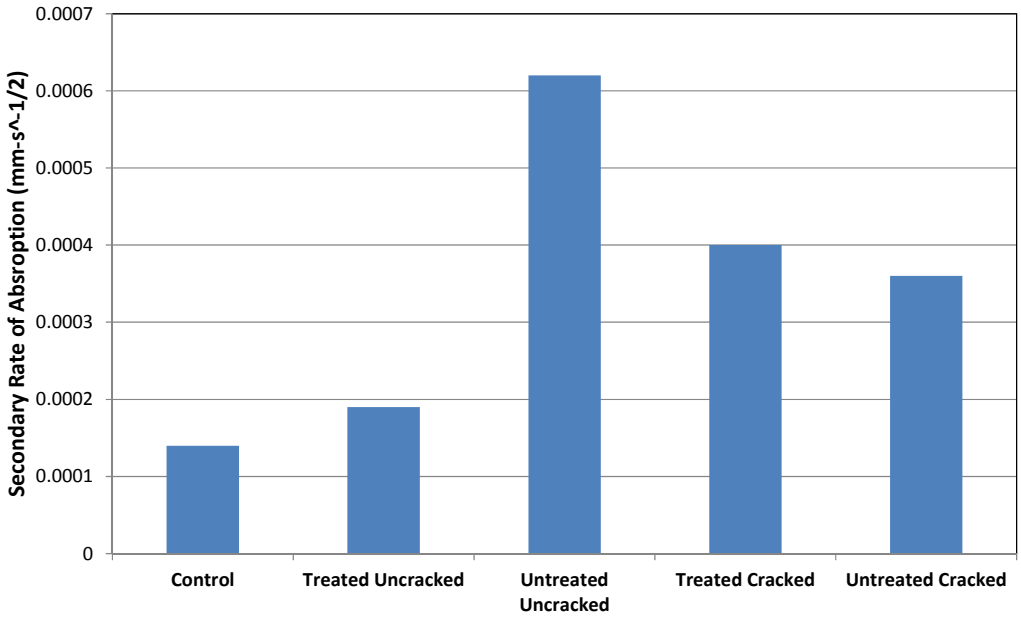

Figure 27: Results from rate of absorption tests on concrete cores.

TESTING

Eight deck panels were tested in this project. Four different HMWM treatment–traffic combinations were evaluated, each with two panels. The treatment times and trafficking levels at completion of testing are summarized in Table 3 for each of the four panel treatment/traffic combinations. Panel names signify the approximate level of trafficking at the time of treatment with HMWM (e.g., M25 signifies the panels that were treated with methacrylate after about 25,000 traffic cycles). Repeated panels are distinguished from each other using the subscripts a and b (e.g., $M25_a$ and $M25_b$). Two panels each were treated at approximately 25,000, 250,000 and one million cycles of loading, and two panels were not treated at all (controls).

Table 3: Test Panel Traffic Levels at Treatment and Completion Times

	Test Panels (2 each)	Traffic Level at Treatment	Traffic Level at Completion
Panel Set 1	$Control_{a,b}$	Not treated	2,122,978
	$M1000_{a,b}$	1,071,820	2,122,978
Panel Set 2	$M250_{a,b}$	242,590	604,932
	$M25_{a,b}$	25,710	604,932

The test panels were placed onto the reaction frame in a manner that ensured full contact between the underside of the concrete panel and the top flange of the reaction frame and to ensure that the vertical elevation between two adjacent test panels was the same. Metal shims of varying thickness were placed along the entire bearing length to fully close any gaps. Gaps were generally less than about 1⁄16-inch thick. Once the shims were in place, ½-inch bolts were installed through the clamping C-channels to the reaction frame through the concrete slab. The nuts were tightened in a step pattern proceeding from lower torque levels beginning with the interior bolts and working outward until all of the bolts were torqued to 90 ft-lb. This torque was checked periodically during trafficking. Plastic pads (⅛-inch LDPE) were also placed between all steel and concrete interfaces to minimize local stresses in the concrete from the clamping forces. The longitudinal gap between the panels was about 1 inch wide.

The ABDT was positioned so that trafficking occurred along the longitudinal centerline of the test panels. Four test panels were tested simultaneously. The ABDT ran continuously 24 hours per day, seven days per week except during times of maintenance, test panel condition assessment, and equipment failure. Temperature in the lab ranged from approximately 55–75° F.

Response Monitoring/Data Collection

Throughout testing, the applied load and the deflection response and physical condition of the deck panels was monitored and recorded, as earlier described. The deflection response and

applied load were used to determine changes in stiffness of the test panels during trafficking. The physical condition of the deck panels was documented at discrete intervals throughout the testing process. These intervals were shorter at the beginning of testing when more rapid changes were occurring in panel condition. The goal of this monitoring process was to allow for correlation of visual condition of the test panels with quantitative changes in their structural stiffness. A timeline of the visual inspections and treatment times for each set of deck panels is shown in Figure 28 and Figure 29, for Panel Sets 1 and 2, respectively. A single value for the average compressive and rupture strength of the concrete was used for the beginning and end of Panel Set 2 because the testing duration was relatively short (2 months). HMWM treatments were applied in consultation with Caltrans at approximately 25,000, 250,000 and 1,000,000 cycles of applied load. A summary of the distress condition of the test panels at the time of treatment is presented in Table 3. In all cases, the panels were in relatively good condition compared to when Caltrans practice would possibly suggest HMWM treatment, as this practice was described earlier in this report. The most distress was present in the panels treated at 1,000,000 load cycles ($M1000_a$ and $M1000_b$ test panels), consisting of cracks up to 0.016 in. wide over 14–19 percent of the top surface of the test panel – under but approaching the threshold of when Caltrans would normally apply HMWM treatment.

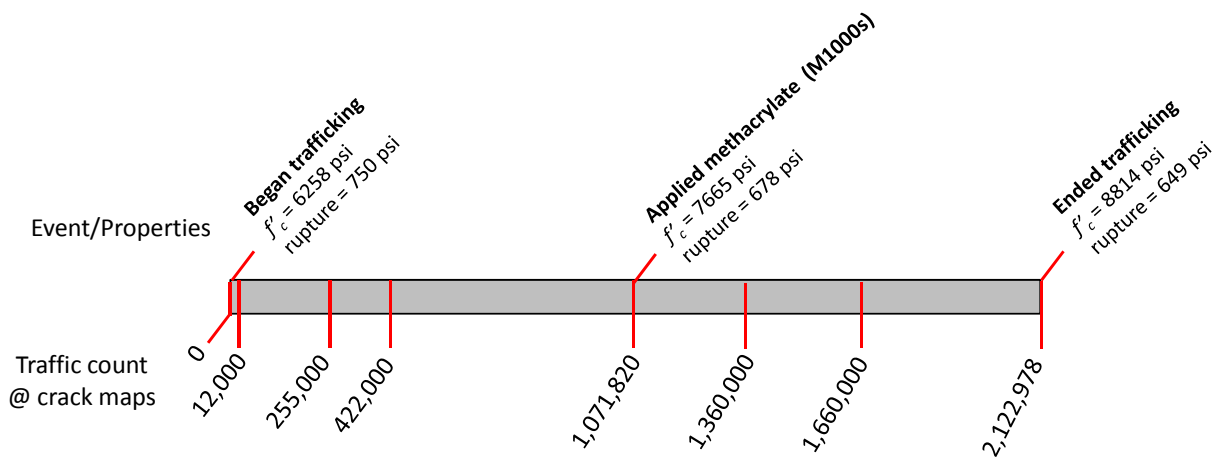

Figure 28: Timeline of events for Control and M1000 test panels (Panel Set 1).

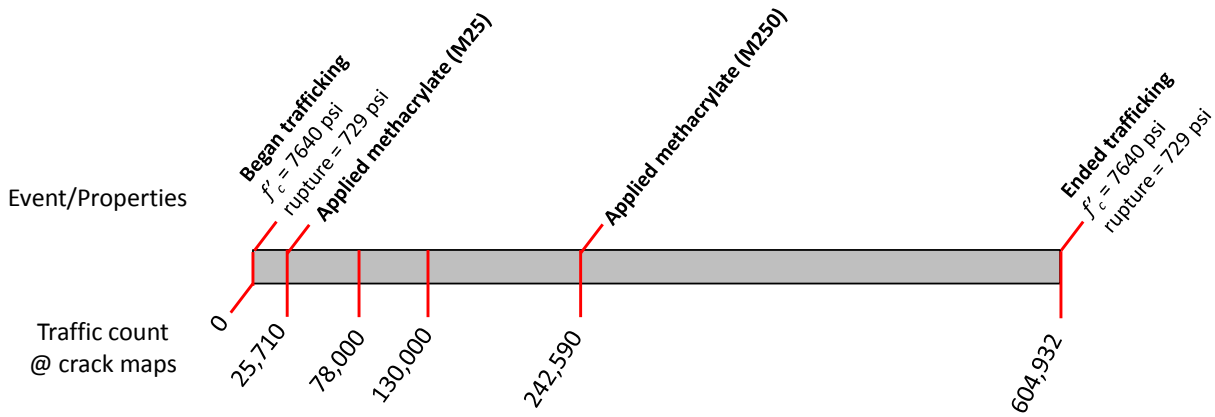

Figure 29: Timeline of events for M250 and M25 test panels (Panel Set 2).

Table 4: Summary of Top Cracking Distresses of Treated Panels Prior to Treatment

Test Panel	Percent Top Cracking	Maximum Crack Width (in.)	Average Crack Width (in.)
$M1000_a$	19	0.016	0.009
$M1000_b$	14	0.016	0.008
M250a	6	0.011	0.004
M250b	19	0.025	0.008
M25a	8	NM	NM
M25b	3	NM	NM

NM = not measured

Deck Rehabilitation

Kwik Bond Polymers (Benicia, CA) KBP 204 HMWM primer/sealer was used as the sole rehabilitation technique during this project (product data sheet in Appendix E). This treatment was applied with the panels clamped in the support frame with the ABDT rolled to one side. Two deck panels were treated at once. The panels were steel shot blasted and cleaned using compressed air in accordance with California's Standard Specifications Section 15-501C(2) *Prepare Concrete Deck Surface*. L & J Construction Group, LLC (Ennis, MT) shot blasted the panels using a Blastrac 2-30 DS Electric Concrete Shot Blaster and 854 Dust Collector in preparation for the HMWM application (Figure 30). The shot blaster made two passes across the deck surface and removed only a very thin layer of material. A comparison of the deck concrete surface before and after shot blasting is shown in Figure 31. The concrete adjacent to cracks was slightly more vulnerable to shot blasting than the rest of the concrete surface, as shown in Figure 32. A four inch strip along each longitudinal edge of the panels could not be shot blasted due to interference between the C-channels and the shot blasting equipment. Therefore these strips

were lightly ground using a handheld 4.5 inch grinder with a diamond cup grinding wheel. The deck surfaces outside of the C-channels (approximately 2 inches of overhang) were not prepared or treated.

Figure 30: Shot blasting the deck panels in preparation for the HMWM application.

Figure 31: Concrete surface before and after shot blasting.

Figure 32: Crack in deck surface after shot blasting.

Subsequent to surface preparation, the KBP 204 (HMWM) was mixed in accordance with Kwik Bond product specifications and applied with a ½-inch nap paint roller (Figure 33). Excess material was rolled to the end of the slab and soaked up or deposited in a trough formed between adjacent test panels. Because cracked areas tended to soak up more methacrylate, special attention was paid to these areas to ensure adequate HMWM was present to fill the cracks prior to curing. The sealer cured for several days before trafficking was resumed. Friction enhancing sand was not added to the surface prior to curing as additional traction was deemed unnecessary in this application, and it was thought that this sand would obscure detection of surface distresses in the deck. A close-up photo of a crack filled with methacrylate is shown in Figure 34.

Figure 33: Application of HMWM surface treatment.

Figure 34: Close-up of methacrylate-filled crack.

ANALYSIS AND RESULTS

Information gathered during the long-term trafficking of the test panels primarily consisted of visual distress assessments and load and deflection data, which was used to calculate test panel stiffness simply as force divided by associated deformation. Presented below is an analysis of the visual distress and stiffness of the test panels as a function of cyclic load history and surface treatment.

Cracking Analysis

All of the test panels experienced cracking as trafficking proceeded, although no spalling or delamination of the concrete was seen. Complete crack maps (by panel and cycle stage) are presented in Appendix F. Presented below is a general description of the progression of the cracking in the panels as trafficking proceeded. This description is followed by a quantitative discussion of various cracking metrics calculated from the crack information, i.e., crack density and overall crack length, in an effort to more objectively delineate differences in panel and treatment performance.

General Cracking Behavior

A typical set of crack maps as a function of cycles of applied load is presented in Figure 35 and Figure 36 for top surface and bottom surface cracking, respectively (test panel Control_a is shown). Cracking in the top surfaces of the panels occurred in many of the specimens by 12,000 to 25,000 load cycles (refer to Figure 35a). This distress often consisted of a single crack along the longitudinal edge of the panel indicative of negative transverse moment, and a few relatively "random" oriented skew and transverse cracks. By the second set of inspections (after 255,000 and 78,000 cycles of applied load, respectively, for panel set one and two), all panels exhibited cracking in their top surfaces. This cracking generally consisted of one or two longitudinal cracks along one or both edges of the panel, and some diagonal cracks across the corners, with occasional skew and transverse cracks. Bottom cracking at these same levels of cyclic load (Figure 36, for test panel Control_a) was confined to the center region of panels. Bottom surface cracking consisted initially of a few longitudinal cracks at or near the center of each panel, consistent with the presence of positive transverse bending moment. Cracking in the bottom surface of the decks definitely reflected the layout of the bars in the bottom mat of reinforcing, and initially, in particular, the longitudinal bars in this mat. Note that the cracking in the top surfaces of the decks did not follow the layout of the top mat of reinforcing steel. The top surfaces of the panels also appeared to generally exhibit less cracking than the bottom surfaces (as is borne out in the quantitative crack analysis presented below). This difference in cracking behavior between the top and bottom surfaces of the decks is believed to be due in part to the relative clear cover on the top and bottom mats of reinforcing steel. The top mat had 2 inches of clear cover, versus 1 inch for the bottom mat.

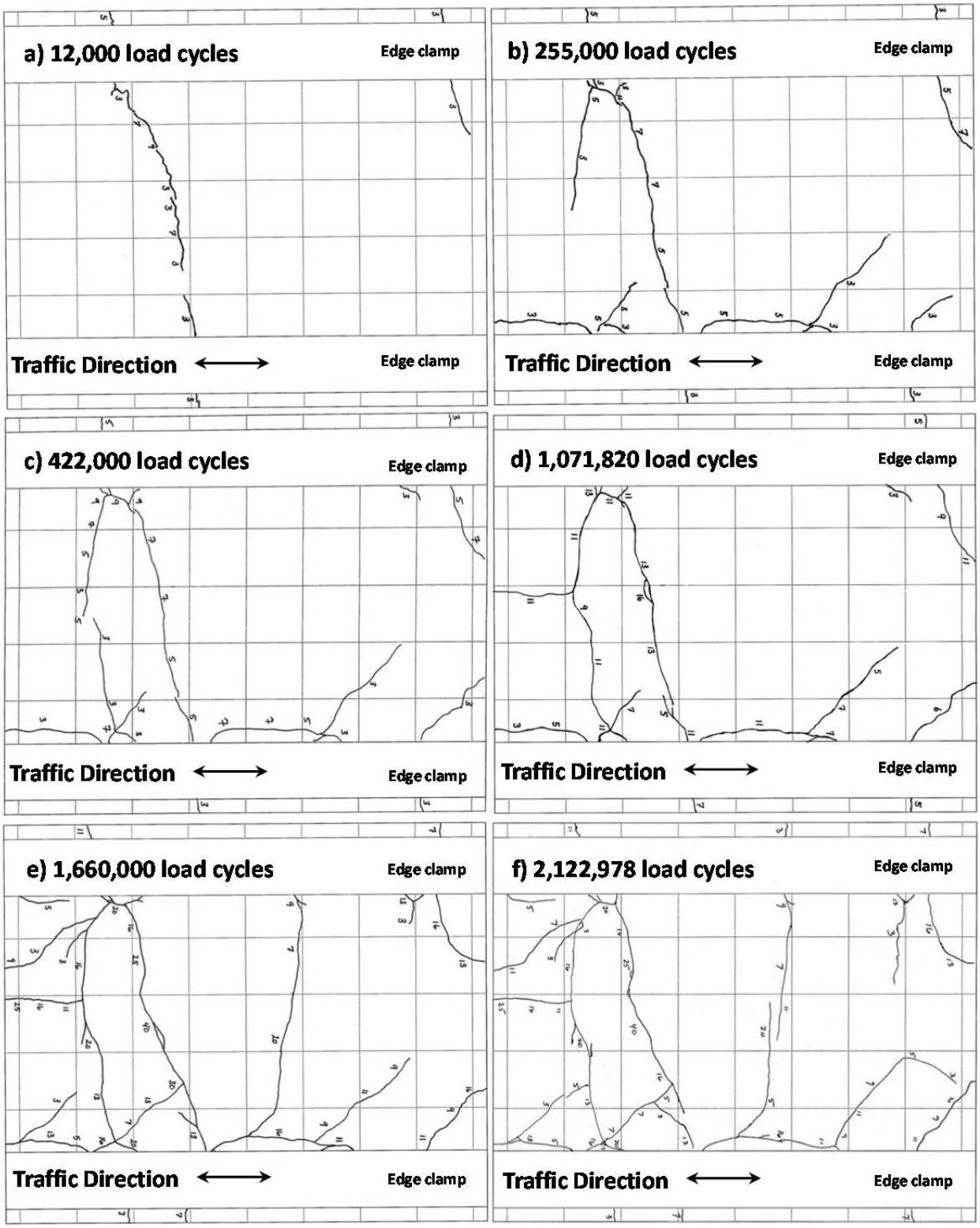

Figure 35: Top cracking in Control$_a$ test panel at various traffic levels.

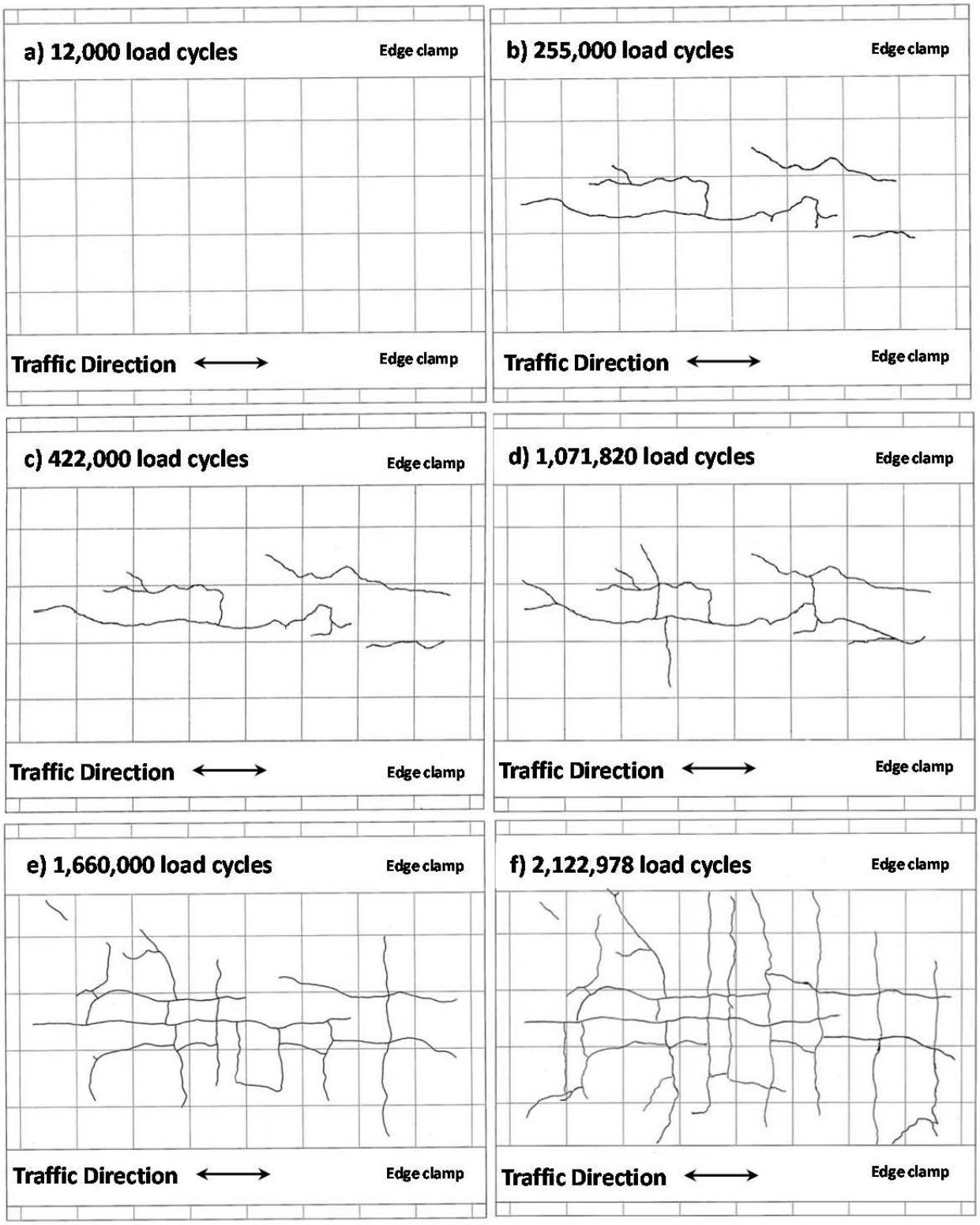

Figure 36: Bottom cracking in Control$_a$ test panel at various traffic levels.

In general, as cycling progressed, cracks continued to increase in extent and width in the top surface of the decks (Figure 35), with this cracking being almost completely arrested when a panel received HMWM treatment. Early crack widths, i.e., at the time of the second set of crack inspections, were typically in the range of only 0.003 to 0.007 inches. At the conclusion of testing of Panel Set 1, cracks in the top surface of the untreated panels (i.e., test panels $Control_a$ and $Control_b$) generally were in the range of 0.016 to 0.020 inches wide, with a maximum width of 0.040 inches. A typical longitudinal crack along a clamped edge is shown in Figure 37 (edge of $M1000_a$ test panel at approximately 1,000,000 load cycles). Note the maximum crack width in each panel at the time the HMWM treatment was applied was previously reported in Table 3.

Figure 37: Longitudinal crack in top surface.

In general, cracking in the bottom surfaces of the test panels generally increased in extent as cycling proceeded. Different from the top surface cracking, however, the progression of cracking in the bottom surfaces of the panels was generally unaffected by the application of HMWM to the top surface. Additionally, while crack widths increased with increased traffic in the untreated top surfaces of the panels, all cracks in the bottom surface never progressed beyond being hairline in width.

Relative to comparative performance between panels, all panels were expected to exhibit similar top surface distress as cycling proceeded until any given panel received HMWM treatment. An excellent opportunity to make such a comparison was after approximately 250,000 load cycles, as six of the eight panels were still untreated at this point, and crack assessments were done on all panels at about this same level of trafficking. The cracking distress in the top surface of these six panels at approximately 250,000 load cycles is presented in Figure 38. Panels $M250_b$ $M1000_a$, $M1000_b$ and $Control_a$ exhibited similar crack patterns, as did panels $M250_a$ and $Control_b$. The difference in the response between these two groups of panels is the presence of longitudinal cracks in the former panels along at least one clamped edge of the panel, while such cracks are absent in the latter panels. The absence of such cracks in Panels $M250_a$ and $Control_b$ could have resulted from differences in the degree of clamping provided by the support frame for these panels, although an associated decrease in the stiffness of these panels was not observed (see stiffness results presented in the subsequent sections below). In the case of panel $M250_a$, the HMWM was applied at 250,000 load cycles, arresting any further crack development. In the case of panel $Control_b$, limited longitudinal cracks did develop along the clamped panel edges after 1,360,000 cycles of applied load.

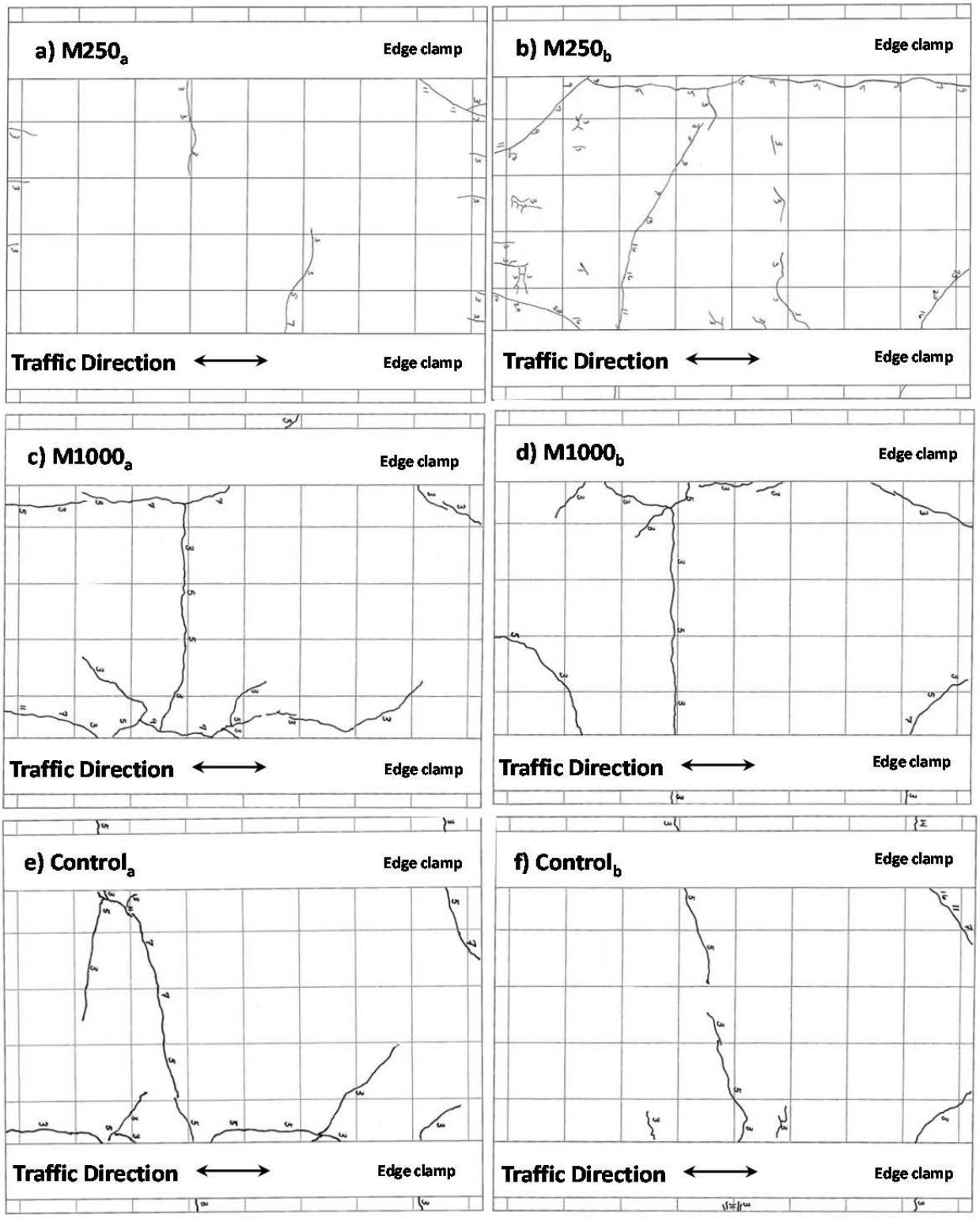

Figure 38: Top cracking in all test panels at about 250,000 traffic passes.

The expected similarity in the distress generated in similarly configured and loaded test panels could also be evaluated using the condition of the slabs in Panel Set 1 at approximately 1,000,000 load cycles, as no treatments were applied to any of these slabs prior to this point. Crack maps of the top surfaces of the four panels comprising this set of panels at approximately 1,000,000 load cycles are presented in Figure 39. Once again, the crack patterns in slabs $Control_a$, $M1000_a$ and $M1000_b$ are similar in nature, while panel $Control_b$ continued to manifest no longitudinal cracks.

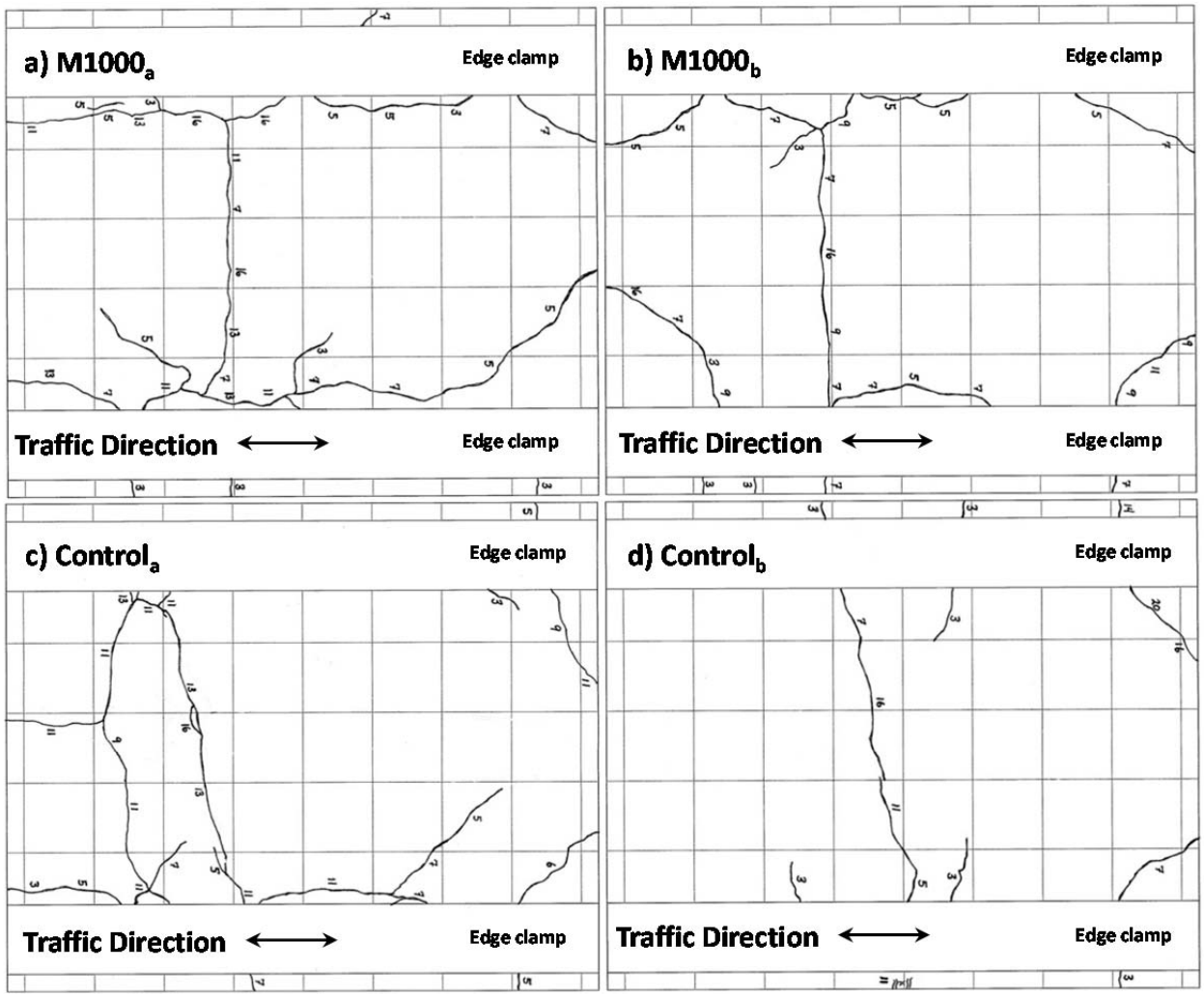

Figure 39: Top cracking in M1000 and Control test panels at 1,071,820 traffic passes.

A comparative analysis of the cracking in the bottom surfaces of similarly configured panels was also possible at about 250,000 and 1,000,000 cycles of applied load. The bottom cracking in the six similarly configured panels available for this comparison at approximately 250,000 cycles of applied load (panels $M250_a$, $M250_b$, $M1000_a$, $M1000_b$, $Control_a$ and $Control_b$) are shown in Figure 40. Considering the information presented in Figure 40, it is apparent panels $M250_a$ and $M250_b$ from Panel Set 2 exhibit more extensive bottom cracking than the other panels. Looking further, it was found that bottom cracking across all the panels in Set 2 was noticeably more

severe than that seen in any of the panels in Set 1. While this difference in behavior between panel sets was not observed in the top surface cracking, it still could result from differences in the concrete used in constructing the two panel sets. The factors that affect cracking in concrete bridge decks are complex, but the reduced clear cover on the bottom versus the top mat of reinforcing steel in these panels could make any cracking that occurs in the bottom surface of the panels more sensitive to some of these factors. In this case and as previously mentioned, the two sets of panels were cast from different batches of concrete, and changes were made in the mix design between batches. The concrete used in Panel Set 2 contained 10 percent more water than was used in Panel Set 1, and this concrete achieved only 90 percent of the 28 day compression strength obtained in Panel Set 1. Both of these differences could conceivably contribute to increased cracking in the bottom surfaces of Panel Set 2 compared to Panel Set 1.

Bottom cracking in the four slabs in Panel Set 1 at 1,071,820 cycles of applied load are shown in Figure 41. At this cycle point the most extensive bottom cracking continued to be seen in panel $Control_b$, with the least bottom cracking in panel $M1000_a$ (closely followed by $Control_a$).

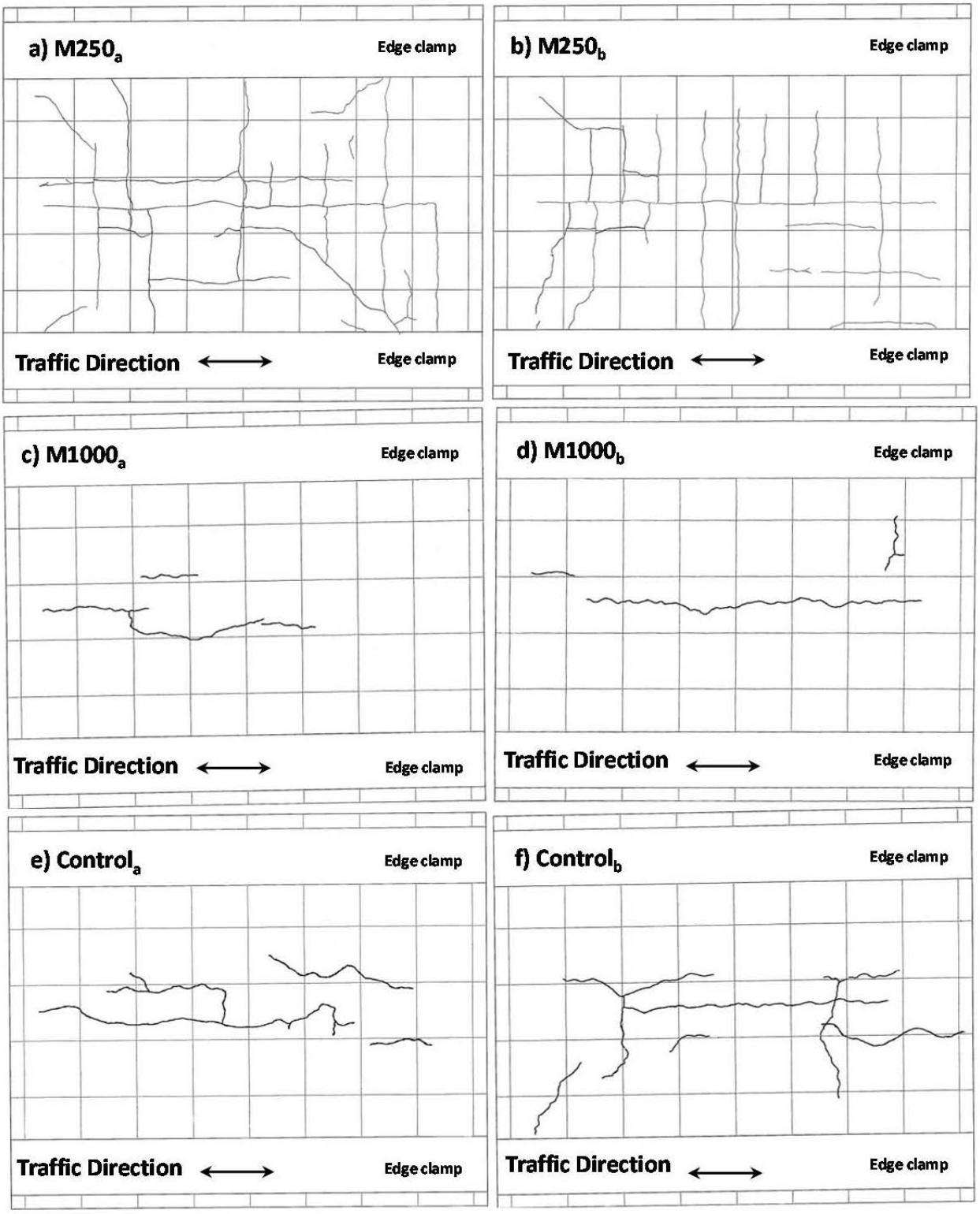

Figure 40: Bottom cracking in M250, M1000 and Control test panels at 250,000 load cycles.

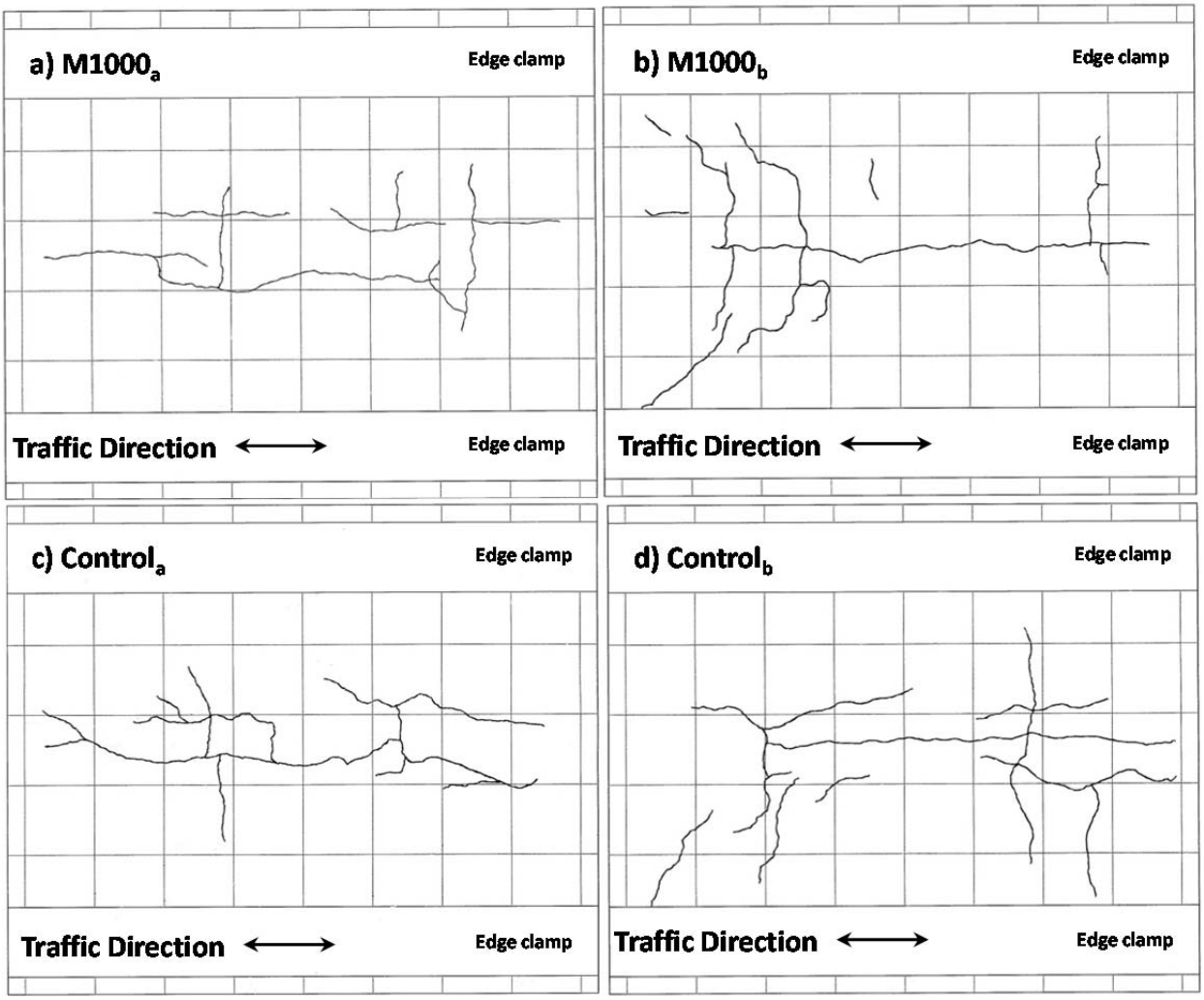

Figure 41: Bottom cracking in M1000 and Control test panels at 1,071,820 traffic passes.

Quantitative Analysis of Cracking Distress

In an effort to more fully and objectively identify distress based differences in slab behavior as a function of applied cycles of load and HMWM treatment, the percent cracked area and total crack length were calculated for each test panel for both the top and bottom surfaces as cycling progressed (using the methodology described in the previous chapter of this report). Progression of cracking in the top and bottom surfaces of the deck panels is presented in Figure 42 and Figure 43, respectively, in terms of percent cracked area and total crack length. Referring to these figures, similarities were immediately evident in the cracking response as quantified by these two parameters. Therefore, the remaining discussion is focused on the percent cracked area results.

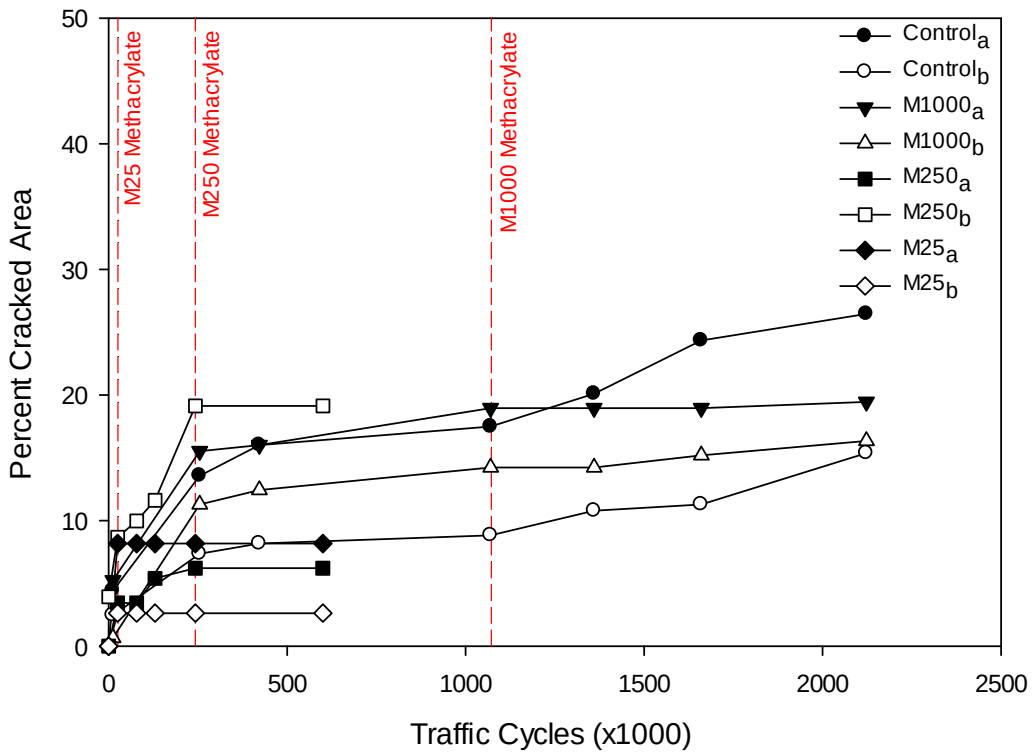

Figure 42: Percent top cracking for both panel sets.

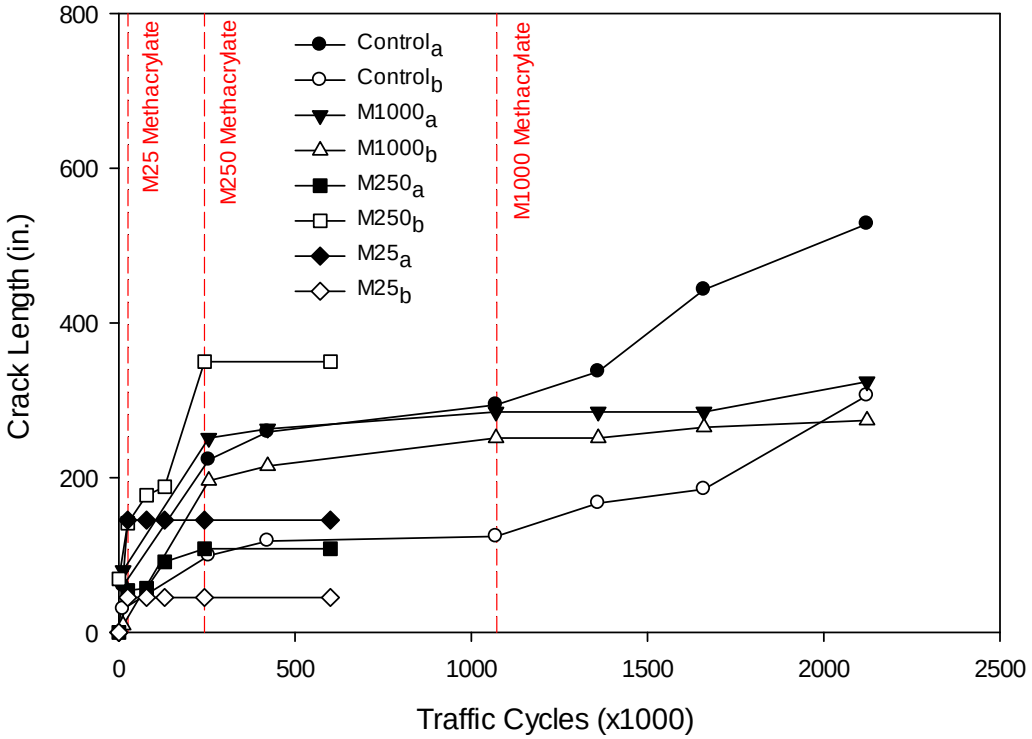

Figure 43: Top crack length for both panel sets.

Referring to Figure 42, and considering first the behavior of Panel Set 1 ($M1000_a$, $M1000_b$, $Control_a$ and $Control_b$), top surface cracking increased relatively rapidly up to the 255,000 inspection point, variously reaching approximately 10 to 20 percent of the area. Between 255,000 and 1,000,000 load cycles, distress in the top surface continued to increase, but at a much more moderate rate. Between 1,000,000 and 2,000,000 load cycles, considering just the untreated control panels, cracking again progressed at a more accelerated rate. At the conclusion of testing, the percent cracked top area of the Control panels ranged from 15 to 18 percent.

While considerable differences are seen in the absolute amount of top surface cracking observed in each panel (attributable to vagaries in materials, fabrication, support condition, etc.), all of the panels exhibited the same pattern in the rate at which this cracking occurred as a function of cycles of applied load. That is, early in the cycle history initial crack formation and growth occurred (up through 250,000 load cycles), followed by a prolonged period of stability with relatively little increase in cracking distress (250,000 to 1,000,000 load cycles), finally followed by a period of renewed cracking activity (in the untreated panels, from 1,000,000 to 2,000,000 load cycles). Referring to Figure 42, it is apparent that little to no additional cracking occurred in the top surfaces of panels $M1000_a$ and $M1000_b$ after the HMWM was applied, while the companion untreated panels ($Control_a$ and $Control_b$) experienced cracking at an accelerated rate.

Extending this discussion to Panel Set 2 ($M25_a$, $M25_b$, $M250_a$ and $M250_b$), these panels were all treated within the first 250,000 traffic cycles, during the period of initial rapid crack growth seen in the first set of panels. While further crack development in the top surface of these panels was subsequently and completely arrested out through the 600,000 cycles of applied load they were exposed to, they need to be tested beyond this point (say, out to 2,000,000 load cycles) if their performance is to be evaluated relative to that of the Panel Set 1.

Cracking in the bottom surfaces of the test panels generally developed as cycling progressed following the pattern described above for top surface cracking, with the notable exception that its progression was not affected by the application of HMWM to the top surface of the panels. In the case of Panel Set 1, and referring to Figure 44, the three stages of crack progression described previously in the top surfaces of the panels is clearly evident in the bottom surfaces, i.e., a period of initial crack development through 250,000 load cycles, followed by a stable period with little change in cracking extent through 1,000,000 load cycles, and concluding with a period of resumed crack growth from 1,000,000 to 2,000,000 load cycles. Unlike the top surface, however, in which cracking was arrested at 1,000,000 load cycles in the panels that were treated with HMWM, cracking resumed at a similar accelerated rate on the bottom surface of all the panels (untreated and treated, alike) through 2,000,000 load cycles, reaching a relatively common extent approaching 40 percent of the panel area.

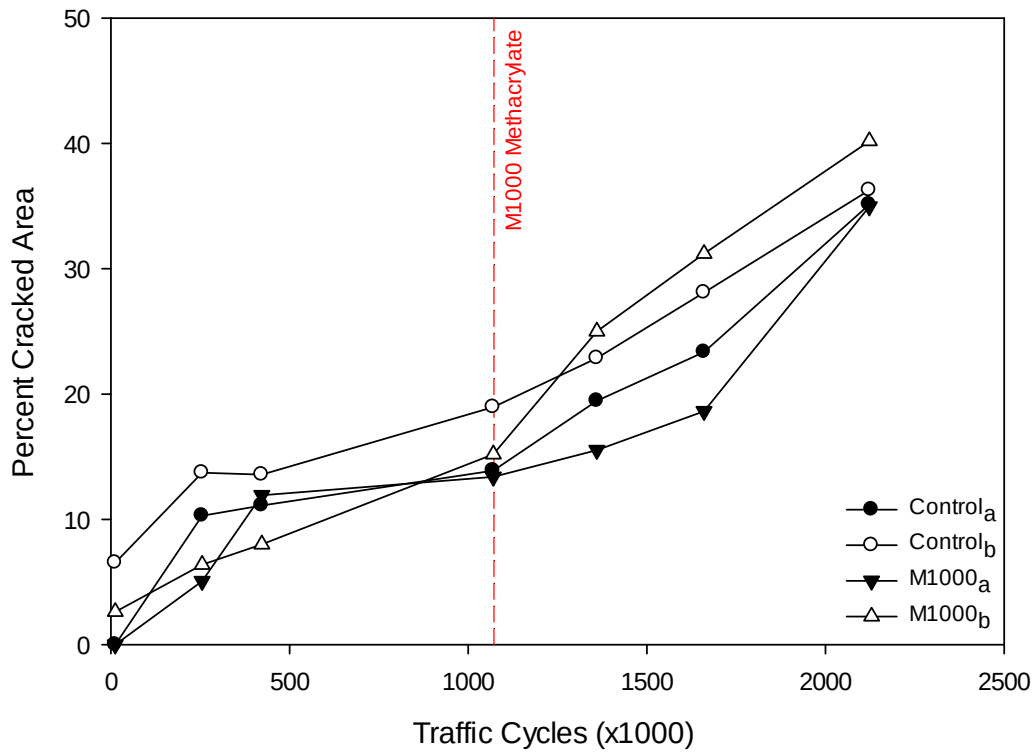

Figure 44: Percent bottom cracking in Panel Set 1.

Crack surveys of the bottom surfaces of Panel Set 2 (summarized in Figure 45) indicate that the second set of panels experienced approximately twice the bottom surface cracking distress (quantified in percent cracked area) as was seen in Panel Set 1 at 600,000 load cycles. As previously discussed, this difference in amount of cracking possibly can be attributed to differences in the concretes used in constructing the two sets of panels. As in the case of Panel Set 1, the progression of bottom cracking was unaffected by HMWM treatment of the top surface, as can particularly be seen in the similarity in cracked condition in all four panels at 250,000 cycles of applied load, while two of these panels were treated at 25,000 cycles of applied load ($M25_a$ and $M\ 25_b$).

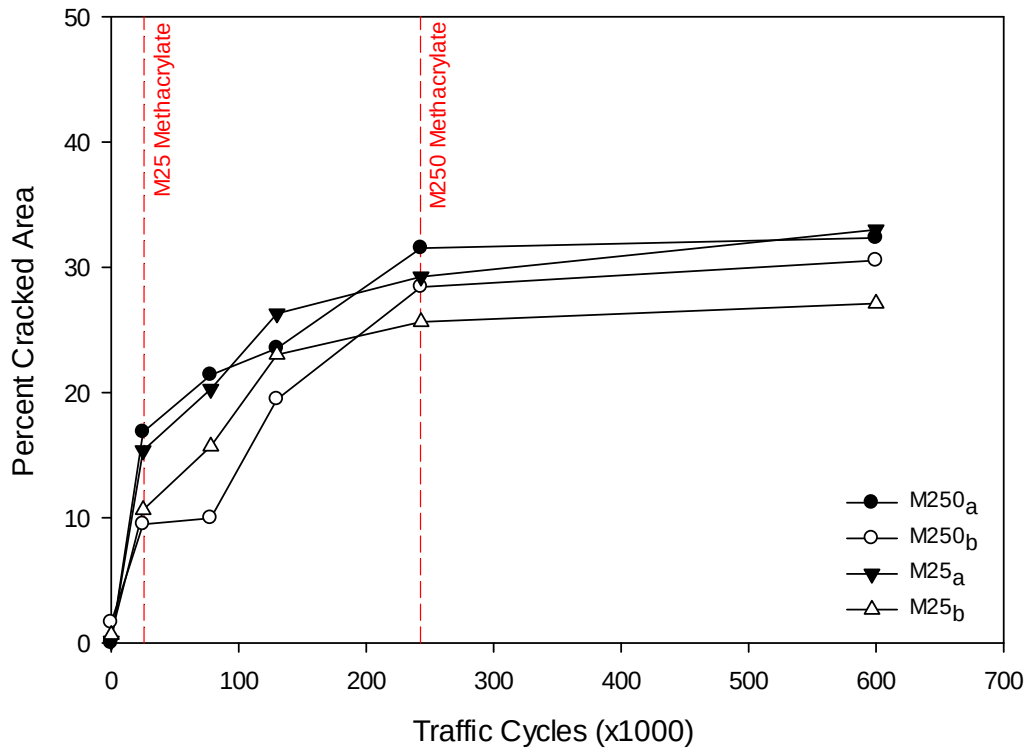

Figure 45: Percent bottom cracking in Panel Set 2.

Conclusions from Cracking Distress

Notable observations based on the cracking distress experienced by the test panels are:

- Top cracking in the test panels was inhibited by HMWM treatment. Existing cracks were sealed and only a few (or no) new cracks formed in the treated test panels when load cycling resumed.
- While HMWM treatments were applied to three different panels at three different points in the cycling process (at about 25,000; 250,000; and 1,000,000 cycles of applied load), additional study is necessary to consider the effect of this timing on overall panel performance. Notably, all treated panels showed little change in their cracked condition after the treatment was applied and the termination of cyclic testing.
- Bottom surface cracking generally was not affected by HMWM treatment of the top surface of the test panels.
- While significant differences were observed in the absolute amount of cracking in similarly configured and loaded test panels, patterns in the progression of this cracking and the effect of HMWM treatment were similar across all panels. Differences in specific panel performance can be attributed to vagaries in material properties and support conditions (i.e., edge fixity) between panels. That being said, panels Control_b, Panel Set 1 and M250_b, Panel Set 2 exhibited a pattern of

top surface cracking distinctively different from the other test panels, and which was indicative possibly of a lesser degree of rotational fixity along the longitudinal edges of these panels.

Flexural Stiffness Analysis

Flexural stiffness of the deck panels was also used to characterize their performance over time during trafficking. Stiffness was simply calculated as applied load divided by attendant deformation. Recall displacements were measured at the center-point, quarter-point and edge of each deck panel along its transverse centerline. Deflection was calculated as the difference in displacement between the interior and edge of the slab. Stiffness was then calculated as:

$$k_{center} = \frac{F_{max}}{\Delta_{center} - \Delta_{edge}} \qquad \text{Equation 3}$$

$$k_{quarter} = \frac{F_{max}}{\Delta_{quarter} - \Delta_{edge}} \qquad \text{Equation 4}$$

The dynamic displacement of the edge was subtracted from both the center and quarter point dynamic displacements in Equations 3 and 4 to account for any nominal global movement of the reaction frame under the traffic load, as all displacement measurements were made with respect to a fixed frame of reference independent of both the panels and the frame. Note that the measured deflections in all panels were very small, with the maximum values observed being less than approximately 0.025 inches at the center of a panel (corresponding to a deflection to span ratio, Δ/L, of 1/2360).

The center- and quarter-point stiffnesses as calculated herein are obviously not independent measures of slab behavior and/or condition, and any changes in stiffness due to slab deterioration as cycling proceeded should have been similarly reflected in the stiffnesses calculated using the deflections at either location. That being said, both stiffnesses are variously used in the analyses below. One use of this paired data was to assist in estimating the stiffness at one location or the other in the event an instrumentation failure was discovered at one of the locations at the end of a cycling interval. A second use of this paired data was to obtain a potentially better general representation of the stiffness condition of the panels as cycling proceeded by averaging the center and quarter point stiffnesses rather than simply studying them independently. These averaged stiffnesses were expected to smooth out any variations in the individual stiffnesses that could have resulted from a) instrumentation introduced variability in the deflection measurements, and b) possible asymmetry in the transverse deflection profile of a panel due to the location and nature of the specific cracking it experienced.

The center point based, quarter point based, and average stiffnesses for Panel Set 1 as cycling proceeded are presented in Figure 46, Figure 47, and Figure 48, respectively. The same sequence of stiffness response is presented in Figure 49, Figure 50, and Figure 51, respectively, for Panel Set 2. Gaps in data in these figures indicate missing values due to instrumentation

problems; "open" data markers in the averaged stiffness results (Figure 48 and Figure 51) indicate cycling intervals in which the response has been estimated based on data available just from either the center-point or quarter-point location. A simple elastic analysis of a homogeneous plate of the test slab dimensions and materials with simply supported and clamped edges would have an apparent center-point load/deflection stiffness of approximately 1600 kips/in. and 3500 kips/in., respectively. Referring to Figure 46 and Figure 49, the corresponding initial stiffnesses of the test panels ranged from about 1600 to 2500 kips/in. Thus, based on this simple analysis, the longitudinal edges offer intermediate fixity relative to the simple and fully clamped cases.

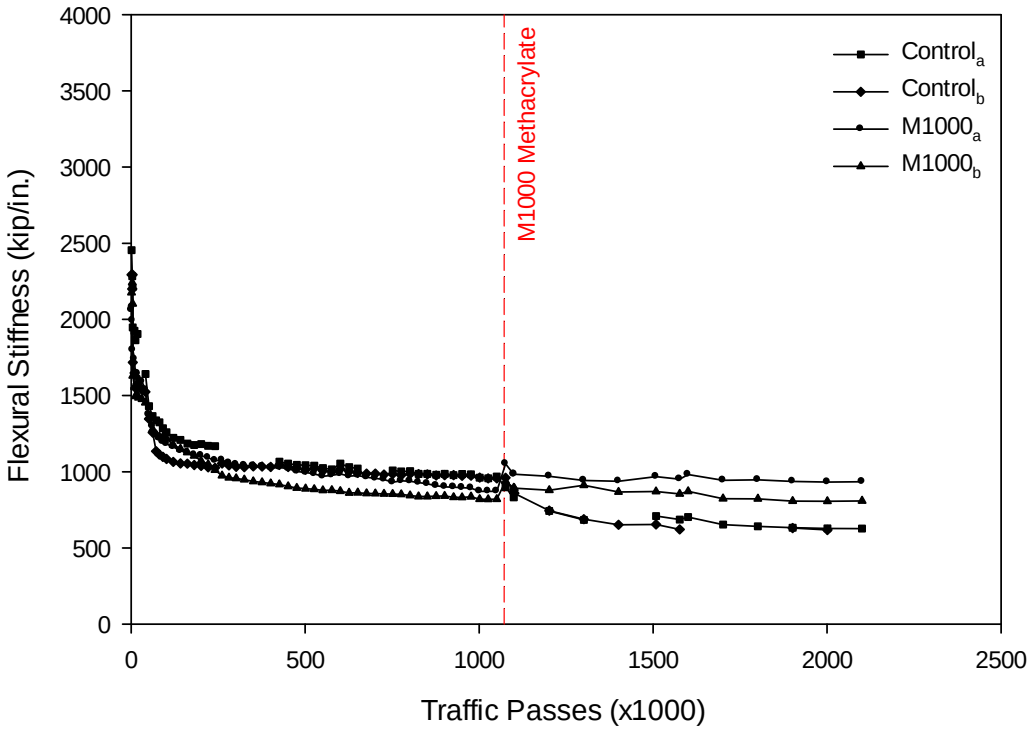

Figure 46: Flexural stiffness of Panel Set 1 based on center-point displacements.

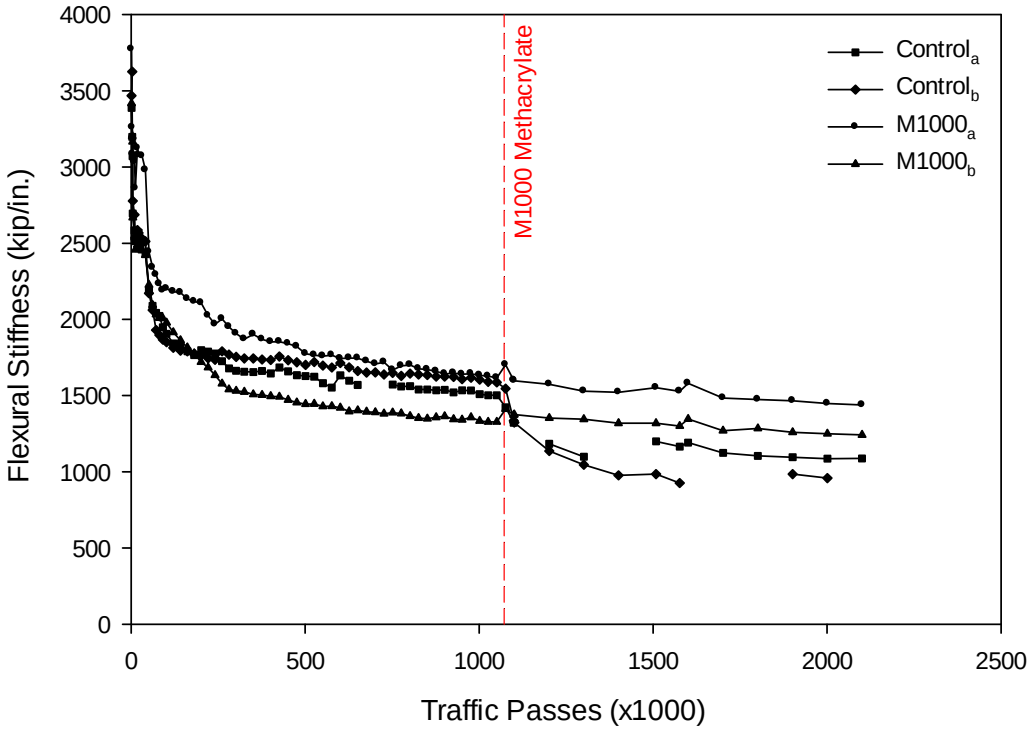

Figure 47: Flexural stiffness of Panel Set 1 based on quarter-point displacements.

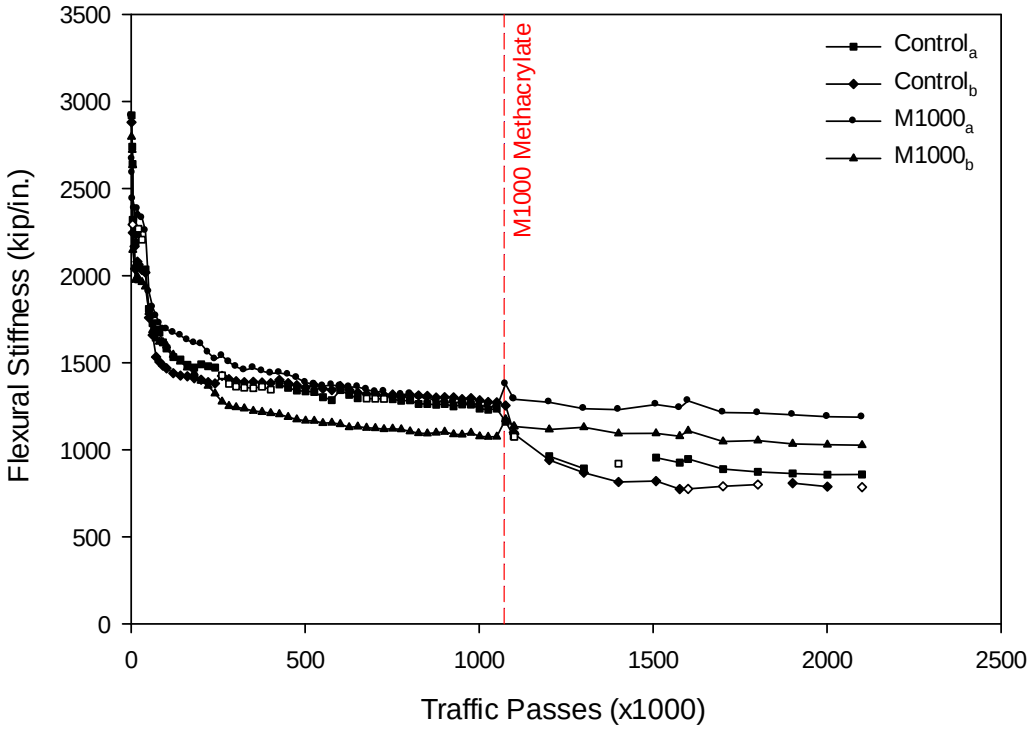

Figure 48: Average flexural stiffness of Panel Set 1.

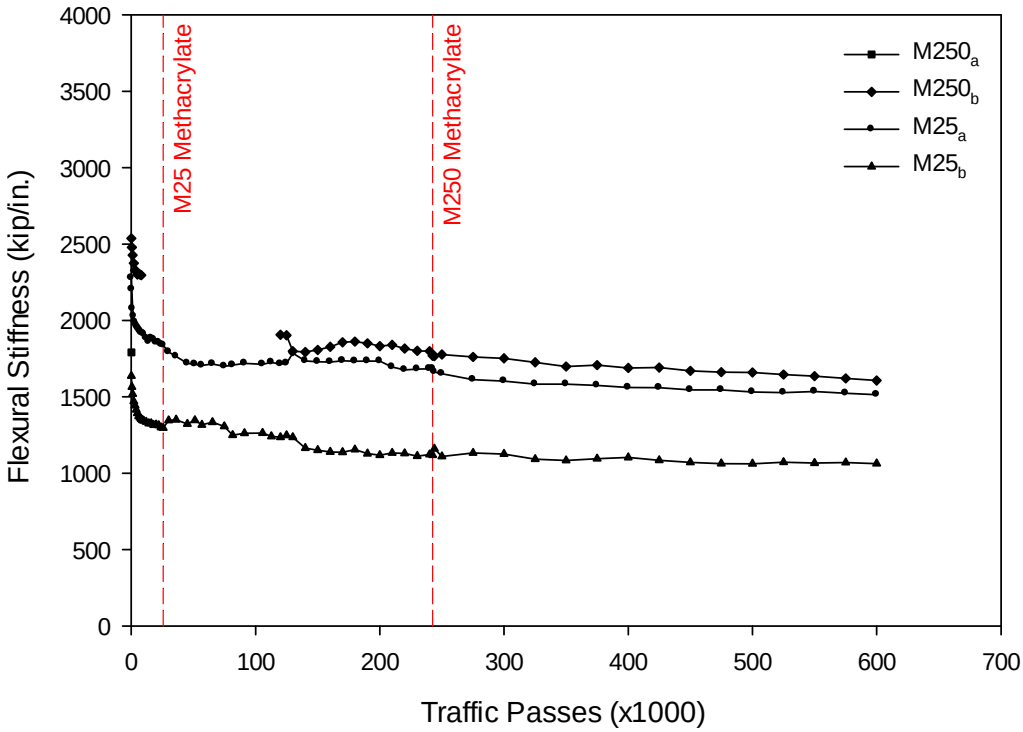

Figure 49: Flexural stiffness of Panel Set 2 based on center-point displacements.

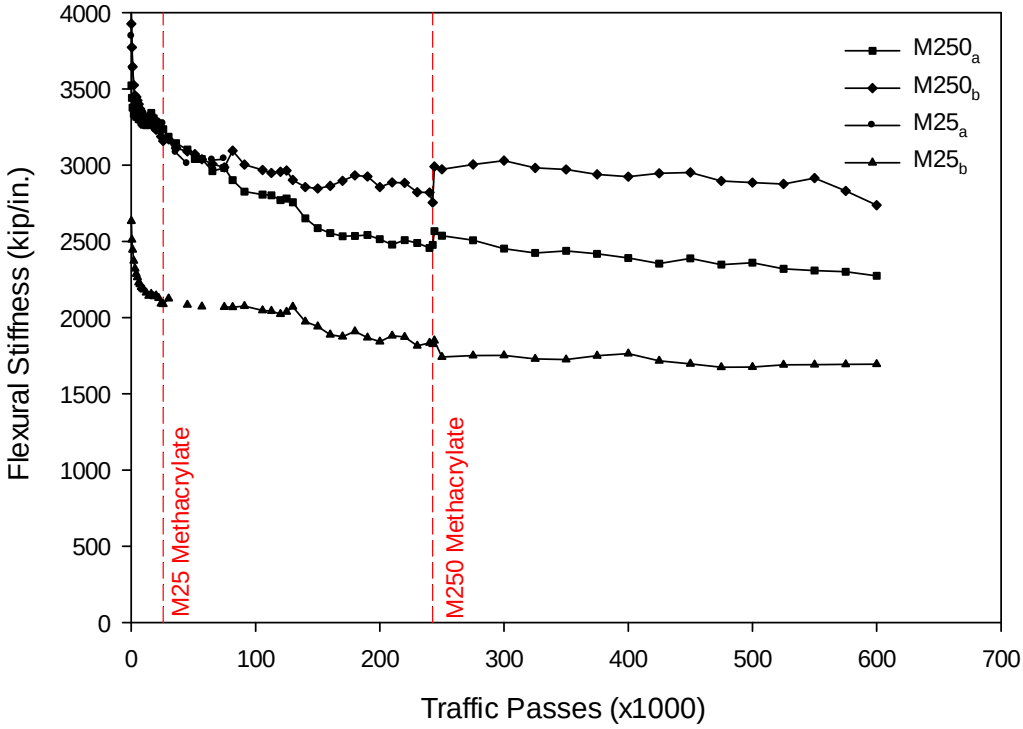

Figure 50: Flexural stiffness of Panel Set 2 based on quarter-point displacements.

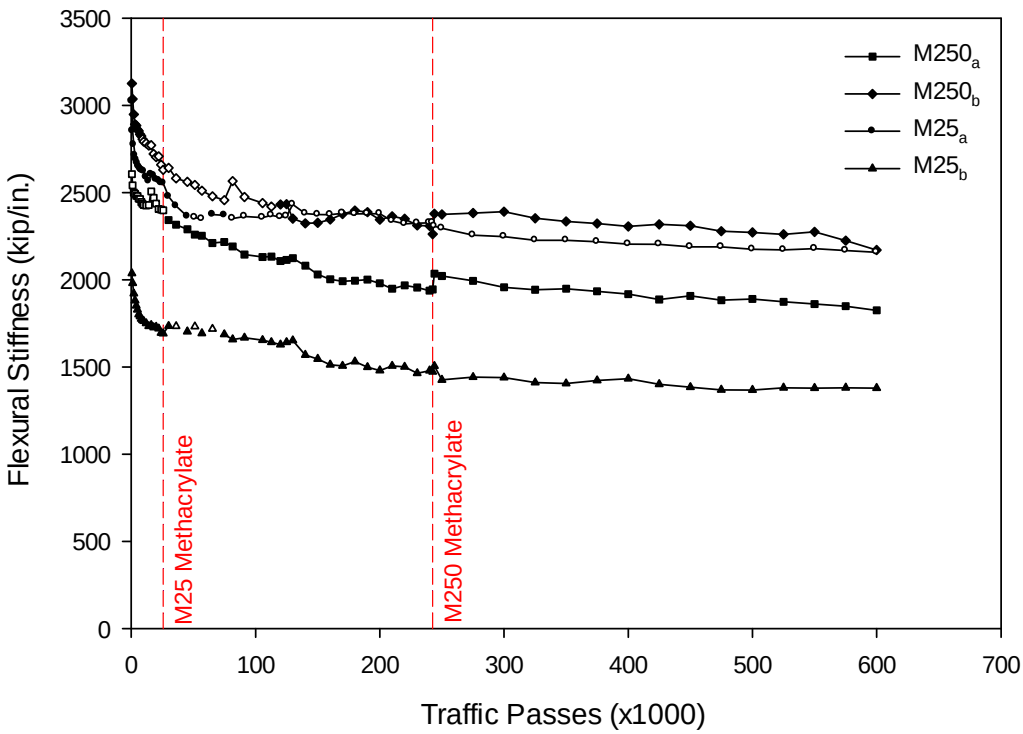

Figure 51: Average flexural stiffness of Panel Set 2.

Referring to Figure 46 through Figure 51, while load and displacement for each of the test panels was measured in the same manner, differences in the support and/or connection conditions between the test panels and the support frame and the material properties of the test panels caused the absolute magnitudes of the stiffnesses of each panel to be different from one another. These differences could have been related to the rigidity of the test frame along the length, placement and fit of the shims, small differences in the concrete or reinforcing steel, or a combination of all of these and other factors. Focusing on the average stiffness values (average of center-point and quarter-point values) reported for each panel in Figure 48 and Figure 51, the slabs in Panel Set 2 tended to be stiffer than those in Panel Set 1. At 250,000 cycles of applied load, for example, the untreated slabs in Panel Set 2 had an average stiffness of about 2200 kips/in., 54 percent greater than the average stiffness of the slabs in Panel Set 1 at this same cycling interval.

Independent of specific level of initial stiffness, all panels demonstrated similar behavior as cycling proceeded, consisting of a) a sharp decline in stiffness in the first 25,000–100,000 load passes (exhibiting about 80 and 25 percent decrease in stiffness in Panel Sets 1 and 2, respectively), b) a subsequently more gentle decrease in stiffness through approximately 250,000 load passes (with a further decrease in stiffness of approximately 12 and 6 percent, respectively in Panel Sets 1 and 2), and c) finally, a very gradual further decay in stiffness until testing was terminated (at 2,122,978 and 604,932 load cycles in Panel Sets 1 and 2, respectively).

Panel stiffness generally increased after HMWM treatment. As may be obvious, HMWM application did not fully restore panel stiffness to precracked conditions, as only the top surface of the panels were treated. The greatest increase in stiffness was observed for the M1000 panels, in which stiffness increased by an average of 10 percent as a result of the HMWM treatment. As would be expected, the percentage increase in stiffness of the treated panels was proportional to the degree of top cracking the panels had experienced at the time of treatment. The average percent change in stiffness for the M25, M250 and M1000 treated panels as a function of average percent of top cracking at the time of treatment is plotted in Figure 52. Across the limited crack conditions and treatment times considered herein, the percent change in stiffness generally appeared to increase at an increasing rate as treatments were applied at higher levels of cracking, with the exception of the $M25_a$ panel which continued to decrease in stiffness after treatment.

The effect of HMWM application on subsequent changes in panel stiffness as cycling proceeded was evaluated by considering the percent change in average stiffness of each pair of treated panels relative to that of other treated and untreated panels across comparable cycles of applied load. Cycle intervals used in this analysis were simply defined by the application points of the HMWM treatments in conjunction with the points at which testing concluded (i.e., at approximately 25,000; 250,000; 600,000; 1,000,000 and 2,000,000 cycles of applied load). Stiffness changes in each interval were simply calculated as the change in panel stiffness across the interval divided by the initial stiffness of the panel immediately prior to the beginning of the interval. The results of this incremental stiffness analysis are presented in Figure 53. In all intervals, greater relative degradation in stiffness occurred in the untreated versus treated test panels. Referring to Figure 53, the difference in relative stiffness degradation following HMWM treatment was similar for the M25 and M250 panels, with the positive effect of the HMWM treatment at 25,000 load cycles beginning to diminish in the 250,000 to 600,000 interval. The most pronounced difference in stiffness performance was seen following the treatment of the M1000 panels at 1,071,820 cycles of applied load, following which the average stiffness decreases by only 4 percent in the treated panels over the next 1,000,000 load cycles, compared to a stiffness decrease of 34 percent in the untreated panels.

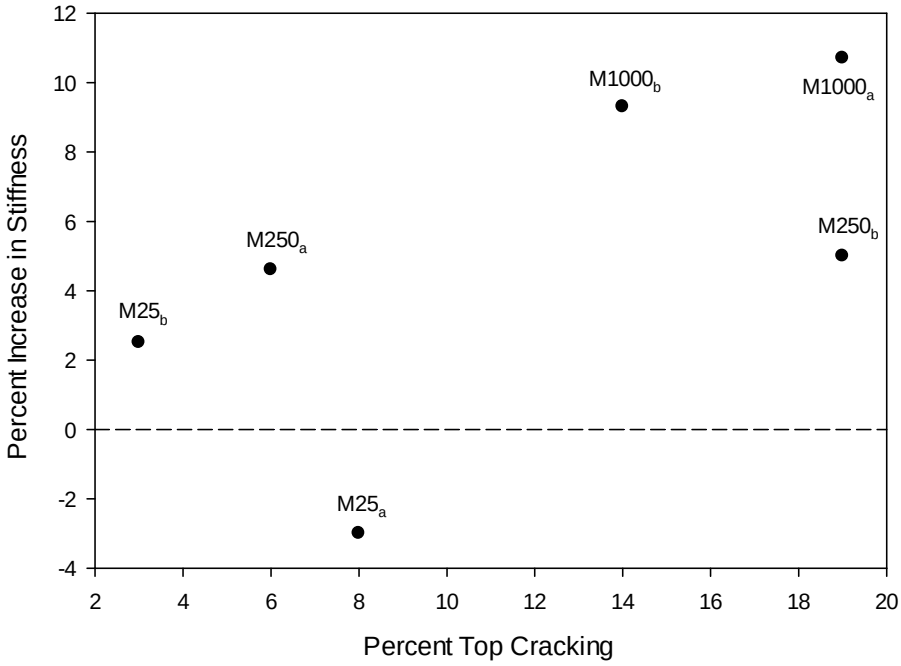

Figure 52: Percent cracking versus percent increase in stiffness.

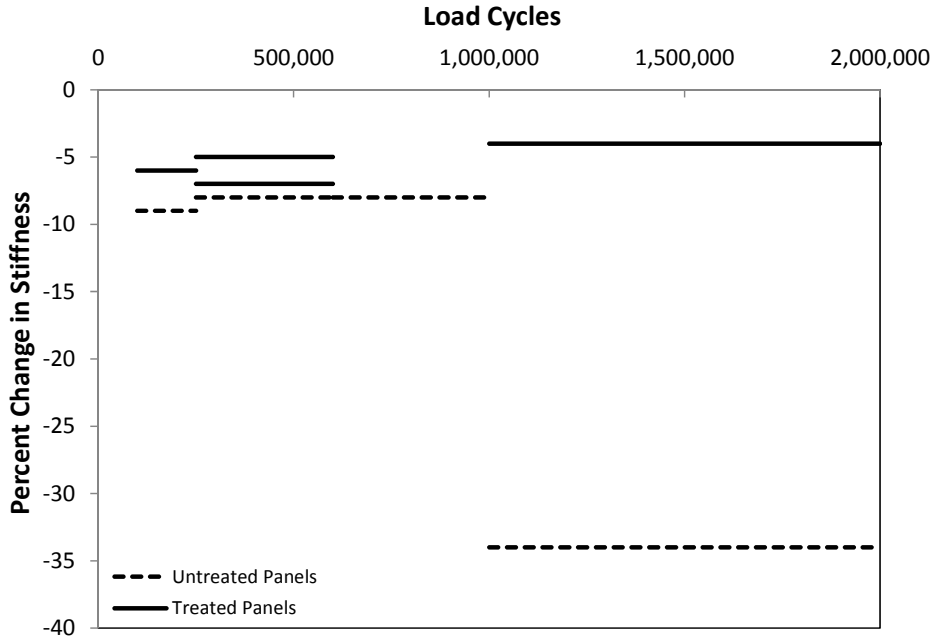

Figure 53: Percent change in stiffness as a function of traffic.

The basic correlation between changes in stiffness and changes in the physical condition of the panels was further explored by plotting stiffness as a function of level of cracking for the control panels. More specifically, stiffness was plotted as a function of percent cracked area at coincident cycle levels for the average flexural response of the two control panels, as shown in

Figure 54. Reference "original" stiffness values were actually taken as the stiffness at approximately 70,000 cycles of applied load, at and after which much of the localized variability in the earlier calculated stiffness values was no longer present. Referring to Figure 54, changes in stiffness well represent accumulated cracking in the top surface of the test slabs over the range of top surface distress generated in this program. The correlation coefficient between these two parameters was 93 percent, indicating that average flexural stiffness possibly can be reasonably used to infer distress condition in deck slabs, at least through 10 to 20 percent cracked area. That being said, and recognizing the limited amount of data used in generating the relationship portrayed in Figure 54, the stiffness could be becoming insensitive to further accumulated distress above 15 percent cracked area.

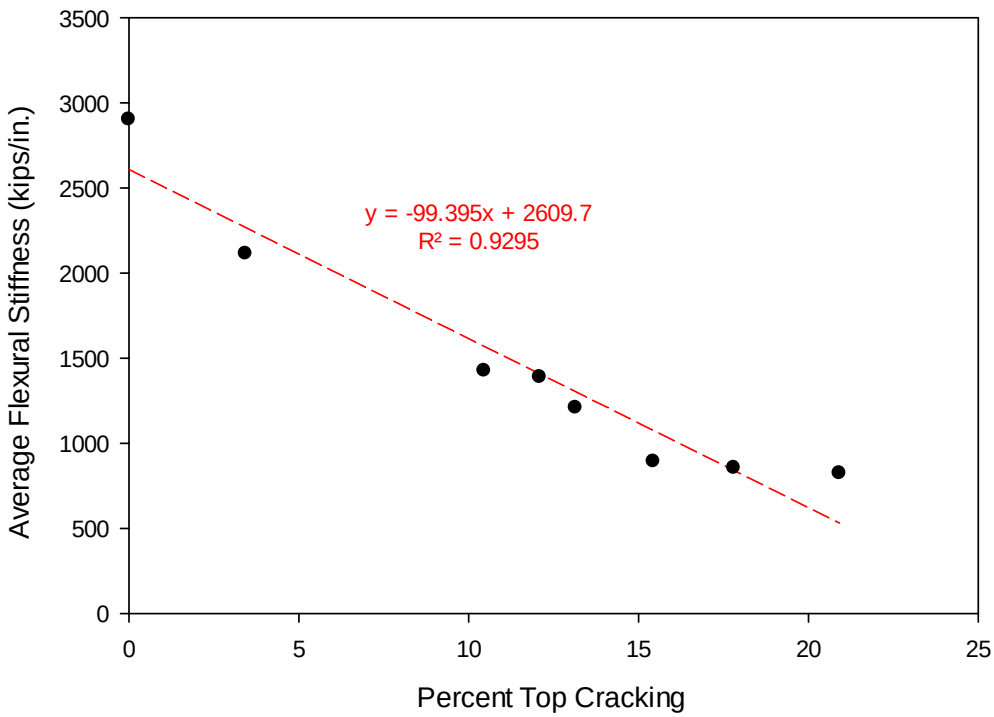

Figure 54: Average flexural stiffness as a function of top cracking for the Control test panels.

CONCLUSIONS AND RECOMMENDATIONS

In this investigation, multiple full-scale concrete bridge deck slabs were trafficked in the laboratory under a cyclic, rolling wheel load to study the effects of HMWM treatments on their fatigue performance. Based solely on traffic-induced stresses, comparisons between test panels treated at various levels of traffic generally indicated that later applications of HMWM will likely result in greater structural benefit. This result was most evident in the two sets of deck panels that were trafficked for over two million load cycles. Panels treated at approximately one million cycles retained about 30 percent more of their flexural stiffness under subsequent trafficking compared to panels that were left untreated. Test panels treated at earlier times (at approximately 25,000 and 250,000 traffic cycles) also showed a benefit, but to a much lesser extent, retaining only 1 to 4 percent more of their stiffness under subsequent load cycles relative to untreated panels. In the case of these earlier treated panels, however, the test program was terminated before they could be trafficked at levels comparable to the later treated panels (due to resource and time constraints), making it impossible to comment with full certainty on the relative benefit of early versus later HMWM treatment. Furthermore, while the results of this project appear to suggest that later application of HMWM may be more beneficial, environmental effects and ingress of water and/or chlorides which are known to accelerate damage in untreated bridge decks was not considered. Early sealing could play an important role in mitigating damage from these mechanisms. The above conclusions are based on trafficking eight test panels under a 20-kip rolling wheel load and visually monitoring their distress condition (crack mapping) and flexural stiffness (based on load-deflection behavior) as trafficking proceeded.

This effort began with the development and design of the specimens and associated support fixtures to reproduce in the laboratory structural stress conditions experienced in full-size box girder bridge decks in the field. Once completed, rolling wheel load testing of representative full size test panels began. Six of the eight test panels subsequently were treated with HMWM at various traffic levels, with two panels being treated at each level, resulting in four treatment/traffic combinations, namely treated at approximately 25,000; 250,000 and 1,000,000 load cycles and untreated (control). Based on the two control panels, the degree/extent of cracking in the top surface of the slabs and their flexural stiffness were found to be directly related to the level of trafficking and distress these test panels experienced. At approximately two million load cycles, the control test panels had experienced approximately 15 to 18 percent of the top surface area was cracked, and maximum crack widths were 0.040 in. Application of HMWM bonded existing cracks together which significantly limited further top surface crack growth and stiffness deterioration. Bottom cracks were not affected by HMWM treatment and continued to grow as trafficking progressed.

None of the panels reached the end of their useful life. Conservative estimates made prior to trafficking suggested that the test panels may reach a serviceability-based fatigue failure in up to

11,000,000 cycles using a 20-kip rolling wheel load. The extent of cracking and its severity were minimal across all panels, even in the control (untreated) test panels that were subjected to two million wheel passes. The damage in these panels was just approaching the level for potential rehabilitative action based on current protocols used by Caltrans maintenance personnel. Because the test panels had not reached their useful life, a life-cycle cost analysis was not able to be performed.

Overall, this research effort successfully met the stated objective in that it resulted in a laboratory based approach to evaluate the effects of HMWM treatments on the fatigue-related distresses in representative concrete bridge deck panels; nevertheless, in moving forward the following suggestions should be considered to potentially improve similar future endeavors.

1. Center-point, quarter-point and edge displacement measurements were used to characterize the deflection profile of the test panel during trafficking, and this information was used to evaluate the flexural stiffness of the test panels over time. Each of these measurements was made at a single point on each test panel (i.e., three sensors were used for each test panel). Malfunctioning instrumentation and sensors resulted in gaps in the data; therefore, it is suggested that any such critical measurements be duplicated to ensure consistent data over time. Additionally, deflection profiles across the panel may not be symmetrical as the panels experience damage.
2. Significant effort was spent designing and building a rigid support system to simulate stress conditions in the flat test slabs consistent with those in a box girder bridge deck. In clamping the panels to the frame, multiple shims of various thicknesses were used to ensure proper contact (i.e., full support) of the bottom edge of the test panel and the top edge of the support frame. Despite the effort put into this clamping operation, flexural stiffness results indicated that support of the panels may have been slightly different, panel to panel. Further investigation is suggested to determine a more reliable method of supporting the test panels to ensure that the desired support conditions are consistently and predictably produced. One such idea is to use the configuration utilized by Yoshitake et al. (2010) to generate translational and rotation fixity along the edge of full size laboratory deck slab models. Rather than using a double row of clamping bolts along each edge of the panel, they elected to use a single row of bolts at the extreme outer edge of the panel, complemented by an adjacent roller, to create a tension/compression moment resisting couple along the panel edge.
3. Time and budget constraints made it necessary to terminate traffic loading of the second set of test panels at about 600,000 traffic passes. Because of this, it is unknown how early applications of HMWM will affect longer term fatigue

performance of the panels (say out through 2,000,000 load cycles). It is recommended, therefore, to continue to traffic the second set of test panels to evaluate their behavior over the same level of trafficking as the first set (i.e., 2,000,000 cycles). It would take approximately four months to apply these additional load cycles.

4. The applied load used during trafficking of the test panels of 20 kips was higher than typical truck loading (usually around 9 kips). In this investigation the wheel loads were purposefully increased to induce fatigue-related distresses in the test panels over a shorter period of time. Even so, fatigue distresses were just approaching the level where treatments such as HMWM are considered. In order to accelerate crack growth and severity it is suggested that the applied load be increased in future testing, or some consideration be given to slightly thinner test panels.

5. There are a variety of concrete bridge deck rehabilitation treatments currently on the market (e.g., polyester concrete overlays, Portland cement overlays, asphalt concrete overlays). Based on the success of this research effort to determine the performance of HMWM, it is suggested that a similar approach be taken to evaluate other available rehabilitation techniques.

REFERENCES

AASHTO – American Association of Highway Transportation Officials, "Guide manual for Bridge Element Inspection," Washington, D.C., 2011.

ACI Committee Report 224.1R-93, Causes, Evaluation and Repair of Cracks in Concrete Structures, American Concrete Institute, Detroit, Michigan, 1993.

ACI Committee Report 345R-91, Guide for Concrete Highway Bridge Deck Construction, ACI Manual of Concrete Practice, American Concrete Institute, Detroit, Michigan, 1991.

ACI Committee Report 503R-93, Use of Epoxy Compounds with Concrete, American Concrete Institute, Detroit, Michigan, 1993.

ACI Committee 345.1R-92, Routine Maintenance of Concrete Bridges, ACI Manual of Concrete Practice, Part 2, pp. 345R-1R-1-13. 1992.

Aktan, H. and Fu, G., Investigate Causes and Develop Methods to Minimize Early-Age Cracking on Michigan Bridge Decks, Technical Report, Wayne State University, Detroit, Mich., 2003.

Al-Qadi, I. L., Weyers, R. E., Galagedera, N. L., "Preformed Membrane Performance under Control Conditions." Transportation Research Record, No. 1371, 1992.

ASTM C39. "*Standard Test Method for Compressive Strength of Cylindrical Concrete Specimens*," West-Conshohocken, PA, ASTM International, 2010.

ASTM C78. "*Standard Test Method for Flexural Strength of Concrete (Using Simple Beam with Third-Point Loading,"* West-Conshohocken, PA, ASTM International, 2010.

ASTM C1202. "*Electrical Indication of Concrete's Ability to Resist Chloride Ion Penetration,"* West-Conshohocken, PA, ASTM International, 2010.

ASTM C1585. "*Measurement of Rate of Absorption of Water by Hydraulic-Cement Concretes,"* West-Conshohocken, PA, ASTM International, 2011.

Attanayaka, A. M., Duyar, O., Liang, X., Aktan, H. M., and Hg, K. Y., "Fundamentals of the Use of Penetrating Sealants for Concrete Bridge Deck Protection," Transportation Research Board (TRB) 2003 CD-ROM, Washington, D.C., 2003.

Babaie, K. and Hawkins, N. M., NCHRP Report 297: Evaluation of Bridge Deck Protective Strategies, Transportation Research Board, National Research Council, Washington, D.C., 1987.

Bousias, S. "Subject: RC Bridge Decks Under Moving Load." E-mail to the author, July, 2009.

Burrows, R. W., "The Visible and Invisible Cracking of Concrete." ACI Monograph No. 11. ACI, Detroit, Mich., 1998.

Byron, T., Choubane, B. and Tia, M. "Assessing Different Loading Configurations in Accelerated Pavement Testing," Florida Department of Transportation Materials Research Park, 2004.

Caltrans Bridge Deck Construction Manual, State of California Department of Transportation, Division of Structures, Office of Structure Construction, 1991.

Caltrans Maintenance Manual, Volume 1, Chapter H: Bridges, pp H-16, 2006.

Caltrans Bridge Deck Investigations and Maintenance Actions: Recommended Investigation Guidelines for Area Bridge Maintenance Engineers, PowerPoint presentation given to maintenance engineers, 2007.

Carden, A. C. and Ramey, G. E., "Weather, Exposure and its Effect on Bridge Deck Curing in Alabama." Practice Periodical on Structural Design and Construction, November 1999.

Doody, M. E. and Morgan, R., Polymer-Concrete Bridge Deck Overlays, Special Report 110, Report FHWA/NY/93/110, New York State DOT, 1993.

El-Gamal, S., El-Salakawy, E.F., and Benmokrane, B. "Behavior of Concrete Bridge Deck Slabs Reinforced with Fiber-Reinforced Polymer Bars Under Concentrated Loads," ACI Structural Journal, Vol. 102, No. 5, pp. 727–735, 2005.

El-Gamal, S., El-Salakawy, E.F., and Benmokrane, B. "Influence of Reinforcement on the Behavior of Concrete Bridge Deck Slabs Reinforced with FRP Bars," ASCE Journal of Composites for Construction. Vol. 11, No. 5, pp. 449-458, 2007.

El-Ragaby, A., El-Salakawy, E., and Benmokrane, B. "Fatigue Life Evaluation of Concrete Bridge Deck Slabs Reinforced with Glass FRP Composite Bars," ASCE Journal of Composites for Construction. Vol. 11, No. 3, pp. 258-268, 2007.

Embacher, R., Snyder, M. and Odden, T. "Using the Minnesota Accelerated Loading Facility to Test Retrofit Dowel Transfer Systems," Transportation Research Record No. 1769, Journal of the Transportation Research Board, 2001.

Engstrom, 1994, Field Performance of High Molecular Weight Methacrylate Monomers and Silanes on a D-Cracked, Jointed Reinforced Concrete Pavement, Mn/RD-94/07.

Gebreyouhannes, E., Chijiwa, N., Fujiyama, C., and Maekawa, K. "Shear Fatigue Simulation of RC Beams Subjected to Fixed Pulsating and Moving Loads," Journal of Advanced Concrete Technology, Vol. 6, No. 1, p. 215-226, 2008.

Gilbert A.M. "Validation of a Laboratory Method for Accelerated Fatigue Testing of Bridge Deck Panels with a Rolling Wheel Load," Thesis submitted in partial fulfillment of the requirements for the degree of Master of Science in Civil Engineering, Montana State University, 2011.

Graddy, J.C., Kim, J., Whitt, J.H., Burns, N.H., and Klingner, R.E. "Punching-Shear Behavior of Bridge Decks under Fatigue Loading," ACI Structures Journal, 903, p. 257-266, 2002.

Hadidi, R. and Saadeghraziri, M. A., "State of the Art of Early Age Transverse Cracking of Concrete Bridge Decks," 82nd Annual Meeting of the Transportation Research Board, Jan. 12–16, 2003, Compendium of Papers (CD-ROM), Washington, D.C., 2003.

Hartt W. H. and Nam, J., "Critical Parameters for Corrosion-Induced Deterioration of Marine Bridge Substructures in Florida." Prepared for the Florida Department of Transportation. 2004.

Hassan, A., Kawakami, M., Niitani, K., Yoshioka, T. "An Experimental Investigation of Steel-Free Deck Slabs," Canadian Journal of Civil Engineering, Vol. 29, p. 831-841, 2002.

Harvey, J., Popescu, L., Ali, A. and Bush, D. "Performance of Dowel Bar Retrofitted Concrete Pavement under Heavy Vehicle Simulator Loading," Transportation Research Record No. 1823, Journal of the Transportation Research Board, 2007.

Hausmann, D. A., "A Probability Model of Steel Corrosion in Concrete," Materials Performance, V. 37, No 10, 1998.

Hobbs, D. W., "Aggregate Influence on Chloride Ion Diffusion into Concrete." Cement and Concrete Research, Vol. 29, No. 12, 1999.

Huang, Y., Adams, T.M., Pincheira, J.A. "Analysis of Life-Cycle Maintenance Strategies for Concrete Bridge Decks," Journal of Bridge Engineering, Vol. 9, No. 3, pp. 250-258, 2004.

Hughes, J.J. Rosphalt-50 Bridge Deck Overlay, Final Report, Pennsylvania Department of Transportation, 1994.

Ibrahim, A.M., and Mahmood, M.S. "Finite Element Modeling of Reinforced Concrete Beams Strengthened with FRP Laminates," European Journal of Scientific Research, Vol. 30, No. 4, pp. 526-541, 2009.

Johnson, K., Schultz, A.E., French, C.E., Reneson, J. "Crack and Concrete Deck Sealant Performance," MN/RC 2009-13, Final report to the Minnesota Department of Transportation, 2009.

Juenger, M. C. G., and Jennings, H. M., "Examining the Relationship between the Microstructure of Calcium Silicate Hydrate and Drying Shrinkage of Cement Pastes," Cement and Concrete Research, Vol. 32, No. 2, 2002.

Kachlakev; D., Miller, T., Yim, S., Chansawat, K., and Potisuk, T. "Finite Element Modeling of Reinforced Concrete Structures Strengthened with FRP Laminates," California Polytechnic State University, San Luis Obispo, CA and Oregon State University, Corvallis, OR for Oregon Department of Transportation, 2001.

Khanna, O.S.; Mufti, A. A.; and Bakht, B. "Experimental Investigation of the Role of Reinforcement in the Strength of Concrete Deck Slabs," *Canadian Journal of Civil Engineering*, V. 27, pp. 475-480, 2000.

Kolb, M., Tidd, M., and Humphrey, D., "Evaluation of Bridge Deck Wearing Surfaces and Protective Systems." FHWA-ME-90-5, Tech Paper 90-5, Maine Department of Transportation, 1992.

Krauss, P. D. and Rogalla, E. A., NCHRP Report 380: Transverse Cracking in Newly Constructed Bridge Decks, Transportation Research Board, National Research Council, Washington, D.C., 1996.

Kuang, J.S. and Morley, C.T. "Punching Shear Behavior of Restrained Reinforced Concrete Slabs," ACI Structural Journal, Vol. 89, No. 1, pp. 13-19, 1992.

Kushner, R. G., Fowler, D. W., and Wheat, D. L., "Mechanical and Durability Properties of a High Molecular Weight Methacrylate Polymer Concrete." Polymer Modified Concrete, ACI SP-99, 1987.

Lee, M.J. and Reis, R.A. "High Molecular Weight Methacrylate Crack Penetration Study," Presentation delivered at Western Bridge Preservation Partnership Meeting, AASHTO TSP·2, Sacramento, CA, 2010. (http://www.pavementpreservation.org/wp-content/uploads/presentations/Lee High Molecular Weight Methacrylate Crack Penetration Study - Compressed.pdf).

Linford, E.T. "Development of an Index for Concrete Bridge Deck Management in Utah," M.S. thesis submitted to Brigham Young University, Department of Civil and Environmental Engineering, Provo, UT, 2006.

Maekawa, K., Gebreyouhannes, E., Mishima, T., and An, X. "Three-Dimensional Fatigue Simulation of RC Slabs under Travelling Wheel-Type Loads," Journal of Advanced Concrete Technology, Vol. 4, No. 3, p. 445-457, 2006.

Mangum, W.D., Bermudez-Goldman, A.J., Whitney, D.P., Fowler, D.W., Meyer, A.H., Repairing Cracks in Portland Cement Concrete Using Polymers, Research Report 385-27, University of Texas, Austin, 122 p., 1986.

Marks, V. J., "High Molecular Weight Methacrylate Sealing of a Bridge Deck." Transportation Research Record 1204, Washington, D.C., 1988.

Matsui, S., Tokai, D., Higashiyama, H., and Mizukoshi, M. "Fatigue Durability of Fiber-Reinforced Concrete Decks under Running Wheel Load," Proceedings: 3rd International Conference on Concrete under Severe Conditions, University of British Columbia, Vancouver, Canada, p. 982–991, 2001.

McGovern, J. F., "Report of the Committee on Bridge and Culvert Maintenance." Highway Research Abstract, Vol. 25, No. 3, 1955.

Meggers, D., "Crack Sealing and Repair of Older Serviceable Bridges Using Polymer Sealers." Kansas Department of Transportation, Report No. FHWA-KS-98-4, 1998.

Mehta, P. K., "Durability of Concrete — Fifty Years of Progress?" Durability of Concrete, SP-126, American Concrete Institute, Farmington Hills, Mich., 1991, pp. 1-31

NCHRP Synthesis of Highway Practice 4: Concrete Bridge Deck Durability, Transportation Research Board, National Research Council, Washington, D.C., 1970.

NCHRP Synthesis of Highway Practice 57: Durability of Concrete Bridge Decks, Transportation Research Board, National Research Council, Washington, D.C., 1979.

NCHRP Synthesis of Highway Practice 220: Waterproofing Membranes for Concrete Bridge Decks, Transportation Research Board, National Research Council, Washington, D.C., 1995.

Newhook, J. P. "The Behavior of Steel-Free Concrete Bridge Deck Slabs Under Static Loading Conditions," PhD thesis, DalTech, Dalhousie University, Halifax, Nova Scotia, Canada, 1997.

Nowak, A., Szerszen, M., and Juntunen, D. Michigan Deck Evaluation Guide, UMCEE 99-14, prepared by the University of Michigan for the Michigan Department of Transportation, 2000.

Page, C. L., Short, N. R., and Holden, W. R., "The Influence of Different Cements on Chloride-Induced Corrosion of Reinforcing Steel." Cement and Concrete Research, 1986.

Perdikaris, P.C., and Beim, S. "RC Bridge Decks under Pulsating and Moving Load," Journal of Structural Engineering, 1143, p. 591–607, 1988.

Perdikaris, P.C., Beim, S.R., and Bousias, S.N. "Slab Continuity Effect on Ultimate and Fatigue Strength of Reinforced Concrete Bridge Deck Models," ACI Structural Journal, 86(4) p. 483-491, 1989.

Perdikaris, P.C. "Subject: RC Bridge Decks Under Moving Load." E-mail to the author, July, 2009.

Petrou, M., Perdikaris P. C., and Wang A. "Fatigue Behavior of Non-composite Reinforced Concrete Bridge Deck Models," *Transportation Research Record 1460*, TRB, National Research Council, Washington, D.C., pp.73-80, 1994.

Petrou, M. "Subject: RC Bridge Decks Under Moving Load." E-mail to the author, July, 2009.

Rahim, A., Jansen, D., and Abo-Shadi, N., Concrete Bridge Deck Crack Sealing: An Overview of Research, prepared by the California Polytechnic State University for the California Department of Transportation, Sacramento, CA, 2006.

Ramey, G. E. and Derickson, J. P., "Performance of Bonded Bridge Deck Overlays in Alabama." Practice Periodical on Structural Design and Construction, ASCE. 2003.

Ramirez, T. L., Polymer Concrete Overlays for Bridge Decks. FHWA-PA-94-015-83-29, Final Report Research Project No. 83-29, 1995.

Rooney, H. A. and Shelly, T. L., Thin Resinous and Aggregate Overlays on Portland Cement Concrete. Report prepared for State of California Department of Public Works, Division of Highways, Materials and Research Department. Report No. 635121, 1969.

Roesler, J.R. and Barenberg, E. J. "Fatigue and Static Testing of Concrete Slabs, TRR 1684, TRB, National Research Council, Washington, D.C., pp 71-80, 1999.

Russell, NCHRP Synthesis 333: Concrete Bridge Deck Performance: A Synthesis of Highway Practice, National Cooperative Highway Research Program, TRB, 2004.

Sagues A. A., and Kranc, S. C., Applied Modeling for Corrosion Protection Design for Marine Bridge Substructures, prepared for the Florida Department of Transportation, 1997.

Samples L. M. and Ramirez, J. A., Methods of Corrosion Protection and Durability of Concrete Bridge Decks Reinforced with Epoxy-Coated Bars, Phase I. FHWA/IN/JTRP-98/15. Purdue University, Indiana, 1999.

Sonoda, K., and Horikawa, T. "Fatigue Strength of Reinforced Concrete Slabs under Moving Loads," Proceedings: IABSE Colloquium on Fatigue of Steel and Concrete Structures, International Association for Bridge and Structural Engineering, Zurich, Switzerland, p. 455-462, 1982.

Soriano, A., Alternative Sealants for Bridge Decks. Final Report No. SD2001-04-D, Prepared for the South Dakota Department of Transportation, 2002.

Sprinkel, M. and DeMars M., (1995) "Gravity-fill Polymer Crack Sealers," Transportation Research Record 1490, Jul 1995, p43-53.

Sprinkel, M. M., Sellars, A. A., and Weyers, R. E., "Rapid Concrete Bridge Deck Protection, Repair, and Rehabilitation." Concrete Bridge Protection and Rehabilitation: Chemical and Physical Techniques, Report No. SHRP-S-344, Strategic Highway Research Program, National Research Council, Washington, D.C., 1993.

Stordahl, A. "Validation of Rehabilitation Strategies to Extend the Service Life of Concrete Bridge Decks," Professional Paper submitted in partial fulfillment of the requirements for the degree of Master of Science in Civil Engineering, Montana State University, 2009.

Transportation Research Circular E-C107, Control of Cracking in Concrete—State of the Art, Transportation Research Board, Washington, D.C., 2006.

Tsiatas, G. and Robinson, J., "Durability Evaluation of Concrete Crack Repair Systems." CD-ROM of the Transportation Research Board Annual Meeting, Washington, D.C. 2002.

Tuttle, R.S. "Condition Analysis of Concrete Bridge Decks in Utah", M.S. thesis submitted to Brigham Young University, Department of Civil and Environmental Engineering, Provo, UT, 2005.

Weiss, W. J., Yang, W. and Shah, S. P., "Factors Influencing Durability and Early-Age Cracking in High Strength Concrete Structures." SP 189-22. High Performance Concrete: Research to Practice, Farmington Hills, Mich., 1999.

Wolanski, A.J. "Flexural Behavior of Reinforced and Pre-stressed Concrete Beams Using Finite Element Analysis," Master's Thesis, Marquette University, Milwaukee, Wisconsin, 2004.

Xi, Y., Shing, B., Abu-Hejleh, N., Asiz, A., Suwito, A., Xie, Z. H., and Ababneh, A., "Assessment of the Cracking Problem in Newly Constructed Bridge Decks in Colorado." Colorado DOT Report No. CDOT-DTD-R-2003-3.

Yohitake, I., Kim, Y.J., Yumikura, K., Hamada, S. "Moving-Wheel Fatigue for Bridge Decks Strengthened with CFRP Strips Subject to Negative Bending," ASCE Journal of Composites for Construction, Vol. 14, No. 6, pp. 784-790, 2010.

APPENDIX A – DECK SLAB REINFORCEMENT DETAILS

Bridge Design Details – September 1993

Deck Slab Reinforcement

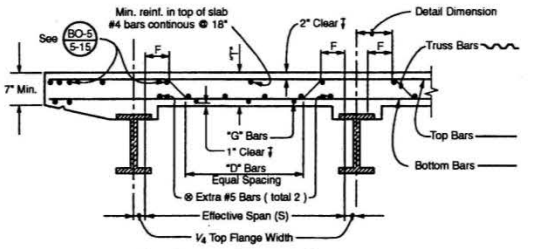

Slab On Steel Girders

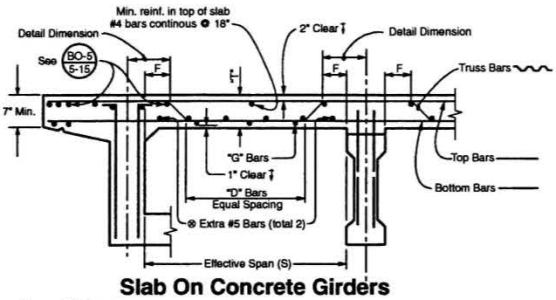

Slab On Concrete Girders

Detail Data:

Designers to specify span to be used and girder width.

⊗ Extra "D" bars to be added when S ≥ 11'.

Notes:

For culverts or bridge slabs supporting fill, note provisions of BDS 6.4.

Design based on decks having 3 or more girders.

For 2 girder decks a special design is required.

Effective overhang shall not be greater than ½ the effective span (s).

T Increase cover over bars and adjust slab thickness if required for environmental conditions. See BDS 8.22 and Memo to Designers 8-2.

Design Data:

Design Stresses: See BDS 8.15

fs = 20,000 lbs. per sq. in.

fc = 1200 lbs. per sq. in.

n = 10

Design Loads: See BDS 3.24

M_{DL} (ft-k) = $\frac{wS^2}{10}$

M_{LL} + I (ft-k) = $\frac{P(S+2)}{32} \times 1.30 \times 0.80 = .52(S+2)$

w = Weight per lin. ft. width of slab.

(includes 35 #/ft.^{2} deck overlay allowance.)

S = Effective span

Impact factor 1.30

Continuity factor 0.08

P = Wheel load = 16^k

Distribution Reinforcement:

220 / $\sqrt{S}$, max. = 67%. See BDS 3.24.10

"S" Effective Span	"T" Top Slab	Dim. "F"	Trans. Bars Size	Trans. Bars Spacing	"D" Bars #5 Bars	"G" Bars #4 Bars
4' - 0"	6 1/2	6"	#5	13"	4	2
4' - 3"	6 5/8"	7"		13"	4	2
4' - 6"	6 3/4"	7"		12"	4	2
4' - 9"	6 7/8"	7"		12"	4	3
5" - 0"	6 7/8"	8"		12"	4	
5" - 3"	7"	8"		12"	4	
5' - 6"	7 1/8"	9"		11"	4	
5' - 9"	7 1/8"	9"		11"	4	
6' - 0"	7 1/4"	9"		11"	4	
6' - 3"	7 3/8"	10"		11"	5	
6' - 6"	7 1/2"	10"		11"	5	
6' - 9"	7 1/2"	11"		10"	5	
7' - 0"	7 5/8"	11"		10"	6	
7' - 3"	7 3/4"	11"		10"	6	
7' - 6"	7 3/4"	1' - 0"	#5	10"	6	3
7' - 9"	7 7/8"	1' - 0"	#6	13"	7	4
8' - 0"	8"	1' - 1"		13"	7	
8' - 3"	8 1/8"	1' - 1"		13"	7	
8' - 6"	8 1/8"	1' - 1"		13"	8	
8' - 9"	8 1/4"	1' - 2"		13"	8	
9' - 0"	8 3/8"	1' - 2"		13"	8	
9' - 3"	8 3/8"	1' - 2"		12"	10	
9' - 6"	8 1/2"	1' - 3"		12"	10	
9' - 9"	8 5/8"	1' - 3"		12"	10	
10' - 0"	8 5/8"	1' - 4"		12"	10	
10' - 3"	8 3/4"	1' - 4"		12"	11	
10' - 6"	8 7/8"	1' - 4"		12"	11	4
10' - 9"	8 7/8"	1' - 5"		11"	12	5
11' - 0"	9"	1' - 5"		11"	12	
11' - 3"	9 1/8"	1' - 6"		11"	12	
11' - 6"	9 1/8	1' - 6"		11"	13	
11' - 9"	9 1/4"	1' - 6"		11"	13	
12' - 0"	9 3/8"	1' - 7"		11"	13	
12' - 3"	9 1/2"	1' - 7"		11"	13	
12' - 6"	9 1/2"	1' - 7"		10"	15	
12' - 9"	9 5/8"	1' - 8"		10"	15	
13' - 0"	9 3/4"	1' - 8"		10"	15	
13' - 3"	9 3/4"	1' - 9"		10"	15	
13' - 6"	9 7/8"	1' - 9"		10"	16	
13' - 9"	10"	1' - 9"		10"	16	
14' - 0"	10 1/8"	1' - 10"		10"	16	
14' - 3"	10 1/4"	1' - 10"	#6	10"	16	
14' - 6"	10 3/8"	1' - 11"	#7	13"	17	
14' - 9"	10 1/2"	1' - 11"		13"	17	
15' - 0"	10 1/2"	1' - 11"		13"	18	5
15' - 3"	10 5/8"	2' - 0"		13"	18	6
15' - 6"	10 3/4"	2' - 0"		13"	18	
15' - 9"	10 7/8"	2' - 1"		12"	19	
16' - 0"	10 7/8"	2' - 1"		12"	19	
16' - 3"	11"	2' - 1"		12"	20	
16' - 6"	11 1/8"	2' - 2"		12"	20	
16' - 9"	11 1/8"	2' - 2"		12"	20	
17' - 0"	11 1/4"	2' - 3"		12"	20	
17' - 3"	11 3/8"	2' - 3"		12"	20	6
17' - 6"	11 1/2"	2' - 3"		11"	22	7
17' - 9"	11 1/2"	2' - 4"		11"	22	
18' - 0"	11 5/8"	2' - 4"		11"	22	
18' - 3"	11 3/4"	2' - 4"		11"	23	
18' - 6"	11 7/8"	2' - 5"		11"	23	
18' - 9"	11 7/8"	2' - 5"		11"	23	
19' - 0"	12 "	2' - 6"		11"	23	
19' - 3"	12 1/8"	2' - 6"		11"	23	
19' - 6"	12 1/4"	2' - 6"		11"	23	
19' - 9"	12 1/4"	2' - 7"		11"	24	
20' - 0"	12 3/8"	2' - 7"	#7	10"	26	7

Deck Slab Reinforcement — *Page 8-30*

APPENDIX B – CALTRANS CONCRETE MIX DESIGN

Approved 07-31-07 RW 666 & 611 CIP Pension

17

Hanson

CONCRETE PROPORTIONS

MIX ID : 4133815 [03] 28.00 MPA 7/17/2007

CONTRACTOR : COFFMAN SPECIALTIES
PROJECT : CALTRANS #11-2358U4 SOLANA BEACH TO ENCINITAS
SOURCE OF CONCRETE : CARROLL CANYON
CONSTRUCTION TYPE : 28 MPA @ 28 DAYS
PLACEMENT : PUMP 4" LINE

WEIGHTS PER CUBIC METER (SATURATED, SURFACE-DRY)

		YIELD, CU M
CEMEX TYPE II/V CEMENT - TAIWAN, KG	308.9	0.098
SRMG CLASS F FLYASH, KG	103.0	0.050
CONCRETE SAND - 41%, KG	680.9 41.0	0.258
25mm x 4.75mm COURSE AGGREGATE - 59%, KG	972.4	0.371
WATER, LITER (GAL-US)	192.22 (50.8)	0.192
TOTAL AIR, %	3.0 +/- 1.0	0.030
	TOTAL	1.000
GRACE WRDA 64 TYPE A, ML	1074.13	
GRACE DARAVAIR, ML	193.4	
WATER/CEMENT RATIO, KGS/KG	0.47	
SLUMP, MM	101.6	
CONCRETE UNIT WEIGHT, KG/M^3	2257.4	

PREPARED BY:

WES JACOBS - QUALITY CONTROL MANAGER

CUSTOMER MAY ADD MESA BUFF #5447M AT 1.84% LOADING OR 11.4KG OF COLOR PIGMENT PER CUBIC METER AT TIME OF PLACING ORDER FOR CONCRETE

Materials	Spgr	% Use	37.5mm	25mm	19mm	12.5mm	9.5mm	4.75mm	2.36mm	1.18mm	600um	300um	150um	75um	F.M.
Carroll Canyon 25mm x 4.75mm	2.62	59%	100	100	86	34	18	3	1	0	0	0	0	0	6.92
Carroll Canyon 9.5mm x 2.36mm	2.62	0%	100	100	100	100	89	15	3	0	0	0	0	0	5.93
Carroll Canyon WCS	2.64	41%	100	100	100	100	100	99	90	65	36	14	3	2.1	2.93
X - Value					75		30			60	37	16			
Combined Gradation			100.0	100.0	91.7	61.1	51.6	42.4	37.5	26.7	14.8	5.7	1.2	0.9	5.28
90 - 3.04			100	90-100	55-100		45-75	35-60	27-45	20-35	12-25	5-15	1-8	0-4	

Gradations are based on continuously updating moving averages and should be verified during actual production.

APPENDIX C – SUPPORT FRAME DESIGN SCHEMATIC

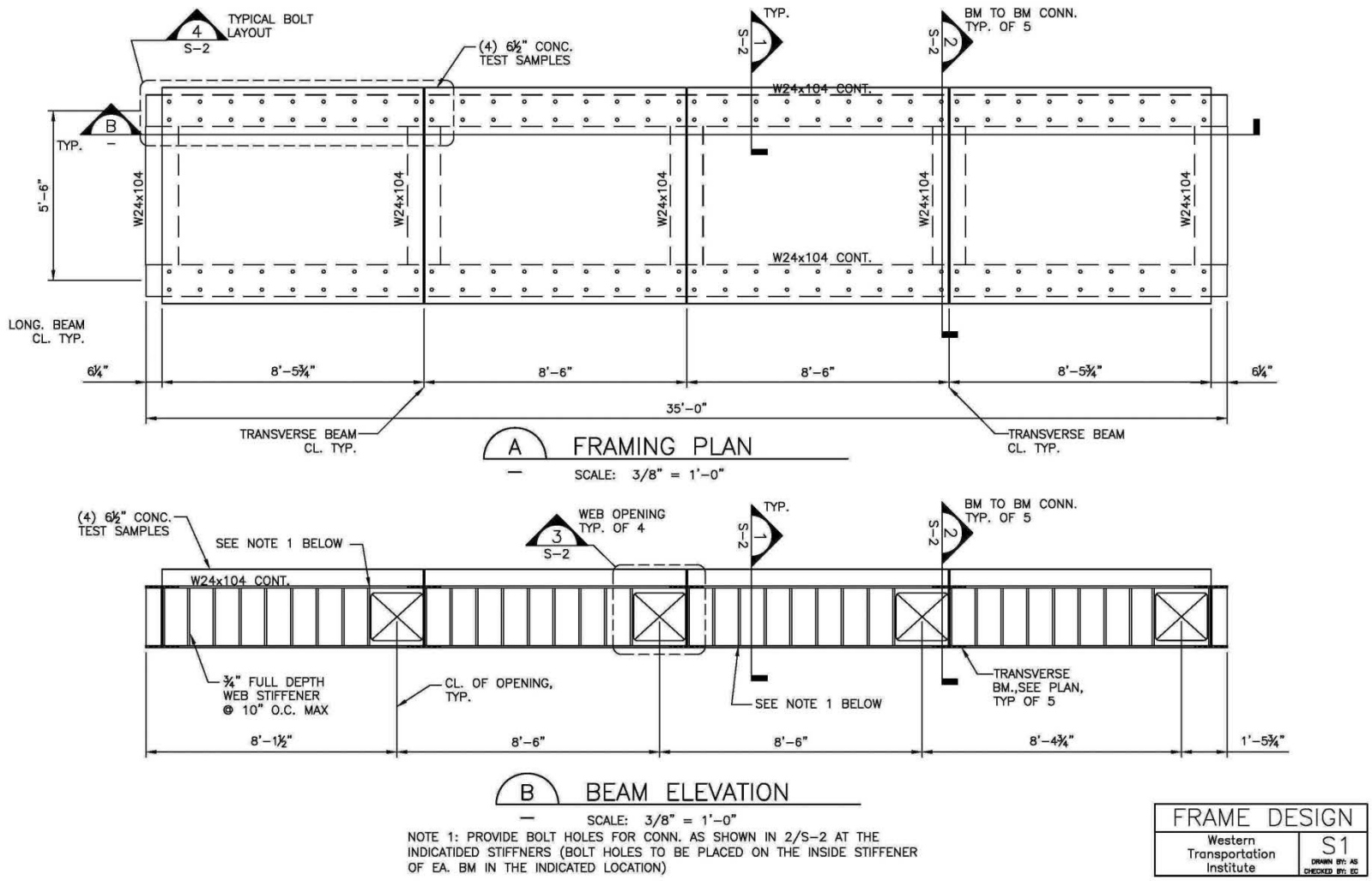

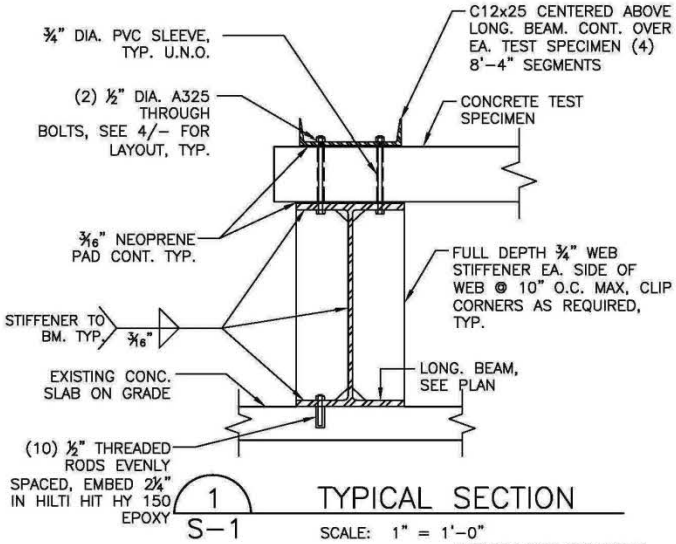

1 S–1 TYPICAL SECTION

SCALE: 1" = 1'–0"

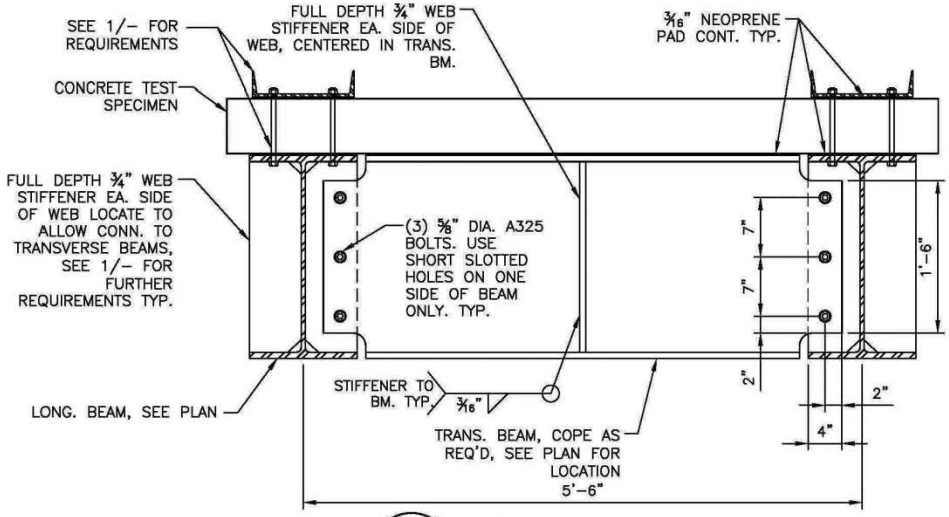

2 S–1 SECTION AT TRANS. BM.

SCALE: 1" = 1'–0"

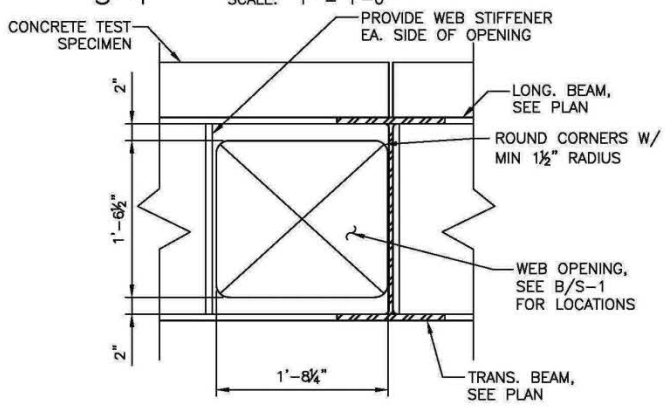

3 S–1 WEB OPENING DETAIL

SCALE: 1" = 1'–0"

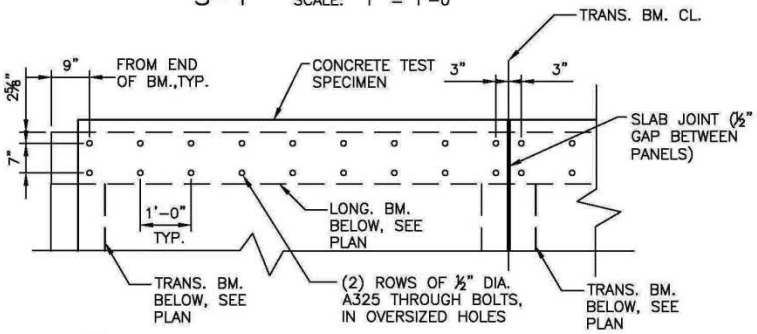

4 S–1 TYPICAL BOLT LAYOUT

SCALE: 1/2" = 1'–0"

FRAME DESIGN	
Western Transportation Institute	S2 DRAWN BY: AS CHECKED BY: EC

APPENDIX D – CRT TEST RESULTS

REPORT NO. T-1405

ON

**RAPID CHLORIDE PERMEABILITY TESTING
AND RATE OF ABSORPTION TESTING
OF SEVERAL CONCRETE SPECIMENS**

TO

**WESTERN TRANSPORTATION INSTITUTE
BOZEMAN, MONTANA**

JULY 5, 2013

Concrete Research & Testing, LLC

RAPID CHLORIDE PERMEABILITY TEST REPORT

Client: Western Transportation Institute **Contact:** Jeremy Miller

Date Received: May 21, 2013 **Date Tested:** June 7, 2013

Test Procedure: ASTM C1202 - Standard Test Method for Electrical Indication of Concrete's Ability to Resist Chloride Ion Penetration

Specimen Identification	Specimen Description	Total Charge Passed, Coulombs	Total Charge Passed, Coulombs	Chloride Ion Penetrability
A1	Untreated Uncracked	3789	3133	Moderate
C1		2477		
A2	Control	3605	3494	Moderate
C2		3384		
A3	Treated Uncracked	786	1405	Low
C3		2024		

Note: The received specimens were 2 in. thick sections that had been saw-cut from 3.69 in. diameter core specimens.

Jason Cummins

Jason Cummins, Laboratory Manager
Concrete Research & Testing, LLC, Columbus, Ohio
CRT Report No. T-1405, pg. 1
Issued: July 5, 2013

Concrete Research & Testing, LLC

Specimens will be discarded 1 month after the report issue date unless otherwise requested.

RAPID CHLORIDE PERMEABILITY TEST REPORT

Client: Western Transportation Institute **Contact:** Jeremy Miller

Date Received: May 21, 2013 **Date Tested:** June 10, 2013

Test Procedure: ASTM C1202 - Standard Test Method for Electrical Indication of Concrete's Ability to Resist Chloride Ion Penetration

Specimen Identification	Specimen Description	Total Charge Passed, Coulombs	Total Charge Passed, Coulombs	Chloride Ion Penetrability
A4	Treated Cracked	2255	2476	Moderate
C4		2696		
A7	Untreated Cracked	4733	3907	Moderate
C6		3080		

Note: The received specimens were 2 in. thick sections that had been saw-cut from 3.69 in. diameter core specimens.

Jason Cummins

Jason Cummins, Laboratory Manager
Concrete Research & Testing, LLC, Columbus, Ohio
CRT Report No. T-1405, pg. 2
Issued: July 5, 2013

Concrete Research & Testing, LLC

Specimens will be discarded 1 month after the report issue date unless otherwise requested.

RATE OF ABSORPTION BY HYDRAULIC-CEMENT CONCRETE
Summary Table

Client: Western Transportation Institute **Contact:** Jeremy Miller

Test Procedure: ASTM C 1585 - Standard Test Method for Measurement of Rate of Absorption of Water by Hydraulic-Cement Concretes

Specimen Identification	Rate of Absorption	
	Initial	Secondary
B1 Untreated Uncracked	56.8×10^{-4} mm/√s (first 30 min)†	6.2×10^{-4} mm/√s
B2 Control	4.3×10^{-4} mm/√s (first 10 min)†	1.4×10^{-4} mm/√s†
B3 Treated Uncracked	3.3×10^{-4} mm/√s	1.9×10^{-4} mm/√s
B4 Treated Cracked	15.4×10^{-4} mm/√s	4.0×10^{-4} mm/√s
B6 Untreated Cracked	75.7×10^{-4} mm/√s (first 5 min)†	3.6×10^{-4} mm/√s

† See page 9 for discussion of test specimens and interpretation of results.

Jason Cummins

Jason Cummins, Laboratory Manager
Concrete Research & Testing, LLC, Columbus, Ohio
CRT Report No. T-1405, pg. 3
Issued: July 5, 2013

Concrete Research & Testing, LLC

Specimens will be discarded 1 month after the report issue date unless otherwise requested.

RATE OF ABSORPTION BY HYDRAULIC-CEMENT CONCRETE

Client: Western Transportation Institute **Contact:** Jeremy Miller

Test Procedure: ASTM C 1585 - Standard Test Method for Measurement of Rate of Absorption of Water by Hydraulic-Cement Concretes

Sample: B1 – Untreated Uncracked		**Test Date:** June 24, 2013
Diameter: 93.7 mm	**Exposed Area:** 6896 mm^2	**Thickness:** 51.8 mm
Conditioned Mass: 811.9g	**Post-sealed Mass:** 817.0g	

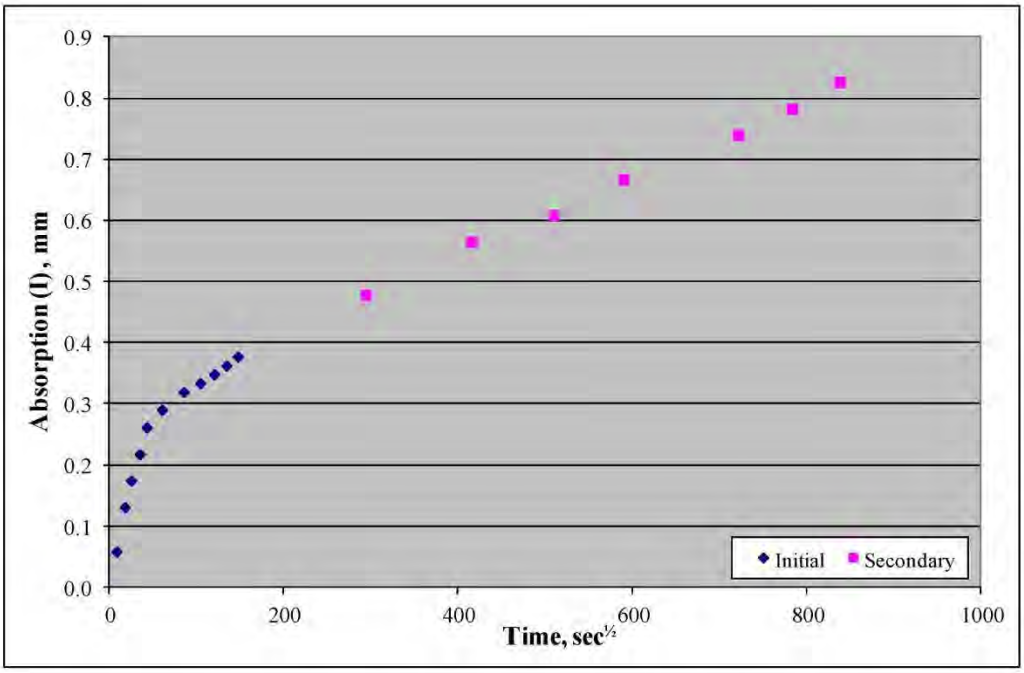

Initial Rate of Absorption: 56.8 x 10^{-4} mm/√s (first 30 min)†	**Correlation Coefficient** = 0.923†
Secondary Rate of Absorption: 6.2 x 10^{-4} mm/√s	**Correlation Coefficient** = 0.999

† See page 9 for interpretation and discussion of results.

Jason Cummins

Jason Cummins, Laboratory Manager
Concrete Research & Testing, LLC, Columbus, Ohio
CRT Report No. T-1405, pg. 4
Issued: July 5, 2013

CRT
Concrete Research & Testing, LLC

Specimens will be discarded 1 month after the report issue date unless otherwise requested.

RATE OF ABSORPTION BY HYDRAULIC-CEMENT CONCRETE

Client: Western Transportation Institute **Contact:** Jeremy Miller

Test Procedure: ASTM C 1585 - Standard Test Method for Measurement of Rate of Absorption of Water by Hydraulic-Cement Concretes

Sample: B2 - Control		**Test Date:** June 24, 2013
Diameter: 93.7 mm	**Exposed Area:** 6896 mm^2	**Thickness:** 52.6 mm
Conditioned Mass: 828.7g	**Post-sealed Mass:** 834.3g	

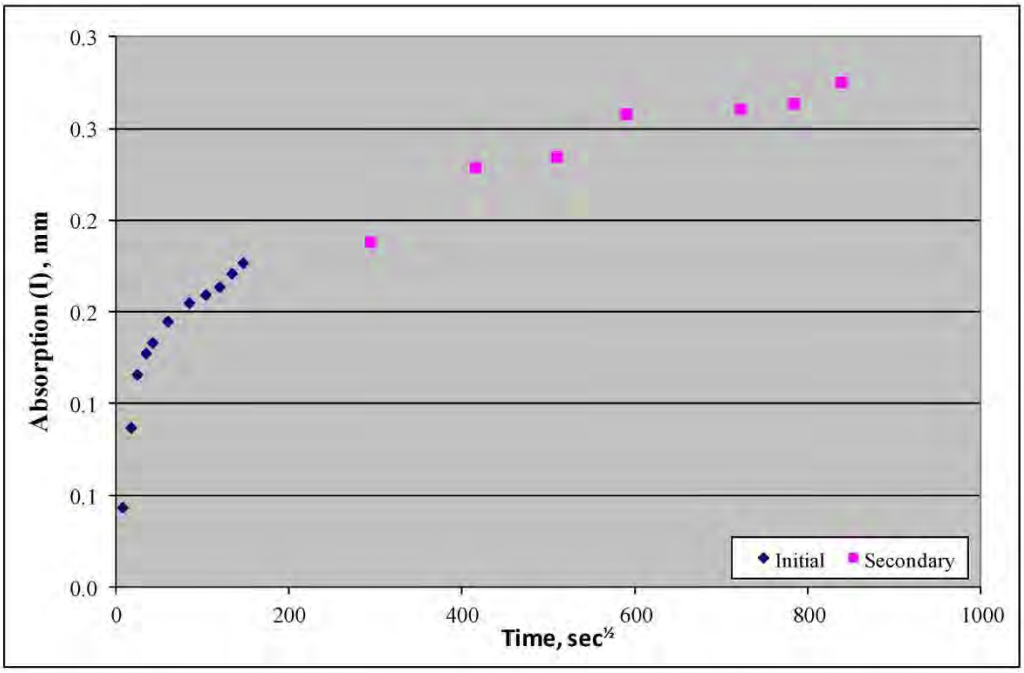

Initial Rate of Absorption: 4.3 x 10^{-4} mm/√s (first 10 min) †	**Correlation Coefficient** = 0.873†
Secondary Rate of Absorption: 1.4 x 10^{-4} mm/√s	**Correlation Coefficient** = 0.946†

† See page 9 for interpretation and discussion of results.

Jason Cummins

Jason Cummins, Laboratory Manager
Concrete Research & Testing, LLC, Columbus, Ohio
CRT Report No. T-1405, pg. 5
Issued: July 5, 2013

CRT
Concrete Research & Testing, LLC

Specimens will be discarded 1 month after the report issue date unless otherwise requested.

RATE OF ABSORPTION BY HYDRAULIC-CEMENT CONCRETE

Client: Western Transportation Institute **Contact:** Jeremy Miller

Test Procedure: ASTM C 1585 - Standard Test Method for Measurement of Rate of Absorption of Water by Hydraulic-Cement Concretes

Sample: B3 – Treated Uncracked		**Test Date:** June 24, 2013
Diameter: 93.7 mm	**Exposed Area:** 6896 mm^2	**Thickness:** 51.2 mm
Conditioned Mass: 821.6g	**Post-sealed Mass:** 826.3g	

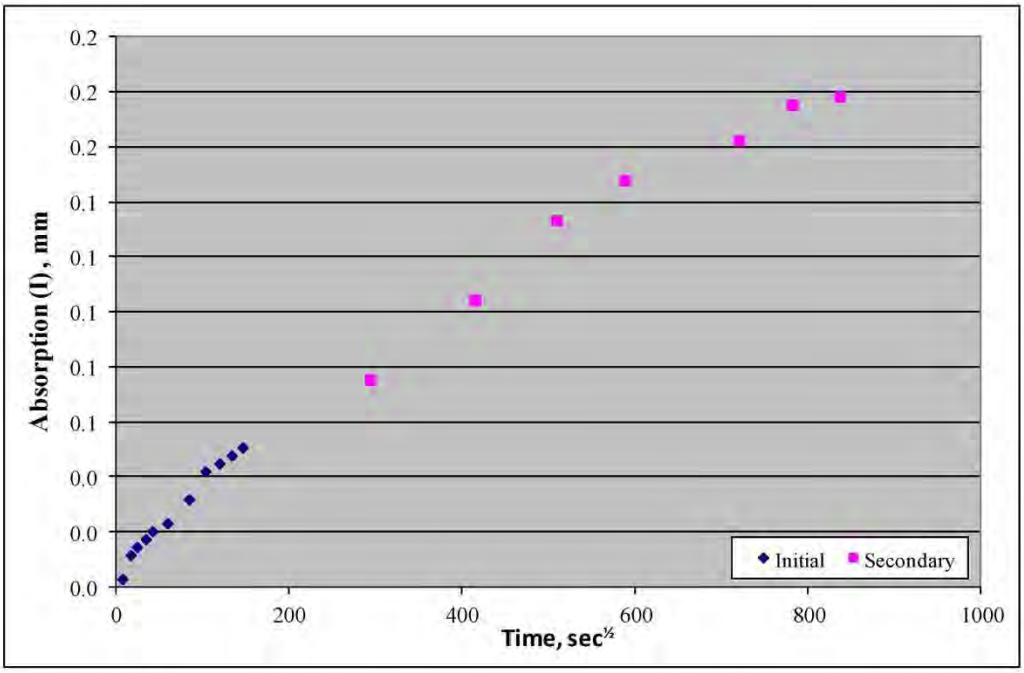

Initial Rate of Absorption: 3.3 x 10^{-4} mm/√s	**Correlation Coefficient** = 0.991
Secondary Rate of Absorption: 1.9 x 10^{-4} mm/√s	**Correlation Coefficient** = 0.983

Jason Cummins

Jason Cummins, Laboratory Manager
Concrete Research & Testing, LLC, Columbus, Ohio
CRT Report No. T-1405, pg. 6
Issued: July 5, 2013

CRT
Concrete Research & Testing, LLC

Specimens will be discarded 1 month after the report issue date unless otherwise requested.

RATE OF ABSORPTION BY HYDRAULIC-CEMENT CONCRETE

Client: Western Transportation Institute **Contact:** Jeremy Miller

Test Procedure: ASTM C 1585 - Standard Test Method for Measurement of Rate of Absorption of Water by Hydraulic-Cement Concretes

Sample: B4 – Treated Cracked†		**Test Date:** June 24, 2013
Diameter: 93.7 mm	**Exposed Area:** 6896 mm^2	**Thickness:** 52.2 mm
Conditioned Mass: 826.1g	**Post-sealed Mass:** 831.1g	

† See page 9 for discussion of test specimen and results.

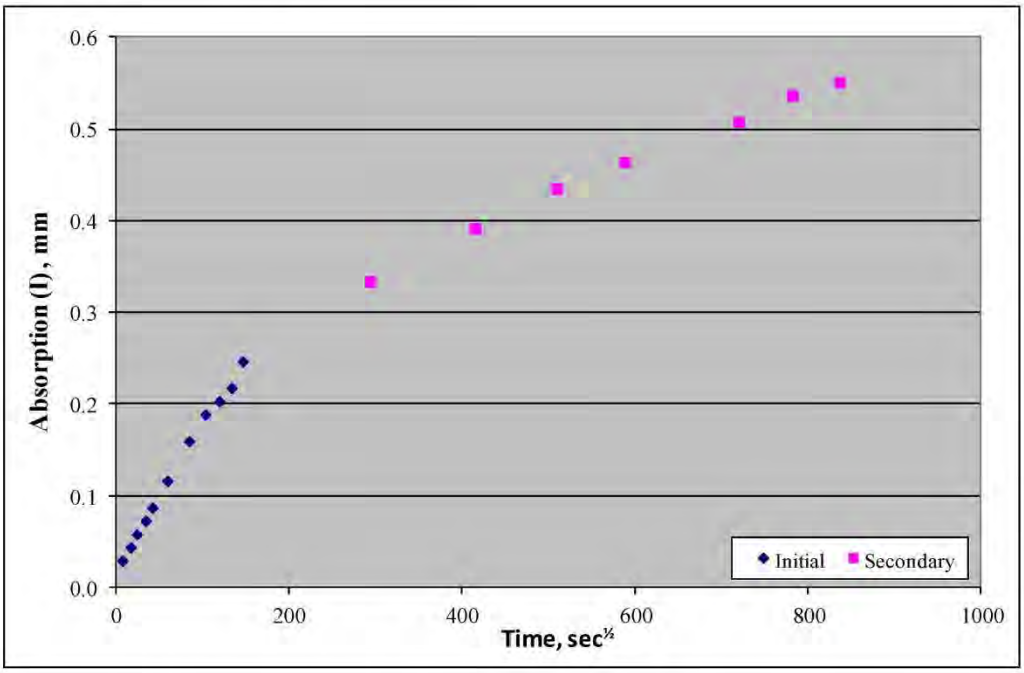

Initial Rate of Absorption: 15.4 x 10^{-4} mm/√s	**Correlation Coefficient** = 0.998
Secondary Rate of Absorption: 4.0 x 10^{-4} mm/√s	**Correlation Coefficient** = 0.997

Jason Cummins

Jason Cummins, Laboratory Manager
Concrete Research & Testing, LLC, Columbus, Ohio
CRT Report No. T-1405, pg. 7
Issued: July 5, 2013

CRT
Concrete Research & Testing, LLC

Specimens will be discarded 1 month after the report issue date unless otherwise requested.

RATE OF ABSORPTION BY HYDRAULIC-CEMENT CONCRETE

Client: Western Transportation Institute **Contact:** Jeremy Miller

Test Procedure: ASTM C 1585 - Standard Test Method for Measurement of Rate of Absorption of Water by Hydraulic-Cement Concretes

Sample: B6 – Untreated Cracked†		**Test Date:** June 24, 2013
Diameter: 93.7 mm	**Exposed Area:** 6896 mm^2	**Thickness:** 51.8 mm
Conditioned Mass: 808.5g	**Post-sealed Mass:** 813.3g	

† See page 9 for discussion of test specimen and results.

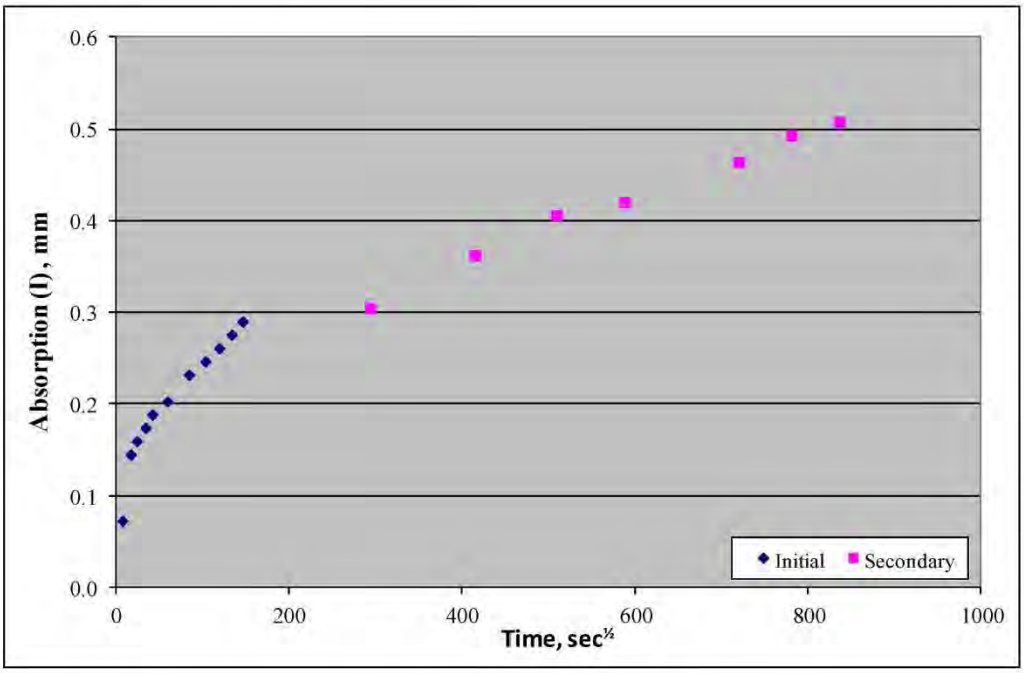

Initial Rate of Absorption: 75.7 x 10^{-4} mm/√s (first 5 min)‡	**Correlation Coefficient** = 0.951‡
Secondary Rate of Absorption: 3.6 x 10^{-4} mm/√s	**Correlation Coefficient** = 0.995

‡ See page 9 for interpretation and discussion of results.

Jason Cummins

Jason Cummins, Laboratory Manager
Concrete Research & Testing, LLC, Columbus, Ohio
CRT Report No. T-1405, pg. 8
Issued: July 5, 2013

Concrete Research & Testing, LLC

Specimens will be discarded 1 month after the report issue date unless otherwise requested.

RATE OF ABSORPTION BY HYDRAULIC-CEMENT CONCRETE

Calculation & Interpretation of Results (ASTM C1585 – Section 10.2 & 10.3)

Initial Rate of Absorption

For the results obtained for Specimen B1, Specimen B2, and Specimen B6, the bolded portion of the following section is relevant for the Initial Rate of Absorption calculations.

10.2 The initial rate of water absorption ($mm/s^{1/2}$) is defined as the slope of the line that is the best fit to I plotted against the square root of time ($s^{1/2}$). Obtain this slope by using least-squares, linear regression analysis of the plot of I versus $time^{1/2}$. **For the regression analysis, use all the points from 1 min to 6h, excluding points for times after the plot shows a clear change of slope. If the data between 1 min and 6h do not follow a linear relationship (a correlation coefficient less than 0.98) and show a systematic curvature, the initial rate of absorption cannot be determined.**

Secondary Rate of Absorption

For the results obtained for Specimen B2, the bolded portion of the following section is relevant for the Secondary Rate of Absorption calculation.

10.3 The secondary rate of water absorption ($mm/s^{1/2}$) is defined as the slope of the line that is the best fit to I plotted against the square root of time ($s^{1/2}$) using all the points from 1d to 7d. Use least-square linear regression to determine the slope. **If the data between 1d and 7d do not follow a linear relationship (a correlation coefficient less than 0.98) and show a systematic curvature, the secondary rate of water absorption cannot be determined.**

Additional Specimen and Test Discussion

The cracks present in two of the specimens have caused an elevated Initial Rate of Absorption (Specimen B4) and significantly elevated early absorptions (Specimen B6). This is due to the wicking of water up through the specimens. Even though the surface of Specimen B4 was treated, the wicking occurred in both specimens; however, the wicking was more pronounced in Specimen B6.

For Specimen B6, if the early accelerated absorption is removed (first 5 minutes), the Initial Rate of Absorption is linear (a correlation coefficient greater than 0.98).

Sample: B6 – Untreated Cracked	
Initial Rate of Absorption (modified): 10.6×10^{-4} mm/√s	R = 0.995

This cannot be done for Specimen B4, however, because even though wicking did occur, the Initial Rate of Absorption was linear (see graph, page 7). A comparison of results from Specimen B3 (uncracked, treated) and Specimen B4 (cracked, treated) shows that the imperfectly-sealed crack in Specimen B4 multiplied the Initial Rate of Absorption by approximately five times.

Jason Cummins

Jason Cummins, Laboratory Manager
Concrete Research & Testing, LLC, Columbus, Ohio
CRT Report No. T-1405, pg. 9
Issued: July 5, 2013

Concrete Research & Testing, LLC

Specimens will be discarded 1 month after the report issue date unless otherwise requested.

APPENDIX E – PRODUCT DATA SHEET FOR KWIK BOND METHACRYLATE

KWIKBOND POLYMERS

923 Teal Drive
Benicia, California 94510

(866) 434-1772
(707) 746-7981 Fax
contact@kwikbondpolymers.com

BRIDGE DECK & ROADWAY REHABILITATION SYSTEMS

PRODUCT DATA SHEET: KBP 204

PRODUCT DESCRIPTION

KBP 204 primer/sealer is a formulated, high molecular weight methacrylate monomer composition that has been developed as a "***healer/sealer***" penetrant for re-bonding and sealing shrinkage or related cracking in Portland cement concrete, latex modified and/or silica fume (micro silica) concrete. KBP 204 has been formulated to conform to published specifications from Cal-Trans, Nevada DOT, Oregon DOT, Virginia DOT, Washington DOT, FHWA, Bureau of Reclamations, and many other specifying authorities.

Formulated high molecular weight methacrylate systems play a distinctly different role than silane, siloxane, or epoxy sealers. KBP 204 is a "***100% solids, completely reactive***", low viscosity penetrant, that wicks deep into cracks, pores, etc and than polymerizes to form a tough plastic seal. The end result is a re-bonded crack that resists the ingress of moisture or other environmental contaminants.

KBP 204 is designed to penetrate quickly and allow return to service within a reasonable period. Typically, materials dry to touch within 1-3 hours during sunlight conditions and temperatures ranging from 55 F-100F. During nighttime and high humidity conditions, 5 hours or more may be needed to obtain proper surface dry times. Surface dry may be accelerated by mechanical means. Deck temperatures, air temperatures, humidity, U.V. light exposure all play a significant role in penetration and drying characteristics. Due to temperature and humidity variations, a test areas should be evaluated under anticipated construction conditions to determine specific catalyst ratios for the expected conditions.

SPECIAL FEATURES

- **Very** Low viscosity for rapid surface penetration
- Fast curing properties during daytime, sunlight conditions
- Excellent adhesion to Portland cement concrete, latex modified concrete, silica fume concrete even under damp conditions
- Low overall odor (This product conforms to Cal-Trans specifications limiting volatile organic content to 30% maximum)
- Easy handling, workability, mixing

kwikbondpolymers.com 1

PHYSICAL PROPERTIES - Typical Values	
Specific Gravity - ASTM D1475	1.06
Viscosity- ASTM D2196 w U/L adaptor, 50 rpm, 25C	<25 cps
Flash Point (Setaflash) ASTM D3278	>180 °F
Adhesion (Saturated Surface Dry Bond Test, Cal-Trans 551)	> 500 psi
Thin Film Tack Free Time (Cal-Trans Test Method, Cal-Trans 551)**	<400 minutes
Vapor Pressure, mm Hg (ASTM D 323)***	1 mm Hg
ASTM D-695 Compressive Strength-RT Cure (2 hours)	>2000 psi
ASTM D-695 Compressive Strength-RT Cure (24 hours)	>3000 psi
ASTM D-638 Tensile Strength (7 Days)	>2000 psi
ASTM C-882 Adhesion (hardened concrete to hardened concrete) @ 2 days, RT Cure	>2500 psi
Surface Coverage Rate*	60-125 sq.ft./gal.

*Coverage rates for penetrants like KBP 204 represent averages only. Field variables such as surface porosity, grooving, tining, heavy brooming, wide cracks, pop offs, etc. consume proportionately higher amounts of materials.

**Primer excluded

*** Calculated

SEALER APPLICATION

Surface Preparation: As a sealer KBP 204 requires minimal surface preparation. On relatively clean decks, free from significant AC deposits, the decks just need to be swept with high-pressure air to remove minor dirt and expose the cracked surface. For decks with higher amounts of contaminants, steel shot-blasting, sandblasting, scarifying or other cleaning processes may be required to provide a surface that will readily absorb the KBP 204 sealer materials.

Mixing: KBP 204 Sealer

Once the deck has been cleaned, catalyze KBP 204 using the following starting point formula:

1) 4 gallons KBP 204
2) 24 fl oz Promoter 8020
3) 12 fl oz Cumene Hydro Peroxide(CHP)
4) 2-15 fl oz Z Cure Accelerator (see temperature chart)

Note: Modifications may be required for working under different temperature conditions or during night time application. For temps above 90 F, night time application should be considered. Reducing CHP levels to 1 fl oz per gallon during elevated temperatures should be evaluated. During cold night time application, both Promoter 8020 and CHP levels may be increased. Adding higher levels ofZ Cure accelerator is also suggested. (See temperature chart)

Mix the CHP peroxide into the KBP 204 monomer first using a variable speed drill motor mixer. Next, add the Promoter 8020 and mix again for about 30 seconds. ***SPECIAL WARNING!!!*** KBP Promoter 8020 and Cumene Hydro Peroxide are INCOMPATIBLE MATERIALS. These materials must NEVER contact each other DIRECTLY! A FLASH FIRE will OCCUR! Each component, separately, must be stirred into the KBP 204 monomer. Always follow the mixing steps outlined above. Mix these materials carefully and recognize the potential hazards. Take precautions by wearing protective clothing as well as having a fire extinguisher and plenty of clean water available.

Placement: KBP 204 Sealer

After proper proportioning and mixing, distribute the KBP 204 mixture on the concrete surface as soon as possible. Spread sealer at a rate of 60-120 square feet per gallon, consistent with the listed project specifications (other application rates are acceptable). Use a squeegee, roller, broom, low pressure sprayer, etc. to distribute the material uniformly. Some areas may selectively absorb greater amounts of KBP 204 sealer and create dry spots. These areas should receive additional amounts of KBP 204 sealer to fill the pores and cracks to the point of refusal to absorb further. Elevated temperatures and UV light significantly increases the reactivity of the KBP 204 sealer and reduces work time. Cold temperatures greatly retard the surface cure of the KBP 204 sealer. Field adjustment of accelerators and/or promoter activators will be required to obtain the proper surface cure within the traffic closure windows. A DEMONSTRATION under EXPECTED JOB CONDITIONS must be conducted PRIOR to actual construction to determine the correct catalyst quantities. Differing levels of catalyst should be evaluated to determine surface cure characteristics obtainable under the prevailing job site conditions. Temperature, humidity, fog, night time versus daylight conditions have an effect on the cure response of the KBP 204 system. Under daytime conditions, traffic may be returned in 1.5-3 hours. Under night time conditions the traffic return time can run from 3-5 hours or longer depending on the exact environmental conditions. *Contact Kwik Bond Polymers technical department for recommendations and suggestions.*

Once the KBP 204 monomer mixture has been distibuted properly, wait approximately 10-20 minutes and then broadcast a commercial grade of 8 x 20 sand blast sand. The intent of broadcasting sand is to provide initial traction to the treated surface. Commonly available grades of sand blast sand, No. 8, 8 x 12, and 20 mesh have been used successfully. The application rate of the broadcast sand is typically 2 lbs per square yard of surface. Sufficient sand should be broadcast to meet the skid resistance requirements of the specification. Any technique may be used to broadcast the sand including hand throwing, fertilizer spreaders, salt spreaders, drop spreaders, etc. Significant quantities of excess loose sand need to be removed from the deck prior to returning traffic.

For night time applications, sealer cure speeds will be reduced. A thin, oily residue may remain on areas of the sealed surface under cold, damp conditions. Temperatures should be 50 F and rising during application. Colder temperatures, low fog, dew, etc. will drastically slow cure times. Under these conditions some un-reacted monomer will leave an oily residue on the surface. The oily residue may alter skid resistance properties of the treated surface even though the surface traction sand has been applied and is well bonded. This residual oiliness can be resolved by distributing approximately 5 lb/100 sf of surface area with diatomaceous earth plus mechanically sweeping the area. A skid tester may be utilized to verify bridge deck friction values.

PRIMER APPLICATION

Surface Preparation: Primer application is an essential component to the success of the PPC 1121 polyester polymer concrete overlay system. The Primer is a part of our ***"Plus" Program*** for our MLS and Easy Patch Products. The Primer not only improves overall bonding characteristics for PPC overlay technology, it additionally acts as ***"Bridge Insurance Policy"*** with its ability to penetrate and re-bond PCC cracks.

For bridge deck overlay applications, the PCC deck surface must be free of curing compounds, oils, deleterious compounds, scaling concrete, and any other condition that may lead to a weakened surface. Preparation methods may consist of micro milling, diamond grinding, steel shot-blasting, hydro-milling, high pressure water blasting, sand blasting, or other mechanical means. Optimally, cement binder paste of the PCC deck surface should be removed, sufficiently, to expose aggregate.

Mixing: KBP 204 Primer

1.	4 gallons	KBP 204
2.	12 fl oz.	6% Cobalt Drier
3.	12 fl oz	Cumene Hydro Peroxide

Modifications may be required under cooler temperature conditions.

Mix in the same manner and follow the identical precautions as in the Sealer application. Because the KBP 204 has a very low viscosity (thin), materials blend together easily. Do NOT over agitate! High speed agitation may lead to splashing. Avoid contact with eyes, skin, clothing. Be sure to read and follow the information provided in this Product Data Sheet and the Material Safety Data Sheet provided. ***DO NOT MIX 6% COBALT and CUMENE HYDRO PEROXIDE directly!!! A FLASH FIRE WILL OCCUR!!***

For information on high volume spray applications, contact Kwik Bond Polymers technical department for suggestions.

Primer Placement: Use the same procedures as listed for the sealer placement. Spread rates are the same. Once the methacrylate primer is placed on the deck, sand is not required. The primer will be covered with the polyester polymer concrete material. The primer should be placed in such a manner that it will be covered with the polyester polymer concrete within the current work shift. Primer should not be placed too far in advance of polyester polymer concrete placement in case of equipment break downs, weather, or other variables. Primer that is not covered within a normal work shift with polyester polymer concrete must a) be removed by some methodology or b) covered with a polyester chip seal during the work shift. The primer, uncovered, will remain slightly oily to the touch and may fail skid resistance requirements.

CLEAN UP

Wipe off excess materials with disposable absorbent materials. Solvents like MEK, acetone, lacquer thinner, orange cleaner are excellent cleaners if used before the KBP 204 sealer hardens. Read and follow the safety and handling recommendations for these materials.

PACKAGING

- Cumene Hydro Peroxide (CHP)- available in 1 gallon containers
- KBP 204 monomer- available in 4 gallon pails, 50 gallon drums, 250 gallon Totes.
- Promoter 8020- available in 4.5 gallon pails.
- 6% Cobalt Drier- available 1 gal and 4 gallon containers.
- Z-Cure is available in 1 gal and 5 gallon pails
- Other packaging may be available

STORAGE

KBP 204, Promoter 8020 and CHP should be stored in a COOL, DRY location and in their original containers at temperatures less than 80 F. Containers need to remain tightly sealed to prevent contamination. Promoters and CHP should be stored in separate locations. The shelf life for these materials is typically twelve months. When stored at elevated temperatures, the KBP 204 reactive monomer may gel prematurely. CHP, Promoter 8020 can have reduced activity after a lengthy storage period. Retest all component materials prior to use
on a project.

SAFETY

NEVER MIX PROMOTER 8020 or 6% COBALT DRIER with CHP together DIRECTLY! A Flash Fire will occur! Take steps to prevent these materials from contacting one another during mixing, storage, clean up, and/or shipping.

Workers should wear appropriate protective clothing, gloves, and eye protection. For most outdoor applications the use of an organic vapor respirator is not required by OSHA. However, sensitive individuals may desire to wear an organic vapor respirator due to the chemical odors. Additional safety equipment includes a fire extinguisher, fresh water for eye rinse. Workers should have a change of clothing in case of accidental contamination of clothing. All KBP 204 components have a very low order of dermal toxicity. However, continued contact with the skin, especially catalyzed material, may lead to redness, swelling, blisters, or other effects. Sensitive workers may react much more rapidly. These effects are typical of other commonly used construction chemicals. All efforts should be made to prevent contact. Read MSDS sheets for additional information and first aid procedures.

The technical data furnished is true and accurate to the best of our knowledge. However, no guarantee of accuracy is given or implied. We suggest that you evaluate these recommendations and suggestions in conjunction with your specific application. Kwik Bond Polymers, LLC warrants its product(s) to be free from manufacturing defects conforming to its most recent material specifications. In the event of defective materials, Kwik Bond Polymers, LLC's liability will be limited to the replacement of material or the material value only at the sole discretion of Kwik Bond Polymers, LLC We assume no responsibility for coverage, suitability of application, performance or injuries resulting from use. 8-15-2011

APPENDIX F – CRACK MAPS

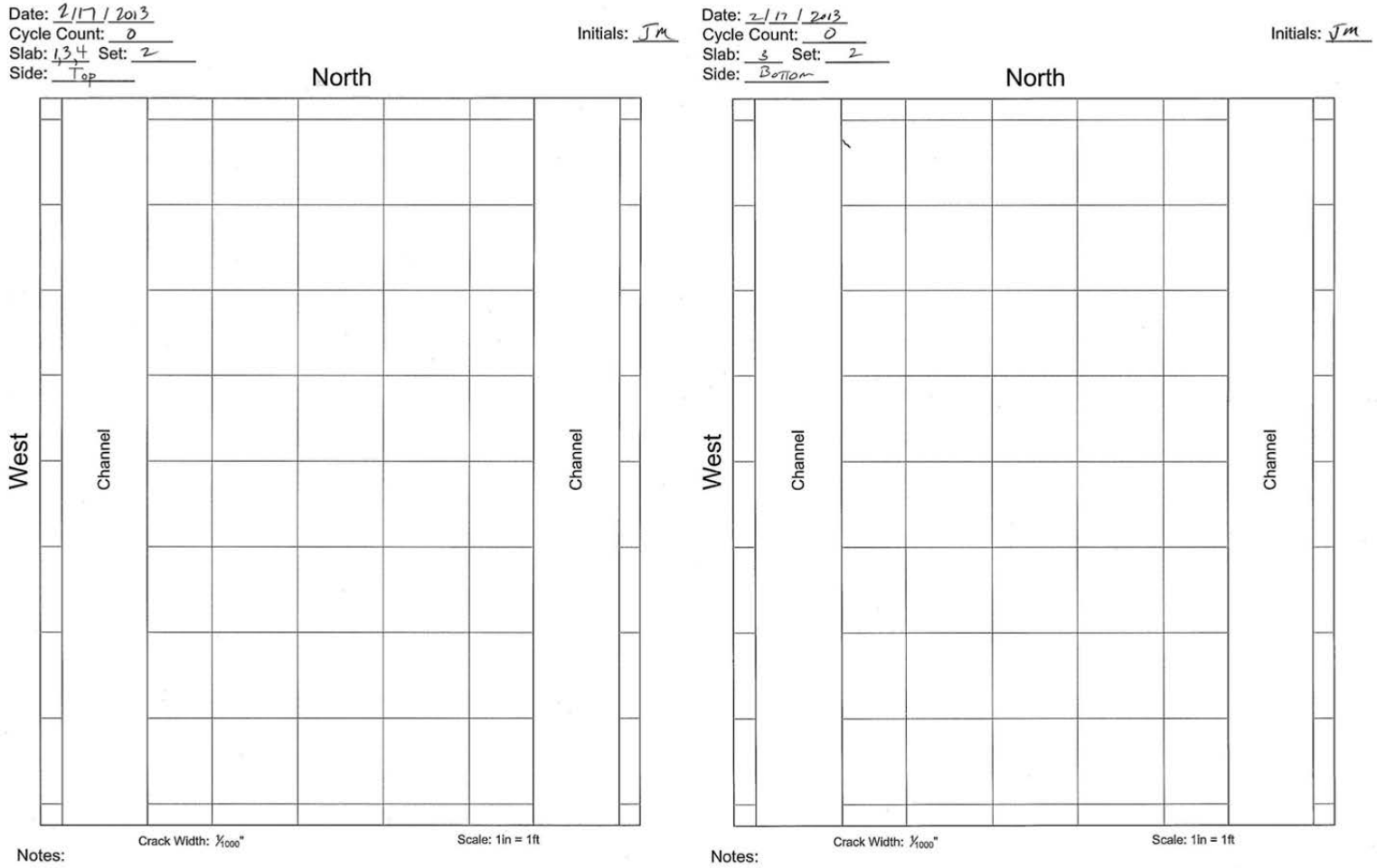

Figure F-1: Crack maps, M25$_a$ test panel, 0 traffic cycles.

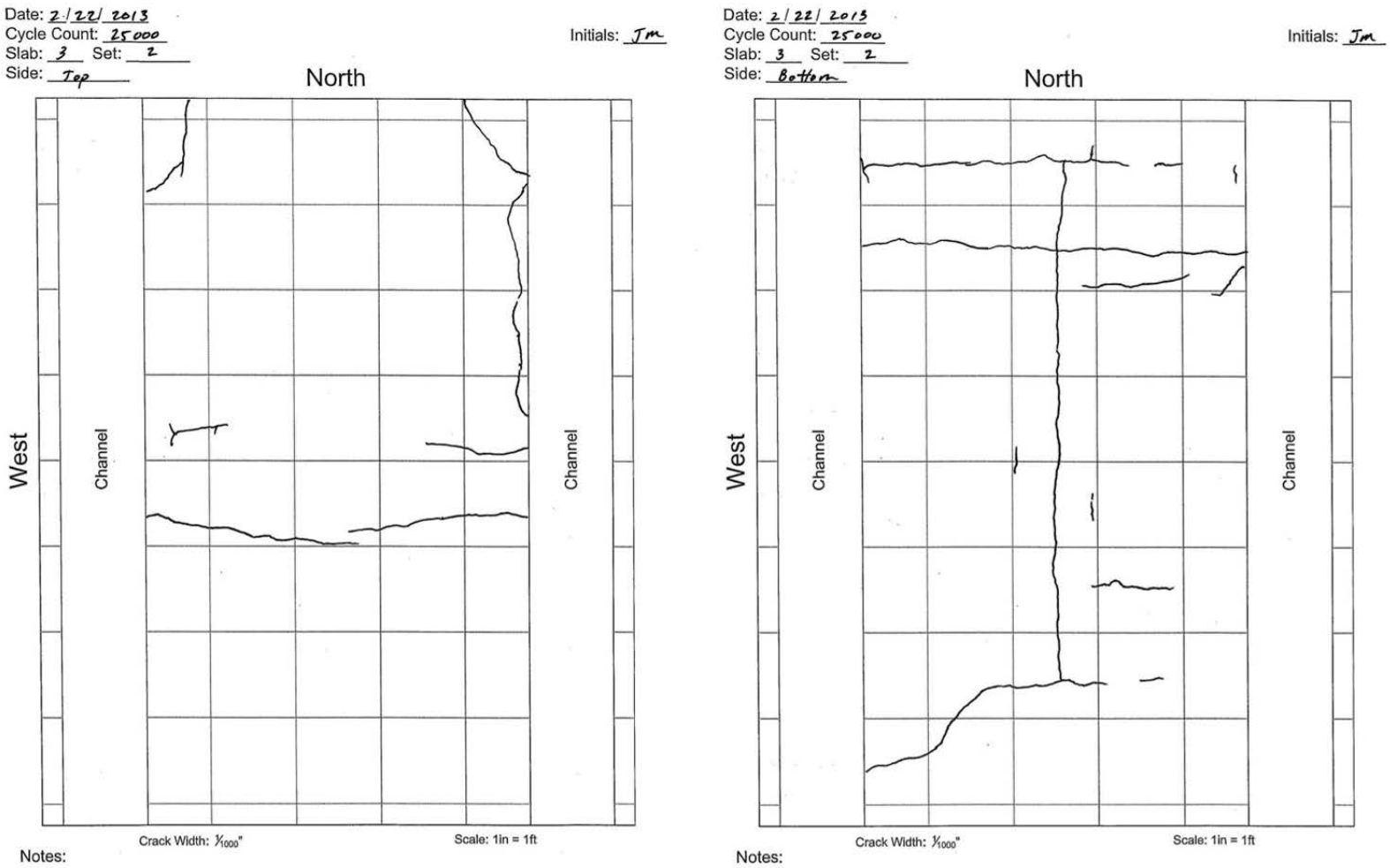

Figure F-2: Crack maps, M25$_a$ test panel, 25,000 traffic cycles.

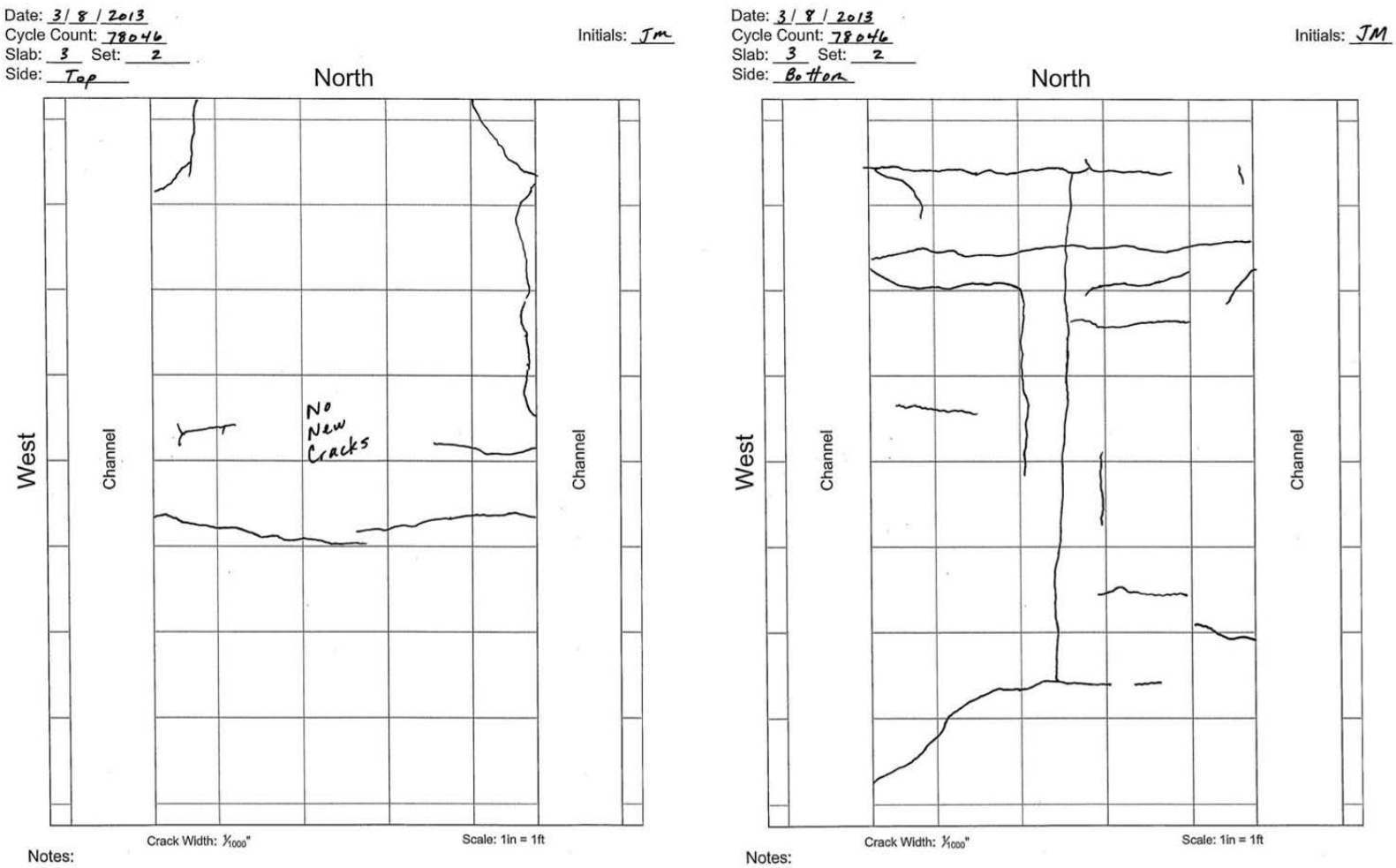

Figure F-3: Crack maps, M25$_a$ test panel, 78,000 traffic cycles.

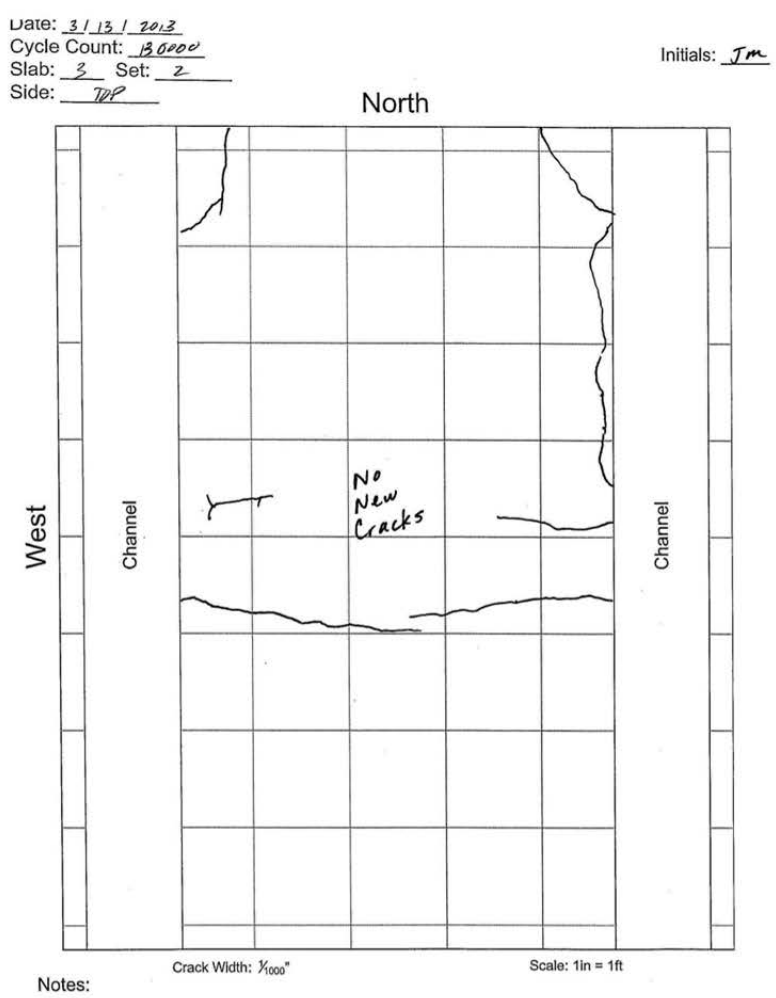

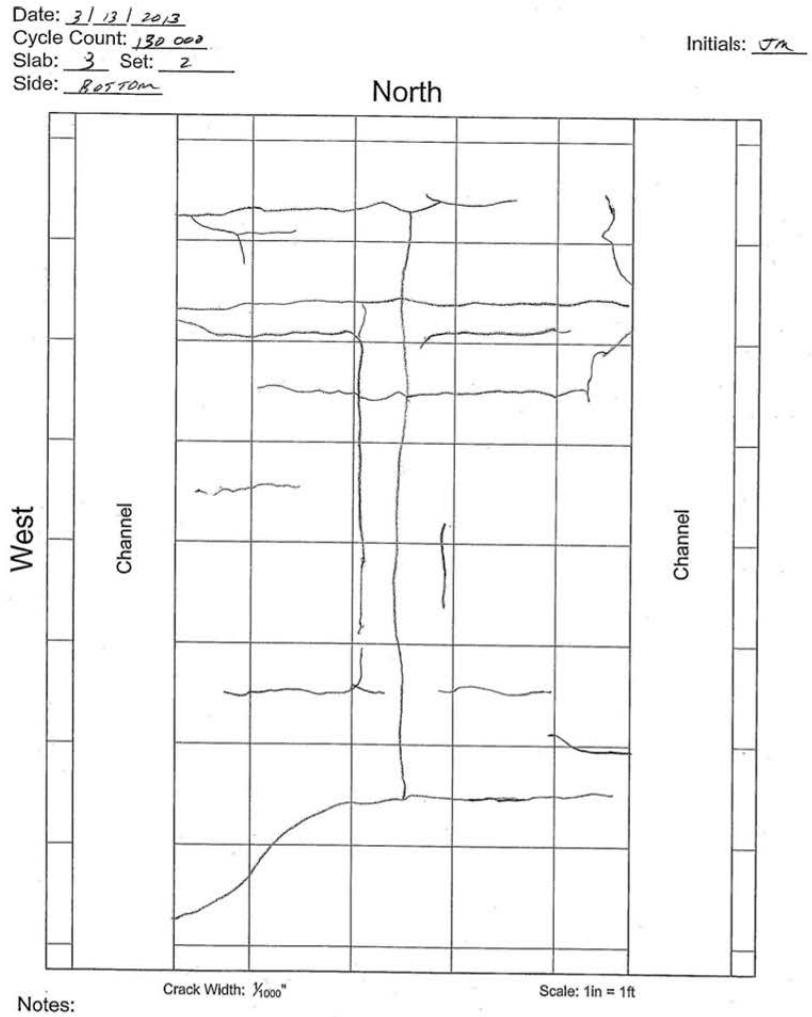

Figure F-4: Crack maps, M25$_a$ test panel, 130,000 traffic cycles.

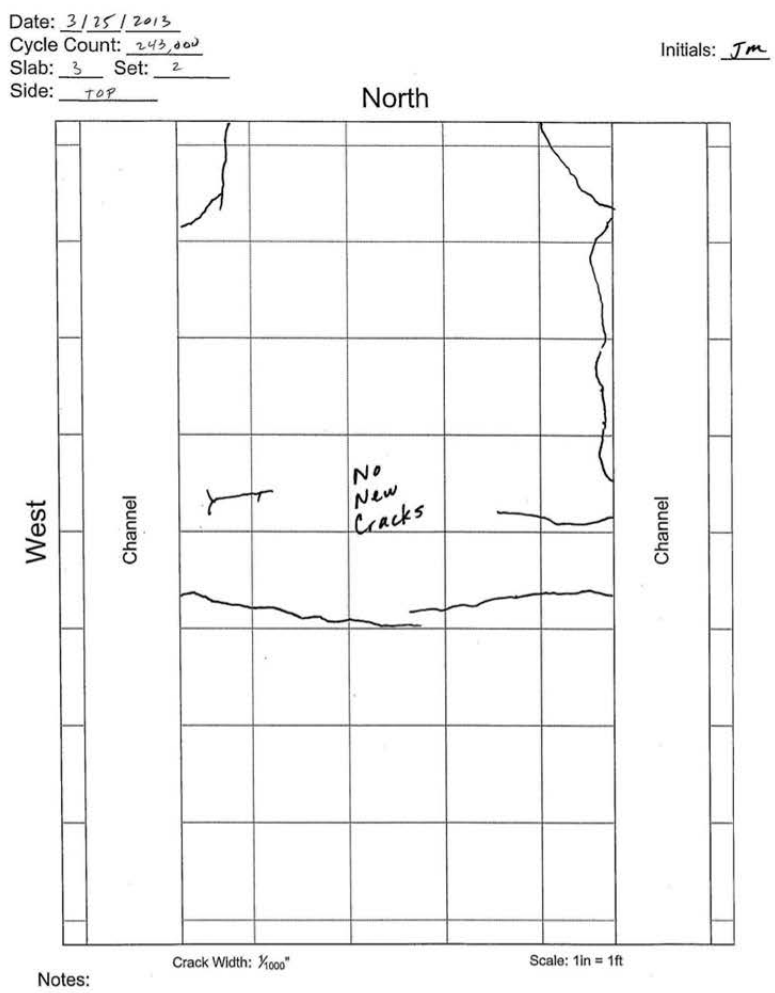

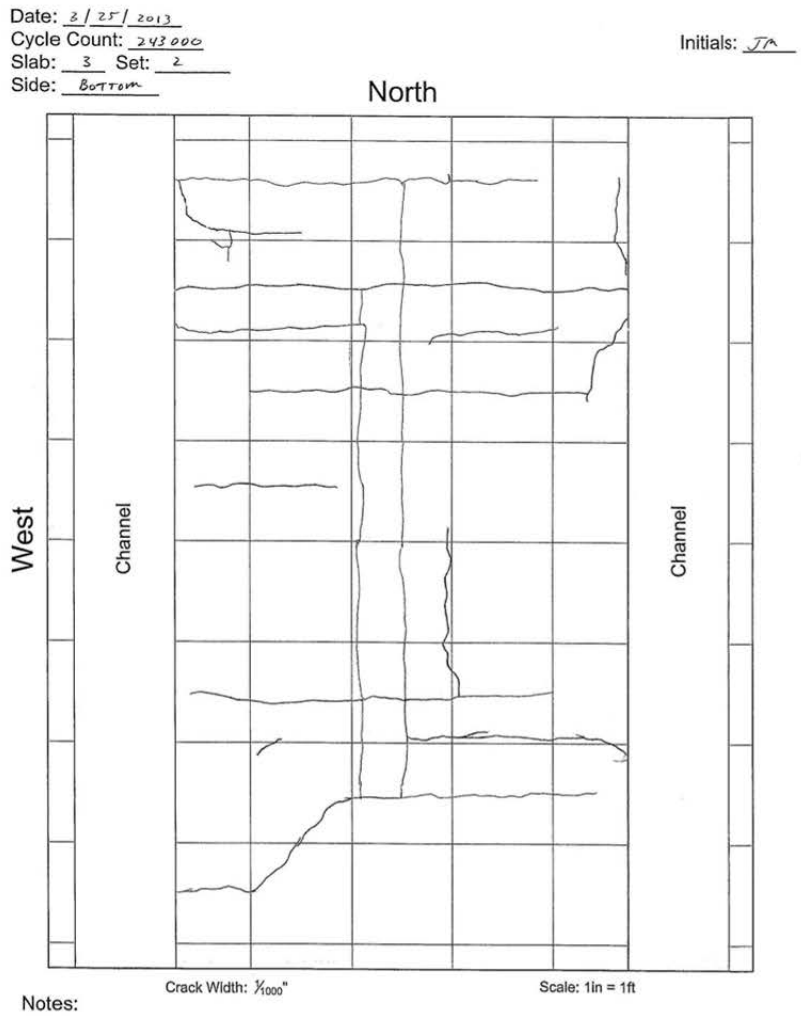

Figure F-5: Crack maps, M25$_a$ test panel, 242,590 traffic cycles.

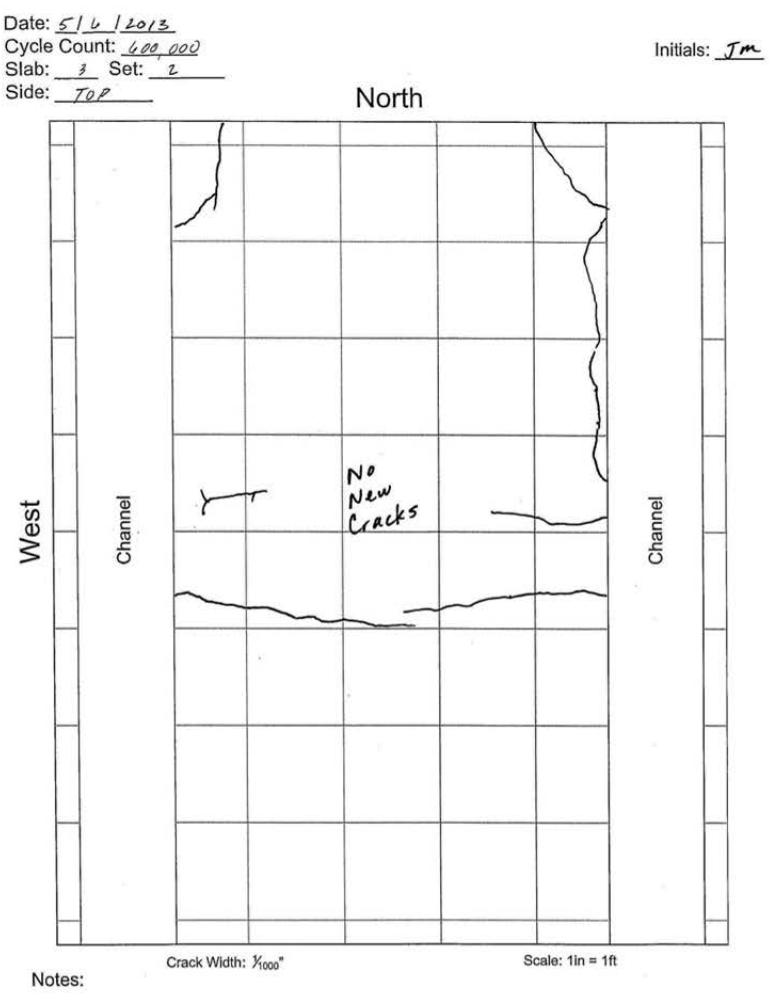

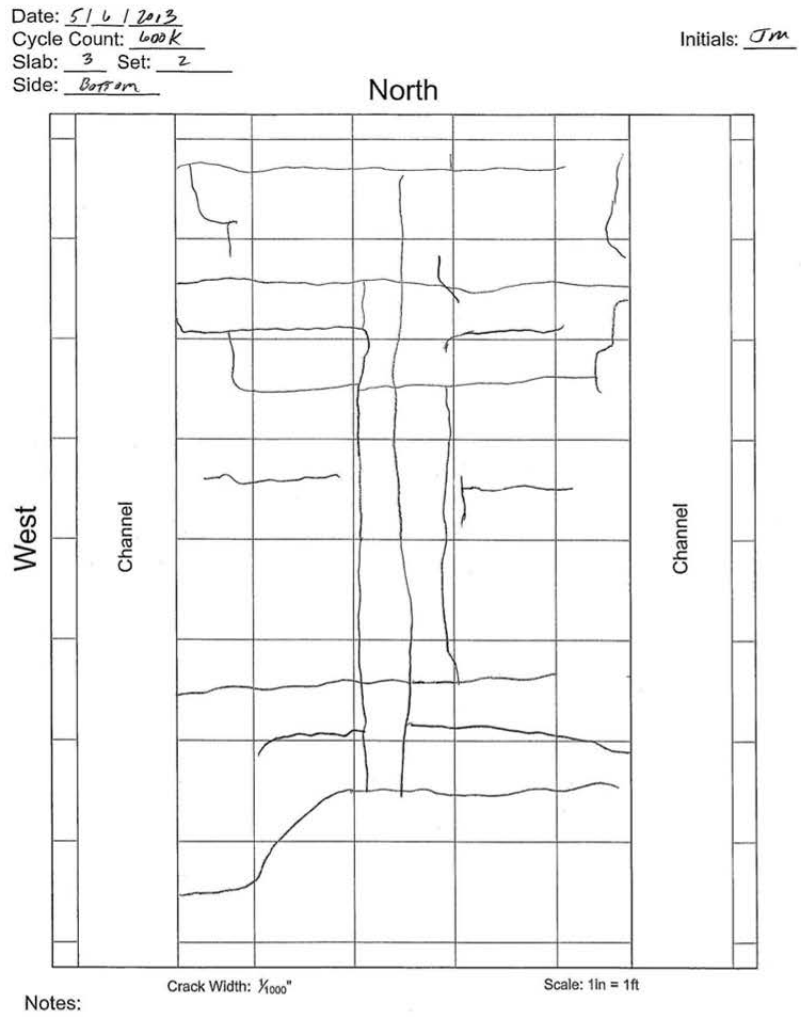

Figure F-6: Crack maps, M25$_a$ test panel, 604,932 traffic cycles.

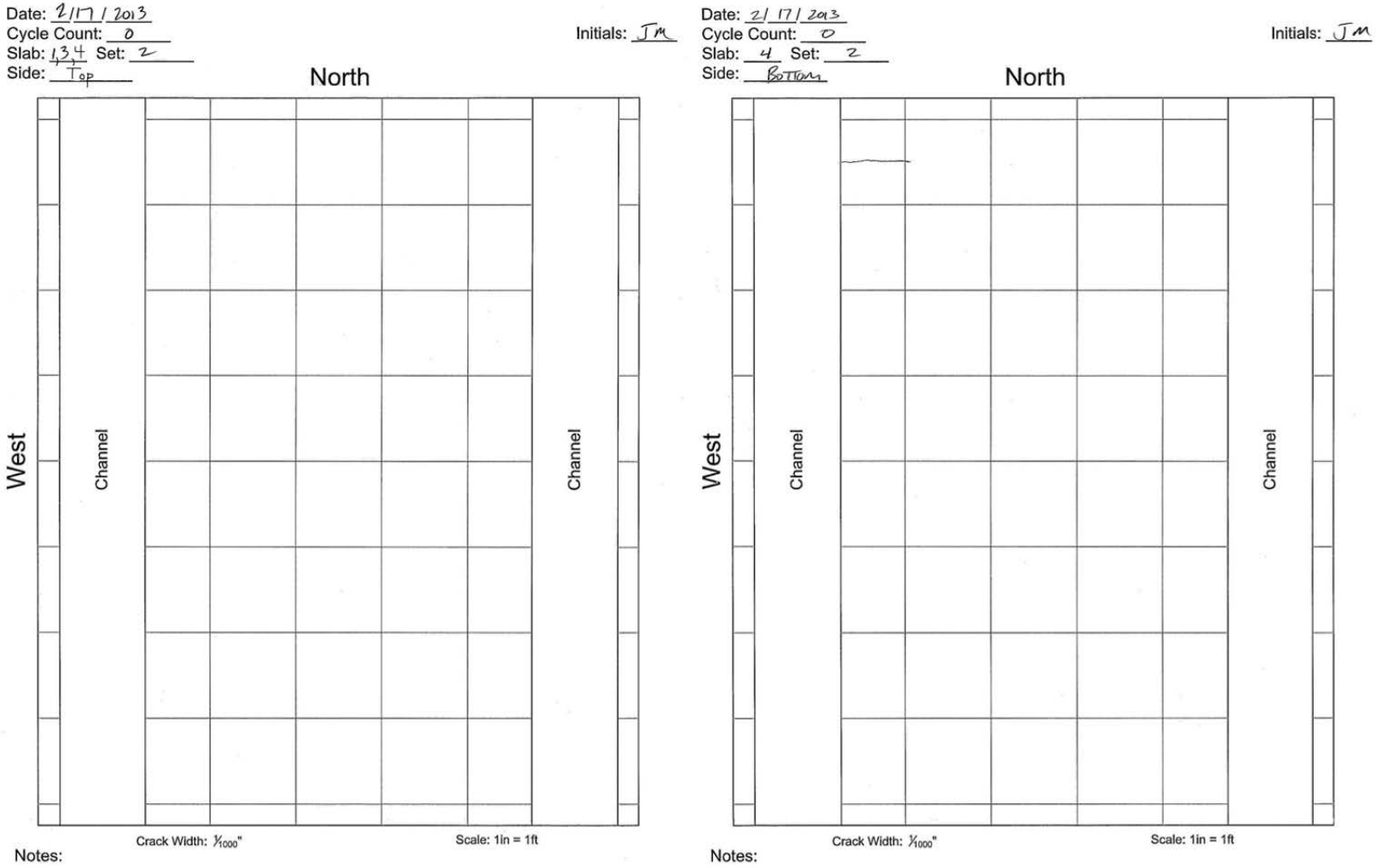

Figure F-7: Crack maps, M25, test panel, 0 traffic cycles.

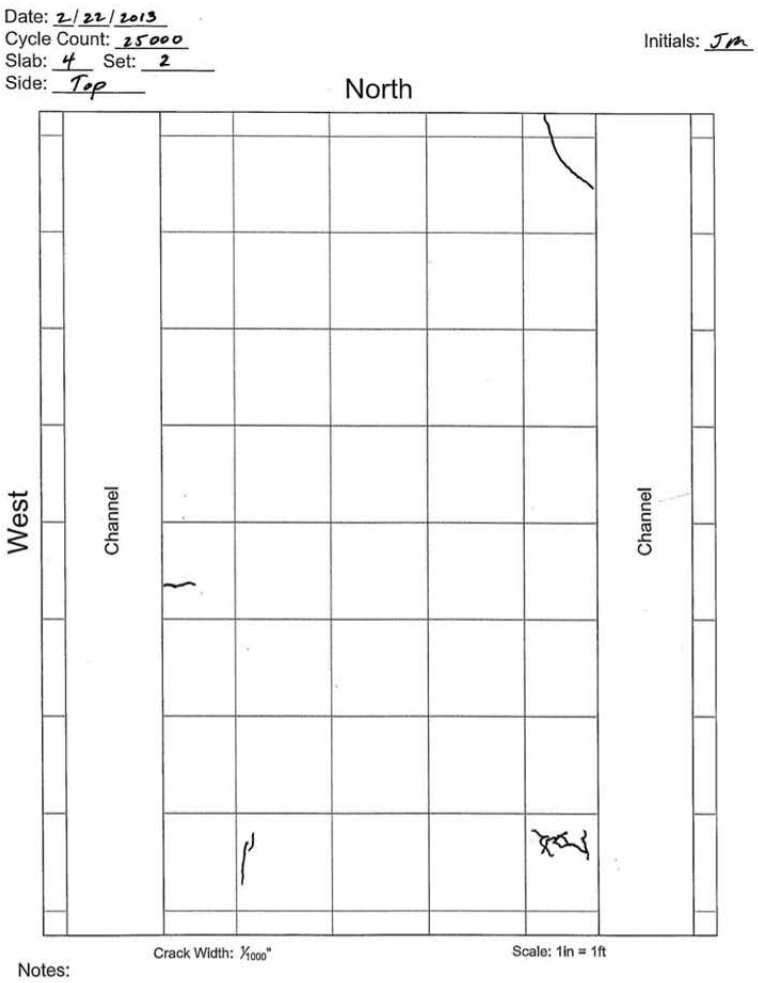

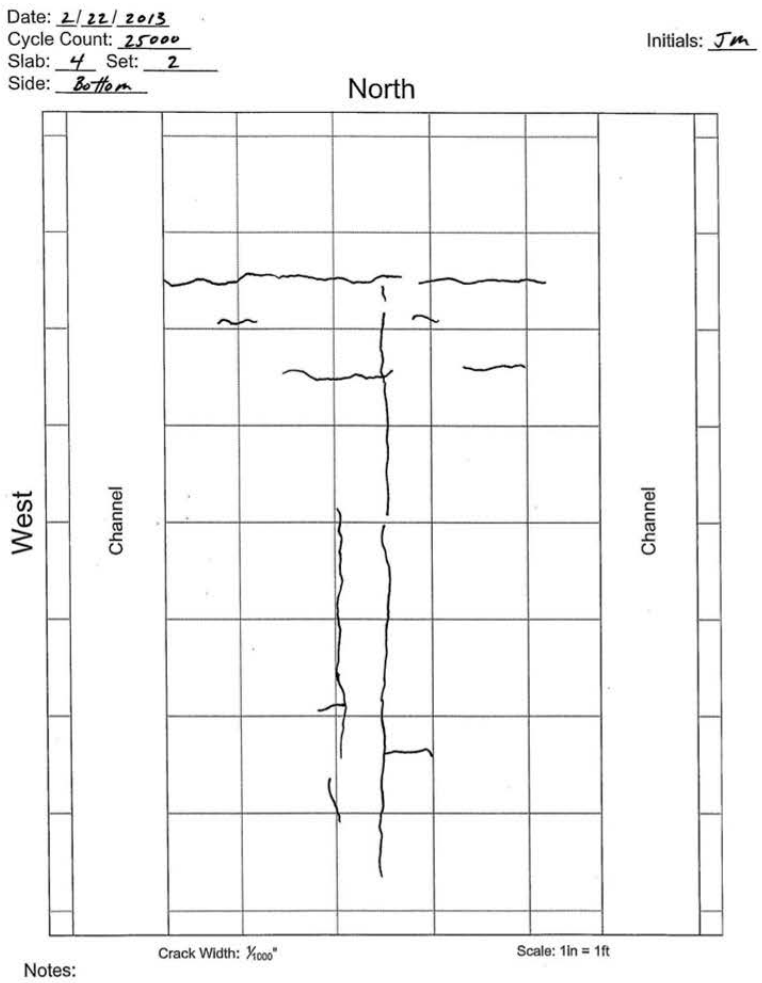

Figure F-8: Crack maps, M25$_b$ test panel, 25,000 traffic cycles.

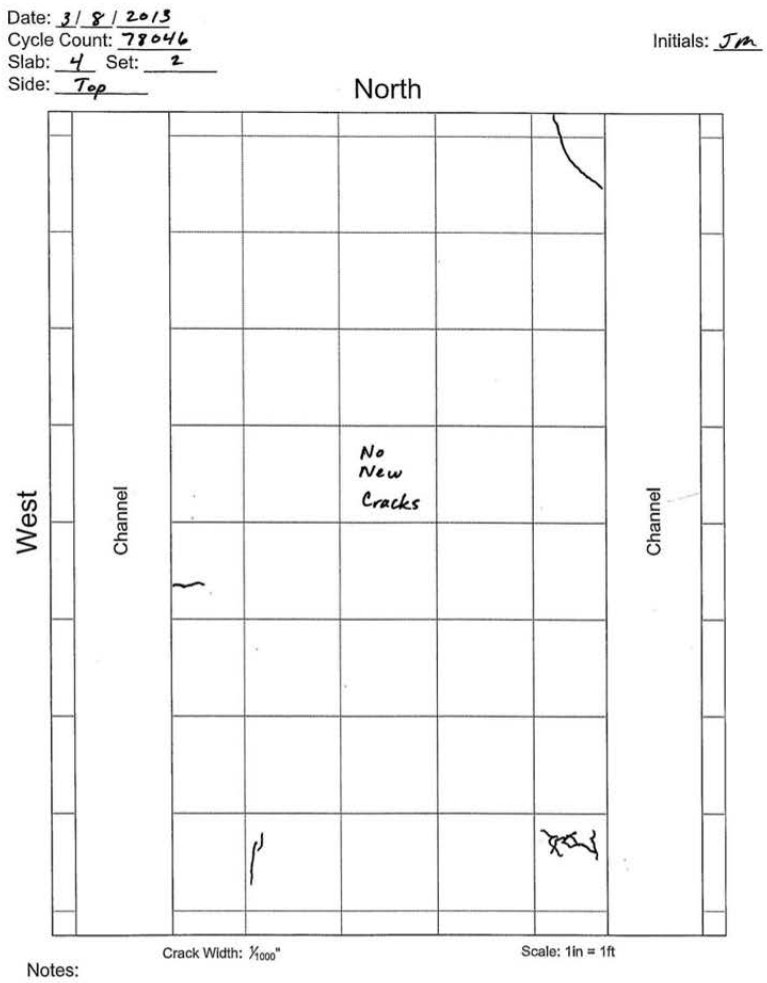

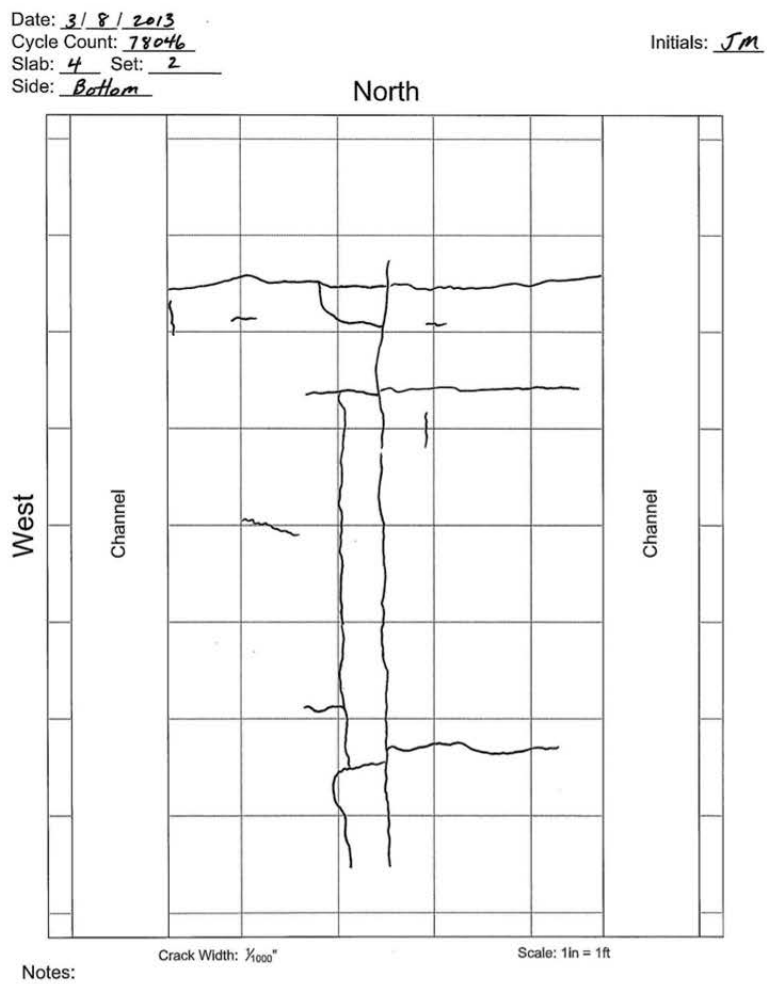

Figure F-9: Crack maps, M25$_b$ test panel, 78,000 traffic cycles.

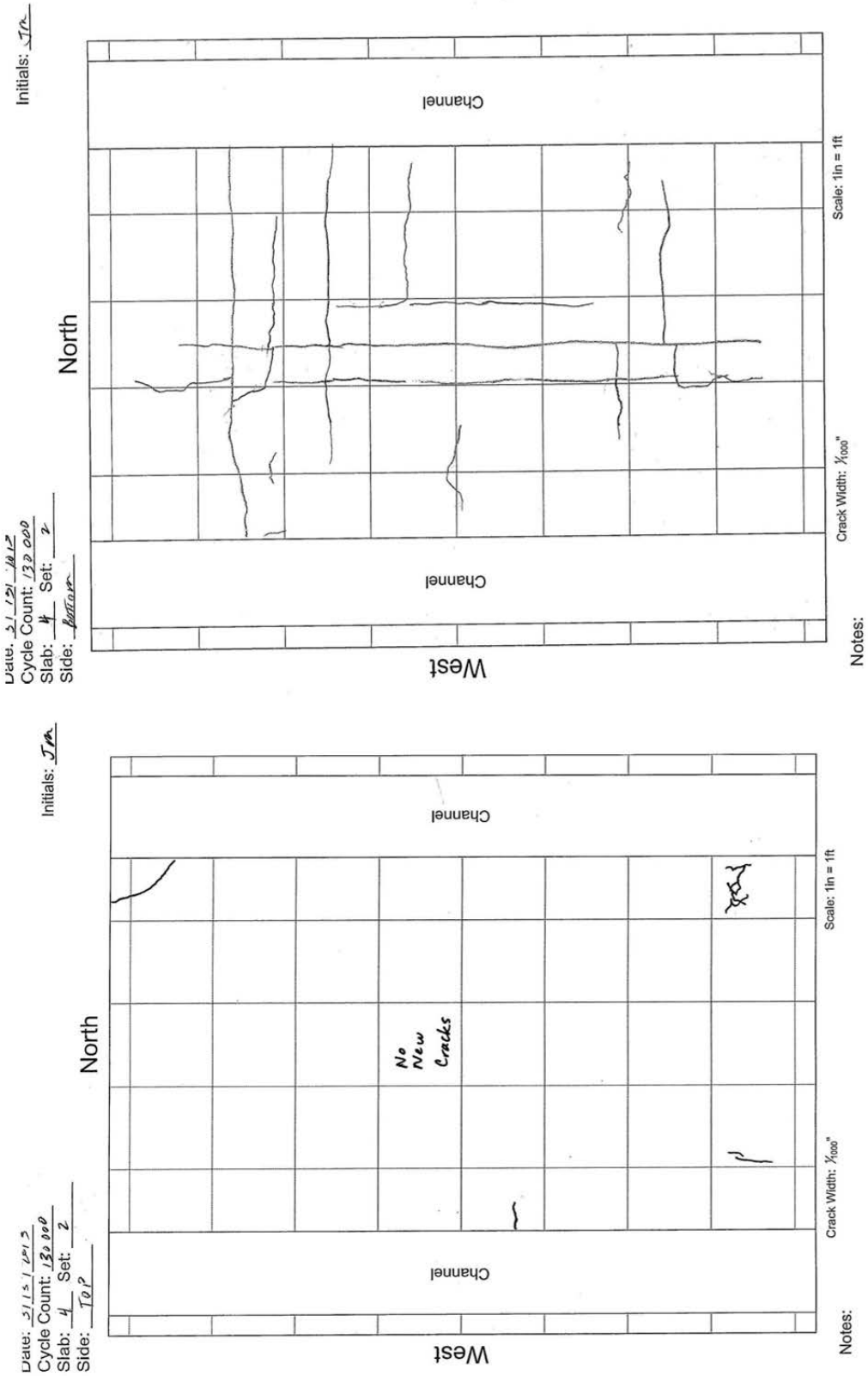

Figure F-10: Crack maps, $M25_b$ test panel, 130,000 traffic cycles.

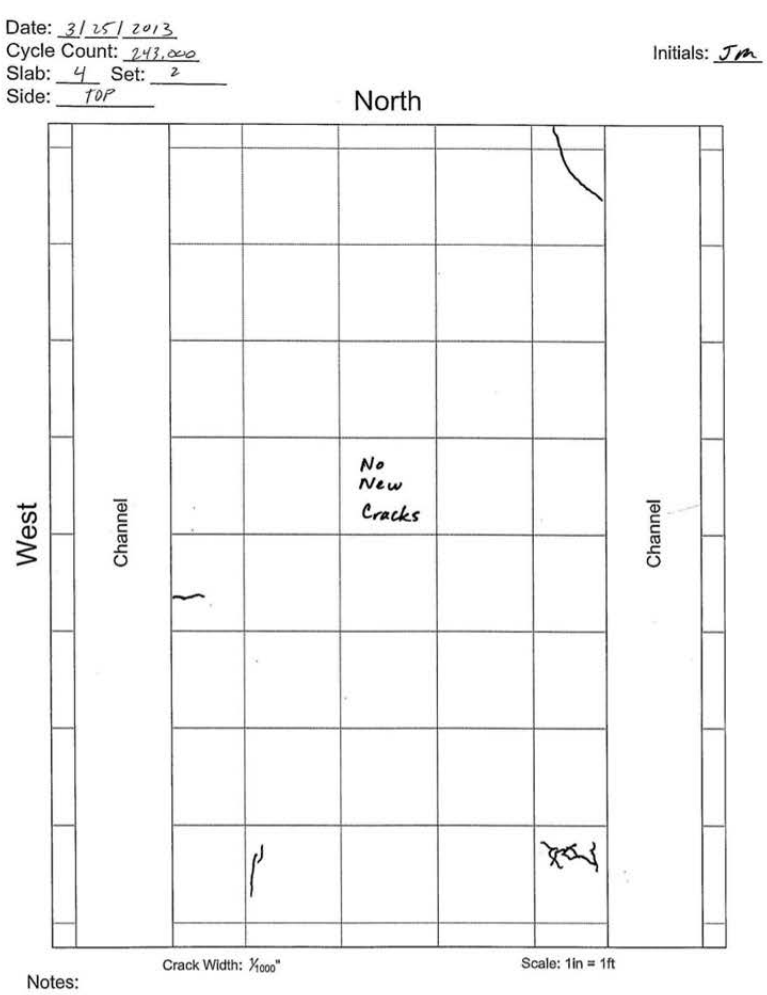

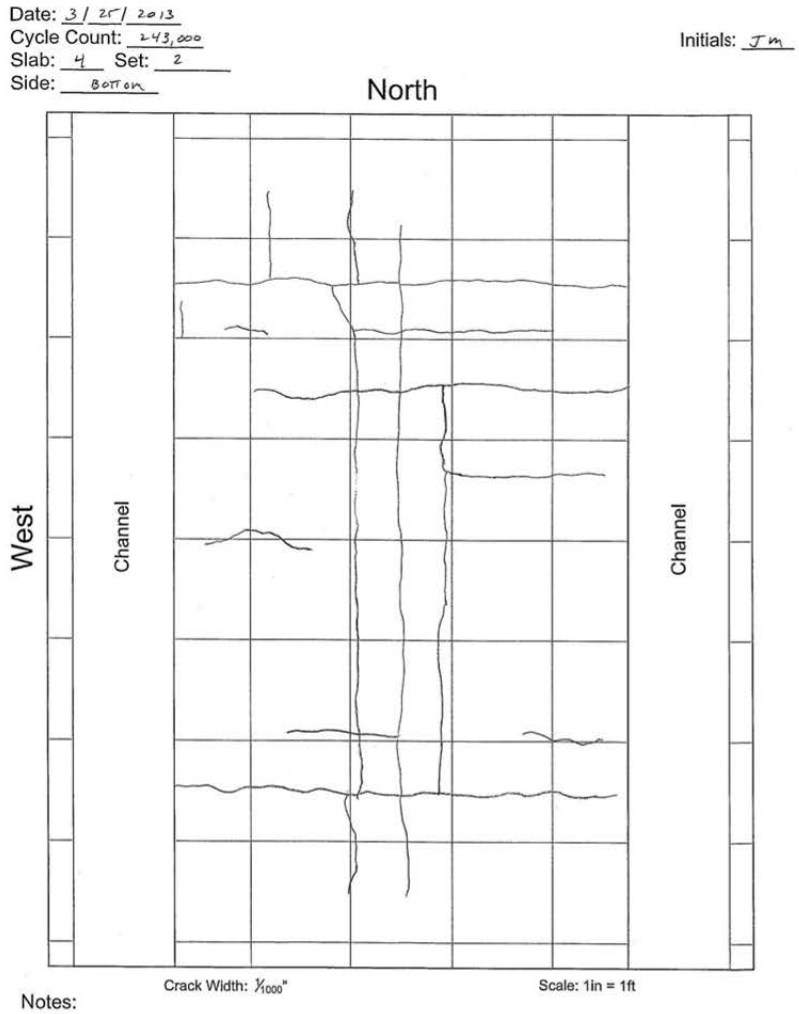

Figure F-11: Crack maps, M25$_b$ test panel, 242,590 traffic cycles.

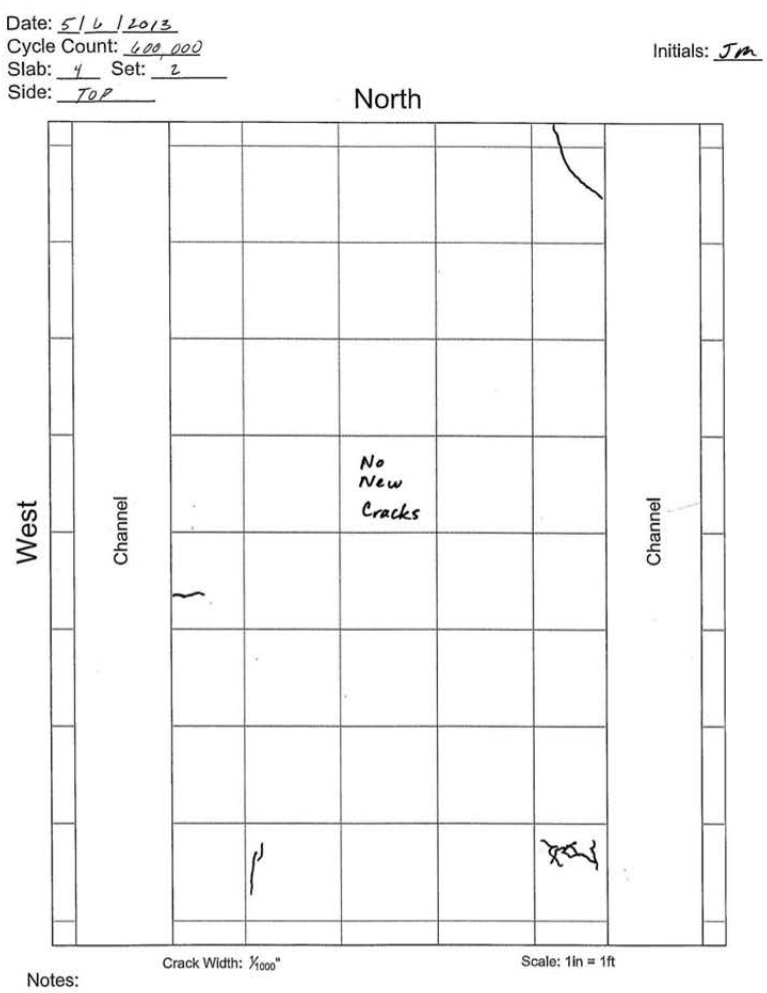

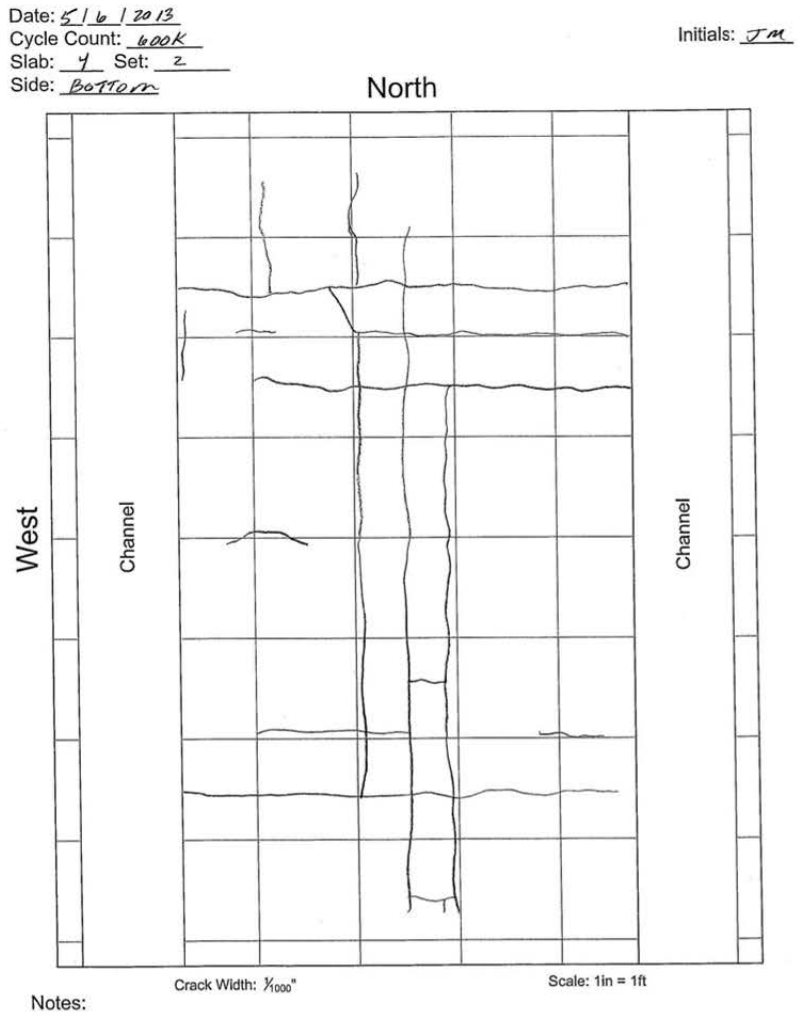

Figure F-12: Crack maps, M25$_b$ test panel, 604,932 traffic cycles.

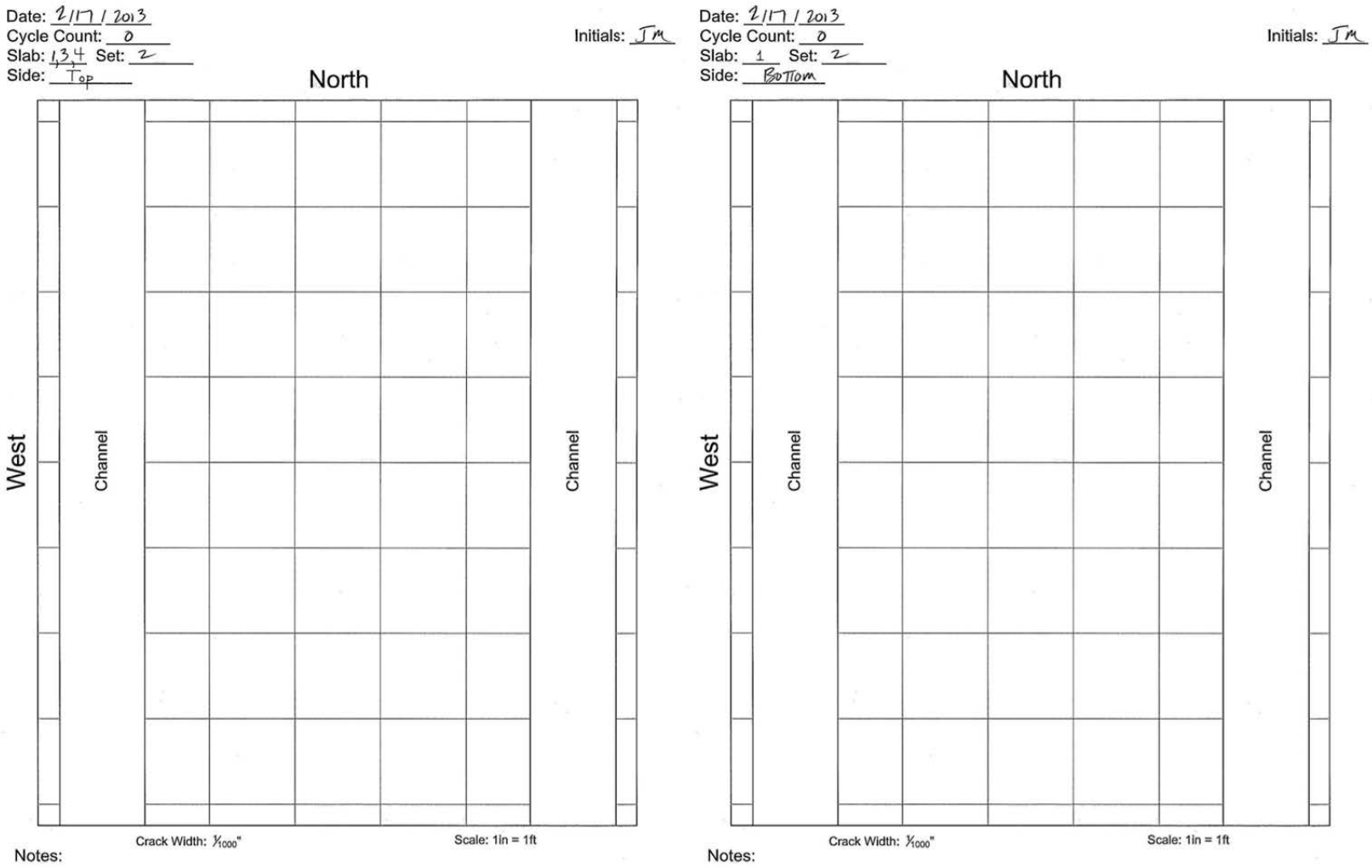

Figure F-13: Crack maps, M250$_a$ test panel, 0 traffic cycles.

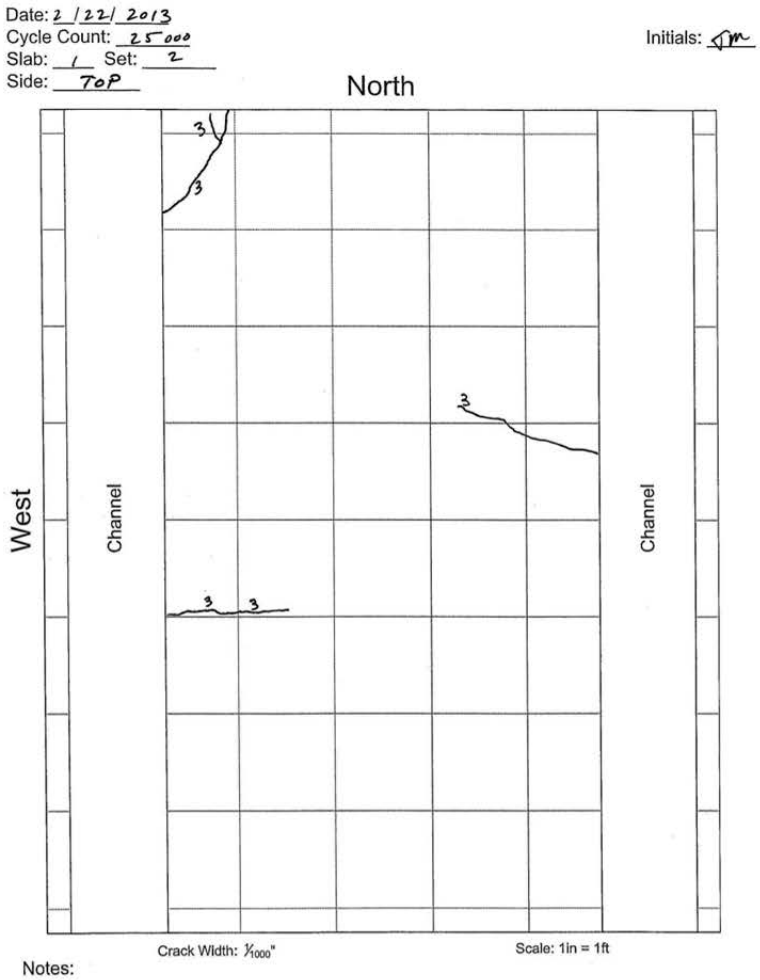

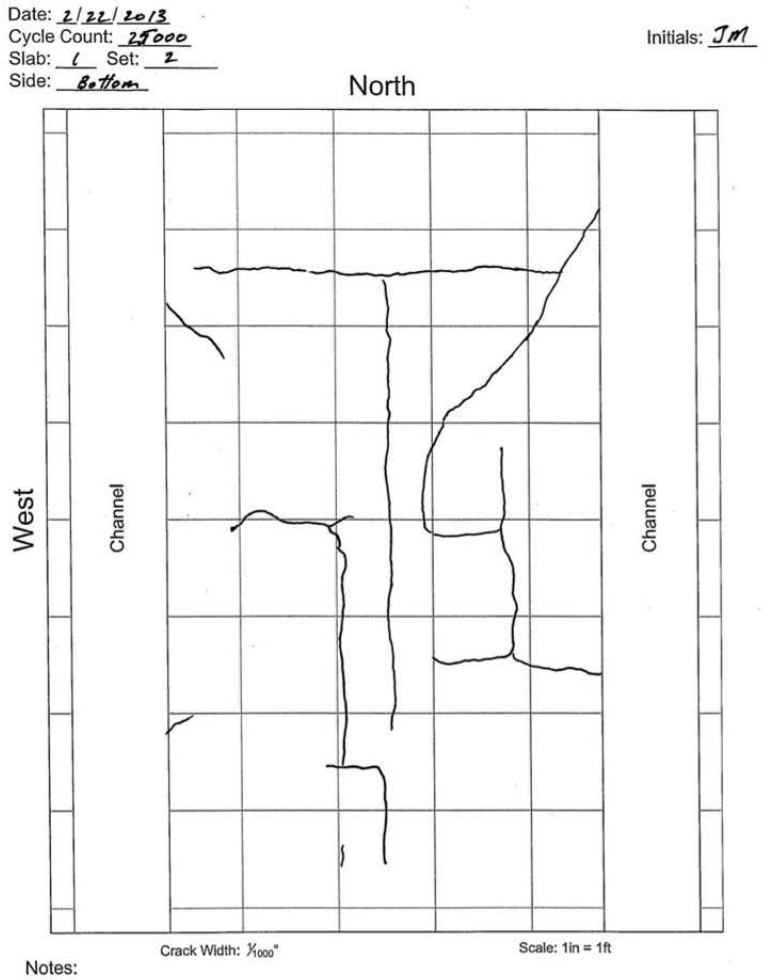

Figure F-14: Crack maps, M250$_a$ test panel, 25,000 traffic cycles.

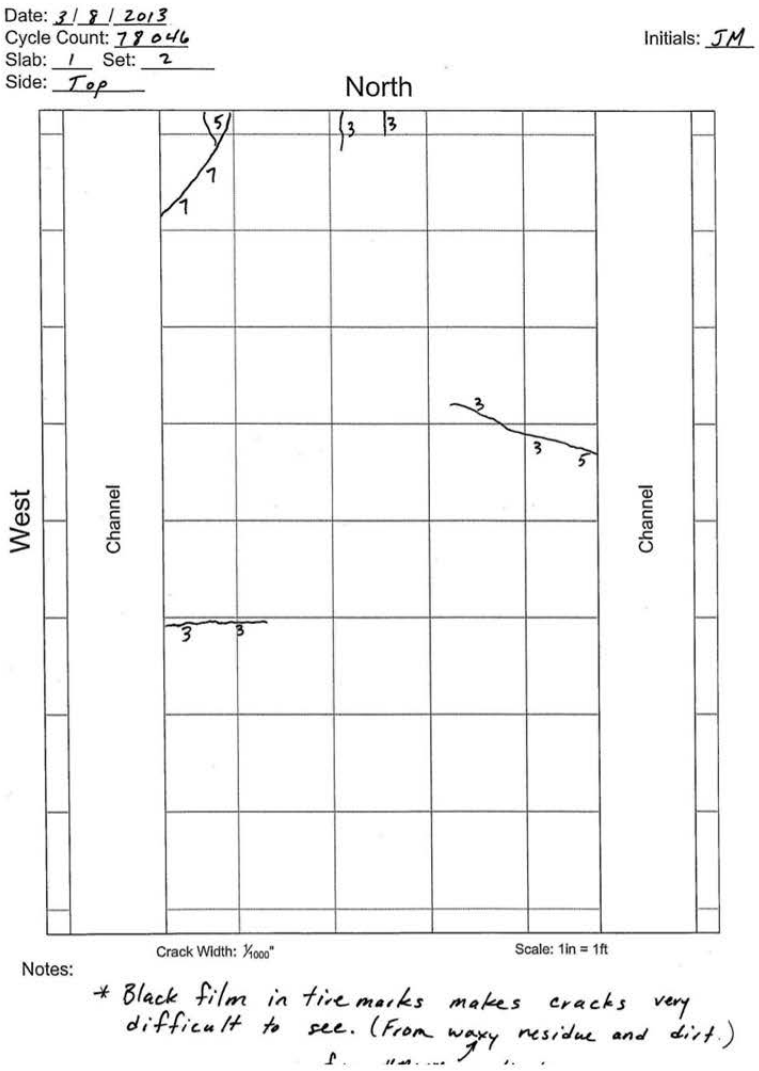

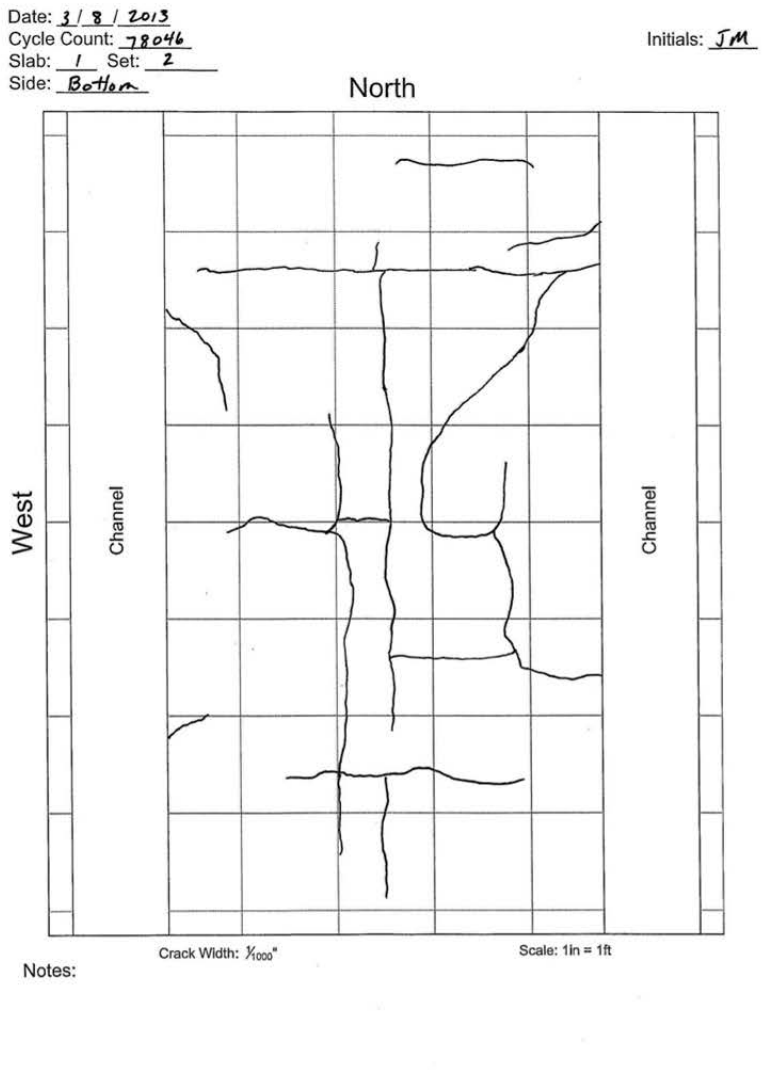

Figure F-15: Crack maps, M250$_a$ test panel, 78,000 traffic cycles.

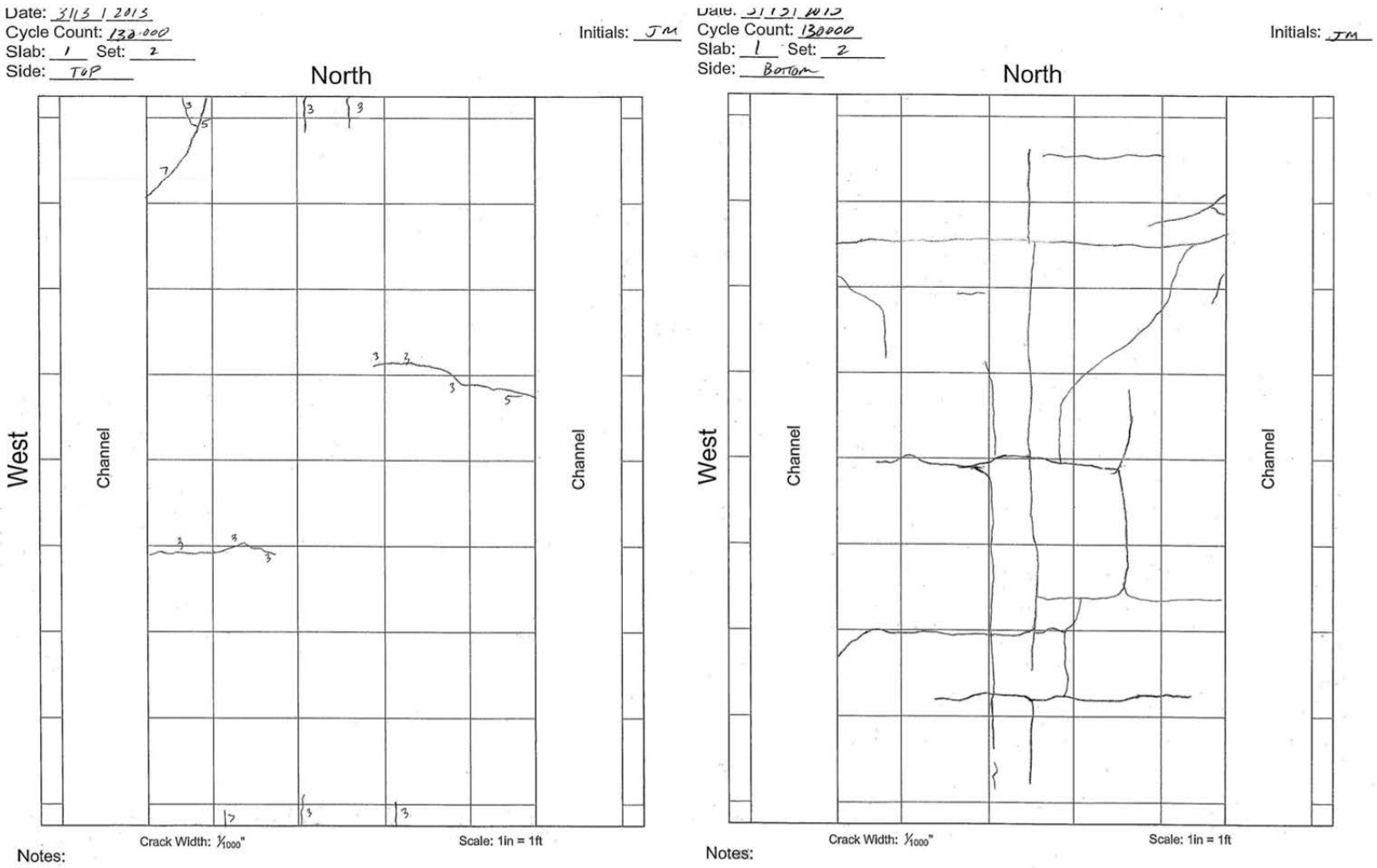

Figure F-16: Crack maps, M250$_a$ test panel, 130,000 traffic cycles.

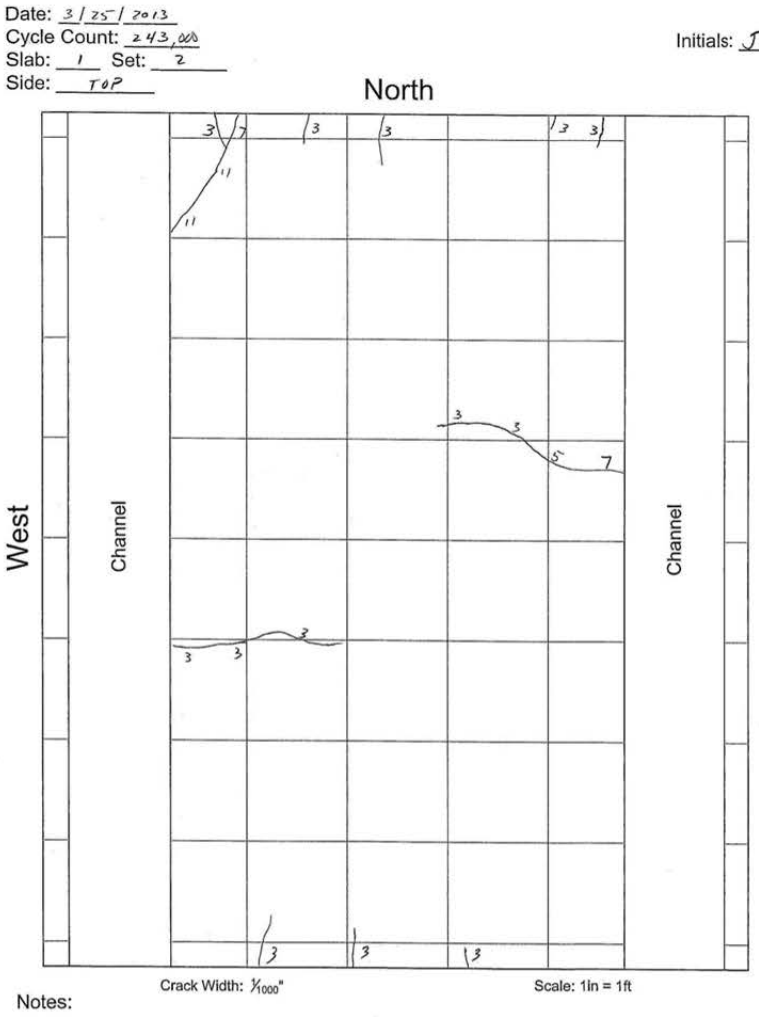

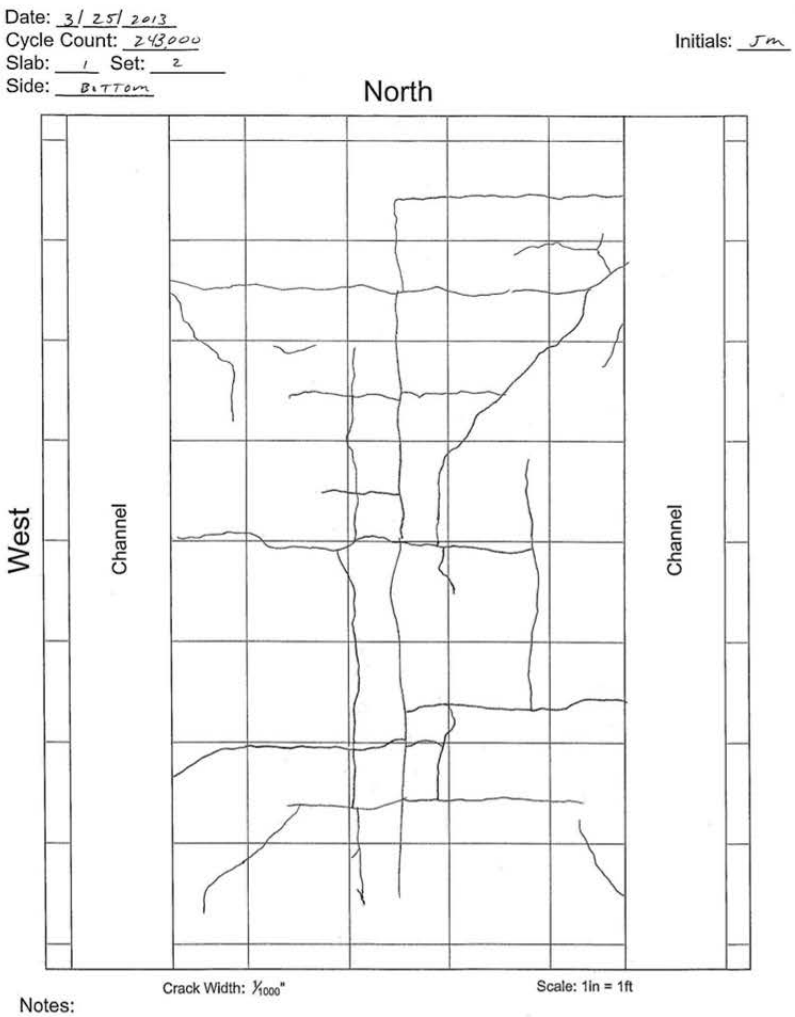

Figure F-17: Crack maps, M250$_a$ test panel, 242,590 traffic cycles.

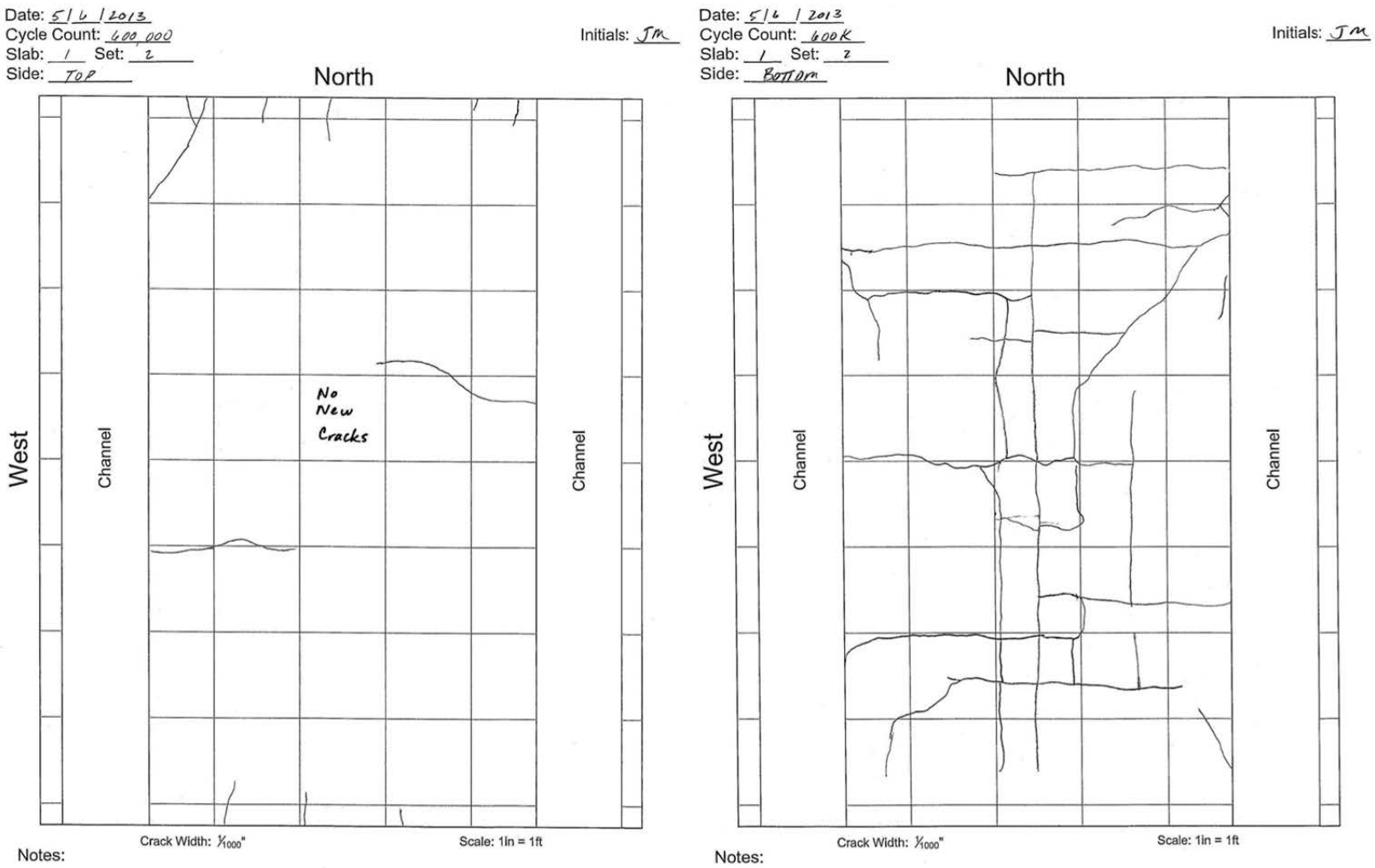

Figure F-18: Crack maps, M250$_a$ test panel, 604,932 traffic cycles.

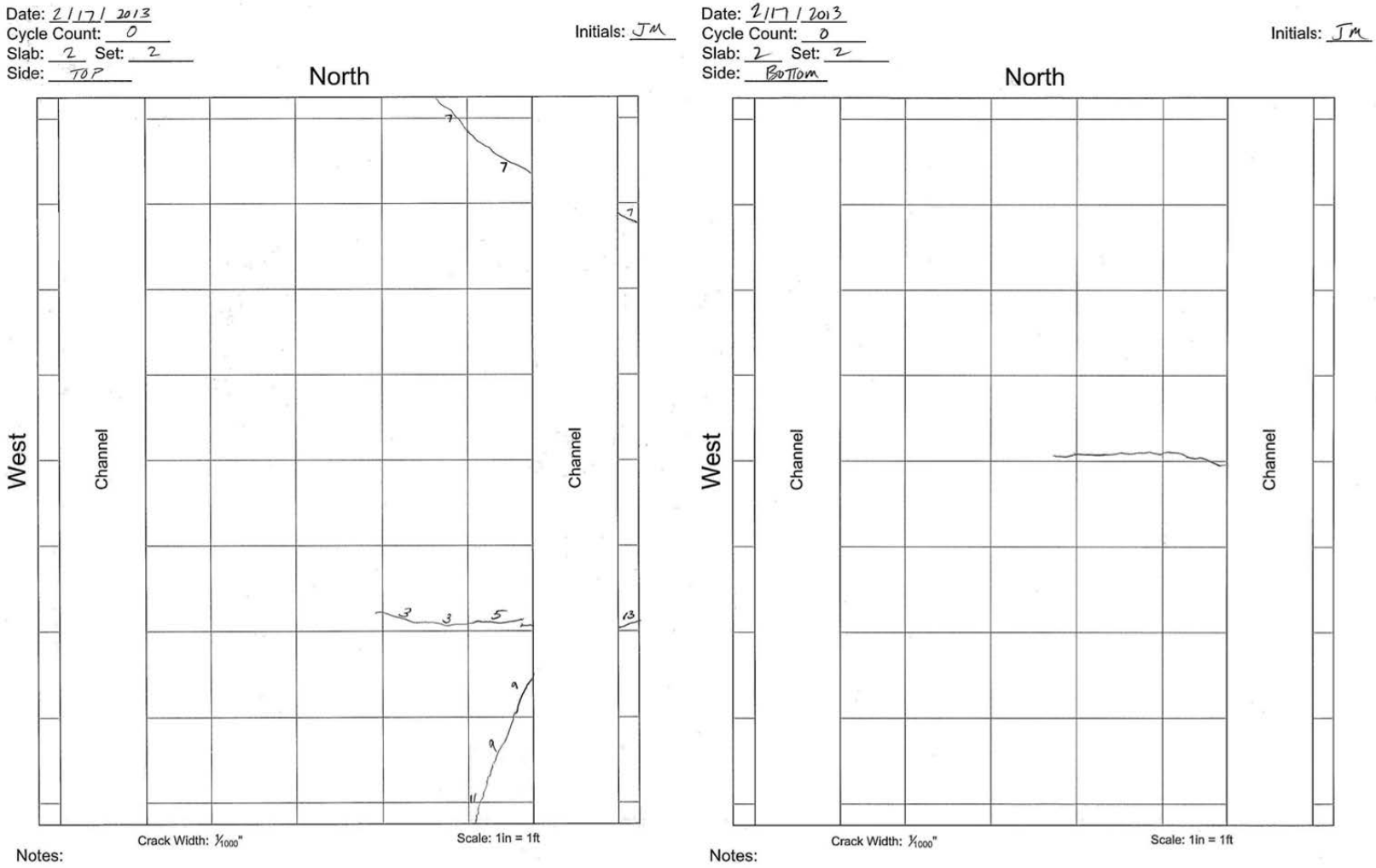

Figure F-19: Crack maps, M250, test panel, 0 traffic cycles.

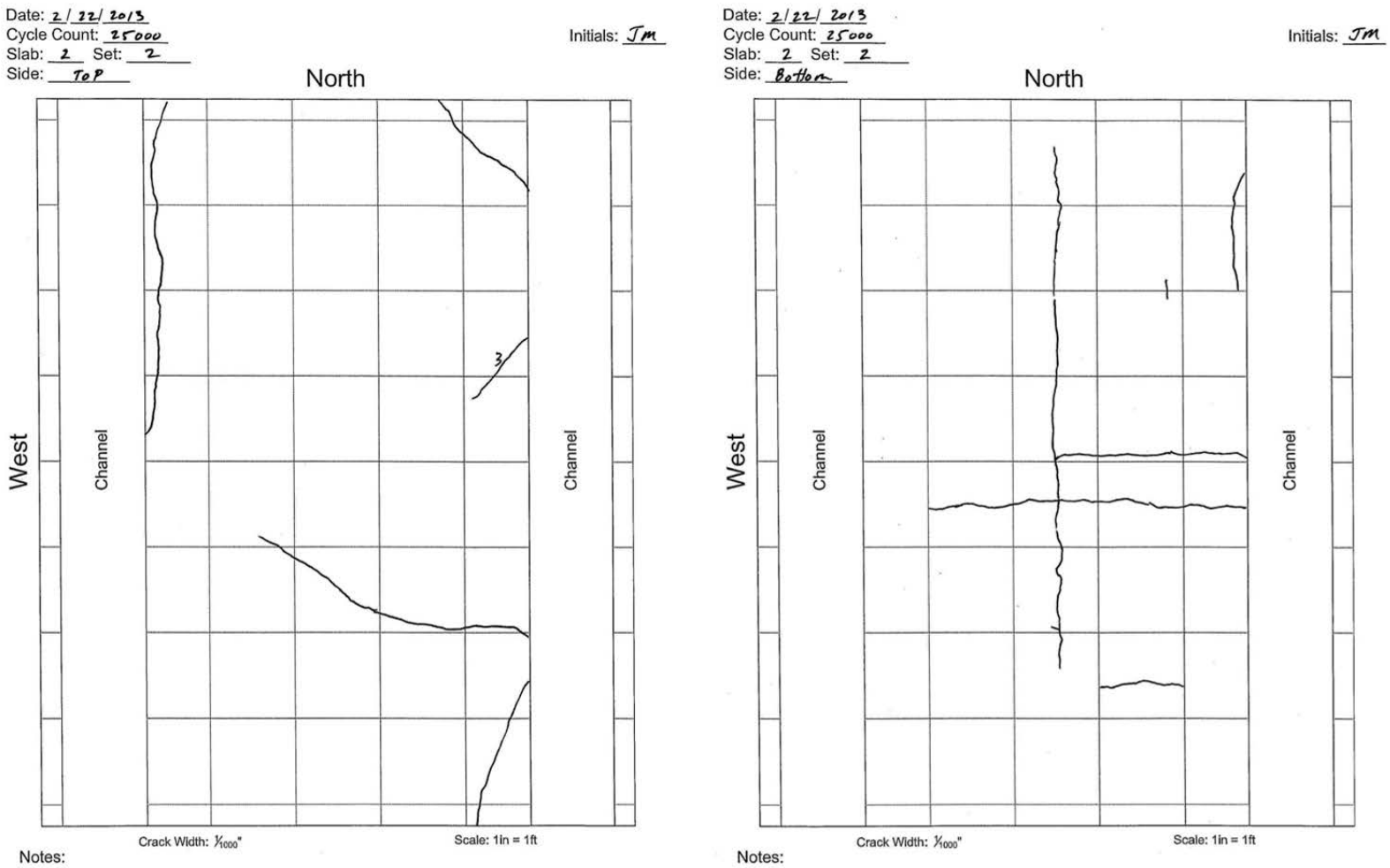

Figure F-20: Crack maps, M250$_b$ test panel, 25,000 traffic cycles.

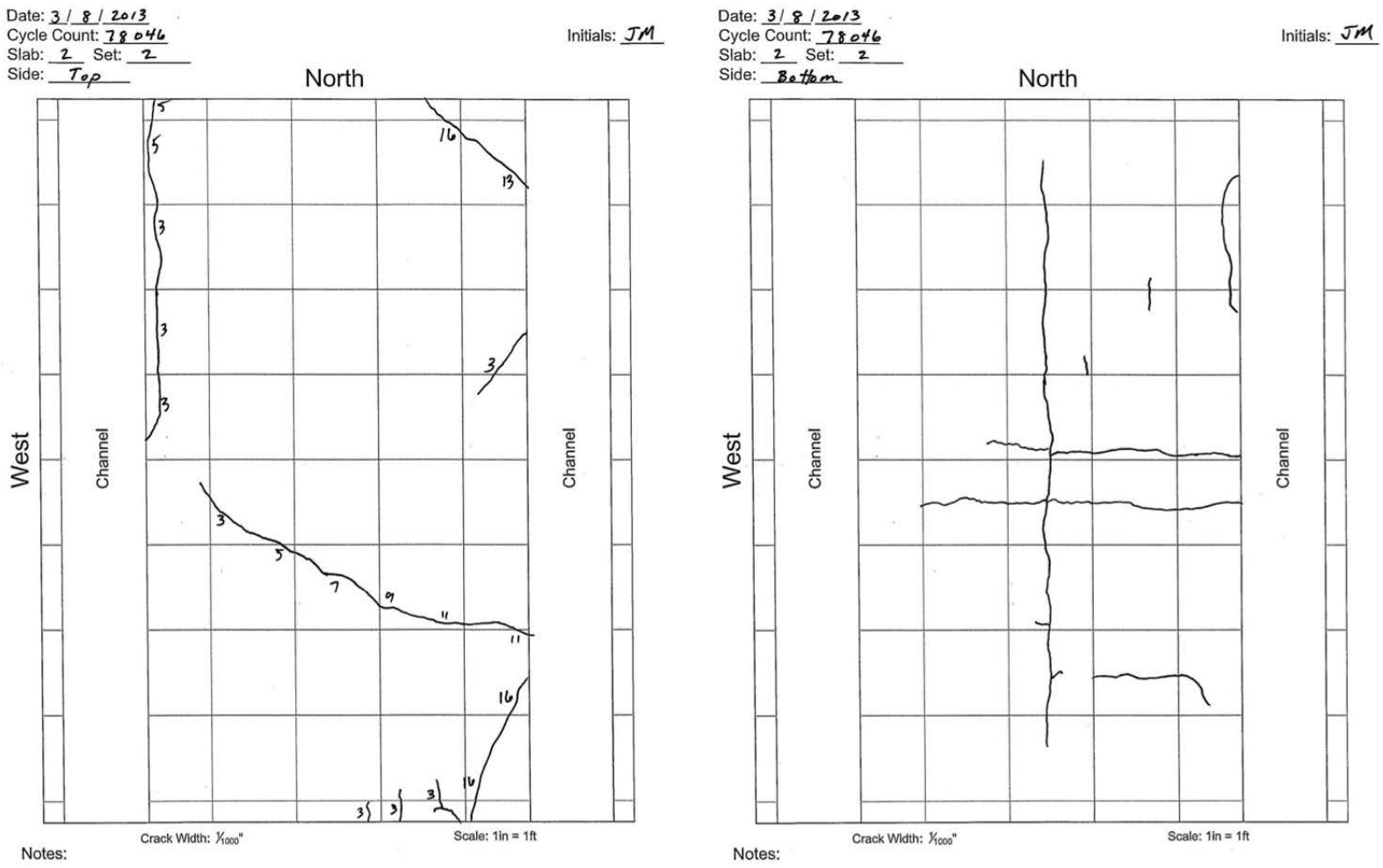

Figure F-21: Crack maps, M250$_b$ test panel, 78,000 traffic cycles.

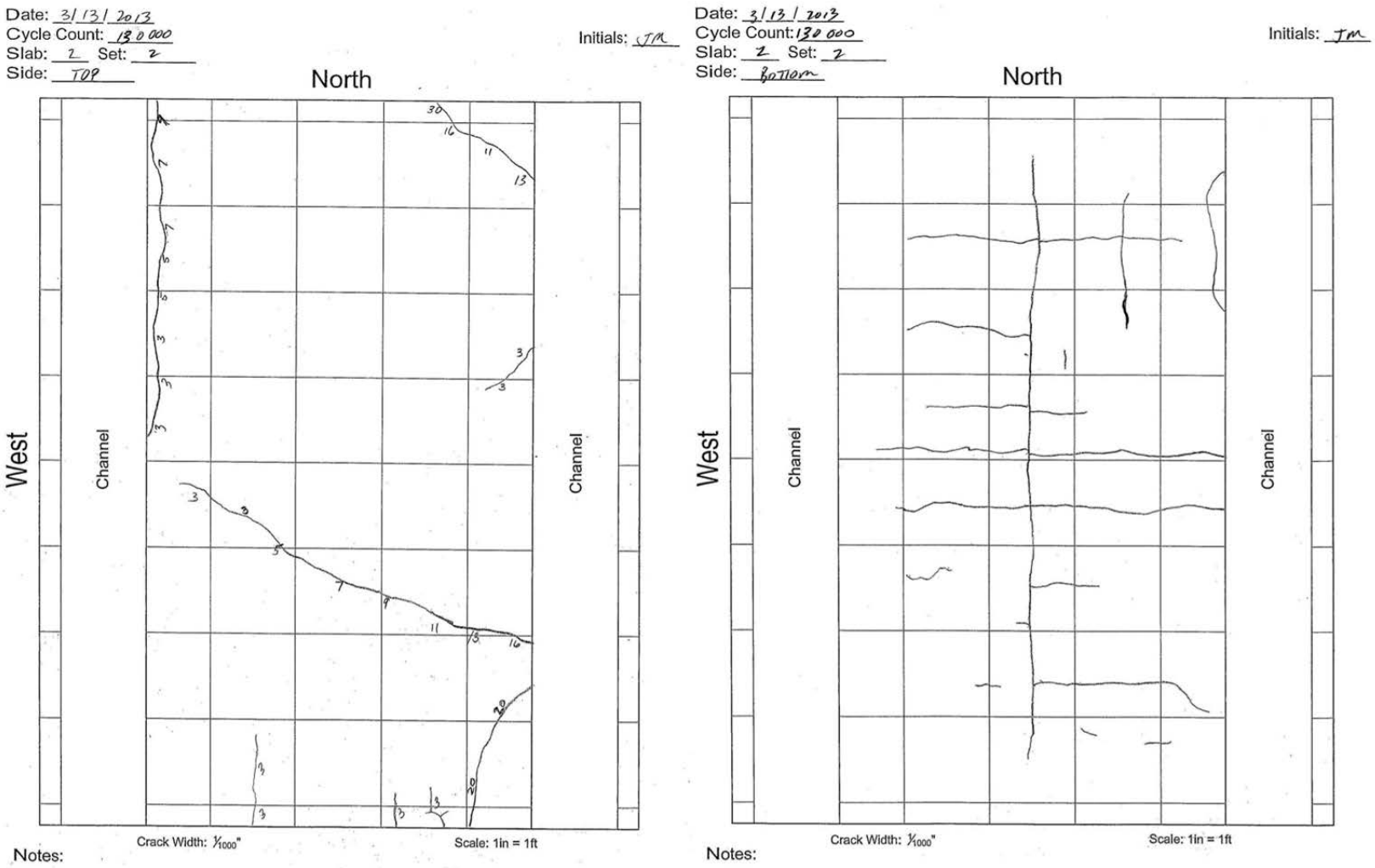

Figure F-22: Crack maps, M250$_b$, test panel, 130,000 traffic cycles.

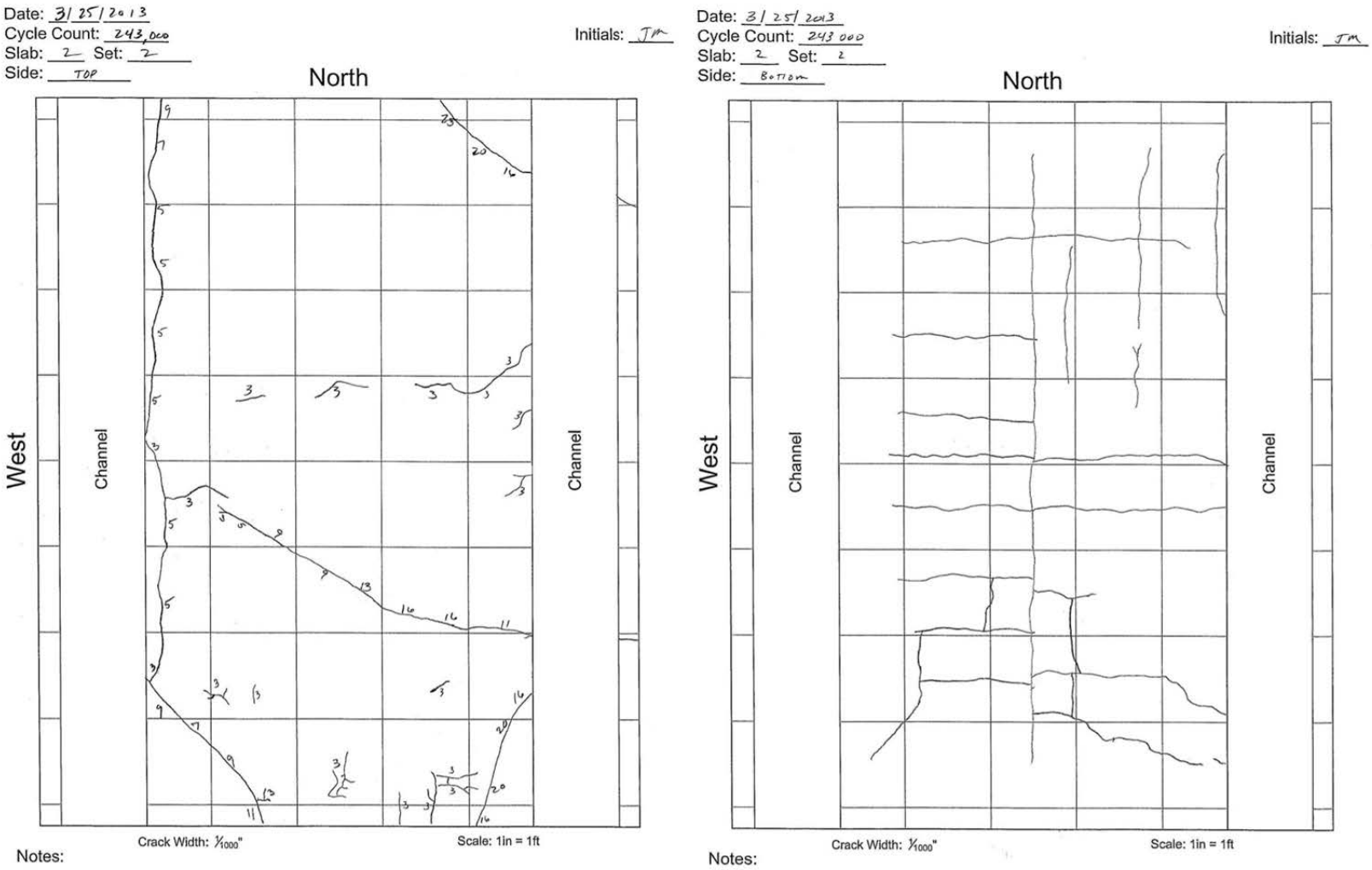

Figure F-23: Crack maps, M250$_b$, test panel, 242,590 traffic cycles.

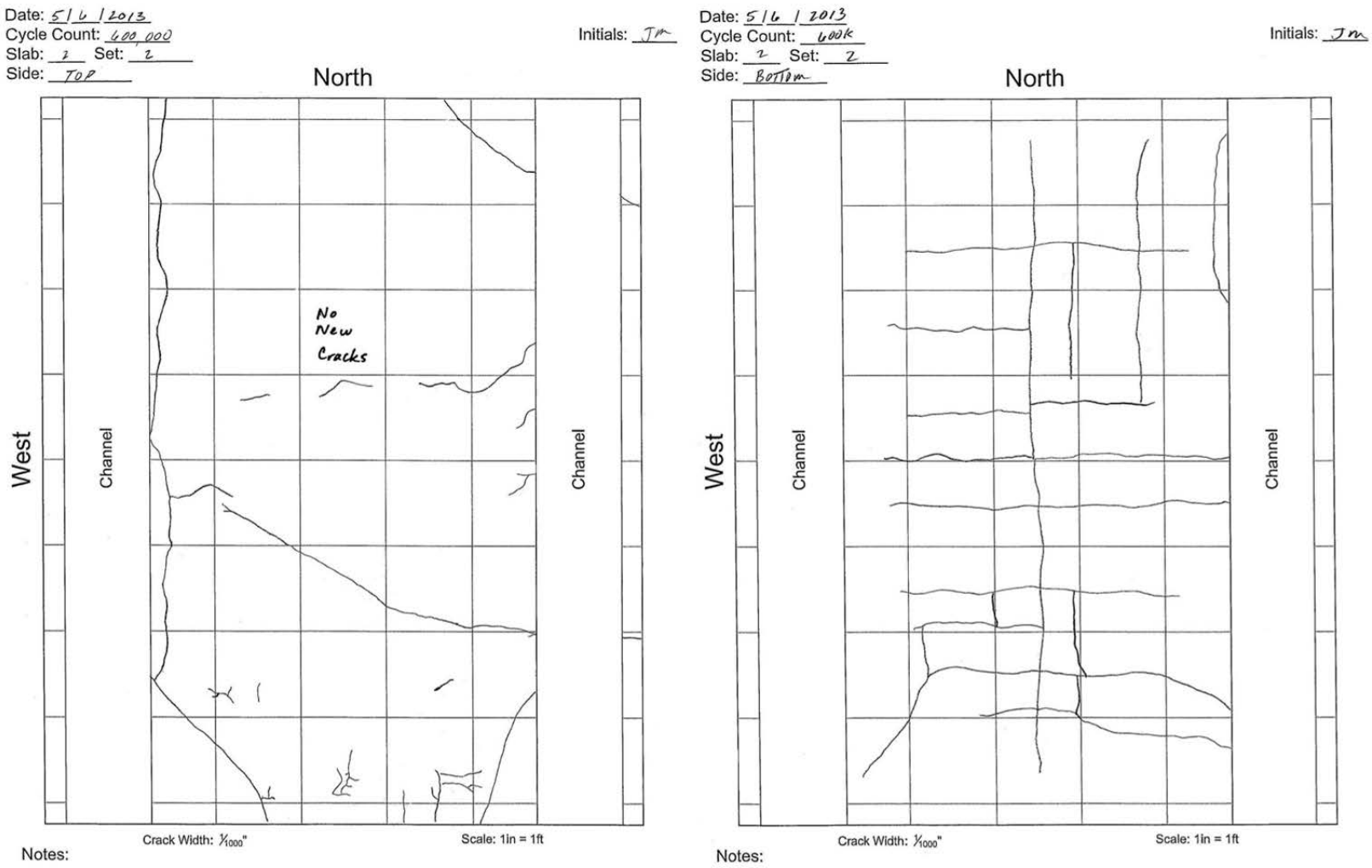

Figure F-24: Crack maps, M250$_b$, test panel, 604,932 traffic cycles.

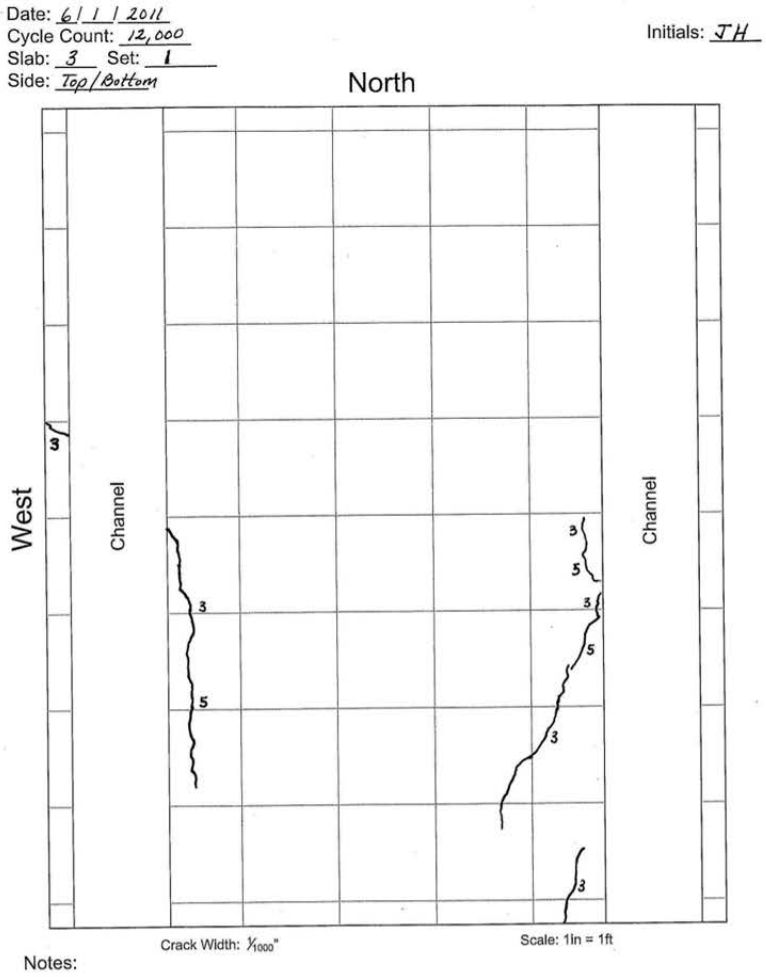

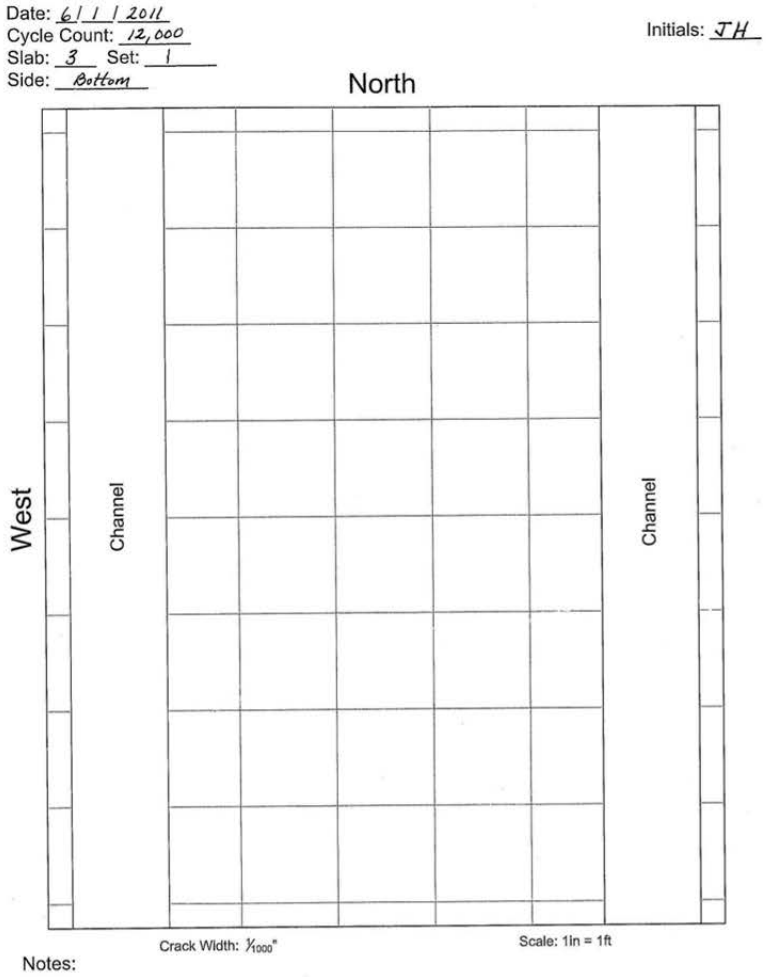

Figure F-25: Crack maps, M1000$_a$ test panel, 12,000 traffic cycles.

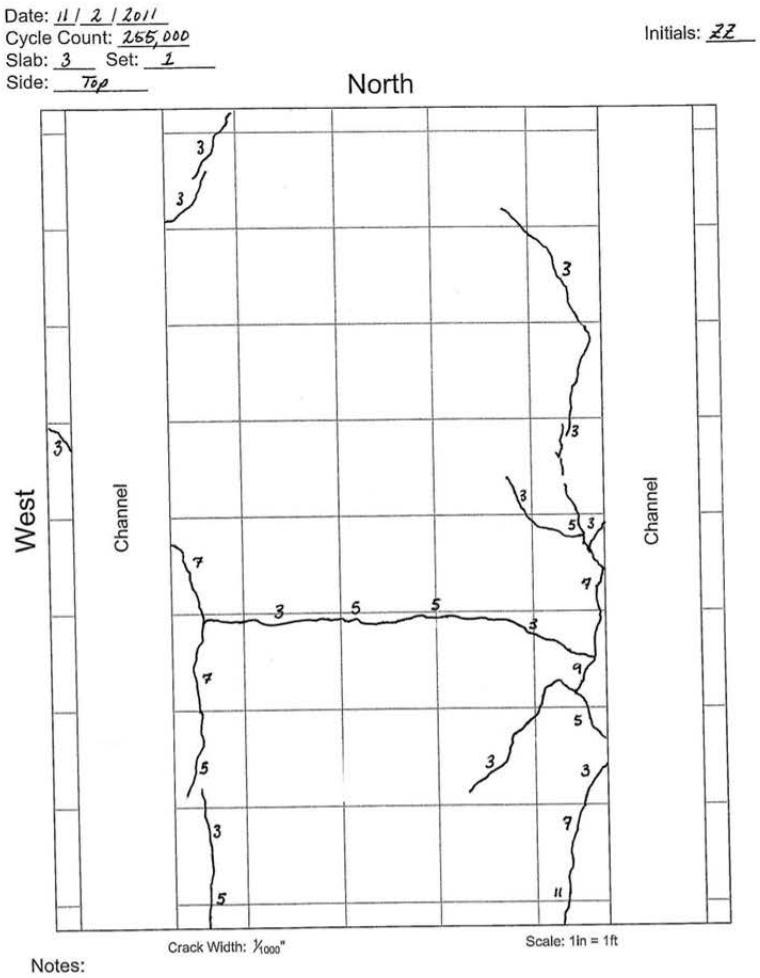

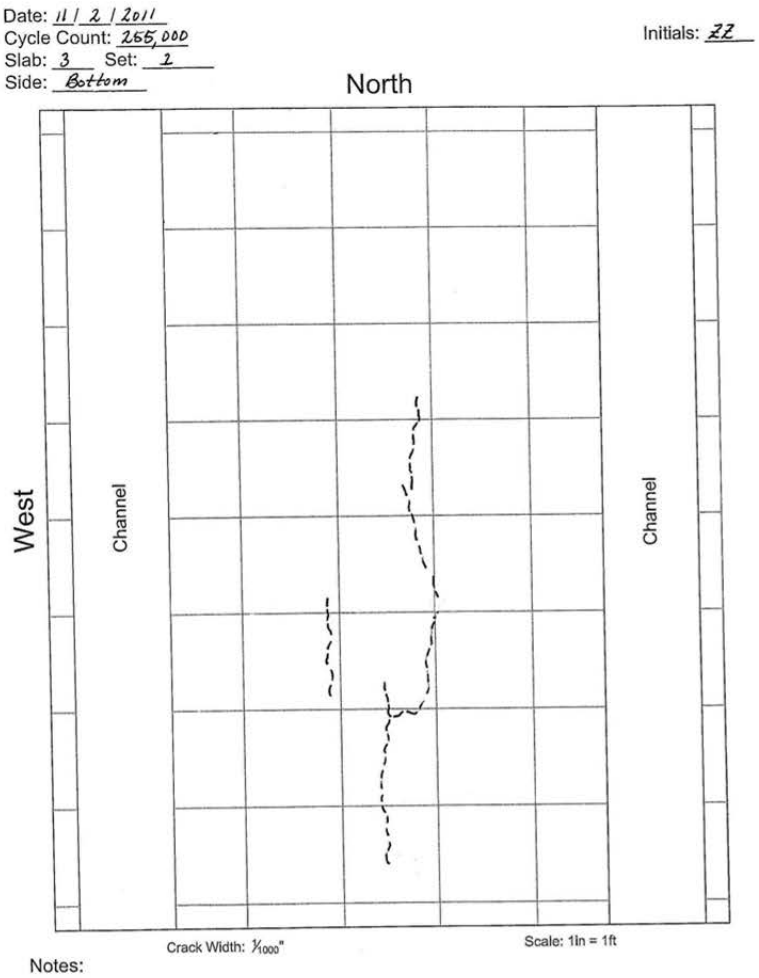

Figure F-26: Crack maps, M1000$_a$ test panel, 255,000 traffic cycles.

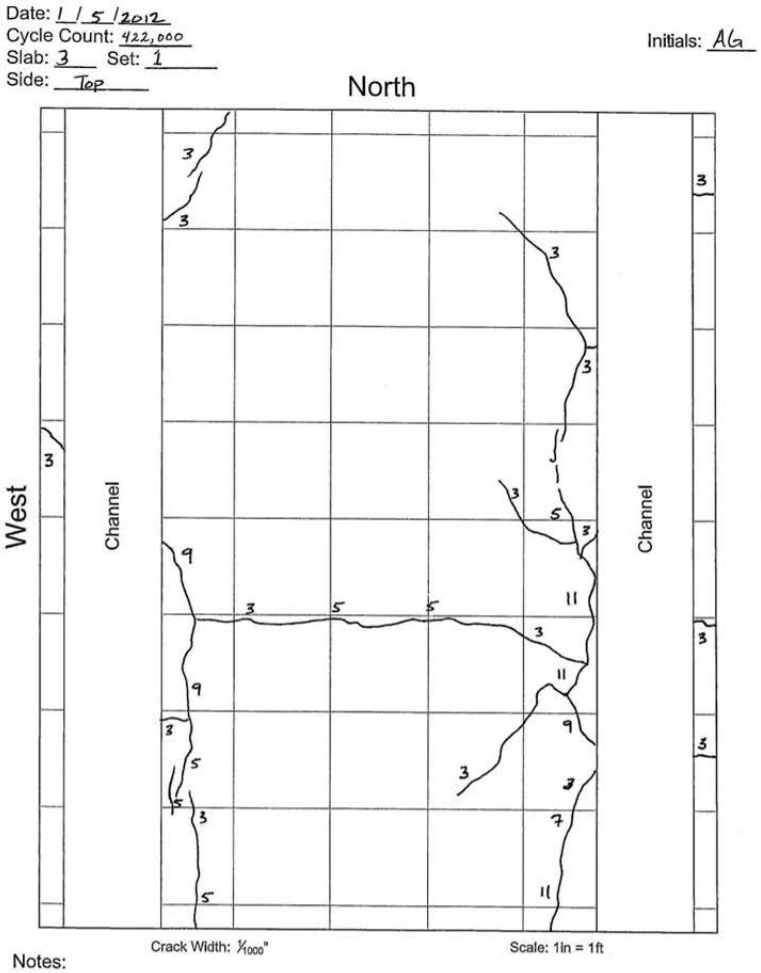

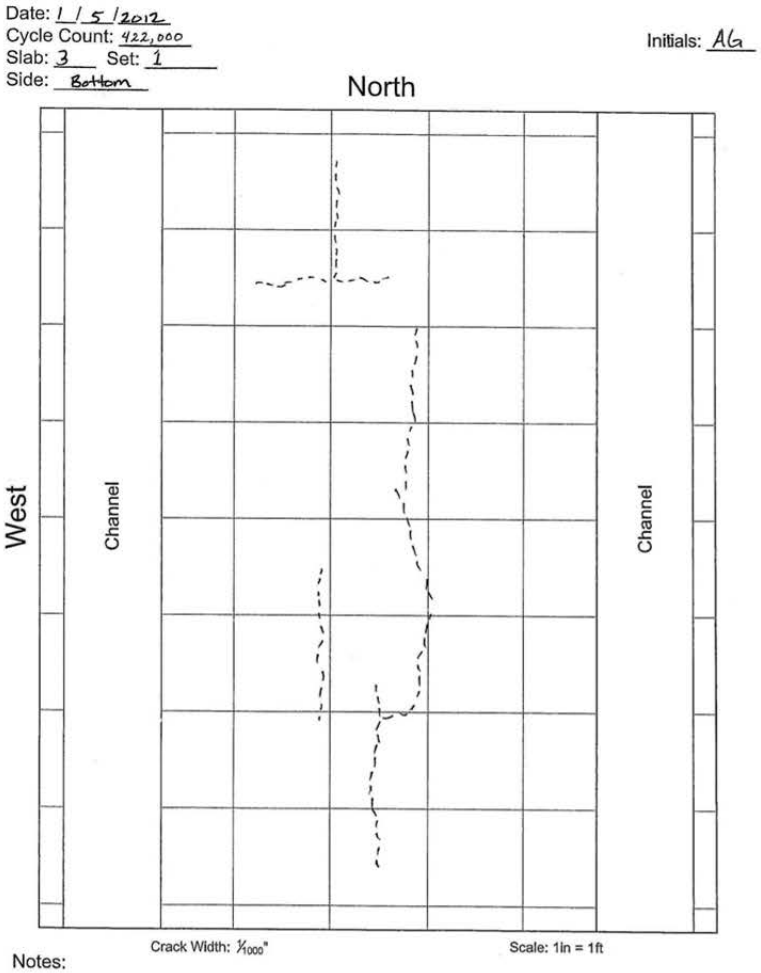

Figure F-27: Crack maps, M1000$_a$ test panel, 422,000 traffic cycles.

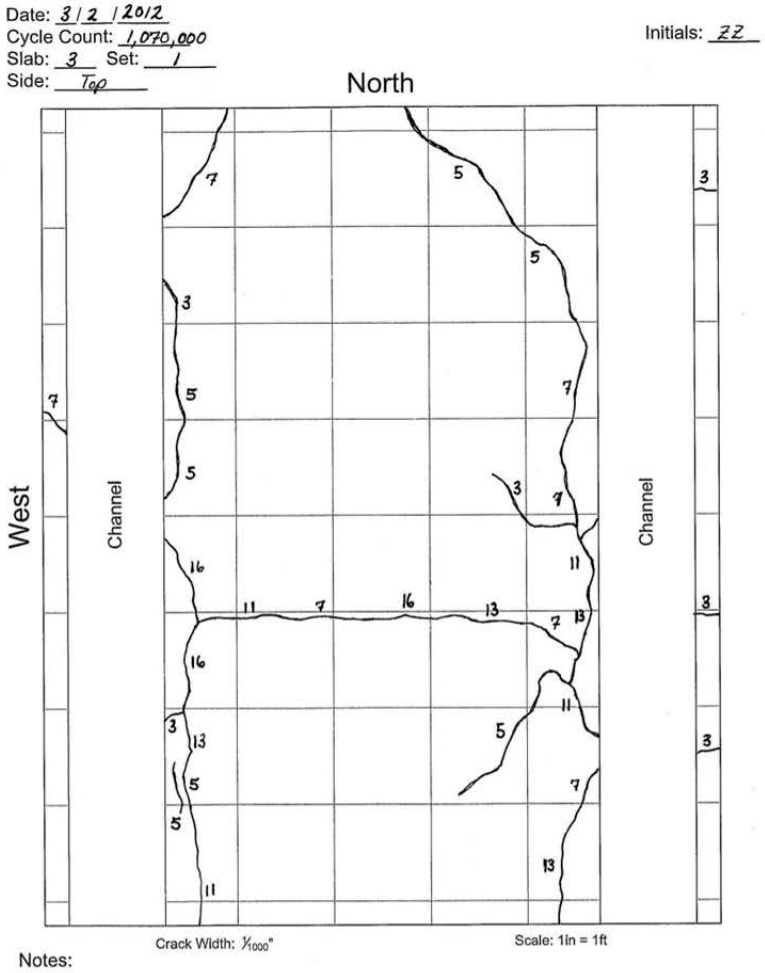

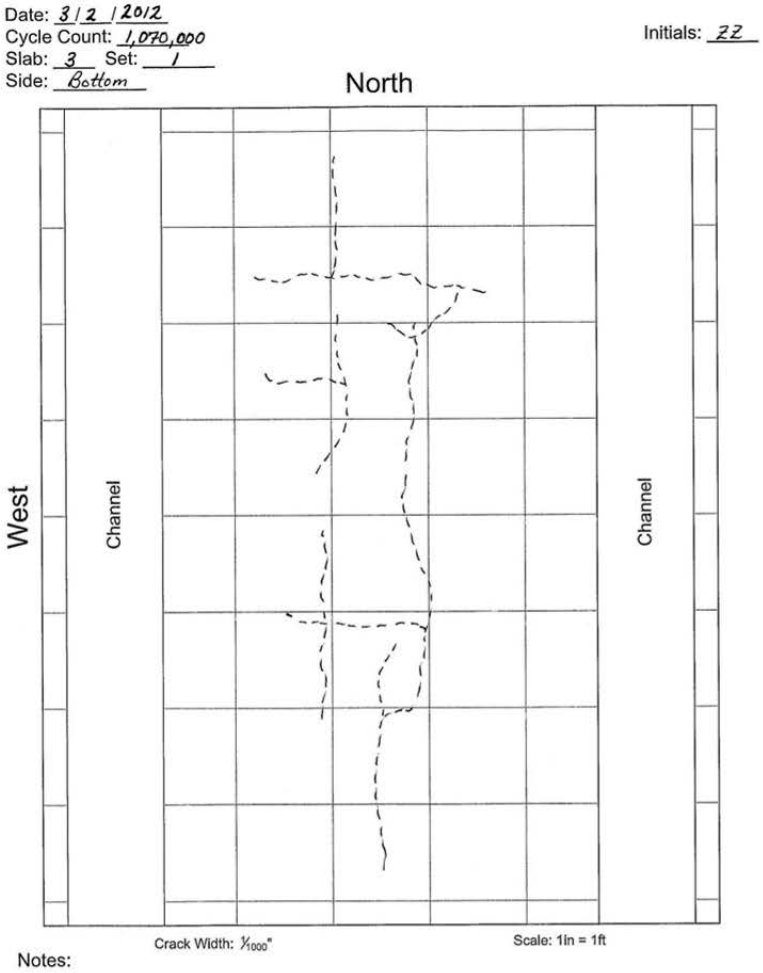

Figure F-28: Crack maps, M1000$_a$ test panel, 1,071,820 traffic cycles.

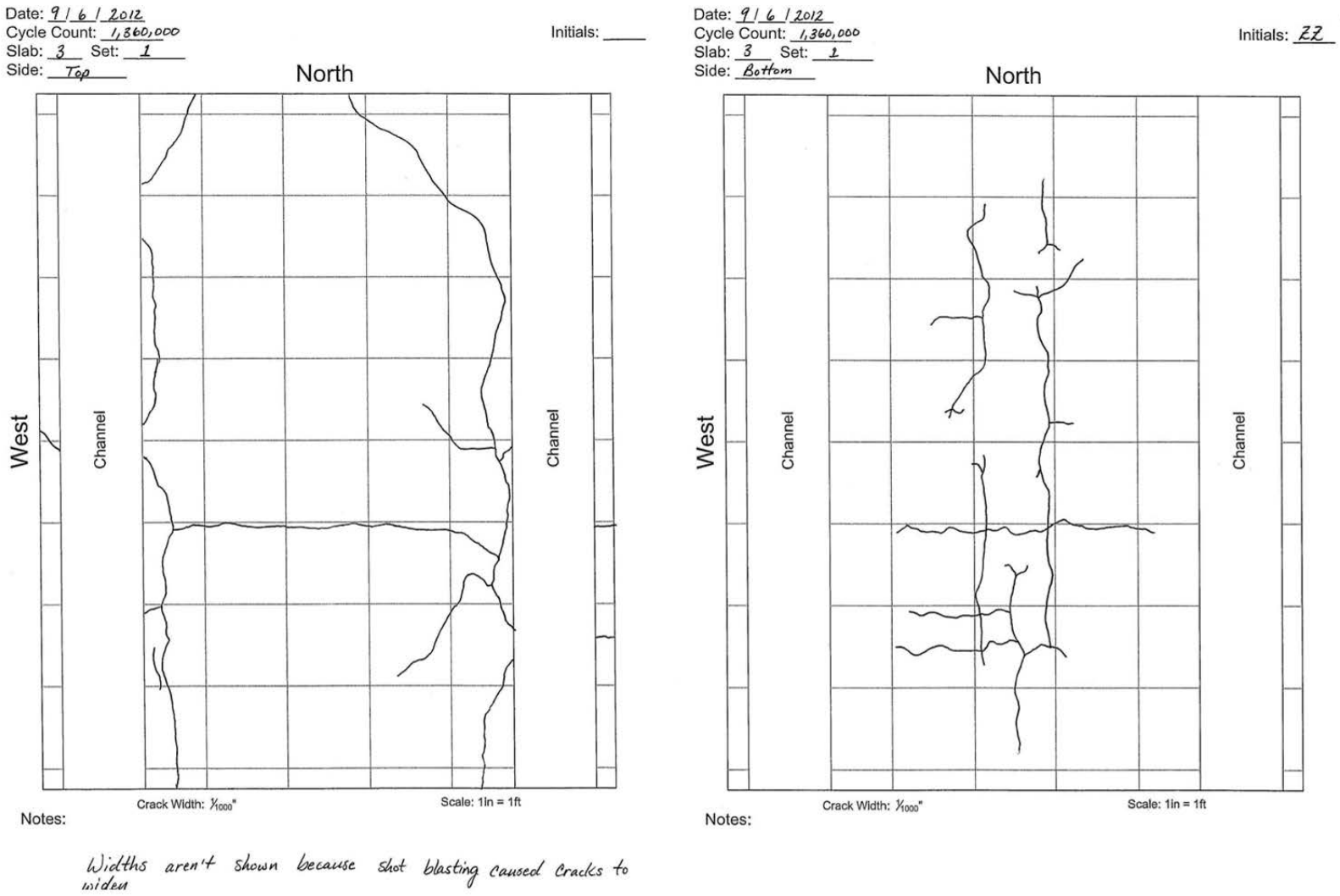

Figure F-29: Crack maps, M1000$_a$ test panel, 1,360,000 traffic cycles.

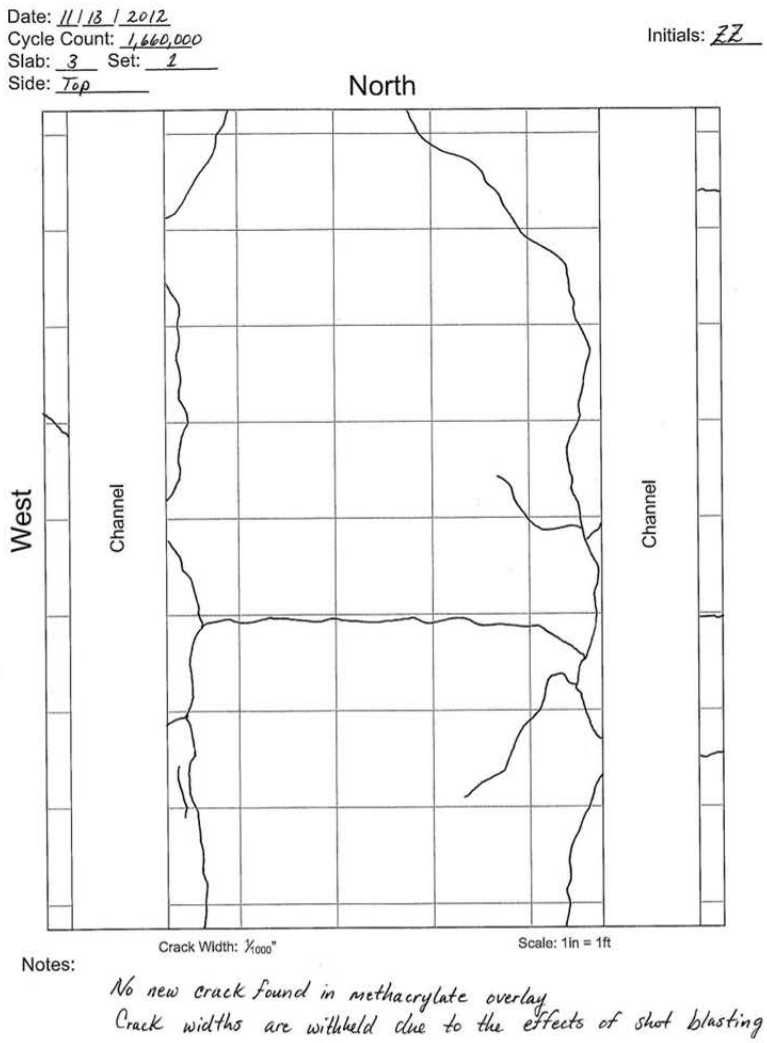

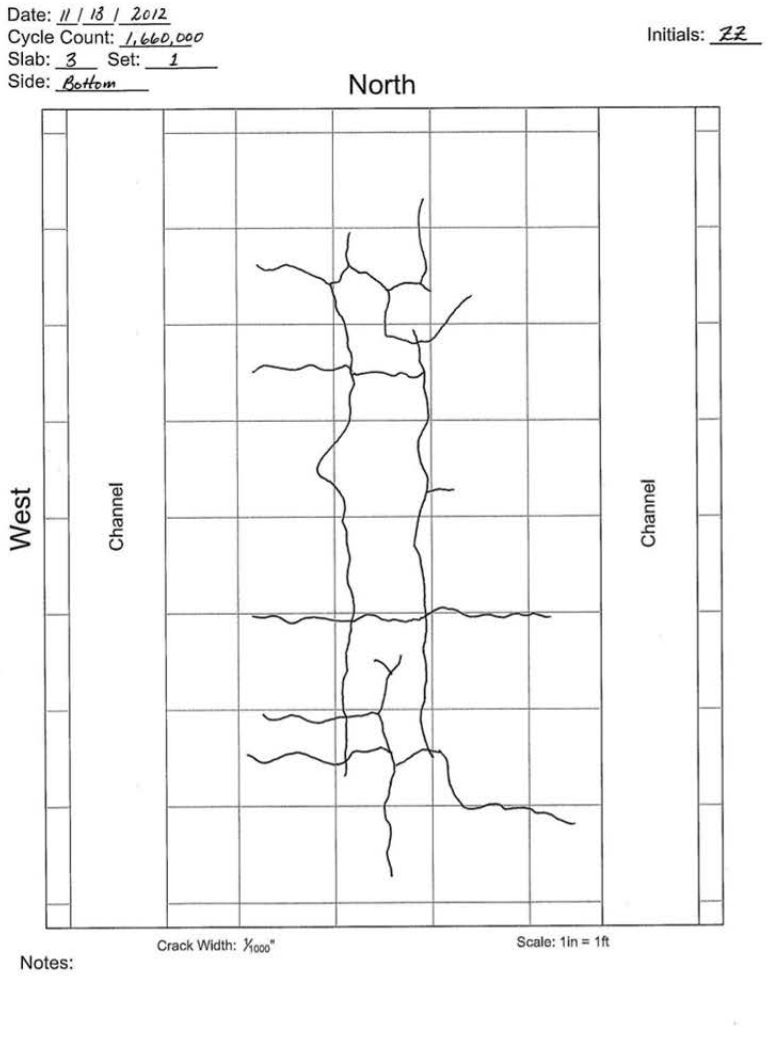

Figure F-30: Crack maps, M1000$_a$ test panel, 1,660,000 traffic cycles.

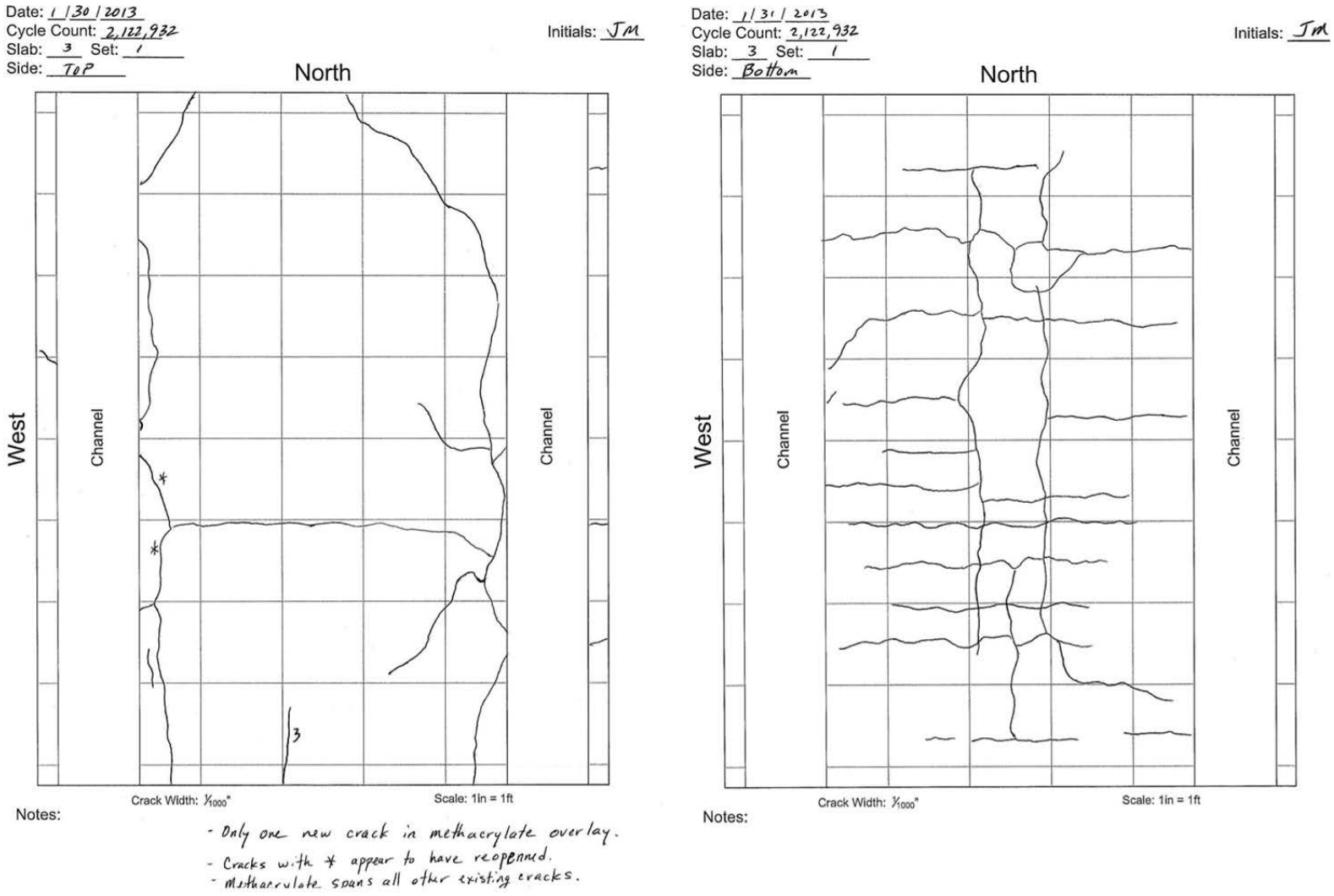

Figure F-31: Crack maps, M1000$_a$ test panel, 2,122,978 traffic cycles.

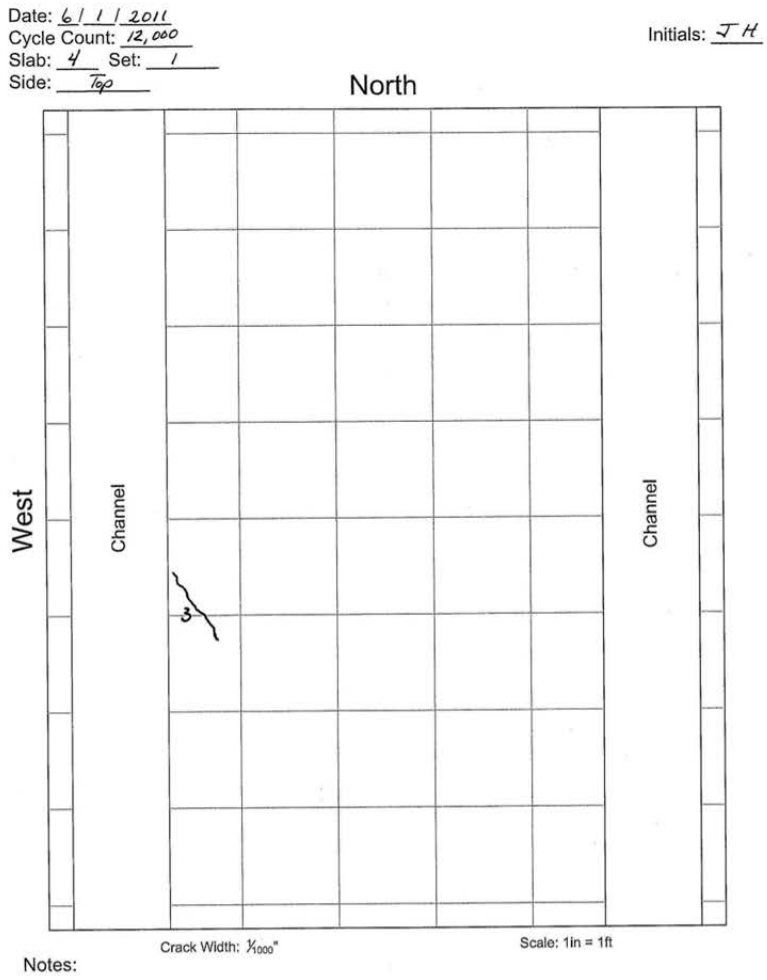

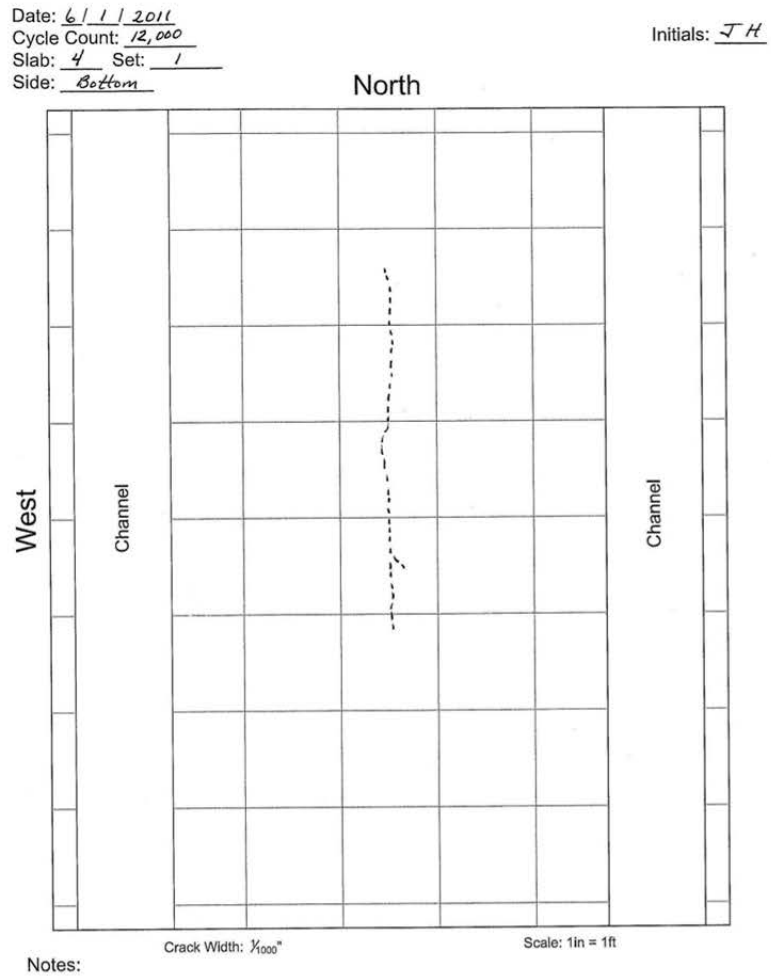

Figure F-32: Crack maps, M1000b, test panel, 12,000 traffic cycles.

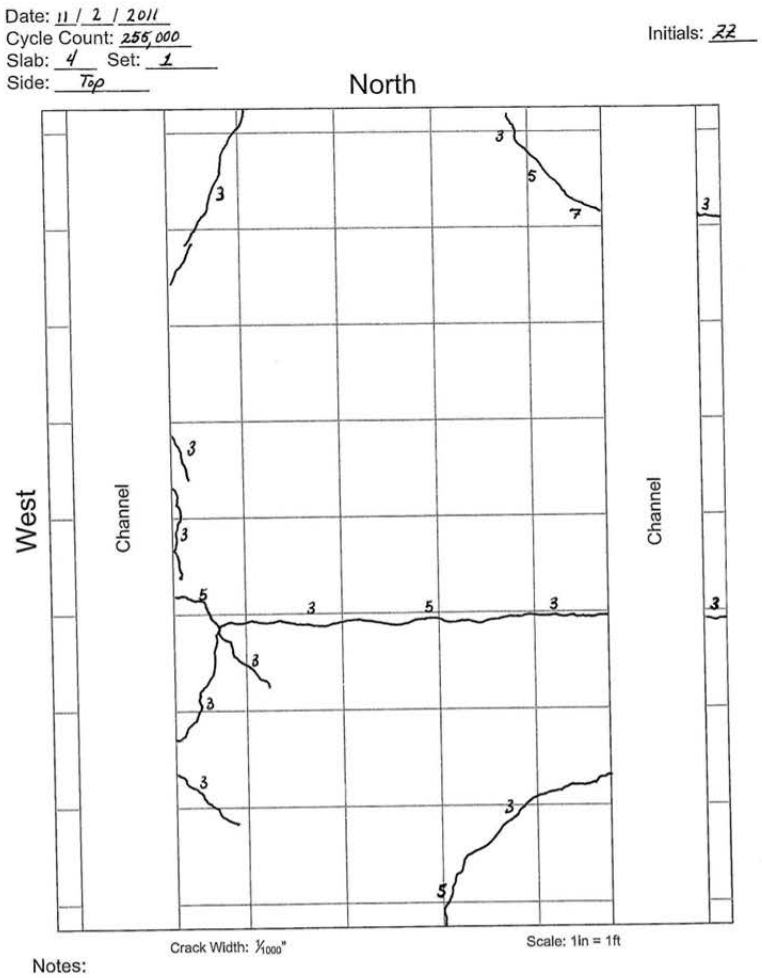

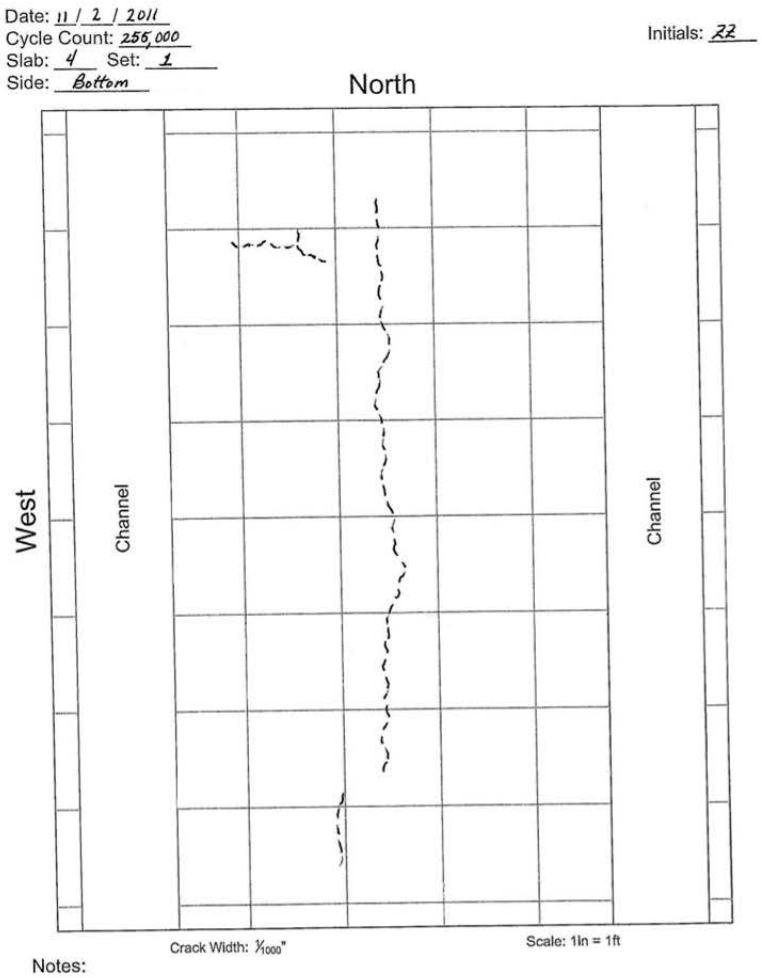

Figure F-33: Crack maps, M1000$_b$, test panel, 255,000 traffic cycles.

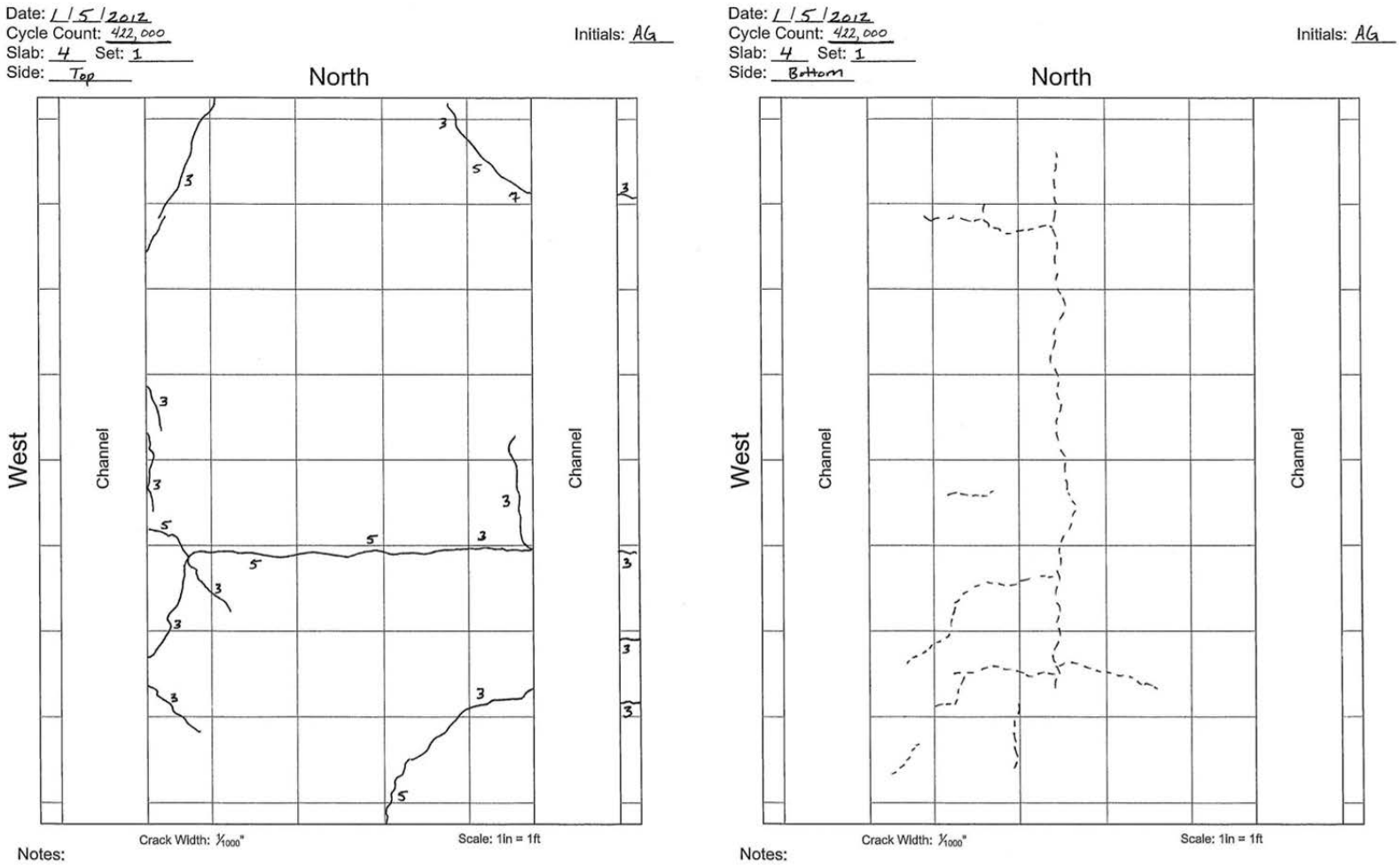

Figure F-34: Crack maps, M1000$_b$, test panel, 422,000 traffic cycles.

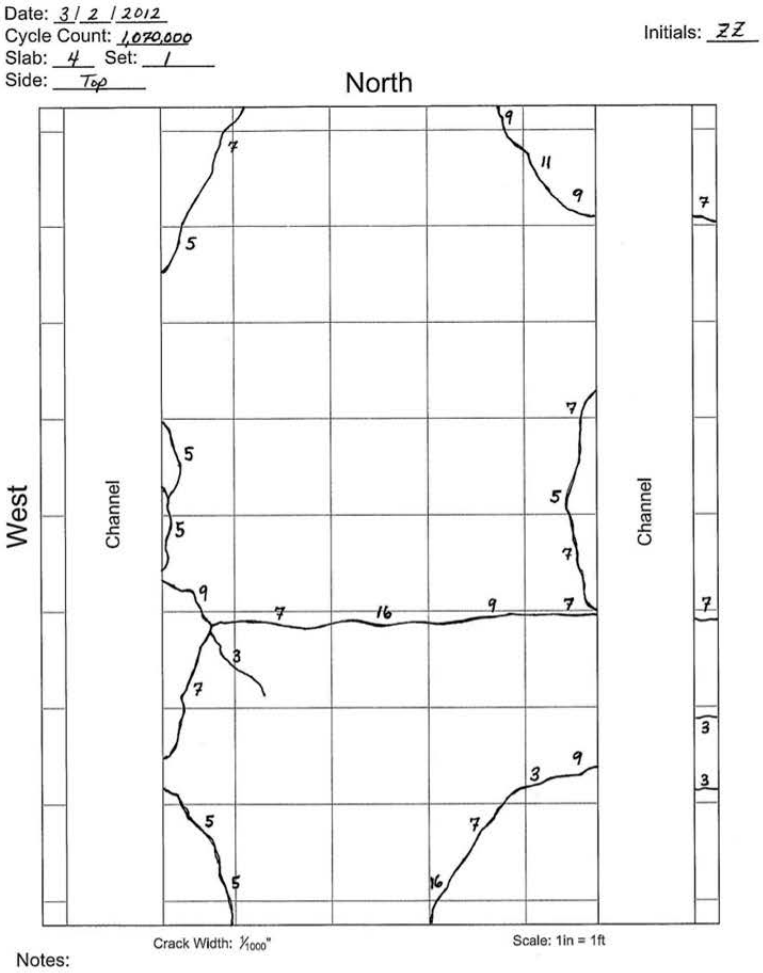

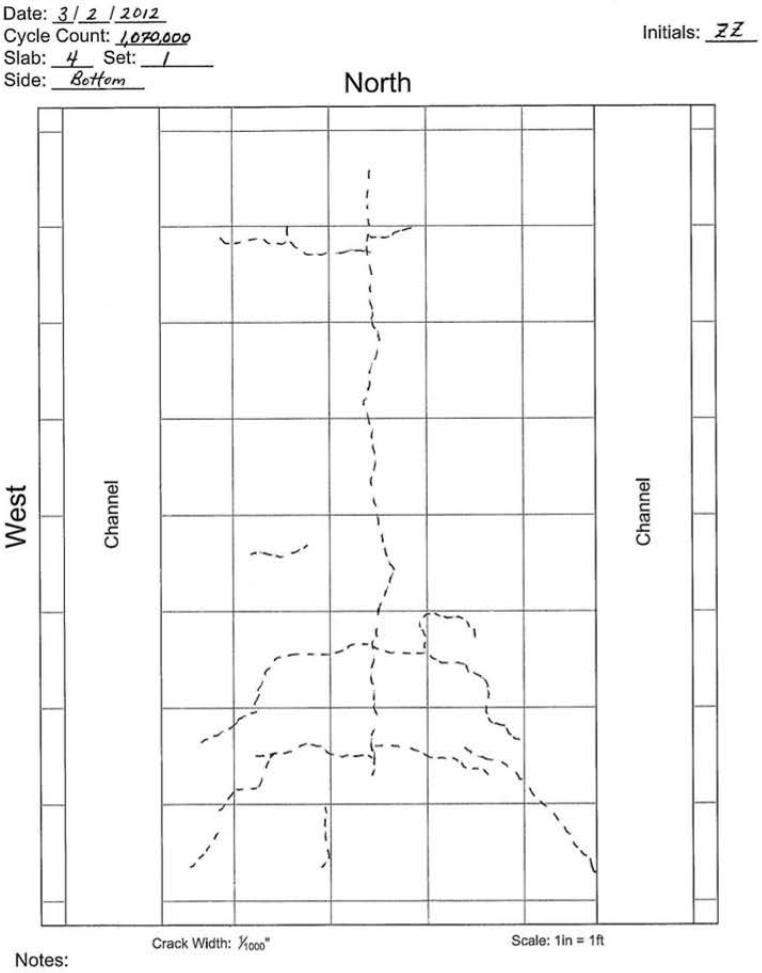

Figure F-35: Crack maps, M1000, test panel, 1,071,820 traffic cycles.

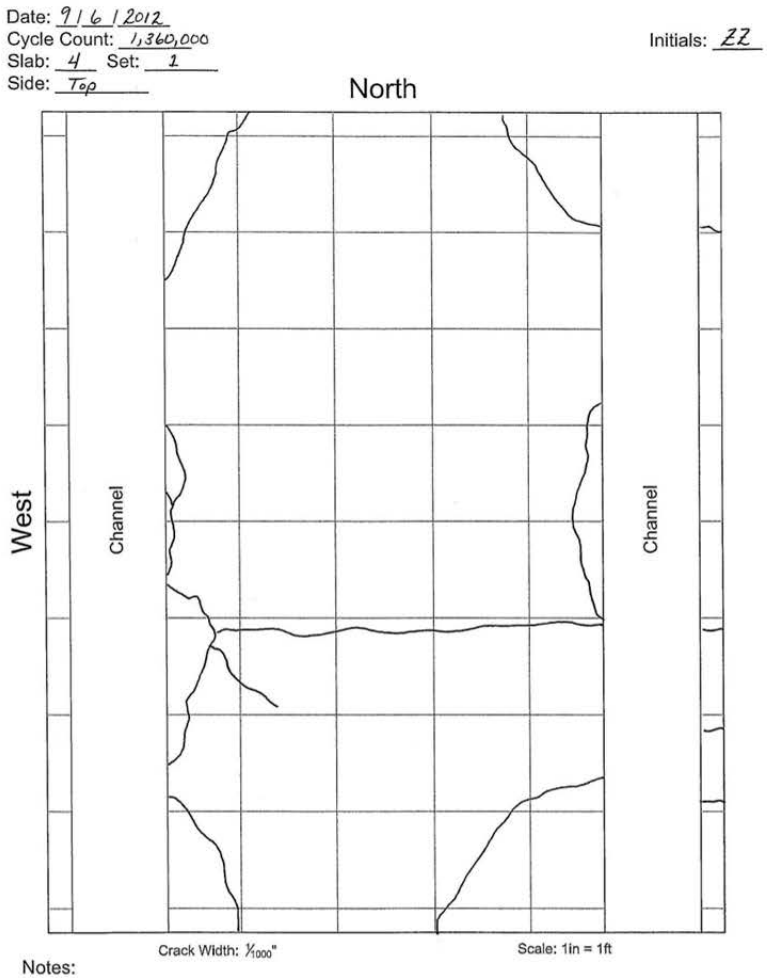

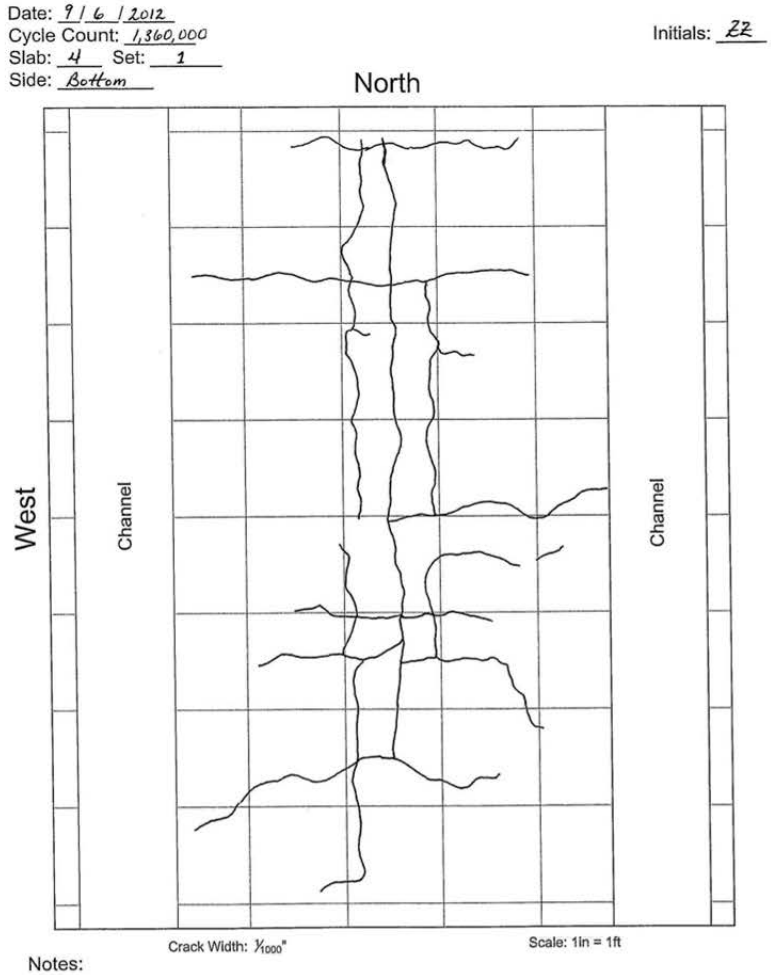

Figure F-36: Crack maps, M1000, test panel, 1,360,000 traffic cycles.

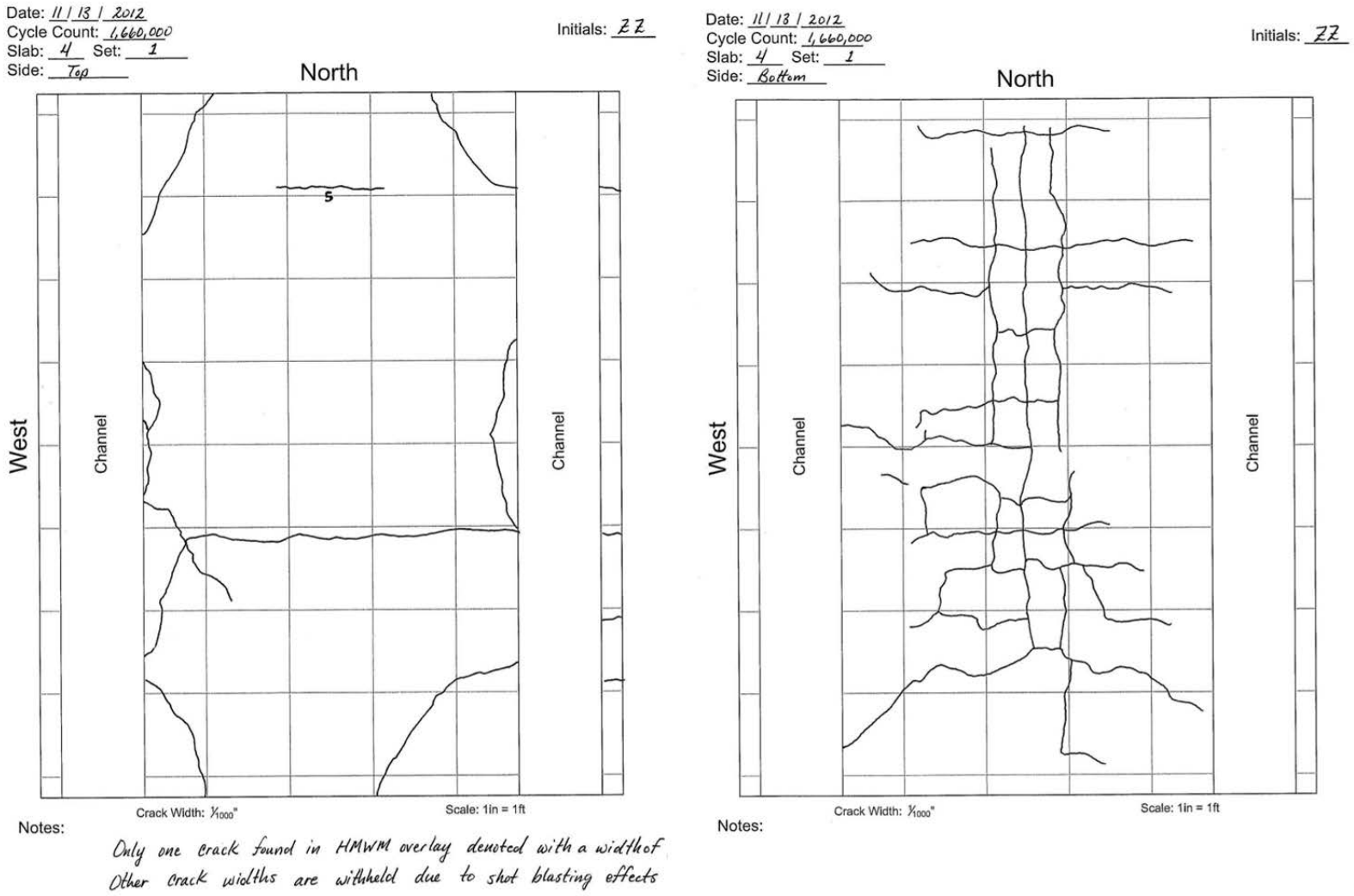

Figure F-37: Crack maps, M1000, test panel, 1,660,000 traffic cycles.

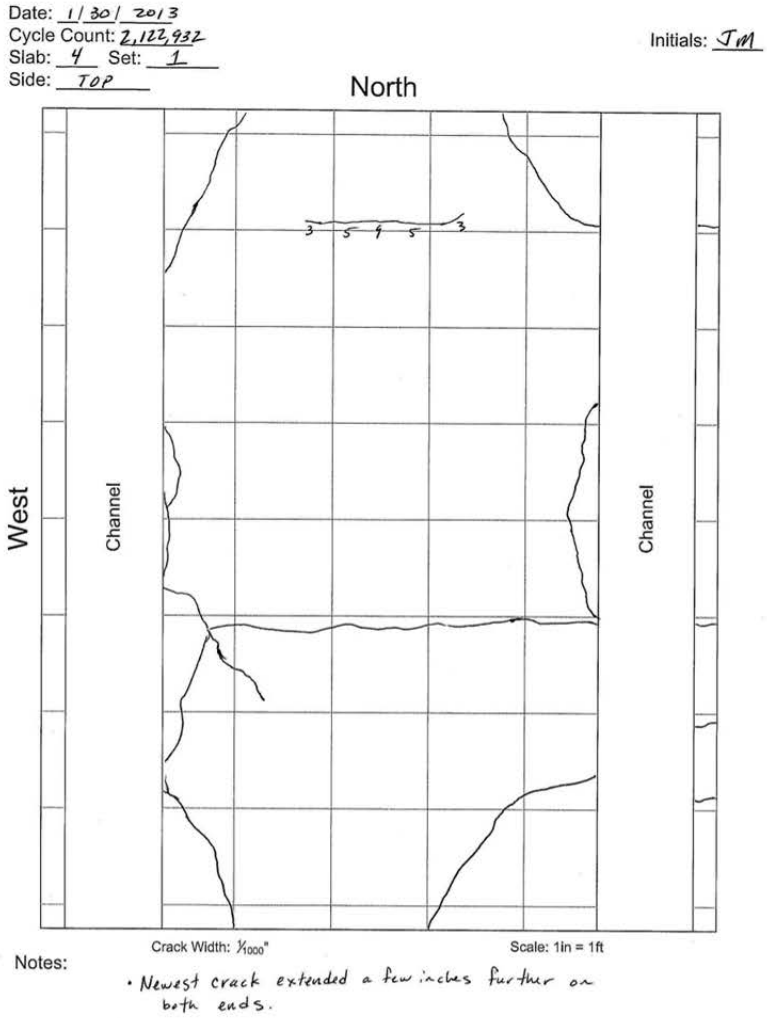

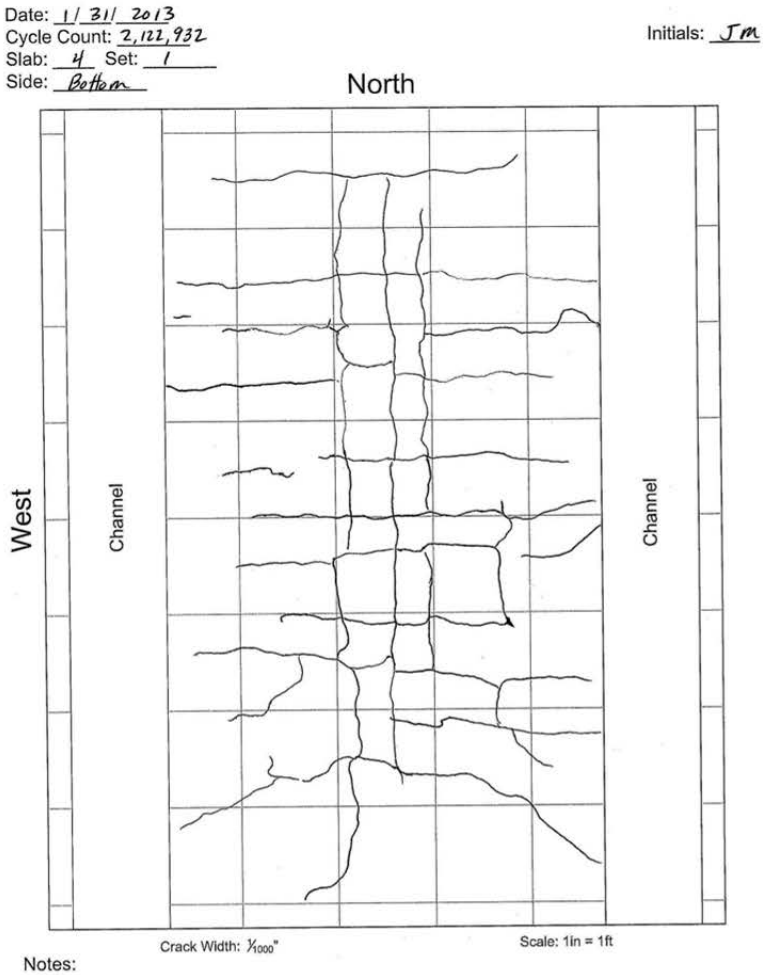

Figure F-38: Crack maps, M1000, test panel, 2,122,978 traffic cycles.

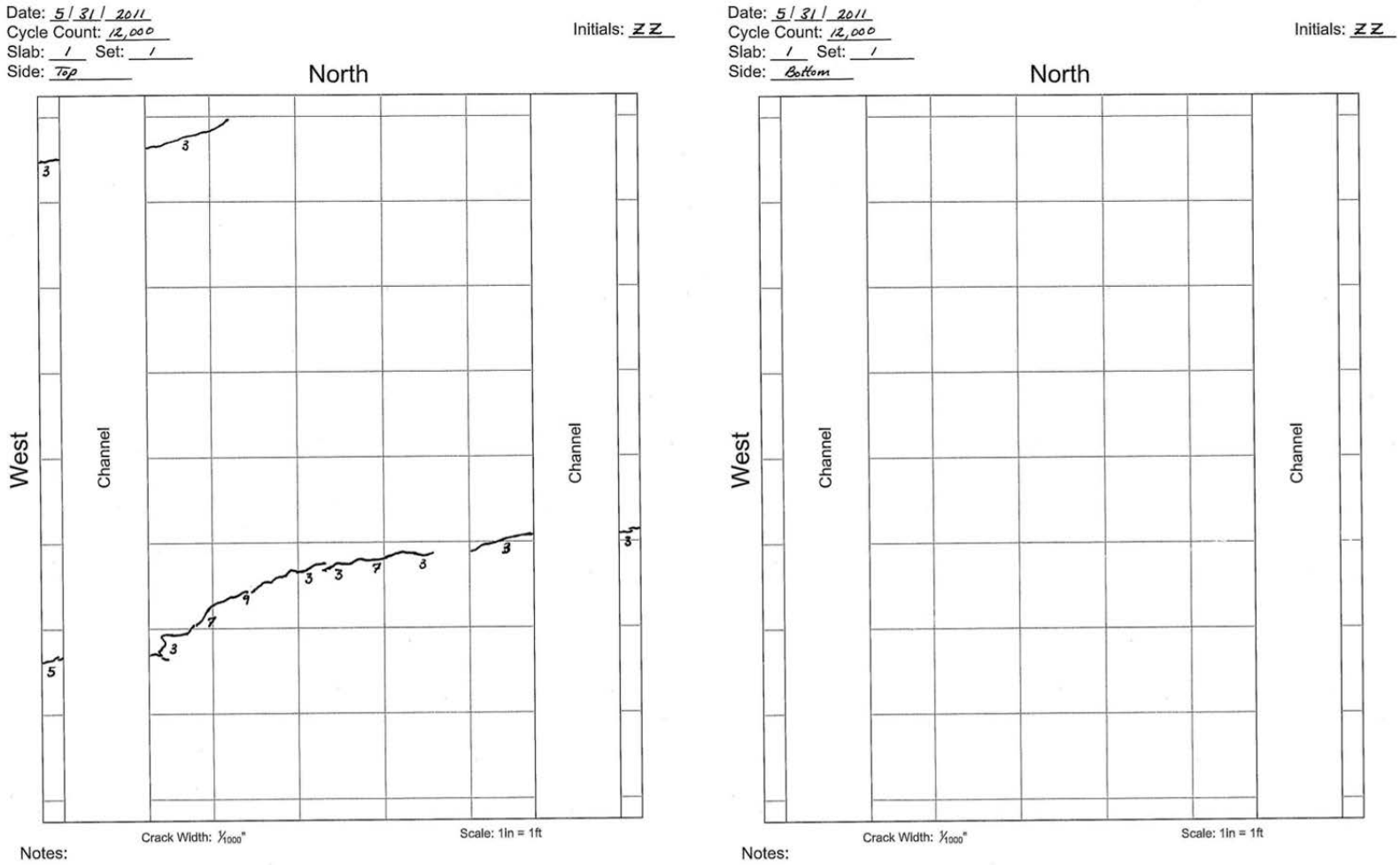

Figure F-39: Crack maps, Control$_a$ test panel, 12,000 traffic cycles.

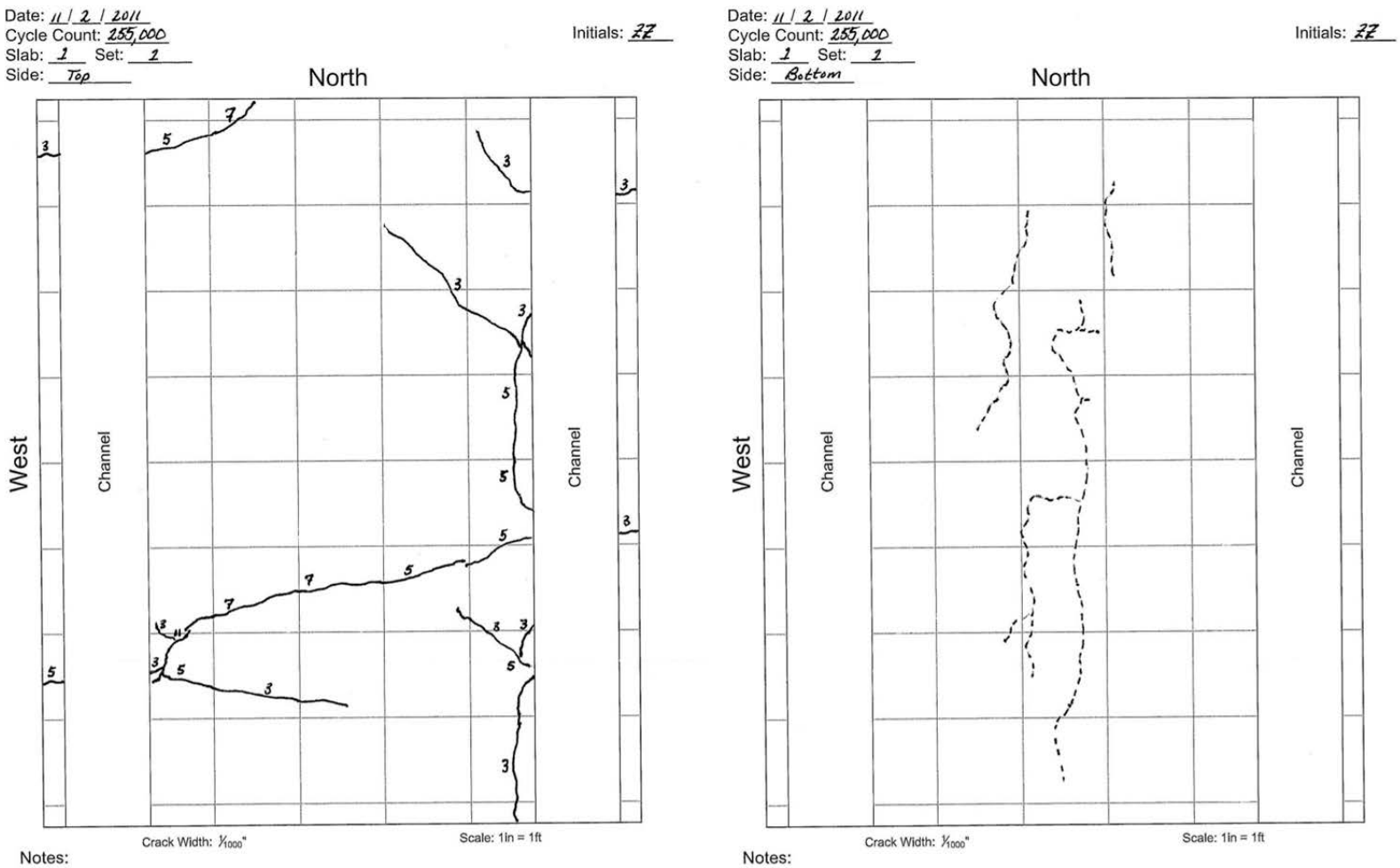

Figure F-40: Crack maps, Control$_a$ test panel, 255,000 traffic cycles.

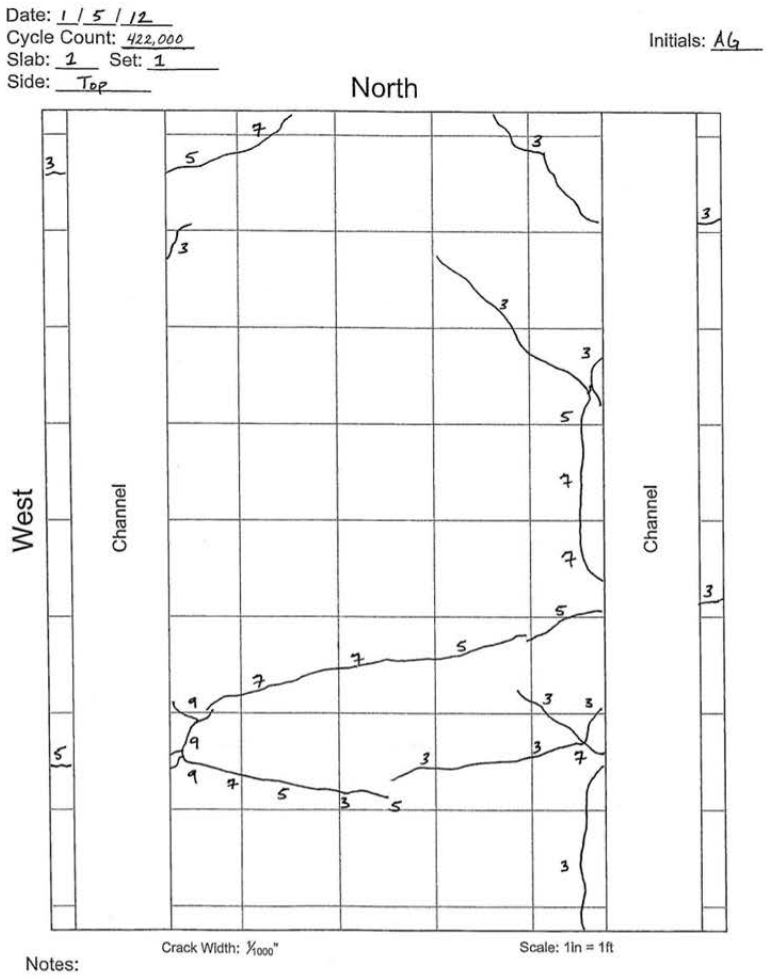

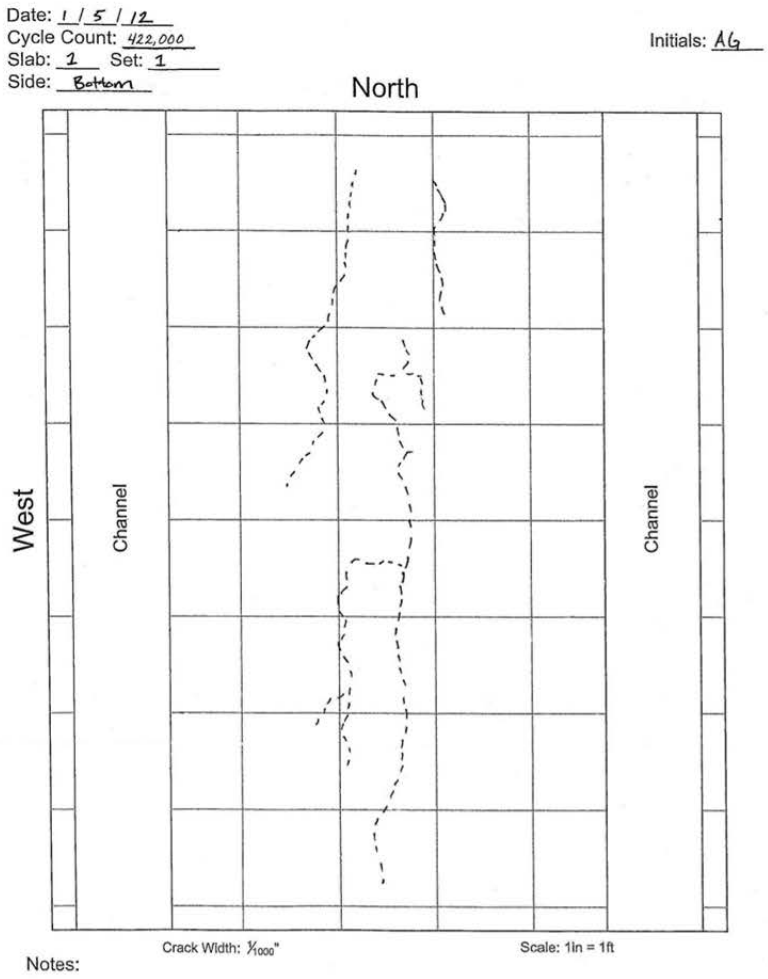

Figure F-41: Crack maps, Control$_a$ test panel, 422,000 traffic cycles.

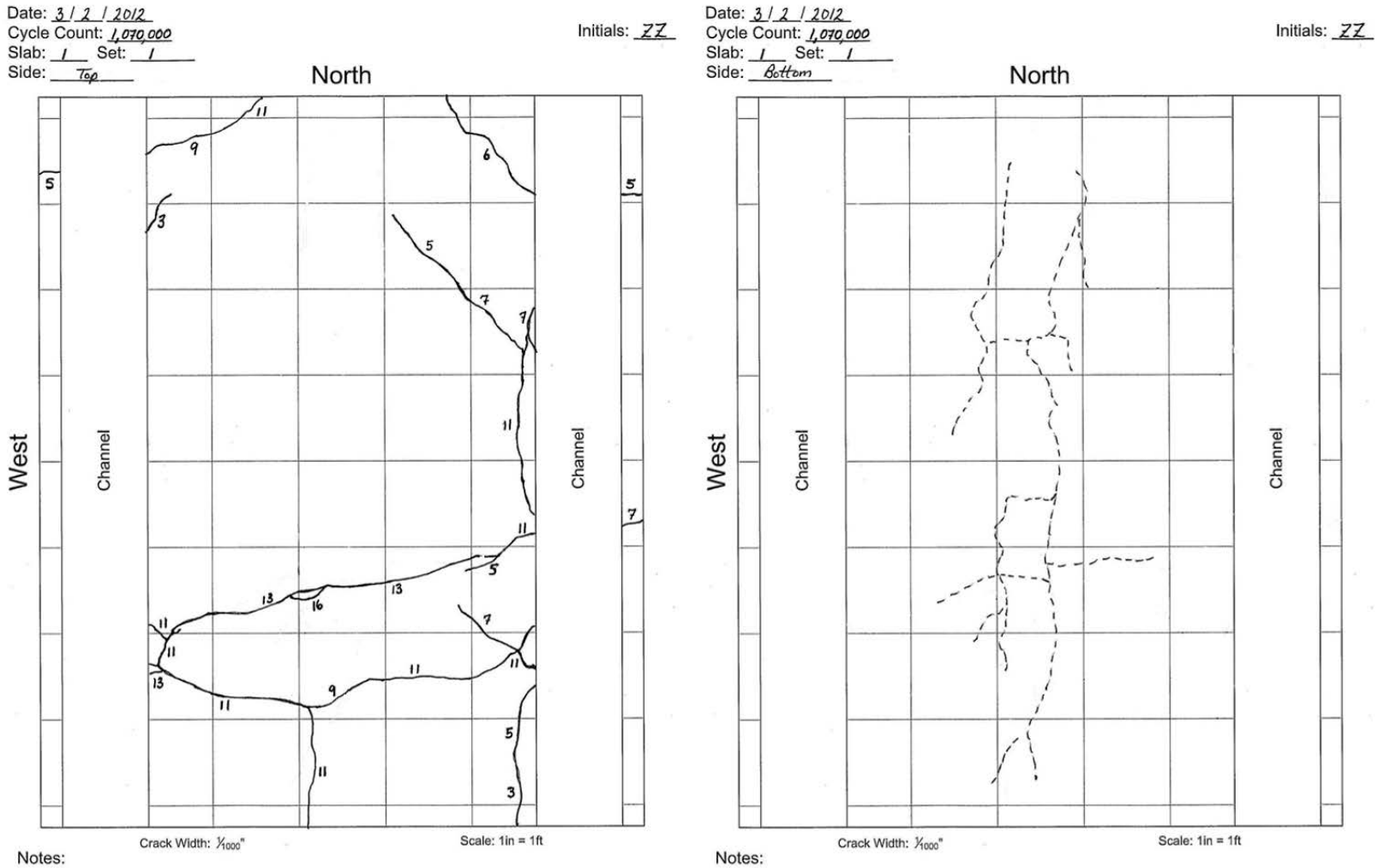

Figure F-42: Crack maps, Control$_a$ test panel, 1,071,820 traffic cycles.

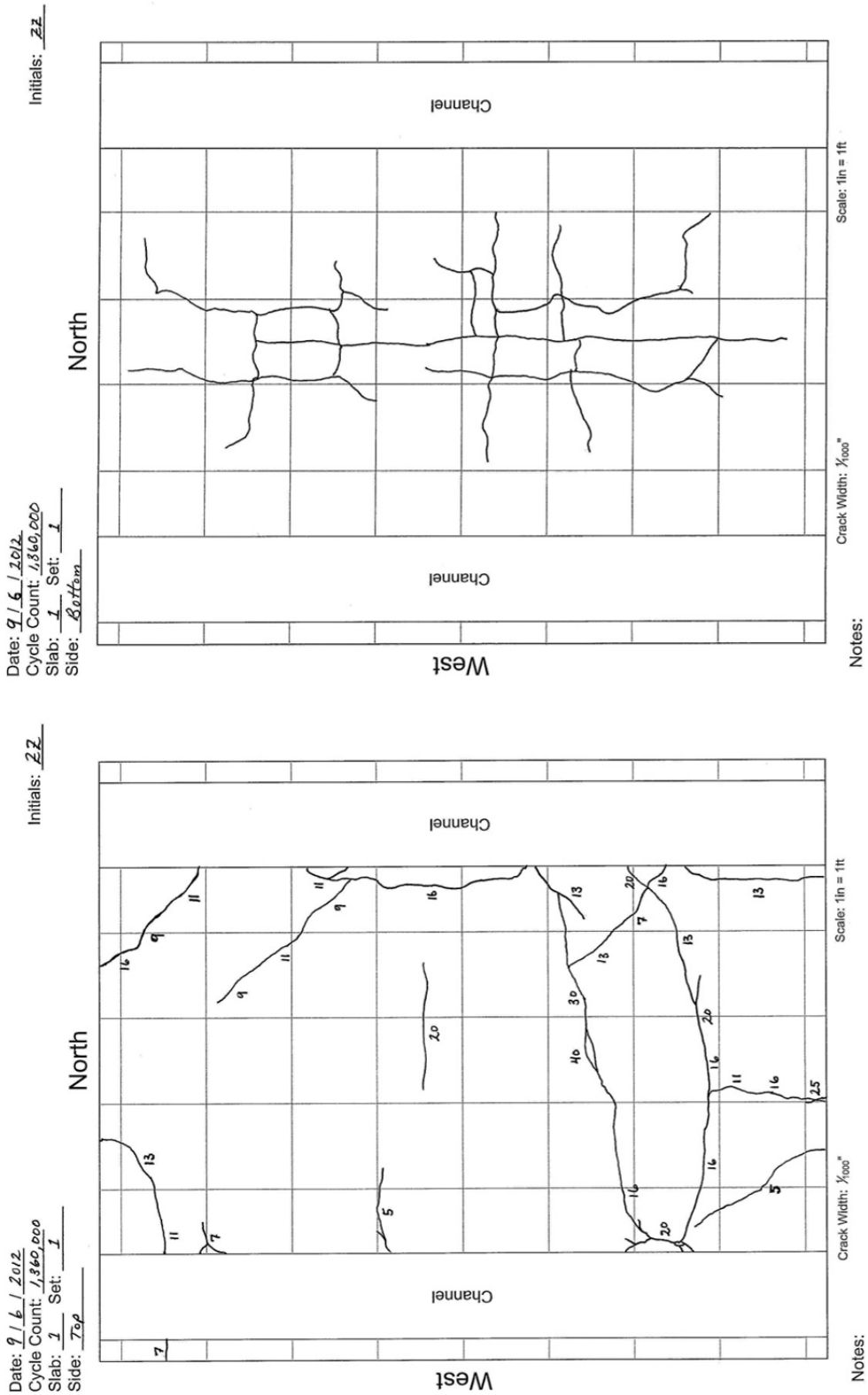

Figure F-43: Crack maps, Control$_a$ test panel, 1,360,000 traffic cycles.

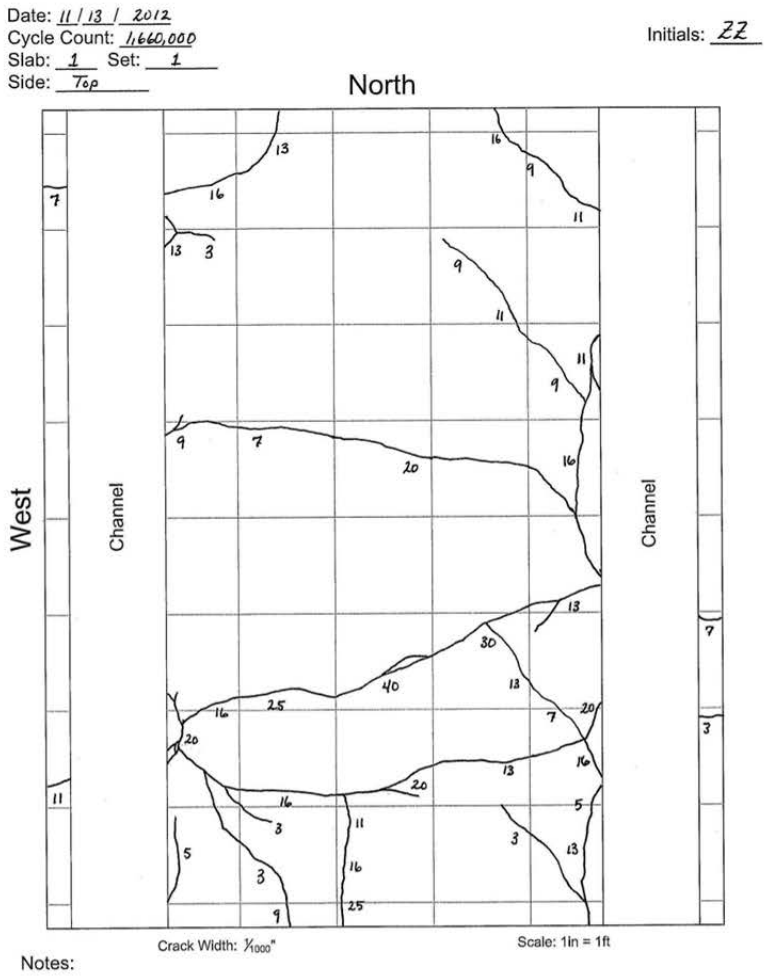

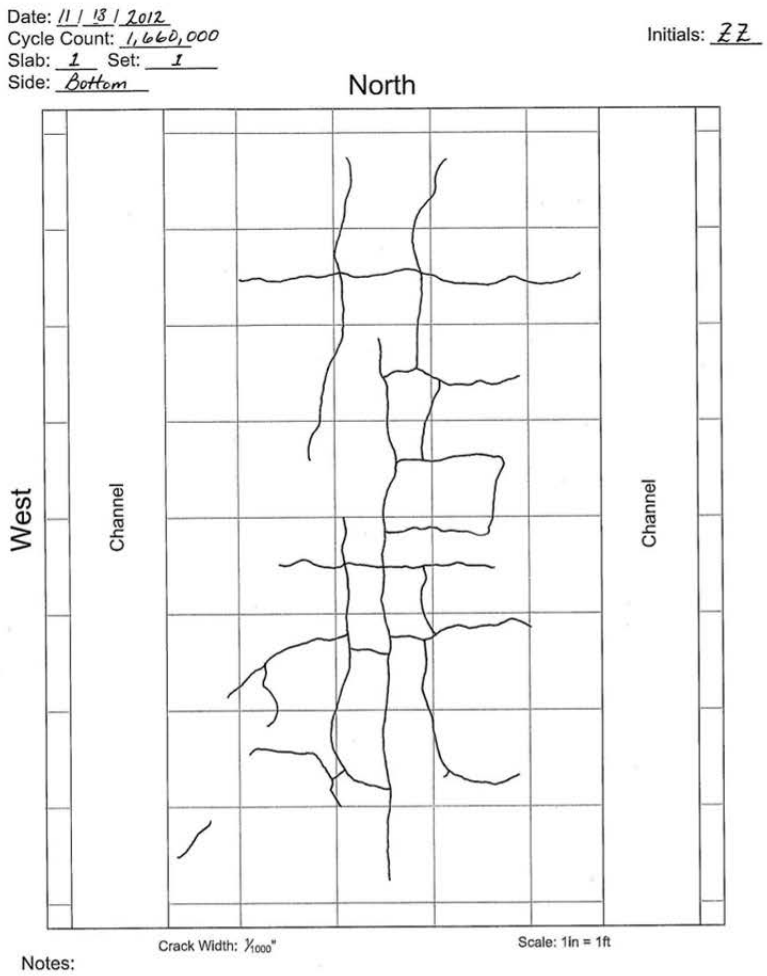

Figure F-44: Crack maps, Control$_a$ test panel, 1,660,000 traffic cycles.

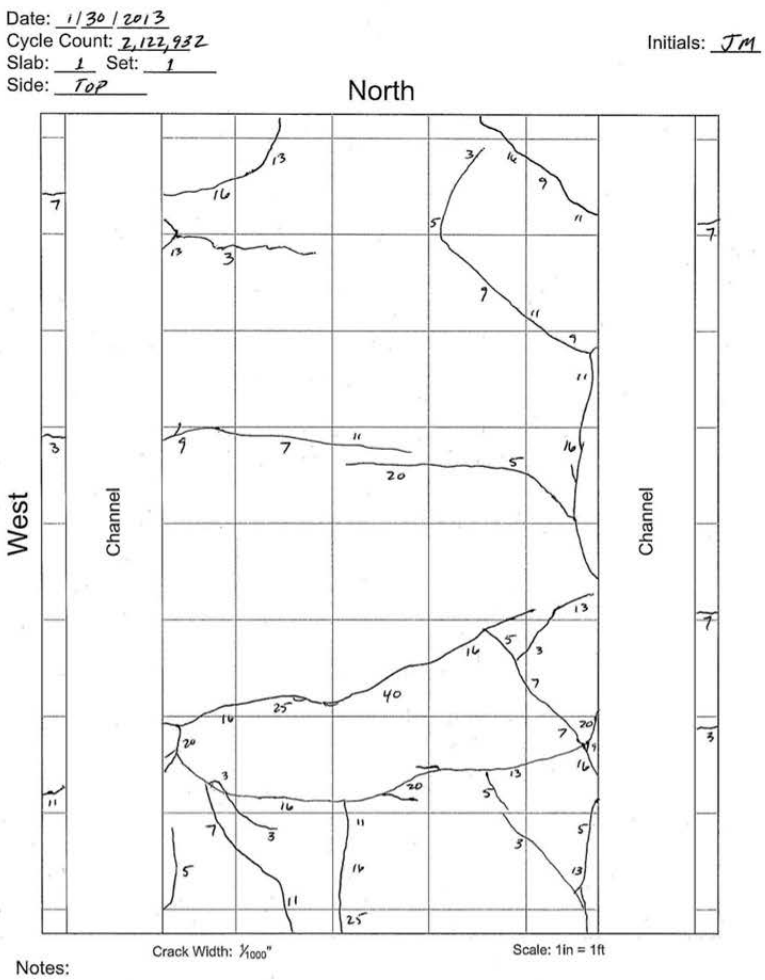

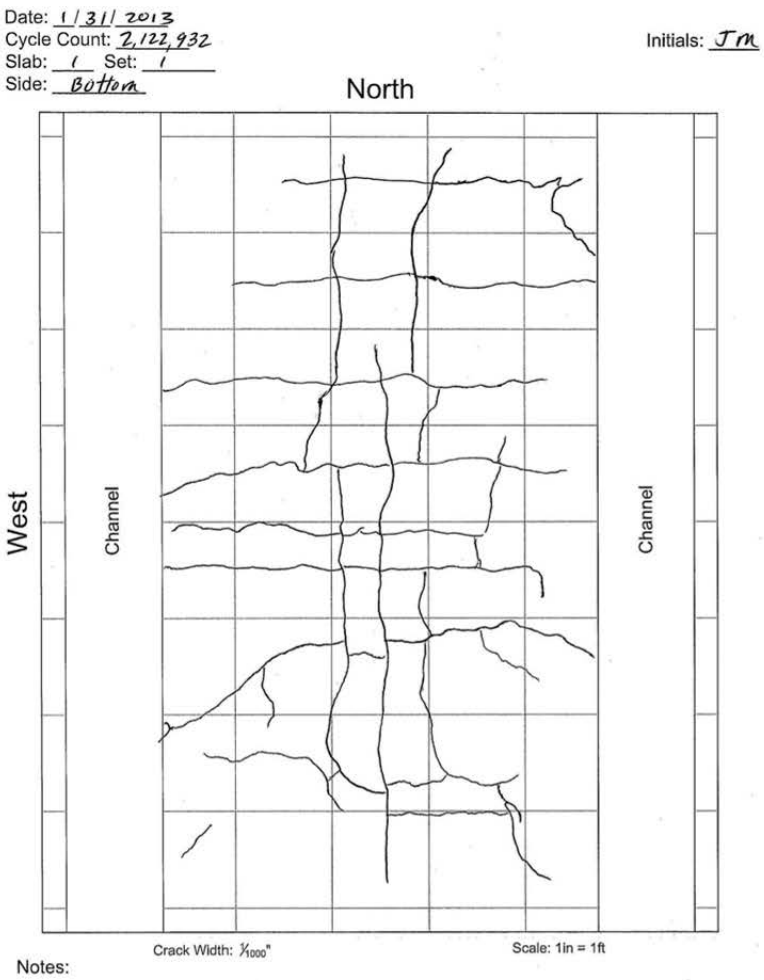

Figure F-45: Crack maps, M1000$_a$ test panel, 2,122,978 traffic cycles.

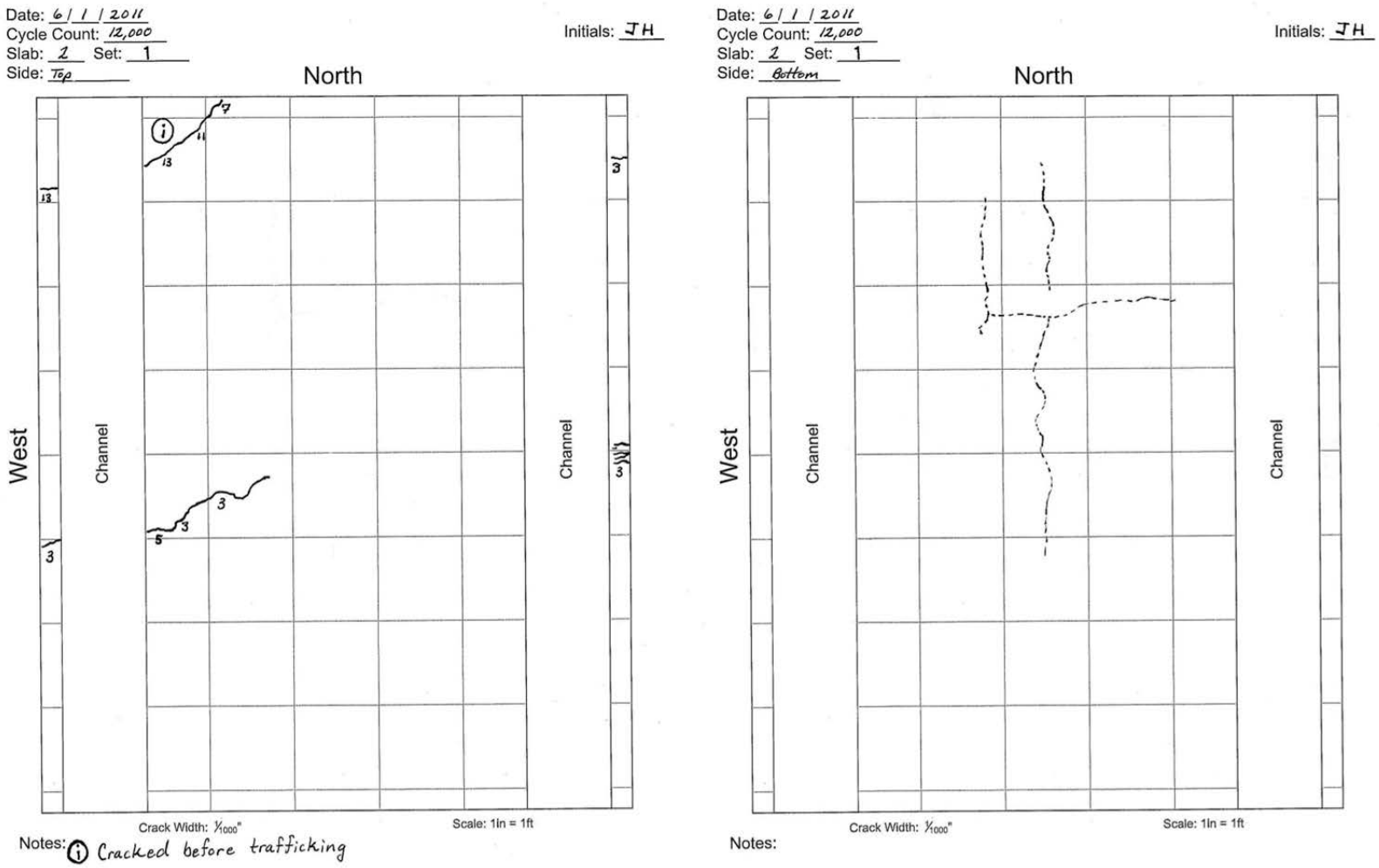

Figure F-46: Crack maps, Control$_b$ test panel, 12,000 traffic cycles.

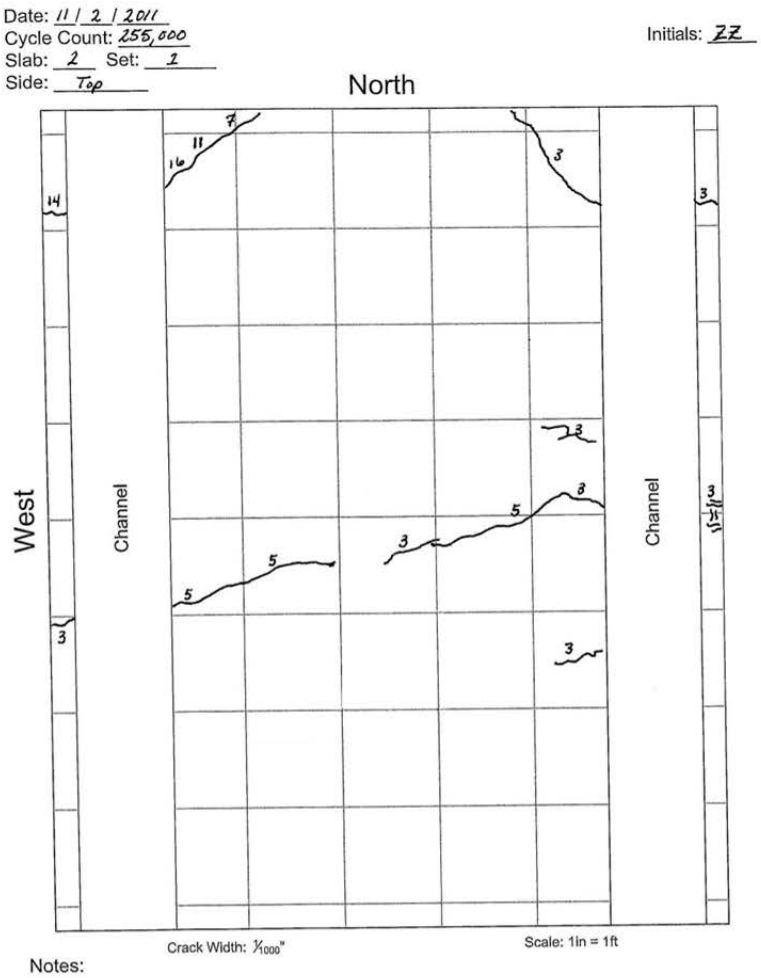

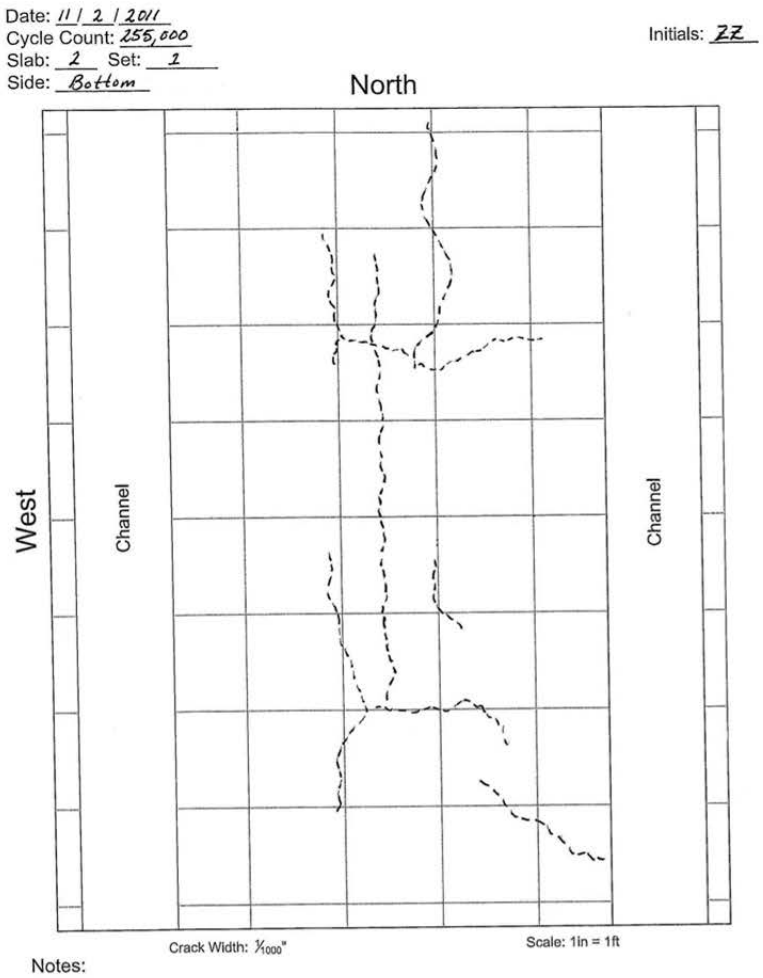

Figure F-47: Crack maps, Control, test panel, 255,000 traffic cycles.

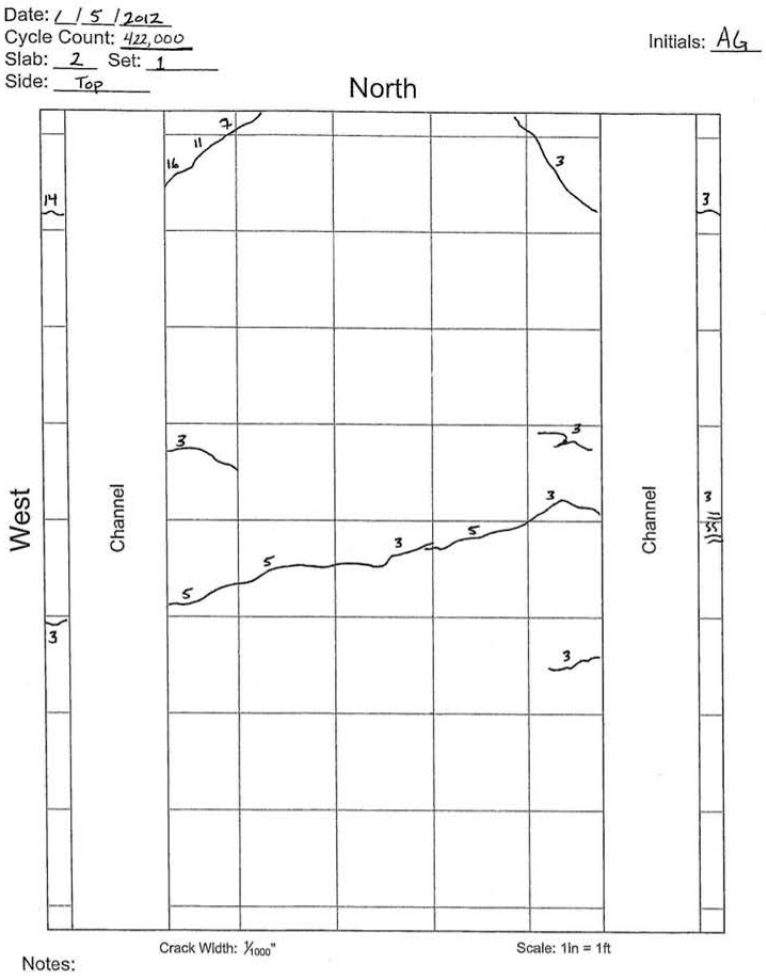

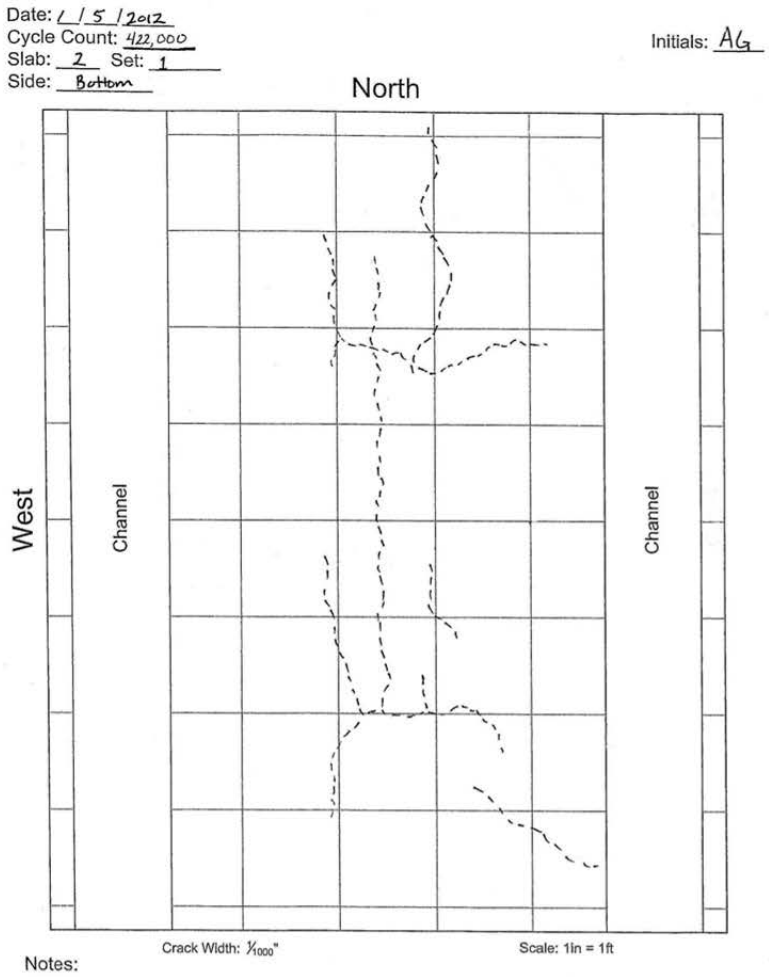

Figure F-48: Crack maps, Control, test panel, 422,000 traffic cycles.

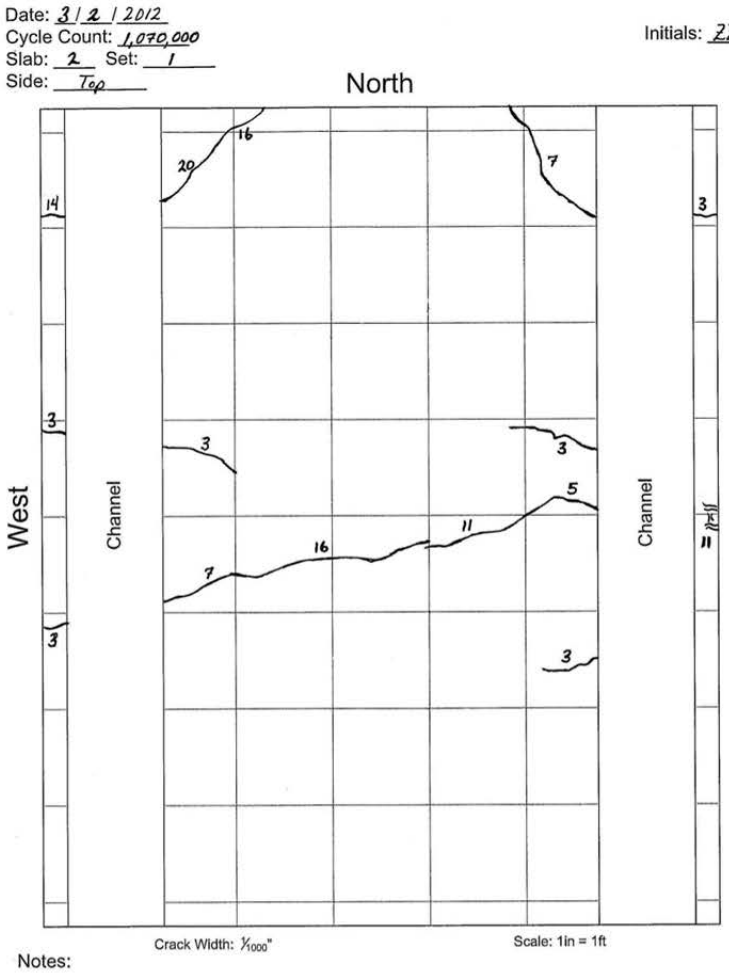

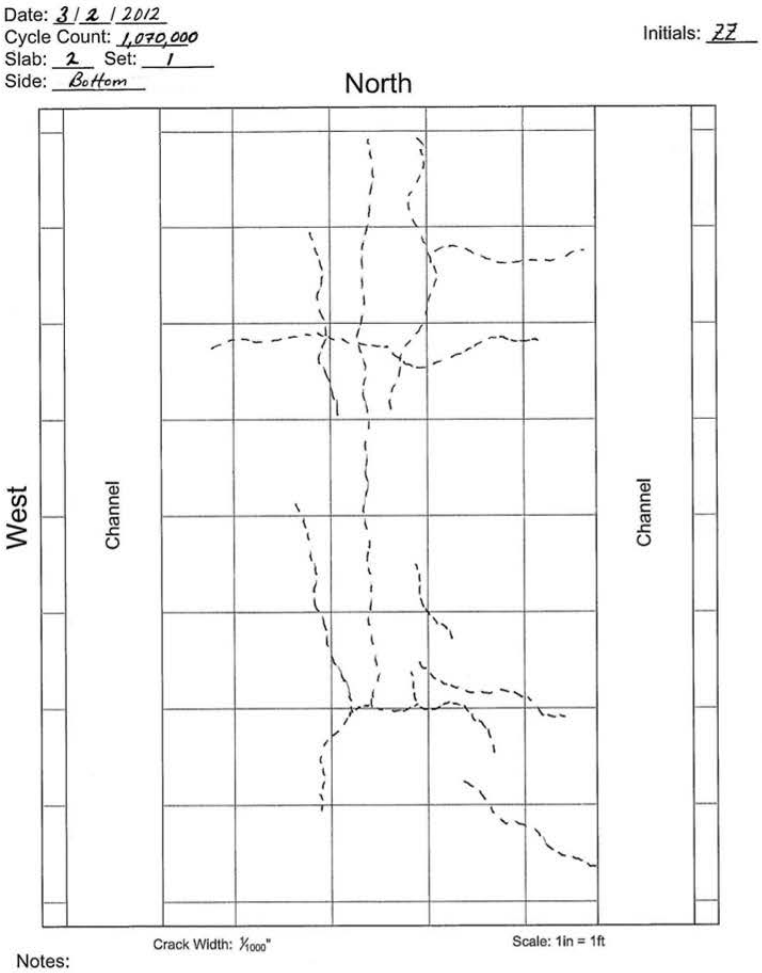

Figure F-49: Crack maps, Control$_b$ test panel, 1,071,820 traffic cycles.

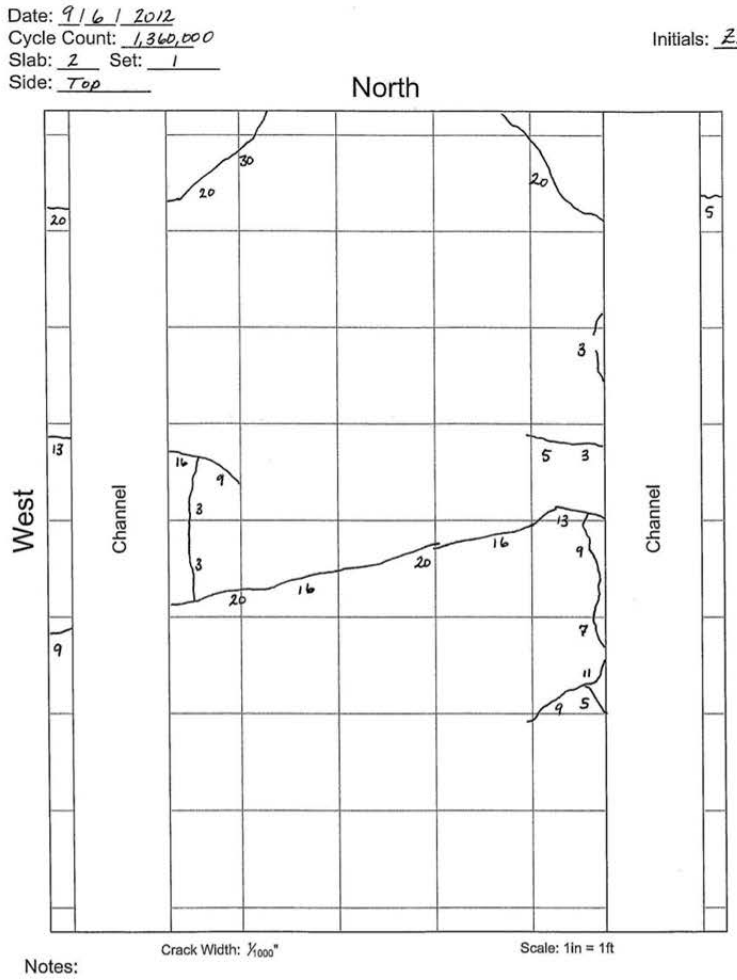

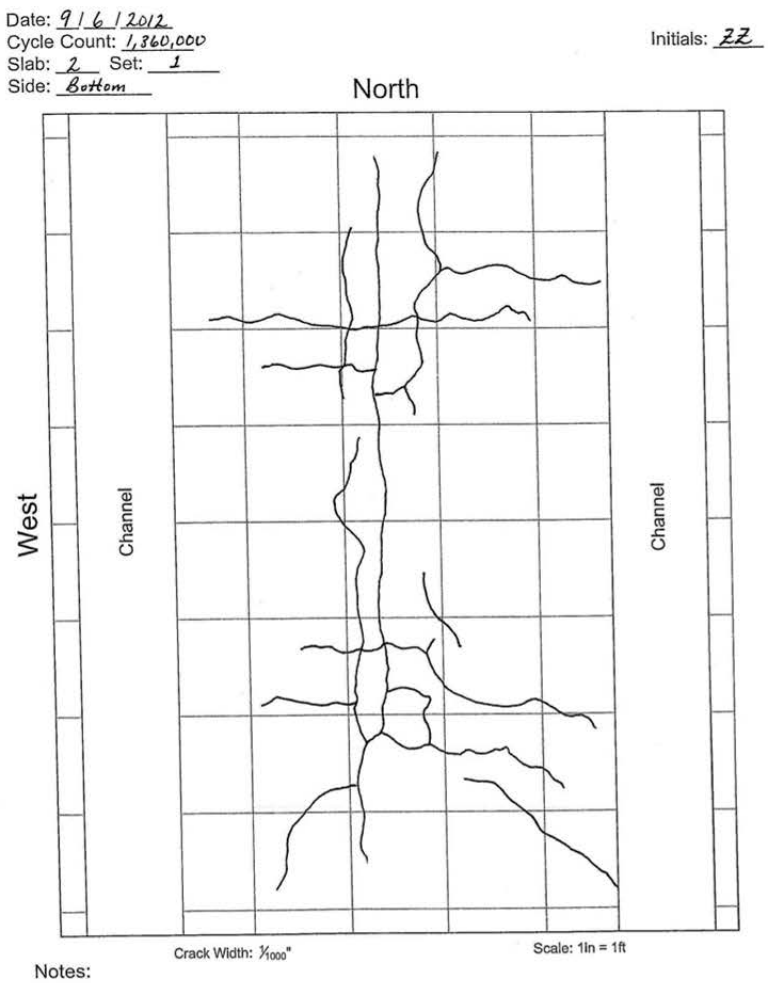

Figure F-50: Crack maps, Control$_b$ test panel, 1,360,000 traffic cycles.

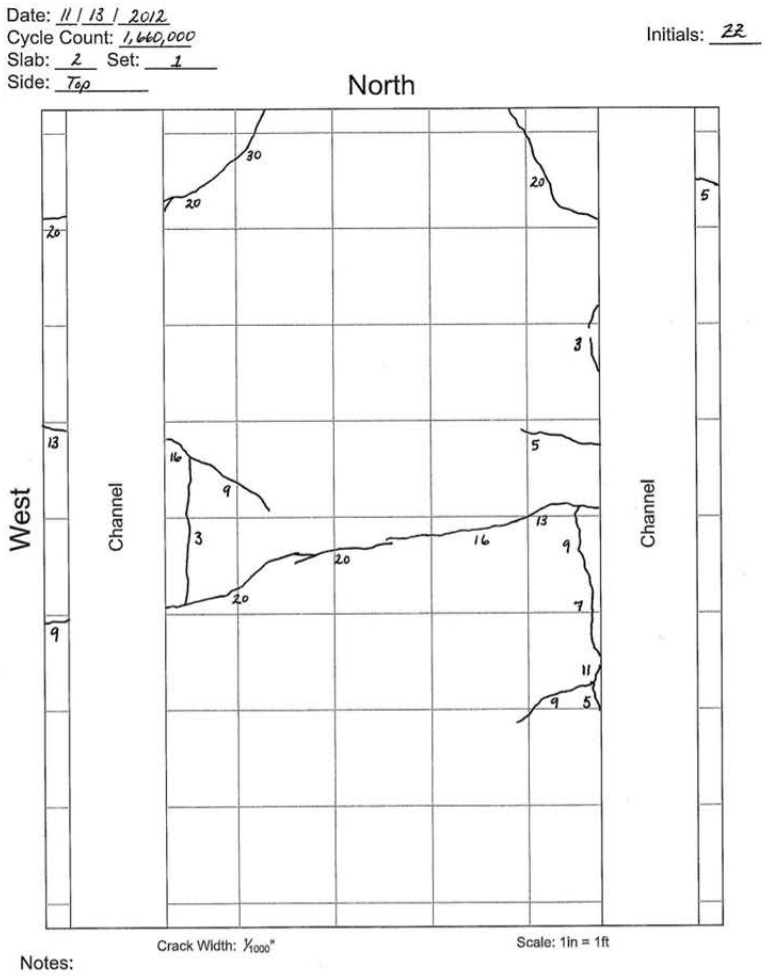

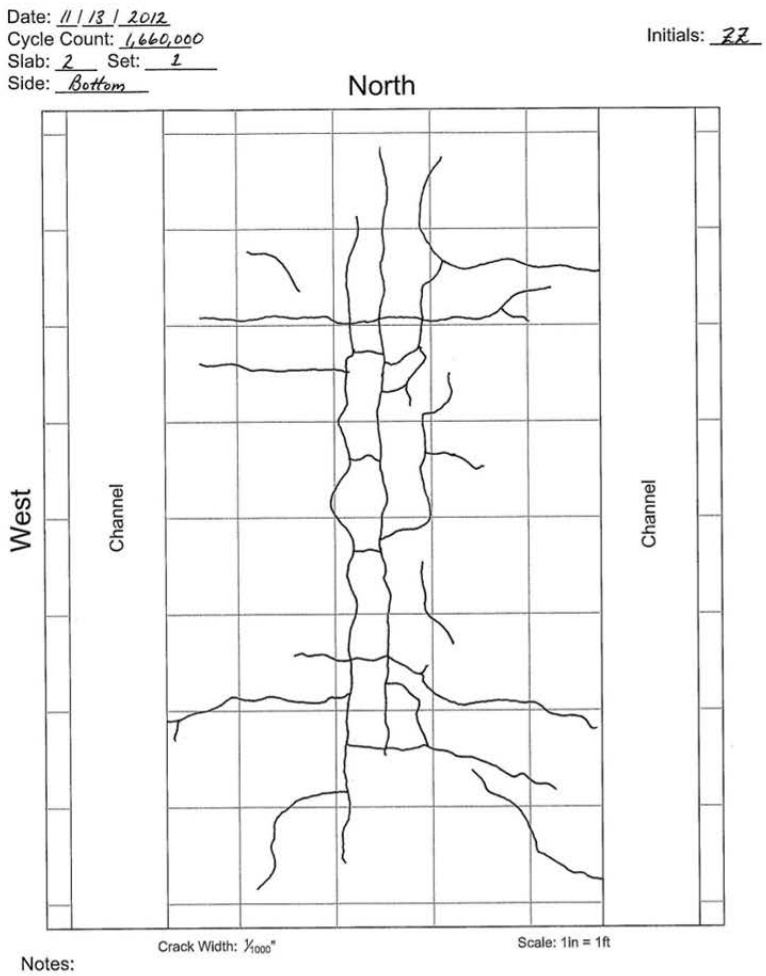

Figure F-51: Crack maps, Control$_b$ test panel, 1,660,000 traffic cycles.

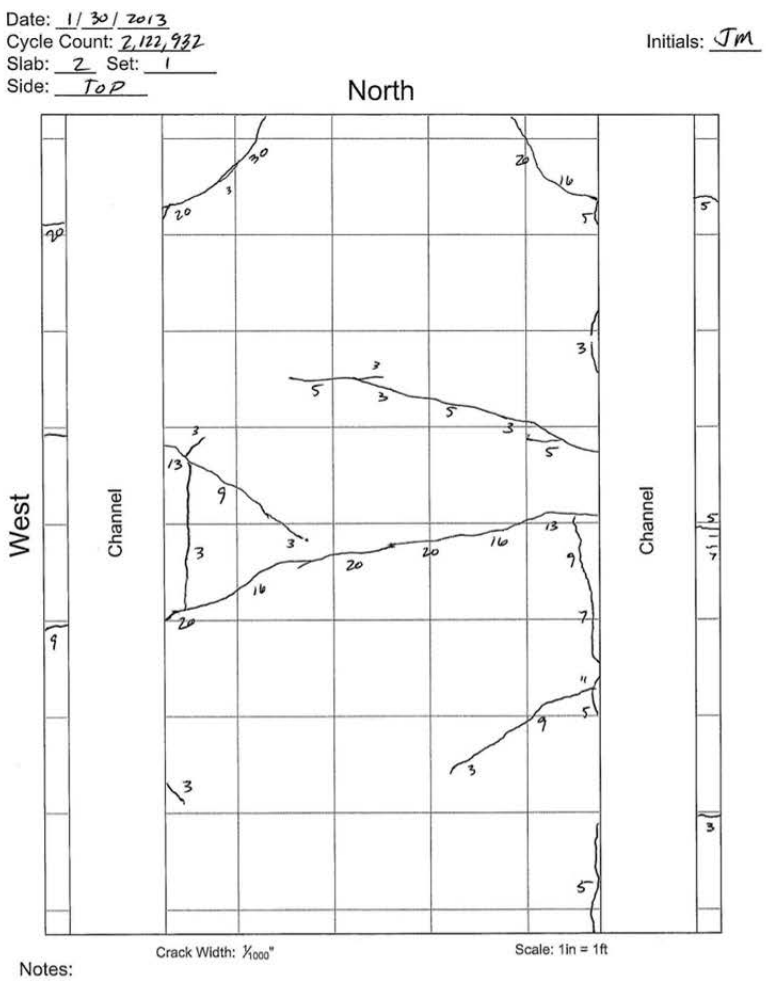

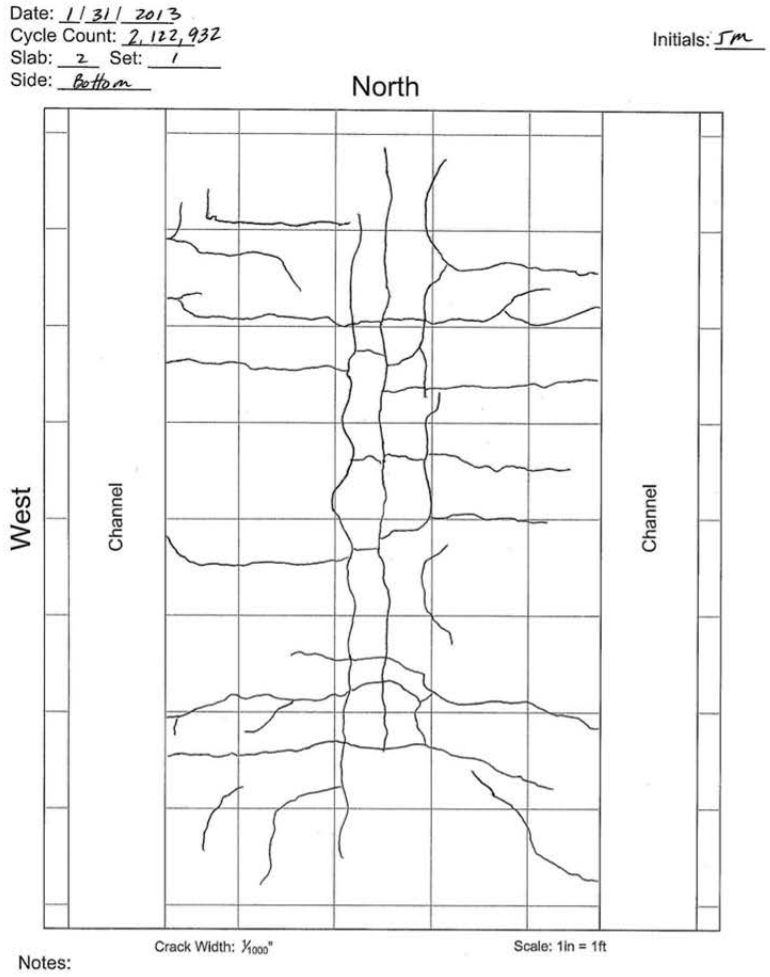

Figure F-52: Crack maps, M1000, test panel, 2,122,978 traffic cycles.